VDES R-Mode positioning system demonstrator

GA5.3/5.4 project report

Issue: 1.1

Issue Status: Approved

Issue Date: 24/10/2021

	Name	Partner	Signature
Provided	Adam Lipka	NIT	
Review	Krzysztof Bronk	NIT	
Approval	Stefan Gewies	DLR	

Document Information

Project Title	R-Mode Baltic
Work Package No.	GA 5.3/5.4
Document Title	VDES R-Mode positioning system demonstrator
Description	The major topic of the document is the analysis of the R-Mode real-time positioning demonstrator
Date	24.10.2021
Lead Author	NIT
Lead Author's Contact Information	National Institute of Telecommunications Wireless Systems and Networks Department Telephone: (+48) 58 341 71 21 E-mail: K.Bronk@itl.waw.pl
Contributing Author(s)	Krzysztof Bronk, Magdalena Januszewska, Adam Lipka, Patryk Koncicki, Rafał Niski, Błażej Wereszko
Approval	Yes

Track Changes

Issue	Date	Pages	Change	Author, Company
0.13	01/06/2021	176	Draft	NIT
1.0	16/06/2021	178	Internal review	NIT (Adam Lipka)
1.1	18/06/2021	179	Internal review	GA 5.4 Leader (Krzysztof Bronk)

This report was created within the framework of the **R-Mode Baltic** project, which aims to develop and demonstrate a new maritime backup system for Position, Navigation and Time (PNT) purposes based on R-Mode technology. Within the project life time of three years the project consortium develops solutions for R-Mode transmitter and receiver prototypes, for independent time synchronisations of broadcasting stations and for a testbed concept and its deployment. The dissemination of R-Mode technology is supported by work in international standardisation bodies. The world's first operational testbed for a transnational R-Mode system will be completed by the project in 2021.

The R-Mode Baltic project is co-financed by the European Regional Development Fund within the Interreg Baltic Sea Region Programme.

This report is available for download on the project website https://www.r-mode-baltic.eu/.

Contents

List of Tables

List of Figures

Abbreviations

AIS	Automatic Identification System
AWGN	Additive White Gaussian Noise
BER	Bit Error Rate
BLER	Block Error Rate
BPSK	Binary Phase Shift Keying
CDMA	Code Division Multiple Access
CRC	Cyclic Redundancy Check
D1,D2	Distances between pairs of samples in a multicorelator
DLL	Delay Locked Loop
EGNOS	European Geostationary Navigation Overlay Service
FDMA	Frequency-Division Multiple Access
FEC	Forward Error Correction
GMSK	Gaussian Minimum Shift Keying
GNSS	Global Navigation Satellite System
GPS	Global Positioning System
I&D	Integration and Dump
INS	Inertial Navigation System
ITDMA	Incremental Division Multiple Access
LNA	Low Noise Amplifier
LOS	Line Of Sight
LPF	Low-pass filter
L1,L2,E1,E2	Sample positions in a multicorrelator
MCS	Modulation and Coding Scheme
MOG	Maritime Office in Gdynia
NCO	Numerically Controlled Oscillators
NLOS	Non Line Of Sight
NRZI	Non Return to Zero Inverted
PLL	Phase Locked Loop
PNT	Position, Navigation and Time
PRN	Pseudorandom noise
PSK	Phase Shift Keying
R-Mode	Ranging Mode
RMS	Root Mean Square
RRC	Root Raised Cosine

SDR	Software Defined Radio
SNR	Signal to Noise Ratio
SOTDMA	Self-organized time-division multiple access
SWR	Standing Wave Ratio
TOA	Time of Arrival
USRP	Universal Software Radio Peripheral
VDES	VHF Data Exchange System
VHF	Very High Frequency
VSWR	Voltage Standing Wave Ratio
QPSK	Quadrature Phase Shift Keying
QAM	Quadrature Amplitude Modulation

1 Introduction

The following report summarises the activities of the National Institute of Telecommunications in the R-Mode's GAs 5.3 and 5.4. The main topic of the document is the description of the tasks that led to the creation of the R-Mode positioning demonstrator. This report is a continuation and supplement to the report entitled "AIS and VDES Ranging – measurements results", therefore there will be some references to this report in the text [1-1].

The report is comprised of eight chapters (including this introduction).

In the second chapter, the greatest attention was paid to the concept of the double delta correlator and its influence on the occurring phenomena of multipath. The focus is on theoretical considerations and mathematical models representing the multicorrelator concept. The implementation method and the influence of the double delta correlator on the accuracy of the determined pseudoranges in the signal correlation application are presented. Extensive analyzes of the obtained results made it possible to examine the effectiveness of the advanced correlators used in the systems to determine the position.

In the third chapter, the main attention is paid to the phenomenon of multipath and the influence of the sample pairs' spacing in the double delta correlator. The tests were carried out for signals in LOS and NLOS conditions, and on the basis of that it was possible to select the most effective sample spacing and to reduce the multipath effect. Thanks to the obtained RMS charts in the SNR domain, it was possible to observe the correlator's influence on the accuracy determination of the calculated pseudoranges.

The next chapter focuses on the construction of the R-Mode positioning system. All modules included in the system were listed and their detailed descriptions were provided. The principle of operation of the system from the physical layer to the layers with data processing in implemented applications was described. Also presented is the method of synchronizing all independent modules, which, when connected to each other, allow for real-time positioning.

The fifth chapter describes in detail the results obtained during the VDES measurement campaign that took place in 2020. All analyzes, charts and conclusions were presented. The existing problems were analyzed and solutions were proposed that could improve the results in the next measurement campaign.

The seventh chapter presents a complete demonstrator of the R-Mode real-time positioning system. Six scenarios that simulated real measurement conditions were presented. During the demonstration, the signal was received, which was transmitted from the station located in the port of Gdynia. The recorded signal was sent to other modules in the R-Mode system and was subjected to digital signal processing. Using the obtained correlation and the calculated pseudo-distances, the last module in the system was able to precisely determine the position of the receiver.

The final chapter presents a summary of the obtained results. The opportunities associated with the R-Mode positioning system were presented. Plans for the future development of the R-Mode system and the upcoming measurement campaigns were also discussed.

2 The concept of a multi-correlator and its implementation in the project in order to reduce the multi-path phenomenon

Correlation is a measure of similarity or mutual dependence. It is a key operation, performed in GNSS receivers, in order to achieve synchronization with the signals coming from each satellite. A single correlator is not enough for this purpose. In fact, even the simplest GNSS receiver supports multiple correlators to achieve proper synchronization.

2.1 Double delta correlator

The double delta correlator uses two pairs of early and delayed samples of the correlation function at different time domain intervals (Figure 2-1). Its purpose is to eliminate the multipath effect [2-1].

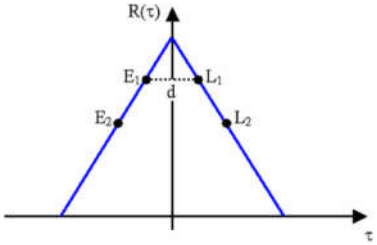

Figure 2-1: Double delta correlator concept

E1 and L1 are one output pair of correlator with an earlier and later correlation peak with d1 spacing, while E2 and L2 are the second output pair with an earlier and later correlation peak with d2 spacing. The distance to be searched can be written by the following formula:

$$D = (E_1 - L_1) - \frac{1}{2}(E_2 - L_2) \quad (1)$$

Since the differences E1–L1 and E2–L2 can be interpreted as narrow correlators, the formula (1) can be written in following form:

$$D = Narrow(d1) - \frac{1}{2}Narrow(d2) \quad (2)$$

The graph of the correlation function under multipath conditions is presented below (Figure 2-2). By taking two pairs of samples into account, the multipath effect can be considered in determining the distance.

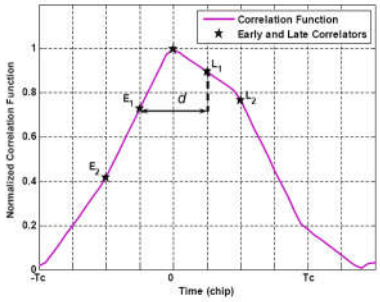

Figure 2-2: The correlation function under multipath conditions

2.1.1 Theory and implementation

The basic concept of baseband processing for a GNSS receiver is to correlate the incoming signal with a local replica of the PRN code (the sequence on which the correlation operation is performed) to obtain an estimated Doppler frequency and code delay. The matched replica here will be referred to as Prompt (P) [2-2].

In practice, even the simplest GNSS receiver supports at least three correlators:

• Prompt (P) - that is aligning the replica with the incoming signal,

• Early (E) - it is a replica that is shifted earlier in the time domain in relation to the Prompt replica,

• Late (L) - this is a replica that is shifted later in the time domain in relation to the Prompt replica.

Figure 2-3 shows an example of the output of these correlators when the Prompt replica is fully aligned with the incoming signal, which is the desired situation, and when the timing has not yet been achieved. The correlation results are the points marked above the autocorrelation function - in this example it is a triangular function taking into account the BPSK modulation (GPS L1 C/A):

- When the signal is being tracked correctly:
    - The power of the Prompt correlator is greater than the power of the Early and Late correlators,
    - Correlator E and L have comparable powers.

- When the signal is not being tracked properly, it is possible for the replicas to be delayed so as to achieve the correct timing. The solution is to analyze the power of the E, P, L correlators. In Figure 2-3 on the left, we can see that the code delay needs to be corrected to move all three replicas towards the right. This process is carried out in the tracking loop.

- The gaps between the E and L correlators are an important parameter in the receiver:
    - They should be smaller than 2 chips (otherwise it will fall out of the autocorrelation function),
    - if it is too small (i.e. close to zero), distinguishing correlators will not be so easy, especially when there is still noise,
    - smaller E-L gaps provide more reliable navigation as they make the correlator results less sensitive to potential autocorrelation distortions outside this region.

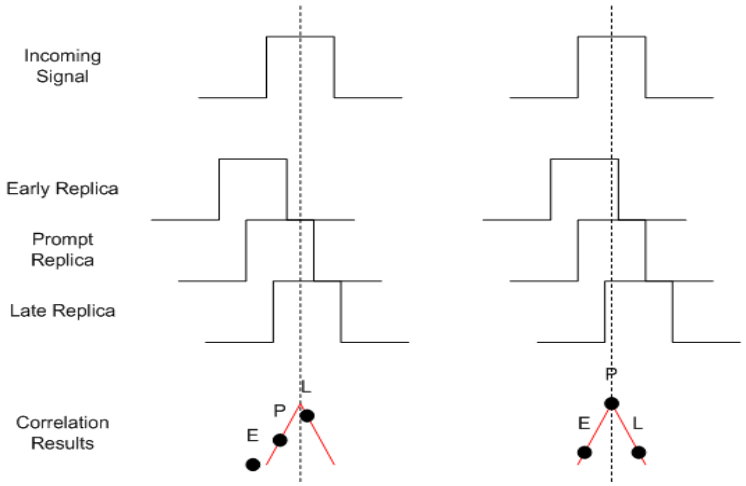

Figure 2-3: On the left, a case where synchronization has not yet been achieved. On the right, a case of complete alignment of the Prompt replica with the incoming signal.

Figure 2-4 shows a block diagram of three correlators for one channel in the baseband. This representation shows how the data at the output of the correlator is computed (both real and imaginary, i.e. using the phase I component and the Q quadrature of the incoming signal, respectively). This output is then used by the tracking loops to compute new estimates:

- Code delay - an additional delay that should be used to adapt local code replicas,
- Doppler frequency - Doppler deviation removal. It is an iterative process.

This is an iterative process that the receiver handles continuously. In the I&D block, we obtain the result of correlation in the time domain, in a coherent or incoherent manner. In parallel, blocking detectors work continuously to distinguish between the useful signal.

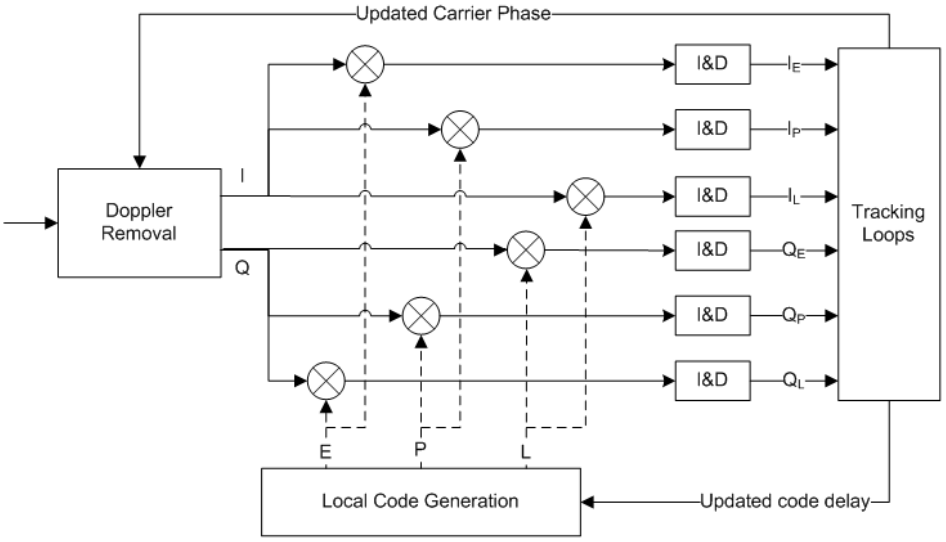

Figure 2-4: Block diagram of a multicorrelator

Without taking noise into account and taking into account the baseband signal, the output of the Prompt correlator can be written as:

$$I_P = AdR_x(\tau_e)\cos(\phi_e) \quad (3)$$

$$Q_P = -AdR_x(\tau_e)\sin(\phi_e) \quad (4)$$

The equations for the Early and Late replicas are expressed as follows:

$$I_E = AdR_x(\tau_e - \delta/2)\cos(\phi_e) \quad (5)$$

$$Q_E = -AdR_x(\tau_e - \delta/2)\sin(\phi_e) \quad (6)$$

$$I_L = AdR_x(\tau_e + \delta/2)\cos(\phi_e) \quad (7)$$

$$Q_L = -AdR_x(\tau_e + \delta/2)\sin(\phi_e) \quad (8)$$

where:

A – signal amplitude

R - signal autocorrelation

d – reference signal

τ_e - is an estimate of the code delay error in the receiver,

ϕ_e - is the estimation of the carrier phase error in the receiver,

E, P and L are indices denoting Early, Promp and Late correlators,

δ – is the distance between the correlation peaks of the Early and Late correlator.

The phase error is understood to mean the following expression: $\phi_e = 2\pi f_e t + \phi_0$, where:

f_e - is the estimated Doppler error in the receiver,

ϕ_0 - is the phase of the incoming signal.

The purpose of GNSS receivers is to synchronize the local replica of the transmitted PRN code with the incoming signal in order to estimate the distance traveled by the incoming signal as accurately as possible. For this purpose, closed-loop tracking loops are used to keep track of the code and the carrier parameters of the incoming signal. These loops are often labeled as code and carrier tracking loops.

In order to extract information from incoming signals, GNSS receivers track them by replicating the PRN code and continuously adjusting the code delay and carrier phase to guarantee synchronization with the incoming signal. In its most common implementation, the receiver implements code and carrier tracking loops to achieve synchronization with the incoming signal, as shown in Figure 2-5.

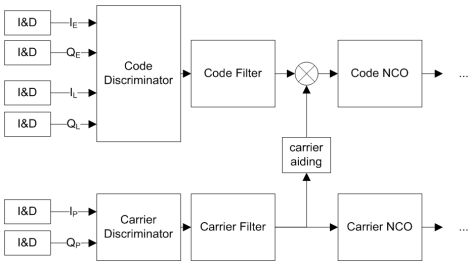

Figure 2-5: Diagram of the tracking loop

The tracking loop includes:

- I&D (Integrate & Dump): blocks that collect the output of correlators and provide their components in phase I and quadrature Q,
- Discriminators: process the output data of the correlators to obtain measurable quantities (e.g. carrier phase information),
- Filters: they filter the signals at the output of the discriminators to reduce noise.
- NCO: The numerically controlled oscillators convert the signals at the filter output into useful Doppler correction factors and code delays, which are returned to the Doppler error removal blocks and the local code generator block, respectively.

While code-tracking loops follow the code delay of the incoming signal using Phase Lock Loops (DLL), carrier-tracking loops can be designed to follow the incoming signal's phase using Phase Lock Loops (PLL), or the Doppler frequency of the incoming signal using Frequency Locked Loops (FLL). Nevertheless, receivers can implement both FLL and PLL: this decision, along with the dimensioning of all components in the tracking loops, is part of a series of trade-offs made in receiver design.

For example, the choice of integration times used in I&D blocks is a compromise between accuracy and resistance to receiver dynamics. On the one hand, the longer the integration time, the less noise is expected at the outputs of the correlators; on the other hand, shorter integration times are more reliable under conditions of dynamic signal change.

Filter loops are used in the receiver for the most accurate synchronization of the incoming signal. The purpose of the filter loop is to filter the signal at the discriminator output to reduce noise. These measurements are fed to the NCO loop and are subtracted from the original input signal to obtain the correction factor. Then this correction is passed back to the first channel blocks of the receiver, namely the Doppler error removal blocks and the local replica generator, to update the current estimates.

The filter loop is constructed by dimensioning the order of the filters and the bandwidth to determine the response to the signal dynamics. The basic design of the filter noise band B_n must take into account the integration time T so that:

$$B_nT << 1 \quad (9)$$

Whenever this condition is not guaranteed, the actual bandwidth is usually greater than desired, leading to filter instability.

The effect of the filter noise bandwidth is shown in Figure 2-6 which shows the filter response to the phase step. On the one hand, it can be seen that lower bandwidths give less noisy

results (because they correspond to longer integration times), and on the other hand, higher bandwidths have faster response times.

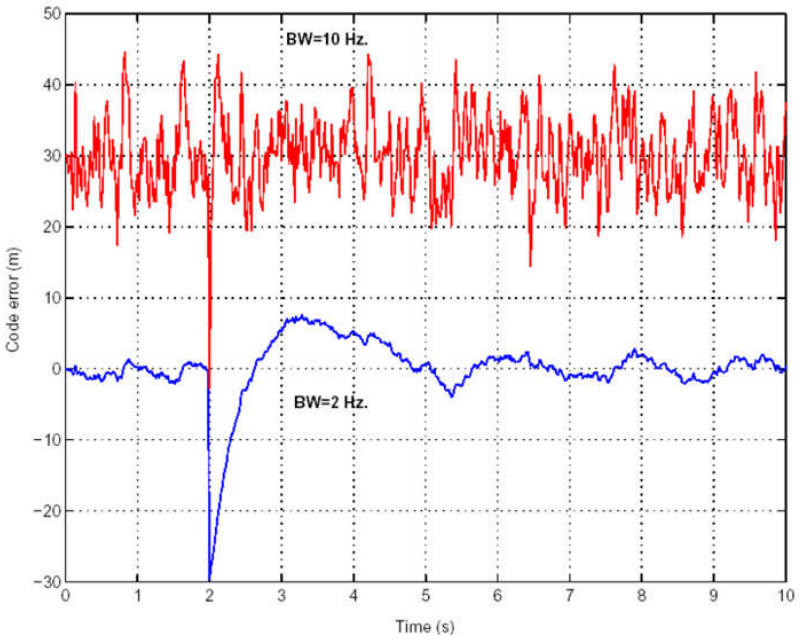

Figure 2-6: Loop response to phase step at time t=2s for different bandwidths

In terms of filter order considerations, the higher the order, the better the filter's ability to track LOS dynamics.

- First order filters are sensitive to changes in speed,
- Second order filters are sensitive to changes in acceleration,
- Third order filters are jerk-sensitive.

As a result, higher-order filters work better under dynamic changes and provide less noisy results (less burdened with noise). The main disadvantage is the additional computational load of the filters, since the order of the filters is directly related to the number of operations. In addition, the order also imposes a filter bandwidth limitation: for example, a third order filter requires a noise bandwidth below 18 Hz to guarantee stability.

Noting that carrier loop jitter is much less noisy than code loop jitter, it is possible to use carrier loop measurements to remove the LOS dynamics of the code loop, with the advantage of being able to lower the order of the code loop filter as well as its bandwidth.

This architecture is often referred to as carrier booster because it allows the PLL tertiary filter to provide information to the DLL's second-order filter, keeping the same level of third-order DLL filter performance as shown in Figure 2-5. To do this, one should apply a scaling factor to the outputs of the carrier filter before including them in the code loop to account for the fact that the Doppler effect of a signal is inversely proportional to its wavelength [2-3]:

$$SF = \frac{Rc}{f_L} \tag{10}$$

where: R_c is the code chip rate for the given signal; f_L is the carrier frequency of the signal.

Another way to remove higher order dynamics from the loop is to use external inertia sensors; this approach can also be used for downstream filters in the trace loops.

The baseband processing block is responsible for processing the down-processed and digitized signal to ensure observability of its parameters: pseudo code ranges and carrier phase measurements, as well as navigation data. It is also possible to obtain a Doppler frequency deviation or a carrier-to-noise ratio. In most GNSS receiver architectures, baseband processing relies on independent channels that track each satellite signal independently. Thereafter, the information from each channel is integrated to obtain a navigation solution.

The baseband processing block is typically replicated over several channels. Each channel processes a given signal from a given satellite to ensure GNSS observability and navigation data. A general diagram of a single channel in a baseband processing block is shown in Figure 2-7.

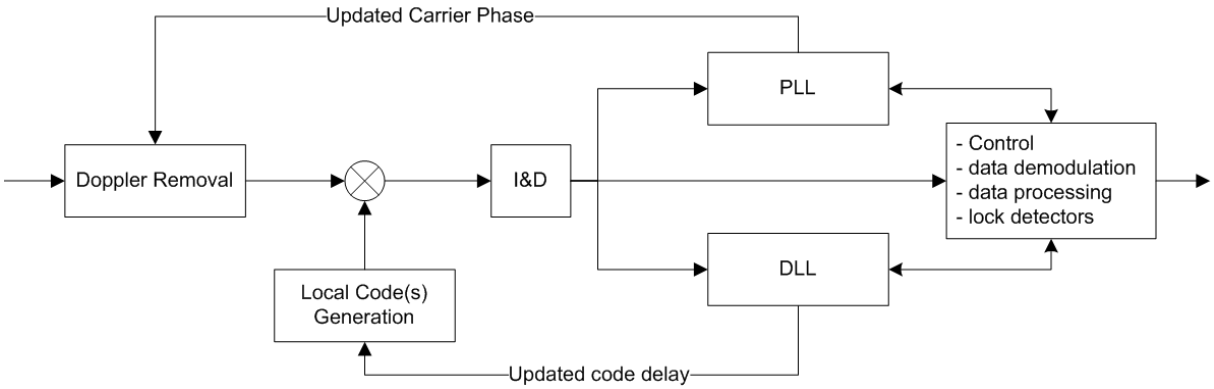

Figure 2-7: Baseband signal processing

The incoming signal is first removed from the Doppler frequency (according to the current estimate) and then correlated with one (or more) locally generated replicas of the PRN code (according to the current code delay estimate). New estimates of the Doppler frequency deviation and the code delay are based on evaluation of the correlation results. Note that in the case of GNSS using FDMA modulation schemes such as GLONASS, the Doppler deviation removal block represents a frequency offset not only corresponding to the estimated Doppler shift due to relative motion between the satellite and the user, but also the center frequency of the available satellite signal.

This process is implemented in an iterative manner, typically using a PLL and DLL trace loop to observe the phase and code delay of the incoming signal, respectively. In parallel, the receiver extracts the navigation data of the incoming signal and provides monitoring and control functions.

The basic principle of GNSS baseband processing is based on the correlation process. The basic idea is that GNSS signals carry different codes that are structured as follows:

- When the code is correlated with an aligned replica of itself, the correlation result is maximal: high autocorrelation properties,
- When the code is correlated with a ragged replica of itself, the correlation score is low,

- When code is correlated with another code in the same family, the correlation score is low: low cross-correlation properties.

The basic principle is shown in Figure 2-8. The receiver first assigns a PRN code to each channel: for CDMA-based GNSS each satellite transmits a dedicated PRN code, while for FDMA-based GNSS (such as GLONASS), the PRN code is the same for all satellites.

At the channel level, the incoming signal is correlated with the local time domain replica of this PRN code. This local replica is generated in such a way that its code delay and phase characteristics differ, representing a two dimensional code and frequency (Doppler) search. Whenever the parameters of the local replica (code and frequency) match those of the incoming signal, the correlation output will reach its maximum and the receiver will take this pair (code and frequency) as a current estimate of these parameters.

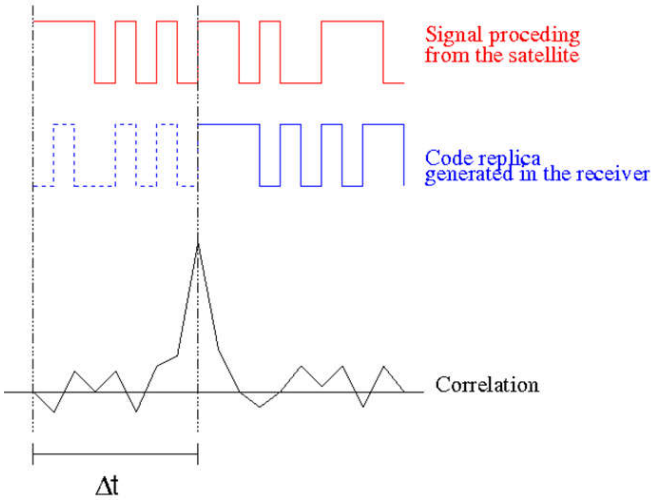

Figure 2-8: Correlation process

Real systems are based on noise signals and highly variable dynamics: as a result, the peak of the autocorrelation seems to change at any moment. This fact justifies the need to track the loop (data accumulators and filters) in order to 'track' the incoming signal continuously, since a 1 ms code delay error would lead to an error of about 300 km in the measurement.

The signal pattern at the baseband RF output (excluding noise) is shown below:

$$s_{BB}(t_k)=\{s(t_k)\exp[j\phi(t_k)]\} \quad (11)$$

where: $s(t_k)=A_I m_I(t_k)d(t_k)-jA_Q m_Q(t_k)d(t_k)$

- A is the signal amplitude,
- $m(t_k)$ – contains PRN code and modulation information,
- $d(t_k)$ - navigation data,
- I and Q - components in phase and quadrature,
- $\phi(t_k)$ takes into account phase information, including Doppler frequency, receiver clock instability, and the initial phase of the signal.

The block with Doppler deviation removal rotates the complex signal in the baseband by the current estimate of the carrier phase:

$$s_{out}(t_k)=s(t_k)\exp[j\phi_e(t_k)]\} \quad (12)$$

where:

- the phase error is determined by $\phi_e(t_k) = \phi'(t_k) - \phi(t_k)$
- $\phi'(t_k)$ phase estimated in the receiver
- $\phi(t_k)$ phase of the incoming signal.

The correlation between the incoming signal and the local code replica corresponds to blocks of correlators and accumulators and can be written as:

$$Corr_{out}(\tau') = \sum_T s^*_{out}(t_k) m(t_k - \tau') \quad (13)$$

where:

- T is the integration time (accumulation interval),
- τ' is estimated code delay at the receiver.

For example, the correlation output for a receiver tracking GPS L1 C/A code would be as follows:

$$Corr_{out}(\tau') = \sum_T (A_I d(t_k) c_I(t_k) + jA_Q d(t_k) c_Q(t_k)) \exp[-j\phi_e(t_k)] c_I(t_k - \tau') \quad (14)$$

where:

- c_I would be the C/A code,
- c_Q would be code P,
- $c_I(t_k - \tau')$ is a local replica generated in the receiver.

Given that the correlation between the C/A code and the P code can be omitted, the expression can be simplified:

$$Corr_{out}(\tau') = \sum_T A_I d(t_k) c_I(t_k) \exp[-j\phi_e(t_k)] c_I(t_k - \tau') \quad (15)$$

Hence, the output data of correlation and accumulation blocks can be written in the I and Q components:

$$I_P = A_I d_I R_{cI}(\tau_e) \cos(\phi_e) \quad (16)$$

$$Q_P = -A_I d_I R_{cI}(\tau_e) \sin(\phi_e) \quad (17)$$

The output from the correlation is then fed to the tracking loops.

In the above considerations it was assumed that the current estimation of the parameter pair (code delay and Doppler frequency) was possible and thus the receiver could generate a local replica of the PRN code using the estimated parameters. However, when a channel is set up for the first time, these estimates are not available, therefore the channel will start 'cold' searching for the signal. The channel is said to be in acquisition mode when searching for signals, and after finding a signal, it enters the tracking mode.

In acquisition mode, each channel searches for all possible pairs (code delay, Doppler frequency), generating a set of possible local replicas and correlating each of them with the incoming signal. The correlator output power is, as it were, a measure of how good (or how close to the real signal) the code delay and carrier phase estimates are. Nevertheless, the correlation results described so far are based on the assumption that the signals are not subject to interference: in fact, the signal is so noisy that the decision process of a single correlation result has a very low probability of detecting the presence of a signal [2-4].

The presence of a signal is assessed by the following decision statistics:

$$z = \sum_{k=1}^{M} |Y(k)|^2 \quad (18)$$

where:

- M is the number of the non-coherent integration interval,
- Y is the output of the correlation of the incoming signal with the local replica at the time T of coherent integration,
- K refers to the k-th coherent integration interval.

After the 'z' statistic has been computed, the statistic is then compared to the detection threshold to judge whether or not a useful signal is present. This detection threshold is defined according to the target false alarm probability.

In this process, the correlation results are actually integrated in time before prior processing: the results are collected in the I&D block. Two types of integration can be considered:

- Coherent integration: This technique uses longer integration times (multiples of the code length) before dropping the correlation output. Although this technique reduces noise, its performance is limited by the number of bits that carry the navigation message: in fact, if the integration time is such that it exceeds the number of bits, the correlation result will surely lose all power.
- Incoherent integration: This technique involves summing the results of a single correlation before entering a decision process block.

Due to possible losses, the first technique is more effective than the second, despite this limit set by the number of beacons. As an example, Figure 2-9 shows the correlation results for all possible code delays at one Doppler frequency. In this case, one coherent and incoherent integration was considered.

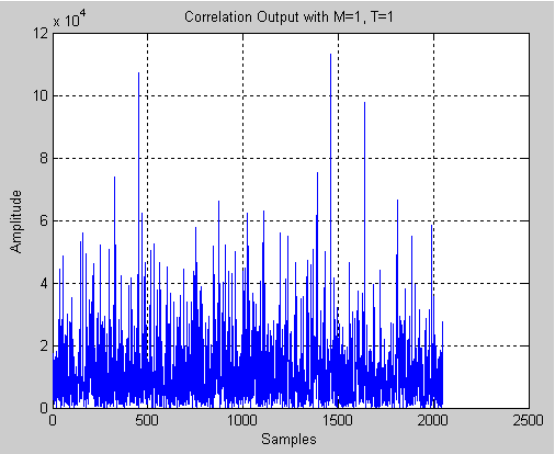

Figure 2-9: Correlation result [2-1]

Due to the noisy GNSS signals, it is clear that the correlation peak is not visible for the result of this correlation. To be able to illustrate this further, Figure 2-10 shows the correlation results for the same signal with different coherent (T) and non-coherent (M) integration times. The increase in power becomes marked with the increase of M and T, hence the peak of the correlation is clearly visible.

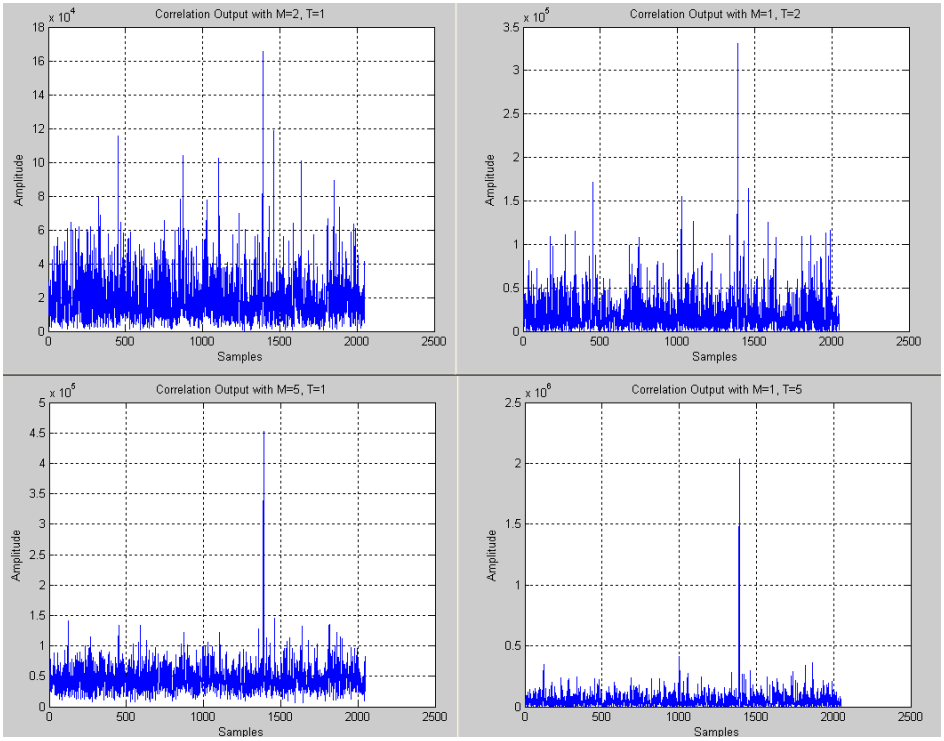

Figure 2-10: Example of a correlation result for different code delays using different integration times [2-1]

On the one hand, the example shown in Figure 2-10 shows how coherent integration produces greater gains (higher power and lower noise levels) than non-coherent integration, which have to deal with the losses due to squaring the output of the correlation function. On the other hand, incoherent integration is safer to travel - done before bit synchronization and the bit limit boundaries in the message structure do not have to be considered.

Finally, the sizing of these techniques must take into account important factors:

- Expected noise conditions,
- The probability of a false alarm,
- Probability of signal detection,
- Acquisition time.

In fact, the longer the integration intervals, the greater the probability of detection (less false alarm probability), but the slower the potential acquisition time is as the receiver will take longer to search in each search interval defined by the pair - code delays and Doppler frequency deviations.

The concepts of coherent and incoherent integration are also applied when the receiver is in tracking mode to reduce the noise level and increase accuracy. The advantage is that after bit synchronization, the receiver can extend the integration time up to bit duration. Long integration times are also used to track weak signals under severe conditions (e.g. indoors), but are limited by both the data bit and the estimated accuracy of the clock/Doppler frequency.

2.1.2 Simulation studies

In order to check the accuracy of the determined correlation, two signals were generated (Fig. 2-11). the first is a sine - 100 samples per period at given moments of time 0 ns, 10 ns, 20 ns, 30 ns...

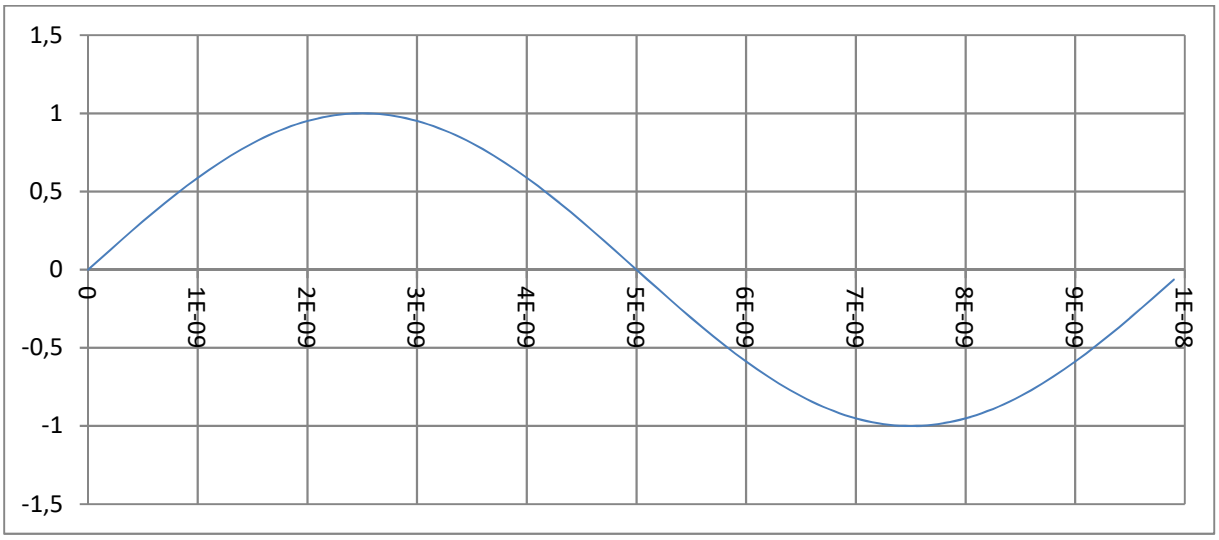

Figure 2-11: Sinus test signal generated

The second signal is delayed in relation to the first by 3 ns (Fig. 2-12), that is at moments 3 ns,13 ns, 23 ns, 33 ns.... Additionally, a delay was introduced by another 15 samples, which gives the total delay time of the second signal by 153 ns.

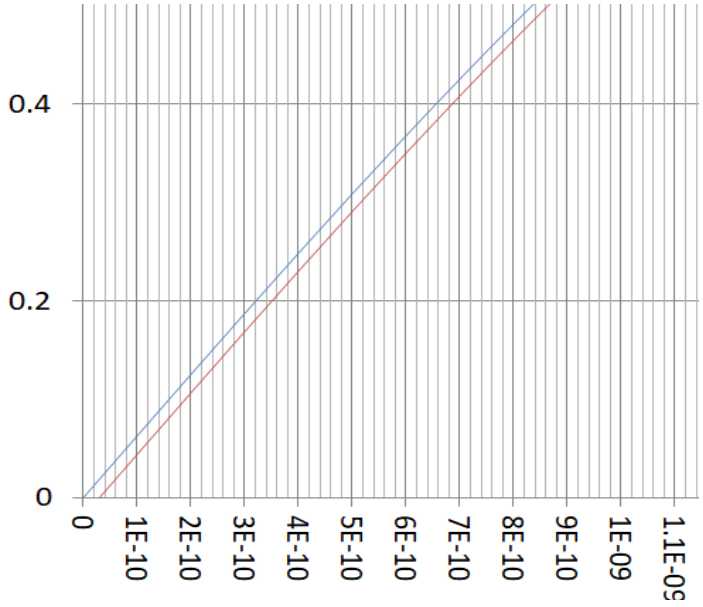

Figure 2-12: The second delay of the test signal

Then, the correlation of these two signals was performed, which resulted in a clear correlation peak (Fig. 2-13).

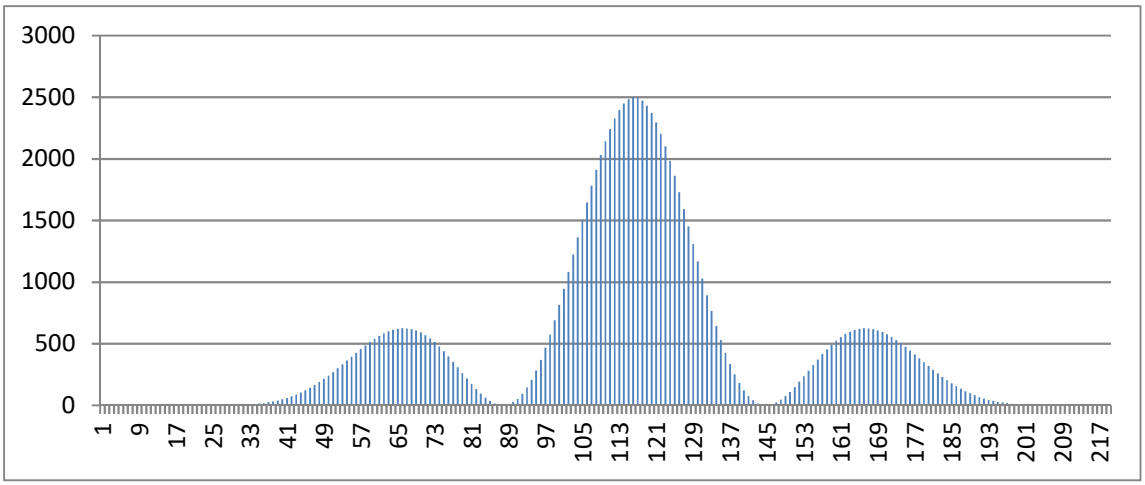

Figure 2-13: The correlation of these two signals

The correlation peak for two cases is shown below (Fig 2-14). The first is the case where the Rx signal is delayed from the Tx signal by 150 ns (by 15 samples). The second case is a delay of the Rx signal by 3 ns and an additional 150 ns in the channel.

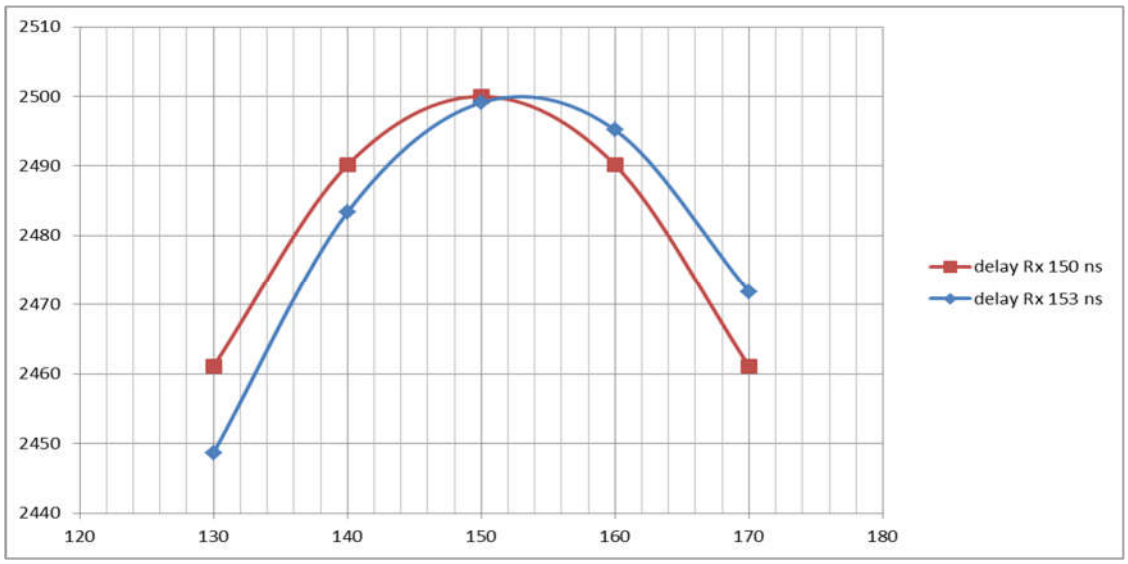

Figure 2-14: The correlation peak for two cases

Now, in order to determine the shift of the two correlation vertices, we need to estimate the position of the apex of this correlation (Fig 2-15, Fig 2-16). This can be determined from the following formulas (19-21).

$$p = \frac{1}{2}\frac{\alpha-\gamma}{\alpha-2\beta+\gamma} = 3 \text{ ns} \quad (19)$$

$$k^* \triangleq k_\beta + p = 153 \text{ ns} \quad (20)$$

$$y(p) = \beta - \frac{1}{4}(\alpha-\gamma)p = 2500 \quad (21)$$

p - exact offset from the sample with the maximum value,

α,β, γ - values of three consecutive bands of the correlation function

k_β - the value of the delay of the band of the correlation function with the highest value

It is based on calculations from the three peaks with the highest value. Thanks to this, we have the distance of the top from the sample with the highest value.

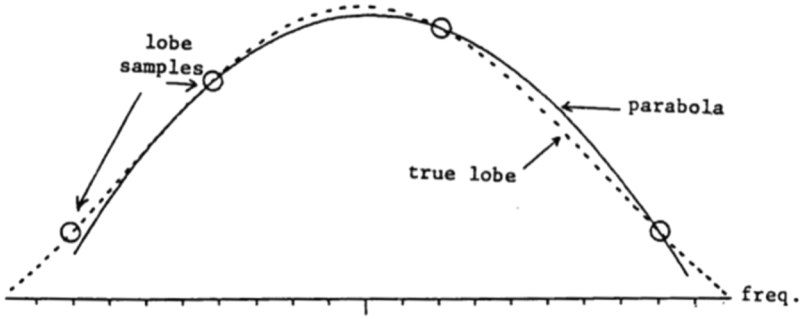

Figure 2-15: Illustrative determination of the correlation peak

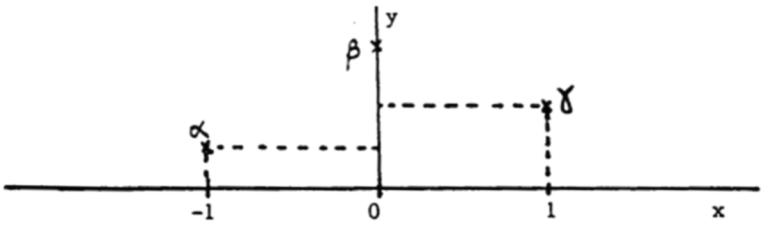

Figure 2-16: Illustrative determination of the correlation peak - markings

Now, we find the location (shift) of the correlation file vertex with respect to the sample with the greatest value (Fig. 2-17):

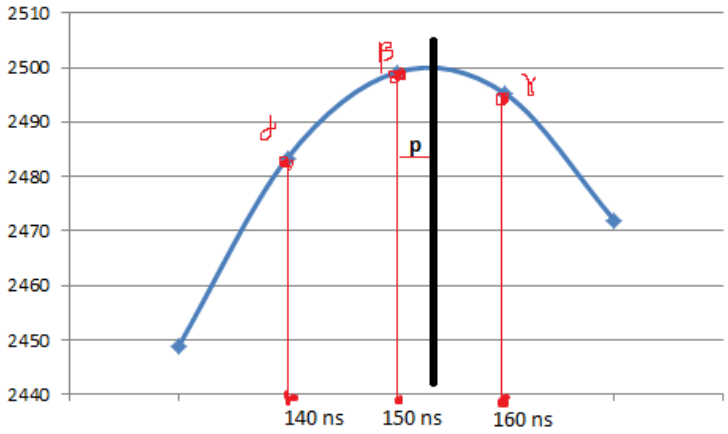

Figure 2-17: Find the location (shift) of the correlation

In order to verify the correctness of the multicorrelator operation, several simulation tests were performed.

In the first scenario (Fig. 2-18), the ideal case was tested when the signals lag behind each other by a full number of samples. In this situation, the sample with the correlation peak has

the greatest power, and the earlier and later samples have comparable powers, and the same delays with respect to one another.

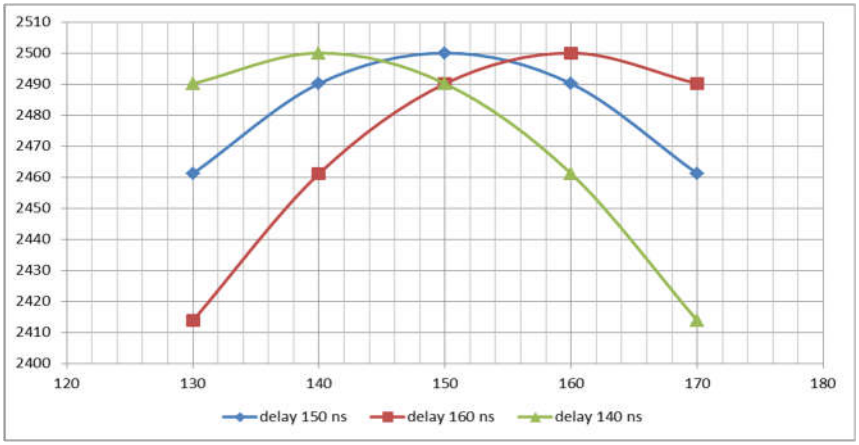

Figure 2-18: Ideal situation when the signals are delayed with respect to each other by the full number of samples

The table 2-1 shows a list of all power values for a given sample depending on the delay value:

Table 2-1: Scenario 1 - list of all power values

delay	Strenght 1	Strenght 2	Strenght 3
110	2413.77	2349.19	2268.71
120	2461.12	2413.77	2349.19
130	**2490.14**	2461.12	2413.77
140	**2500**	**2490.14**	2461.12
150	**2490.14**	**2500**	**2490.14**
160	2461.12	**2490.14**	**2500**
170	2413.77	2461.12	**2490.14**

The table 2-2 shows the exact calculated peak correlation delays for each of the signals:

Table 2-2: Calculated peak correlation delays for each of the signals

Calculated correlation	Correlation 1	Correlation 2	Correlation 3
$k^* \triangleq k_\beta + p,$ $where$ $p = \frac{1}{2}\frac{\alpha - \gamma}{\alpha - 2\beta + \gamma}$	**140 ns**	**150 ns**	**160 ns**

In the second case, we shift by a fragment of the sampling period, and exactly by half the samples (Fig. 2-19). For comparison, the results for three correlations are included. Signals shifted relative to each other by 145, 150 and 155 ns. In each case, the vertex of the correlation was correctly calculated.

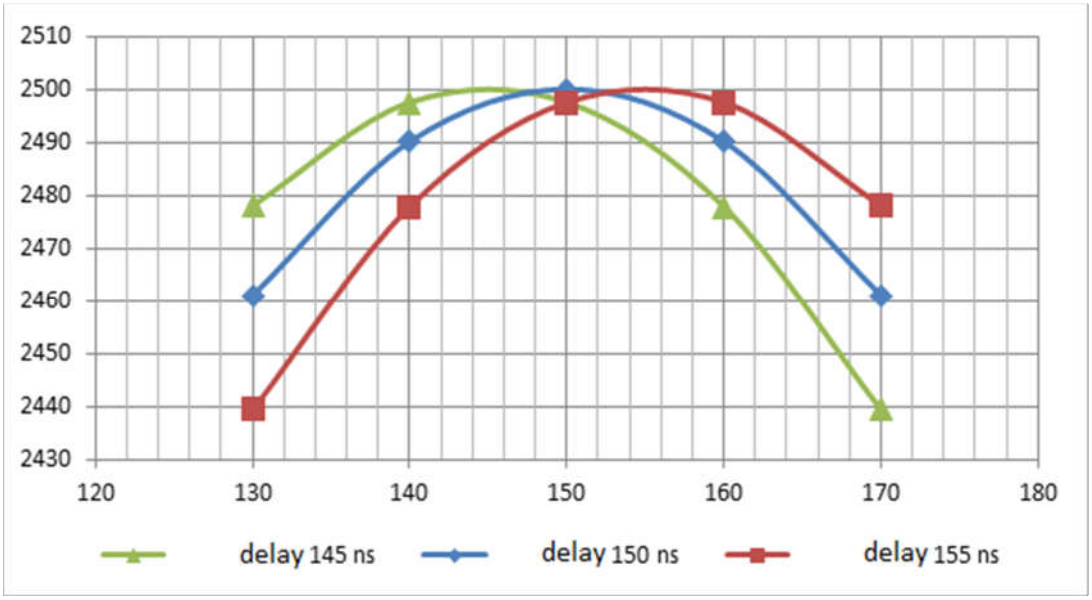

Figure 2-19: Half sample advance

The table 2-3 shows a list of all power values for a given sample depending on the delay value:

Table 2-3: Scenario 2 - list of all power values

delay	Strenght 1	Strenght 2	Strenght 3
110	2383.72	2349.19	2310.3
120	2439.79	2413.77	2383.14
130	**2478.06**	2461.12	2439.4
140	**2497.53**	**2490.14**	2477.86
150	**2497.53**	**2500**	**2497.53**
160	2477.86	**2490.14**	**2497.53**
170	2439.4	2461.12	**2478.06**
180	2383.14	2413.77	2439.79

The table 2-4 shows the exact calculated peak correlation delays for each of the signals:

Table 2-4: Calculated peak correlation delays for each of the signals

Calculated correlation	Correlation 1	Correlation 2	Correlation 3
$k^* \triangleq k_\beta + p,$ $gdzie$ $p = \frac{1}{2}\frac{\alpha - \gamma}{\alpha - 2\beta + \gamma}$	145 ns	150 ns	155 ns

In the last case, we have a shift by any part of the sampling period fragment by: (a) 3 ns and (b) 0.3 ns (Fig 2-20). For this case, the offset has also been calculated correctly.

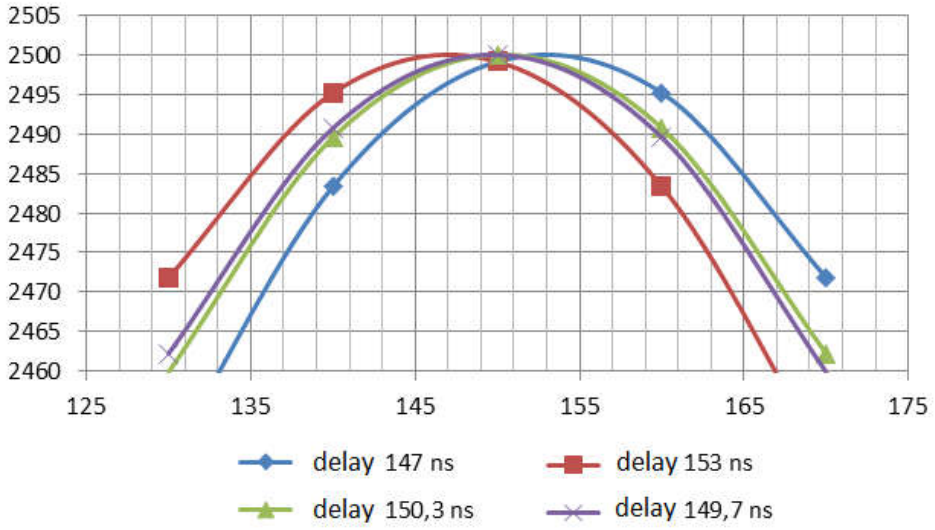

Figure 2-20: Shift by any fraction of the sampling period

The table 2-5 shows a list of all power values for a given sample depending on the delay value:

Table 2-5: Scenario 3 - list of all power values

delay	Strenght 1	Strenght 2	Strenght 3	Strenght 4
130	2448.66	2471.86	2459.95	2462.27
140	**2483.36**	**2495.17**	**2489.54**	**2490.73**
150	**2499.11**	**2499.11**	**2499.99**	**2499.99**
160	**2495.17**	**2483.36**	**2490.73**	**2489.54**
170	2471.86	2448.66	2462.27	2459.95

The table 2-6 shows the exact calculated peak correlation delays for each of the signals:

Table 2-6: Calculated peak correlation delays for each of the signals

Calculated correlation	Correlation 1	Correlation 2	Correlation 3	Correlation 4
$k^* \triangleq k_\beta + p$, $gdzie$ $p = \frac{1}{2}\frac{\alpha-\gamma}{\alpha-2\beta+\gamma}$	**153 ns**	**147 ns**	**150,3 ns**	**149,7 ns**

The accuracy of determining the correlation depending on the sampling frequency was also checked. The formula used to calculate the exact shift of the correlation peak is based on calculations normalized to 1 (eq. 22), so that the obtained result is enough to be multiplied by the sampling period.

$$p' = \frac{1}{2}\frac{\alpha-\gamma}{\alpha-2\beta+\gamma} * 1/F_s \quad (22)$$

Below is an example (Tab. 2-7) for signals delayed by 157.5 ns from each other with a sampling period of 25 ns.

Table 2-7: Signals delayed by 157.5 ns from each other with a sampling period of 25 ns

symbol	delay	sample power
α	120	2478.06
β	145	2497.53
γ	170	2497.53

$$p = \frac{1}{2}\frac{\alpha-\gamma}{\alpha-2\beta+\gamma} = 0.5 \quad (23)$$

$$p' = p * \frac{1}{F_s} = 0.5 * 25ns = 12{,}5\ ns \quad (24)$$

Signal delay= 145 +12.5=157.5 ns

2.1.3 Tests based on the real R-mode signal

In the next case, tests were carried out on the π/4-QPSK signal generated using the modulator (Fig. 2-21) and constellation scheme (Fig. 2-22) below. The result was a modulated signal. For testing purposes, a second signal was generated, shifted in relation to the first signal by half samples. This study was aimed at checking the effectiveness of the **basic correlator**, i.e. a correlator based only on the maximum value of the peak of the correlation function and the extended **correlator** - based on adjacent samples around the peak with the maximum value.

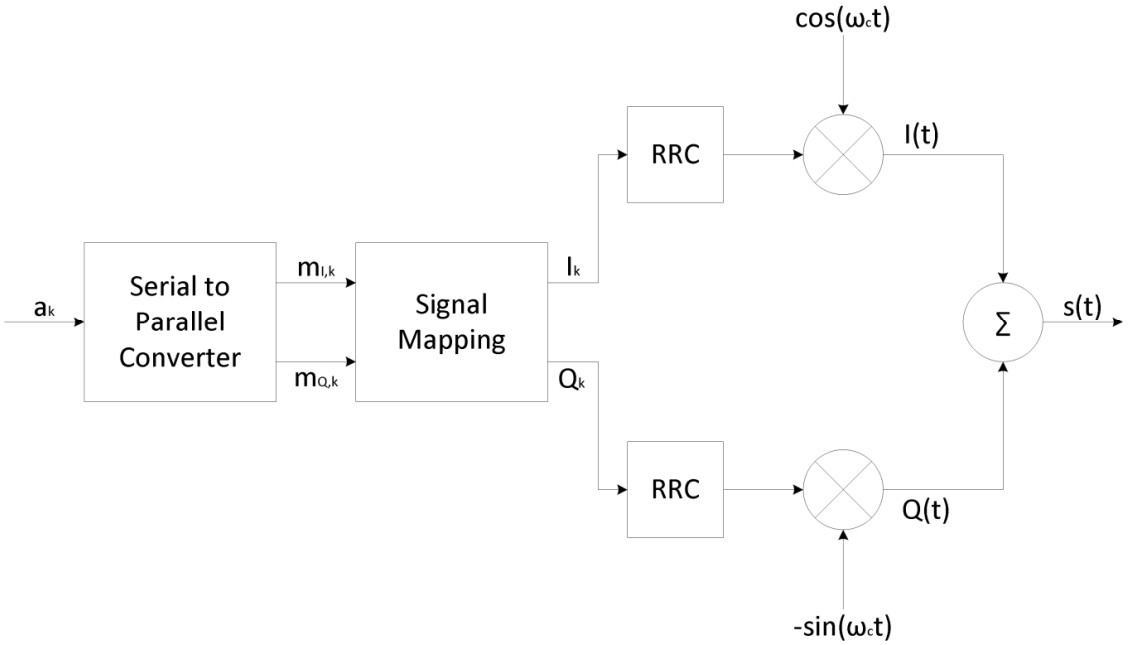

Figure 2-21: Transmitter for generating a signal for testing

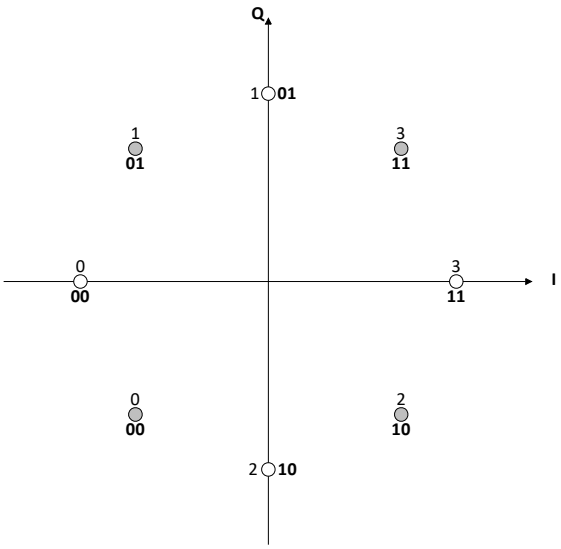

Figure 2-22: Constellation for π/4-QPSK modulation

The generated signal is shown below (Fig. 2-23):

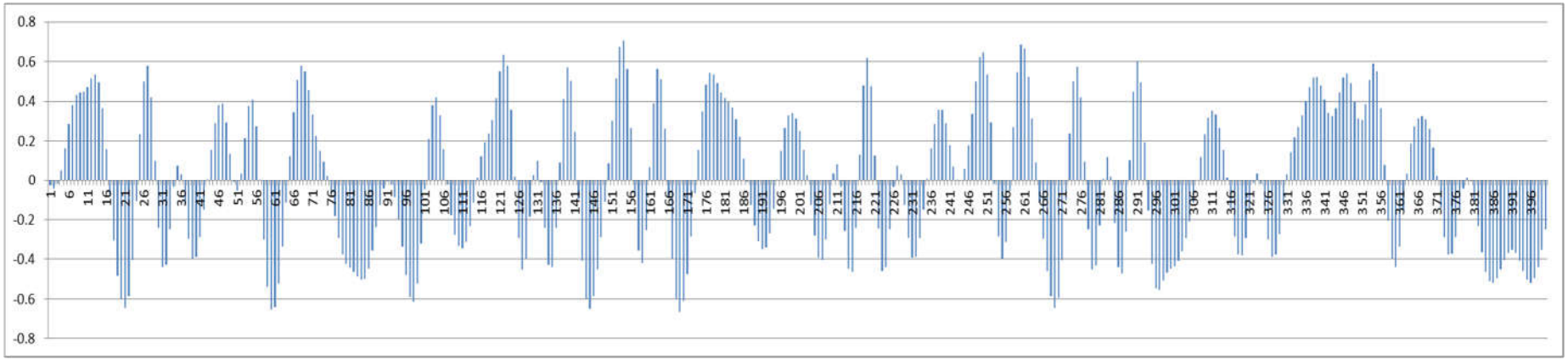

Figure 2-23: Generated signal π/4-QPSK

A second signal shifted from the first signal by half the sample was also generated (Fig. 2-24):

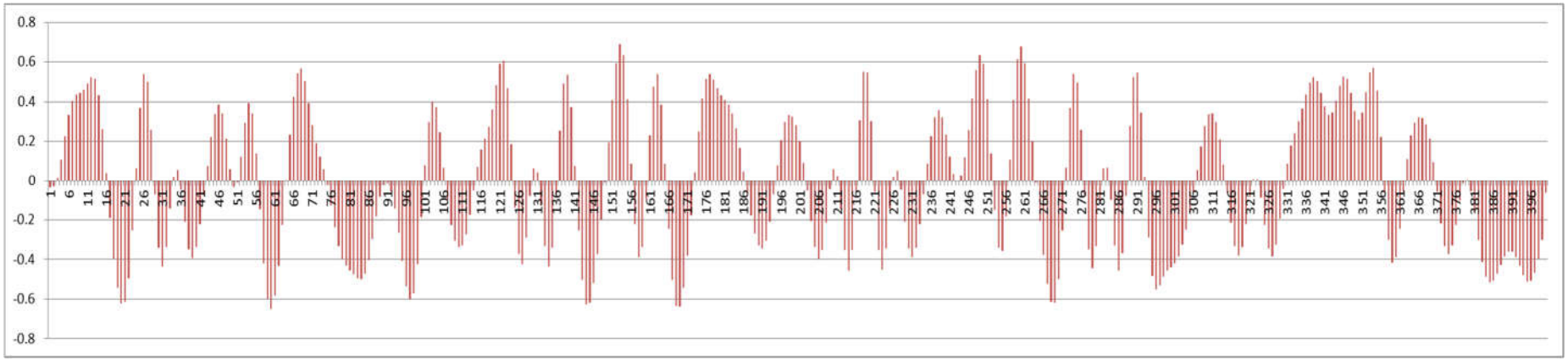

Figure 2-24: Generated signal π/4-QPSK shifted by half the sample

The superimposed signals are presented below in 3D form so that we can see the minimum delay introduced between them (Fig. 2-25):

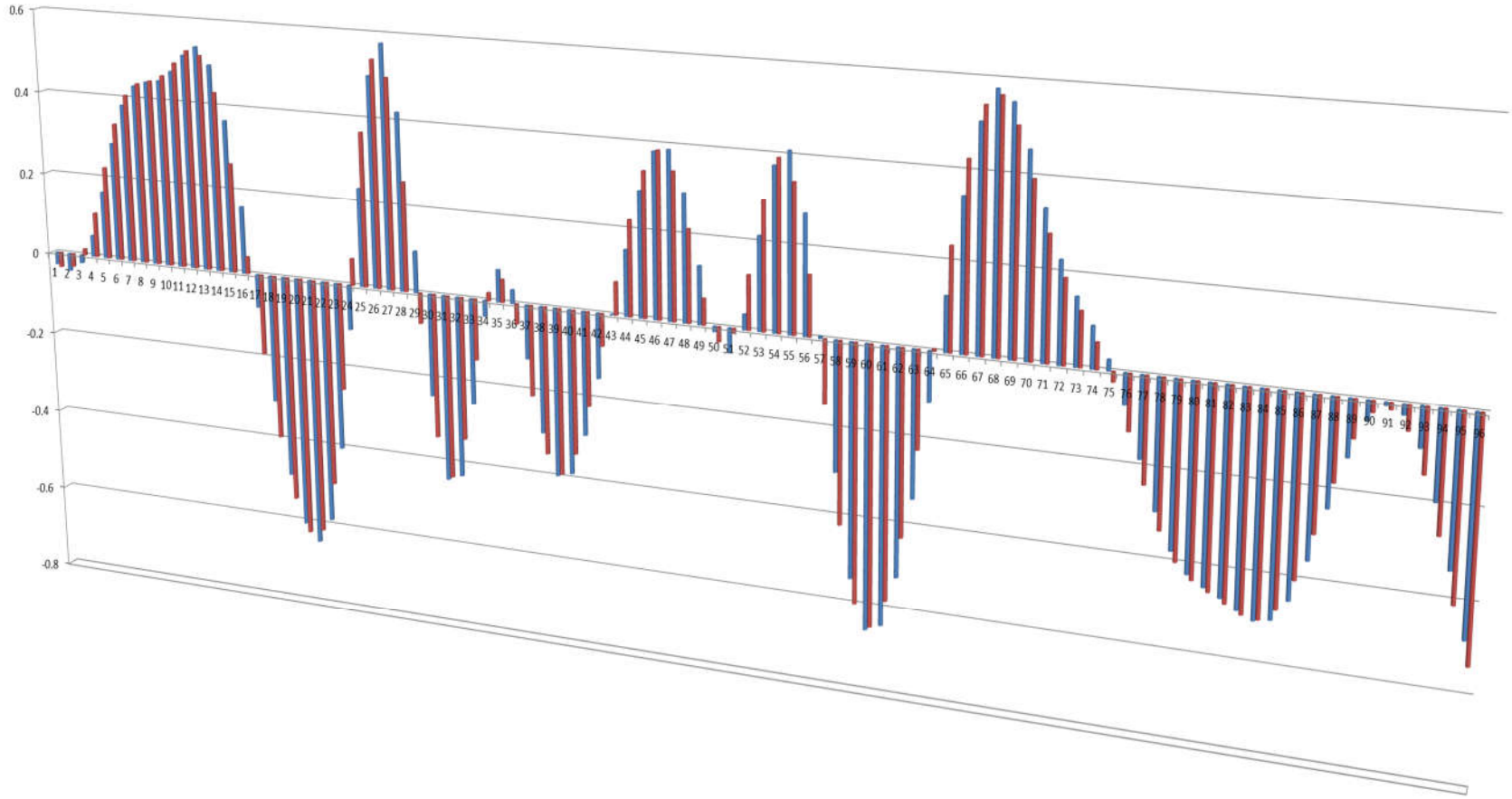

Figure 2-25: Overlapping signals in the 3D form

Correlation results for the basic and extended correlator (Fig. 2-26):

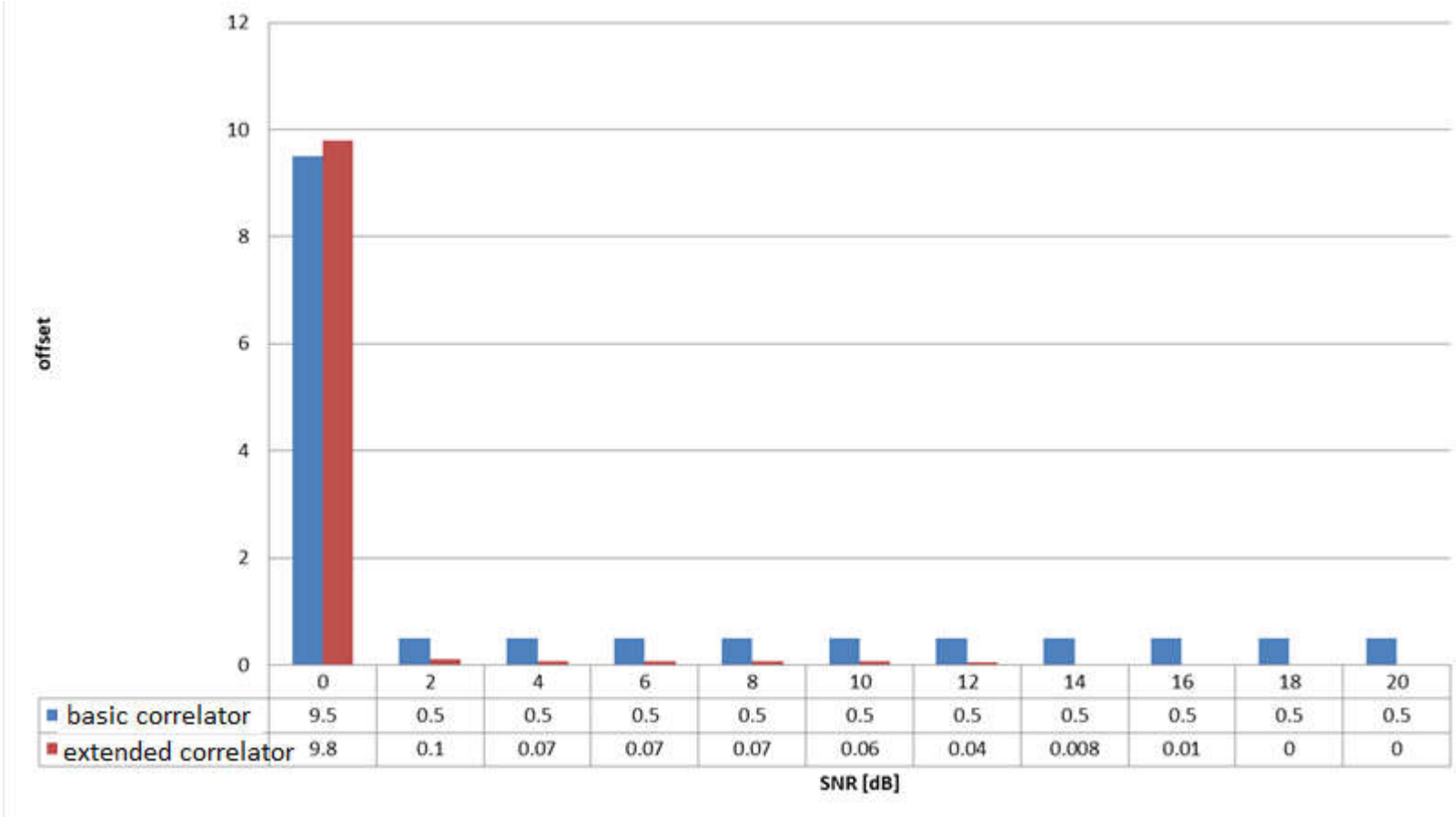

	0	2	4	6	8	10	12	14	16	18	20
basic correlator	9.5	0.5	0.5	0.5	0.5	0.5	0.5	0.5	0.5	0.5	0.5
extended correlator	9.8	0.1	0.07	0.07	0.07	0.06	0.04	0.008	0.01	0	0

Figure 2-26: Correlation results for the basic and extended correlator

2.2 Analysis of the ranging accuracy in relation to the SNR for various measurement scenarios and for different spacing of the samples in the multi-correlator

To test the double delta correlator, a π / 4 - QPSK signal was generated (100 symbols, 16 samples / symbol) (Fig. 2-27):

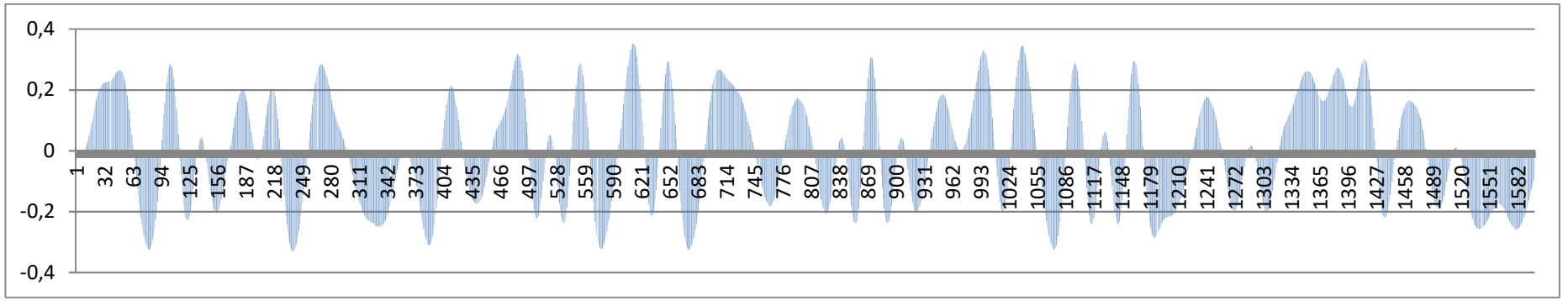

Figure 2-27: π / 4 - QPSK signal (100 symbols, 16 samples / symbol)

A second signal shifted from the first signal by half of the sample was also generated (Fig. 2-28):

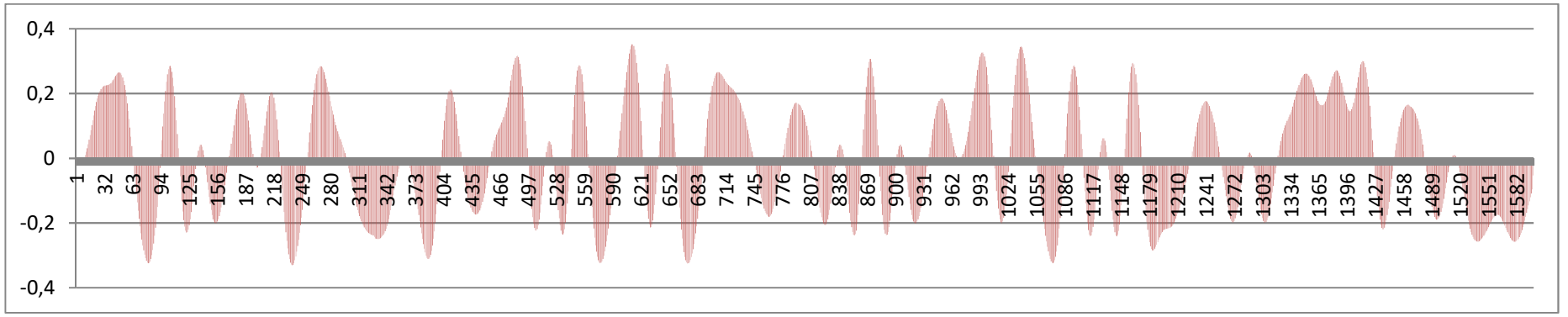

Figure 2-28: π / 4 - QPSK signal (100 symbols, 16 samples / symbol) shifted by half of the sample

For a better visualization, the signals have been superimposed to make the shift visible (Fig. 2-29):

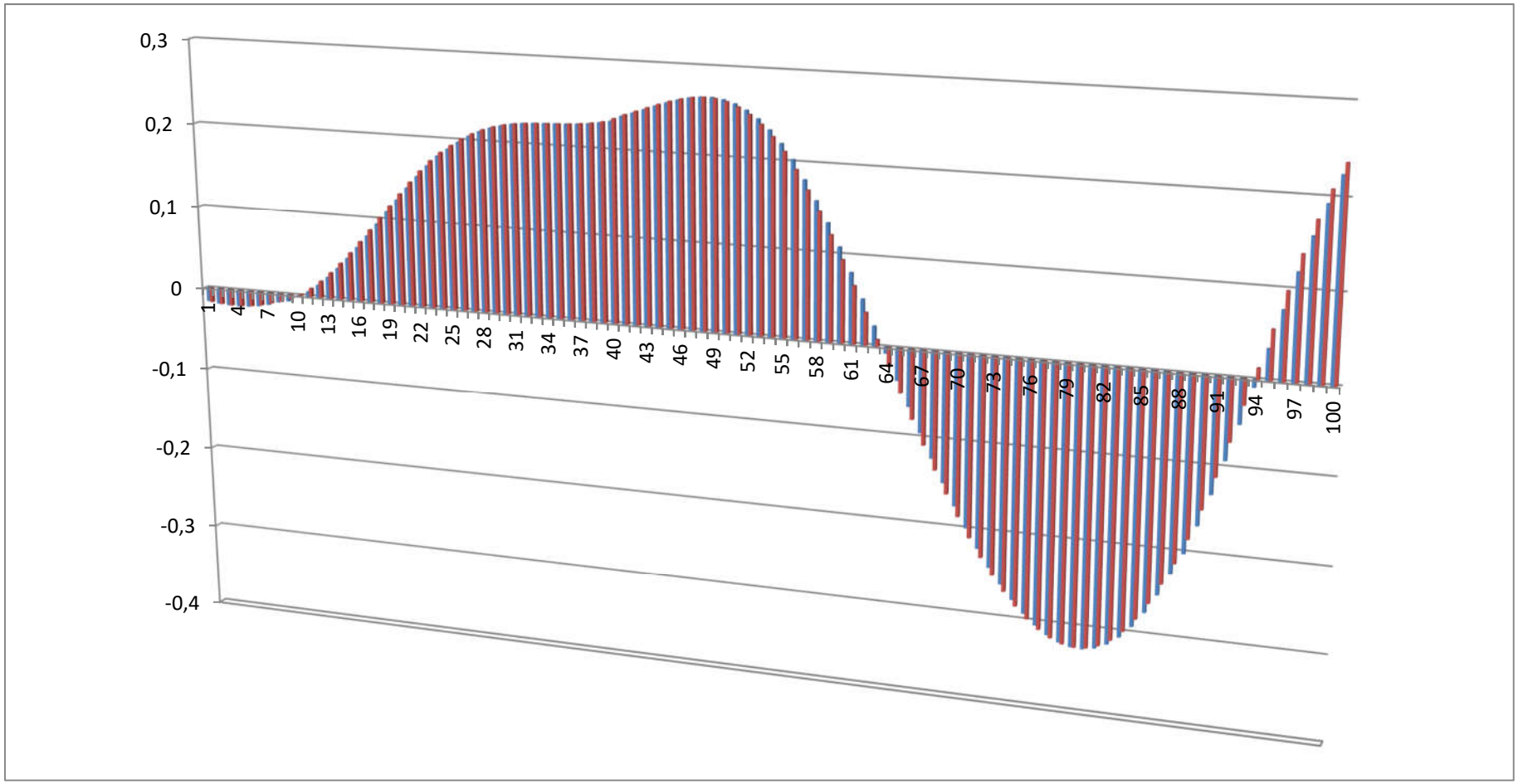

Figure 2-29: Overlapping signals in the form of 3D

In fig. 2-30, the correlation power plot is shown:

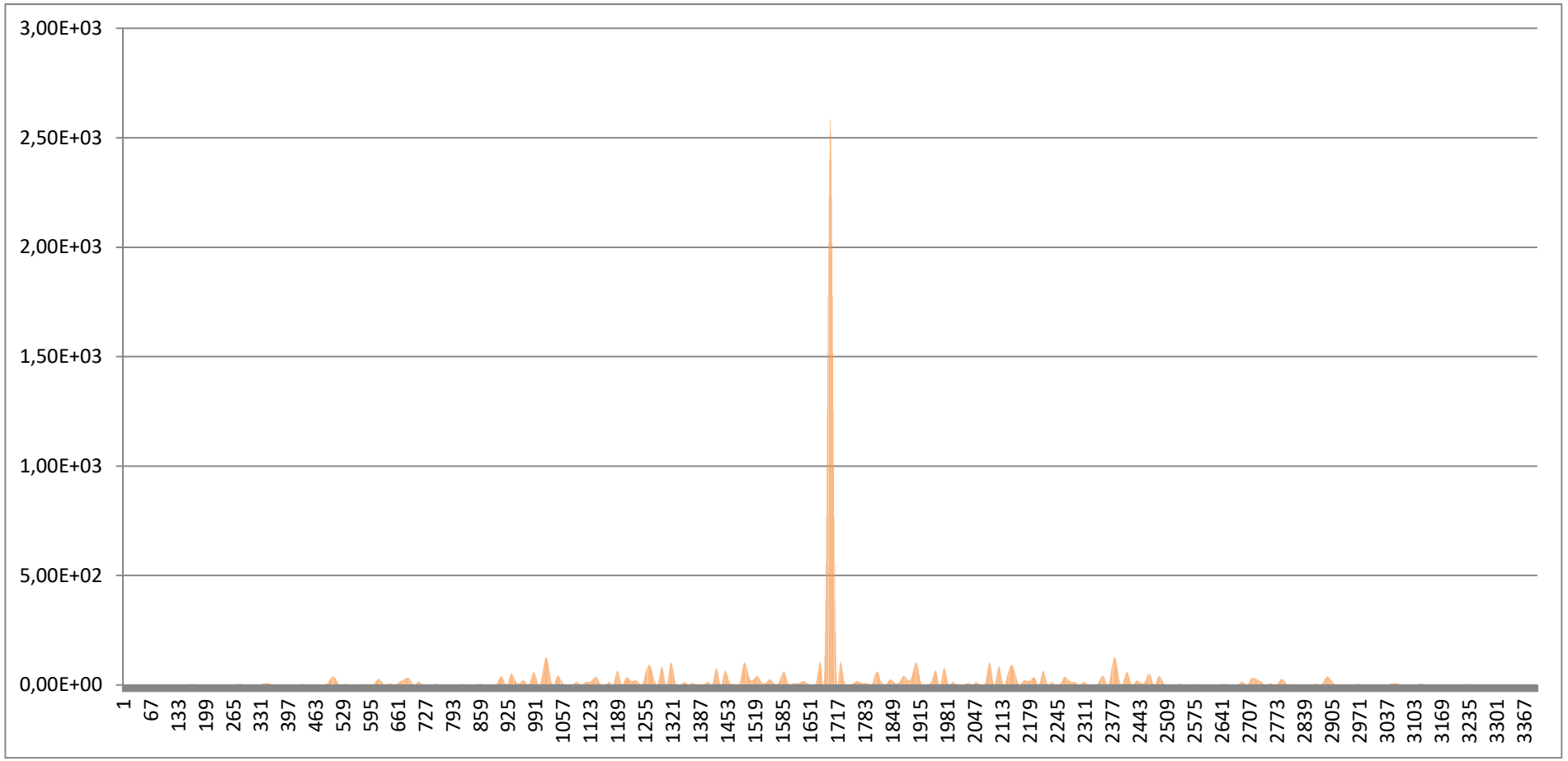

Figure 2-30: The correlation power plot

Let us consider two correlation scenarios (Fig. 2-31, Fig. 2-32) to test the effectiveness of determining the exact shift:

Scenario 1

$d_1 = 2 * T_s$

$d_2 = 4 * T_s$

Scenario 2

$d_1 = 2 * T_s$

$d_2 = 8 * T_s$

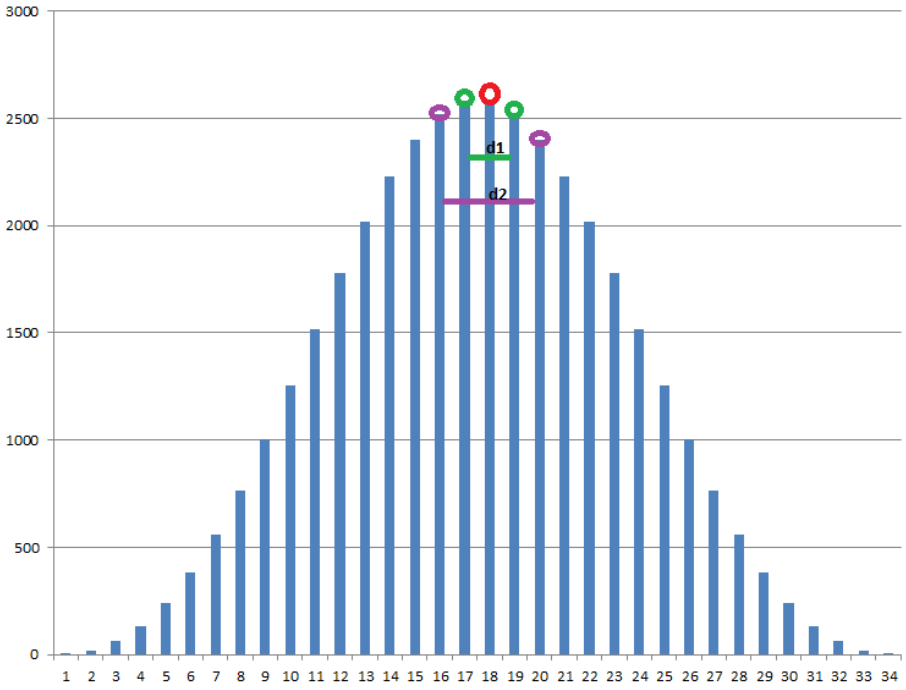

Figure 2-31: Scenario with a smaller spacing of the second pair of samples

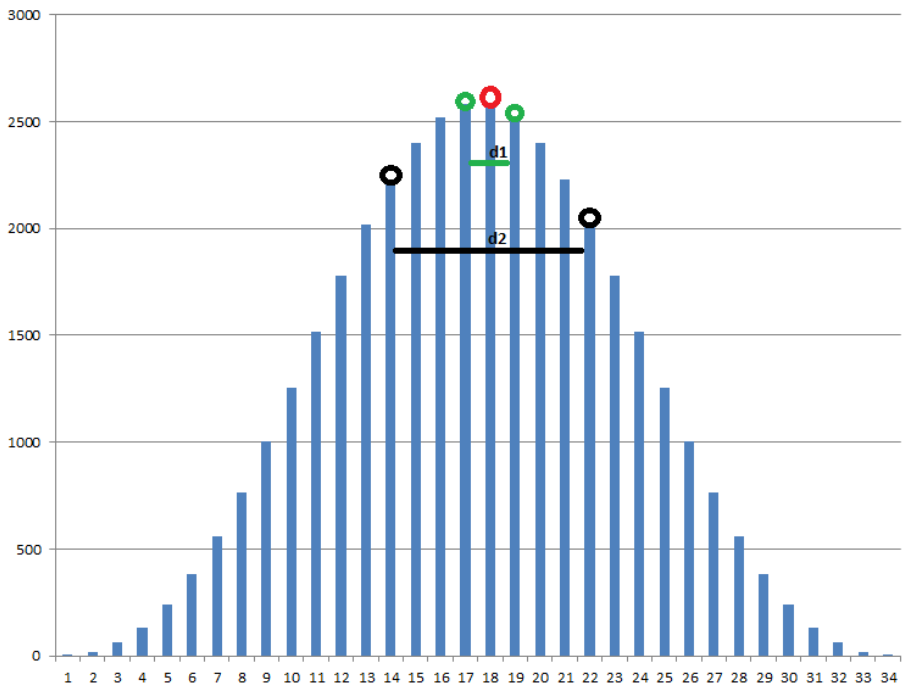

Figure 2-32: Scenario with a larger spacing of the second pair of samples

The efficiencies obtained for various correlator configurations are presented below (Fig. 2-33). It can be seen how the double delta correlator reduces the error in determining the offset of the samples. Compared to the basic correlator, this error is smaller by as much as half the sample.

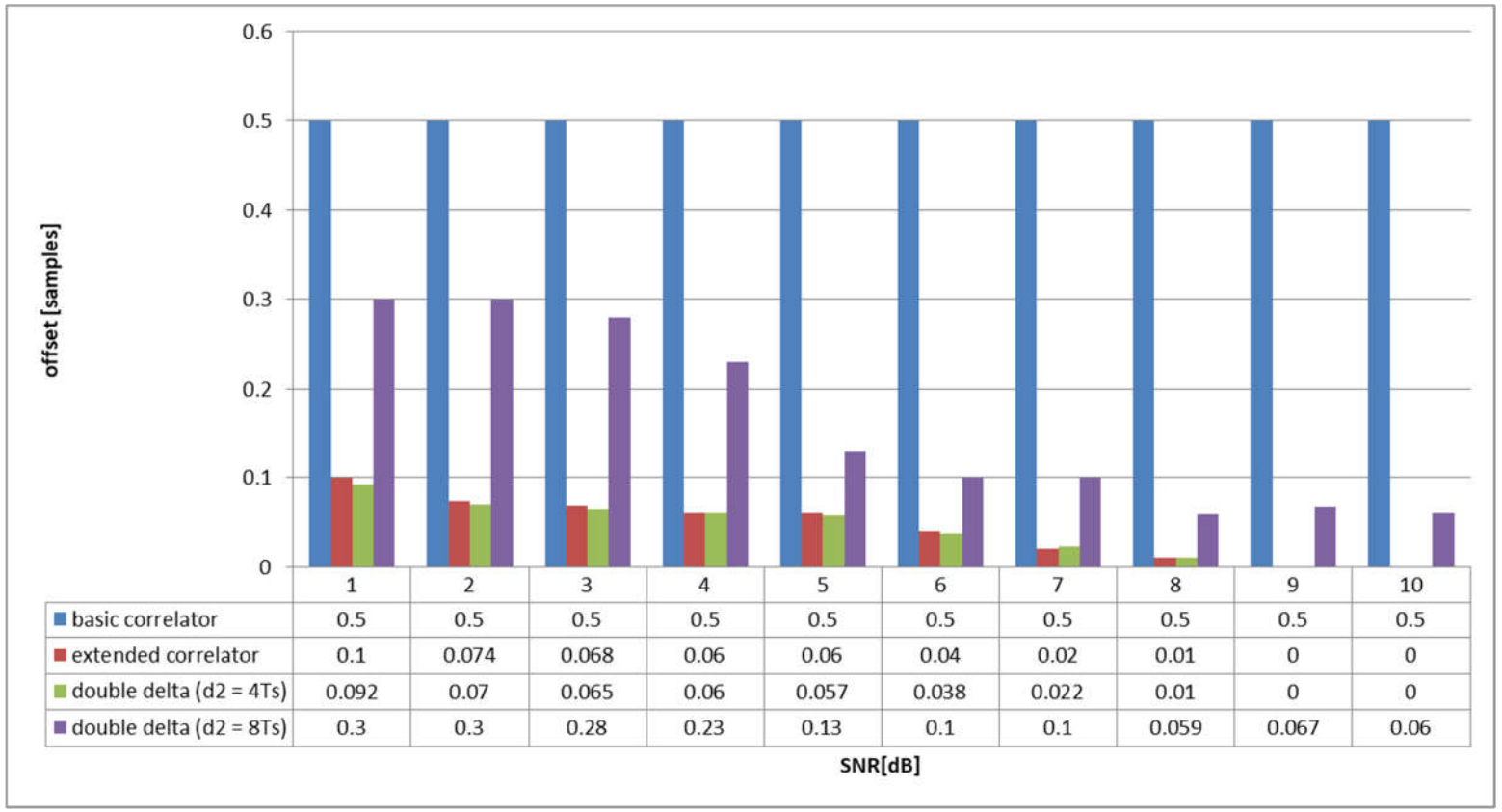

	1	2	3	4	5	6	7	8	9	10
basic correlator	0.5	0.5	0.5	0.5	0.5	0.5	0.5	0.5	0.5	0.5
extended correlator	0.1	0.074	0.068	0.06	0.06	0.04	0.02	0.01	0	0
double delta (d2 = 4Ts)	0.092	0.07	0.065	0.06	0.057	0.038	0.022	0.01	0	0
double delta (d2 = 8Ts)	0.3	0.3	0.28	0.23	0.13	0.1	0.1	0.059	0.067	0.06

Figure 2-33: The obtained efficiencies for various configurations of the correlator

The next simulation tests were aimed at checking the effectiveness of the multi-correlator for signals with a large number of samples per symbol (Fig. 2-34). To test the double delta correlator, a π/4 - QPSK signal was generated (100 symbols, 64 samples/symbol).

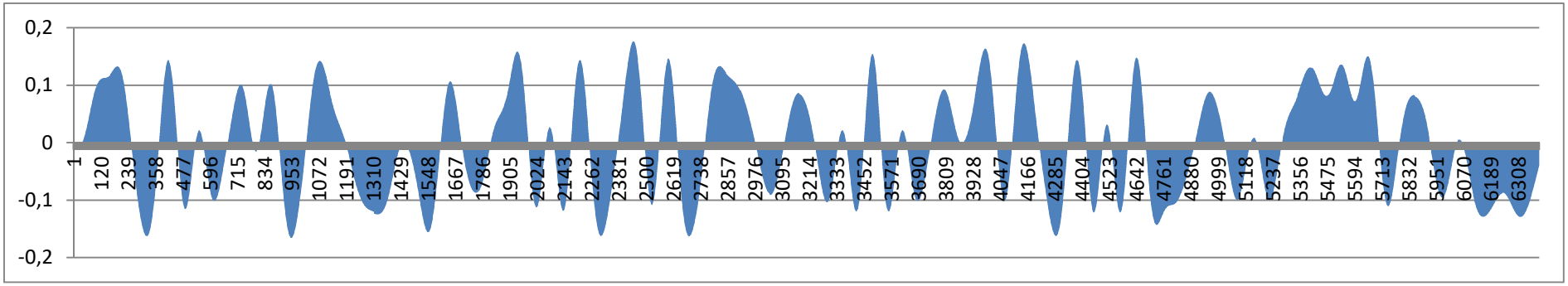

Figure 2-34: π/4 - QPSK signal (100 symbols, 64 samples/symbol)

A second signal shifted from the first signal by half of the sample was also generated (Fig. 2-35):

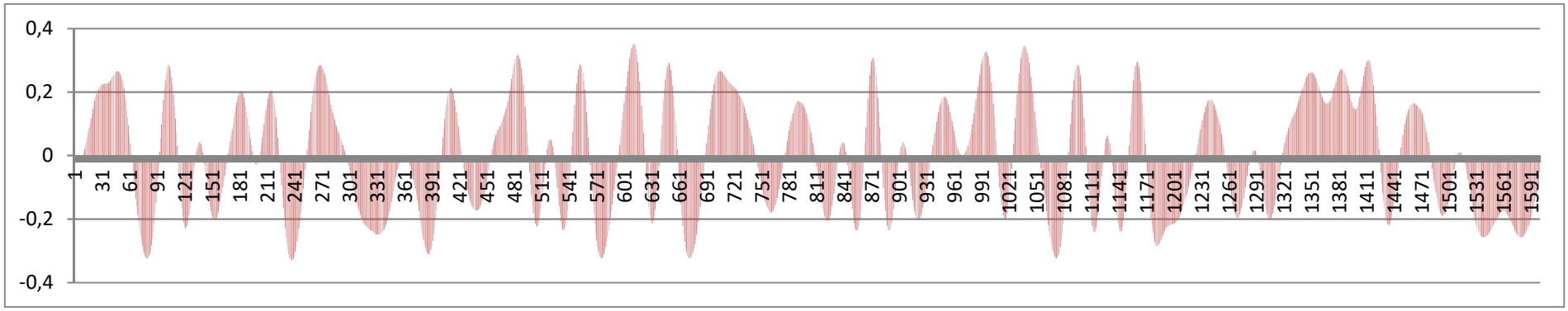

Figure 2-35: π/4 - QPSK signal (100 symbols, 64 samples/symbol) shifted by half of the sample

For better visualization, the signals have been superimposed to make the shift visible (Fig. 2-36):

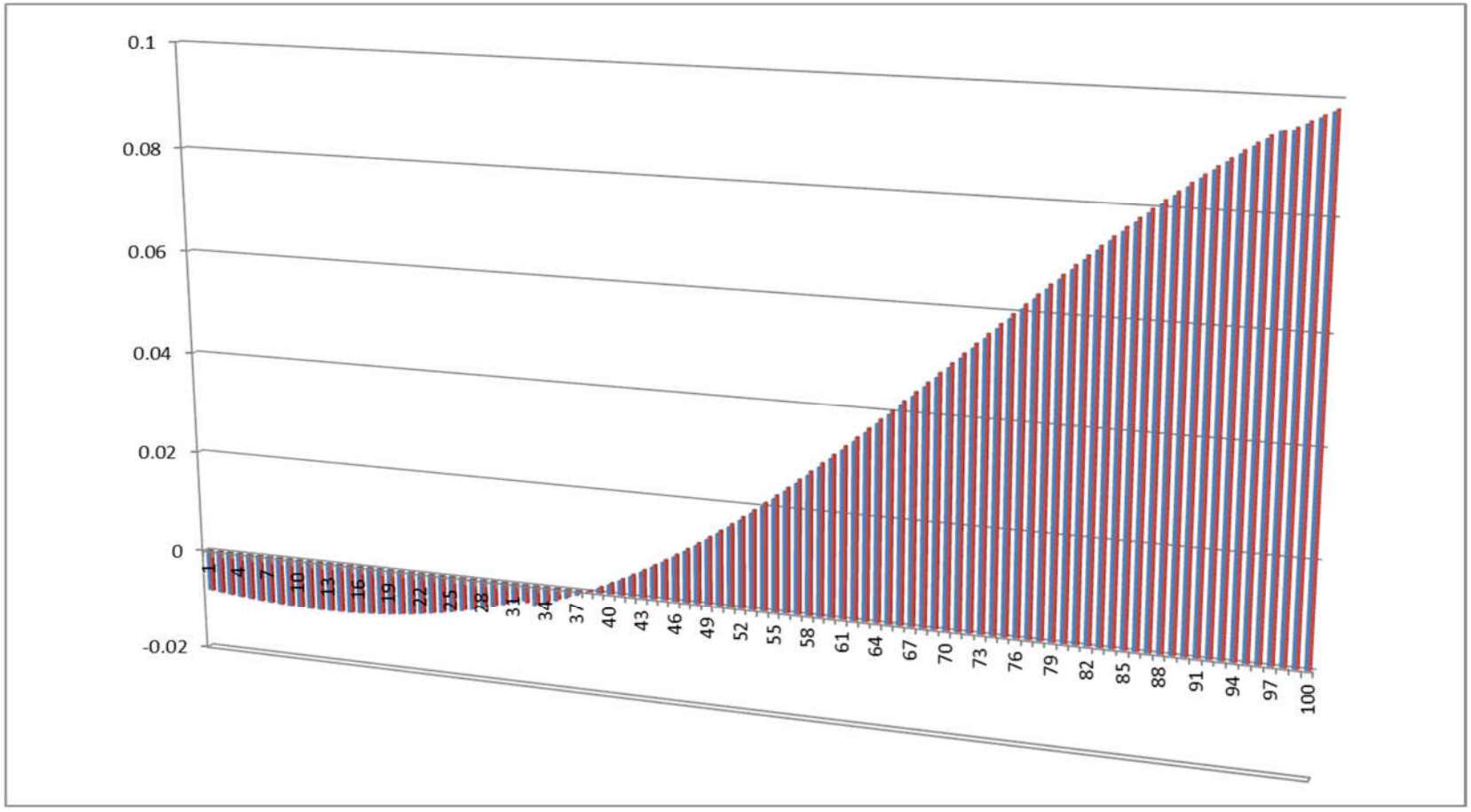

Figure 2-36: Overlapping signals in the form of 3D

Below is a correlation graph of the above signals (Fig. 2-37):

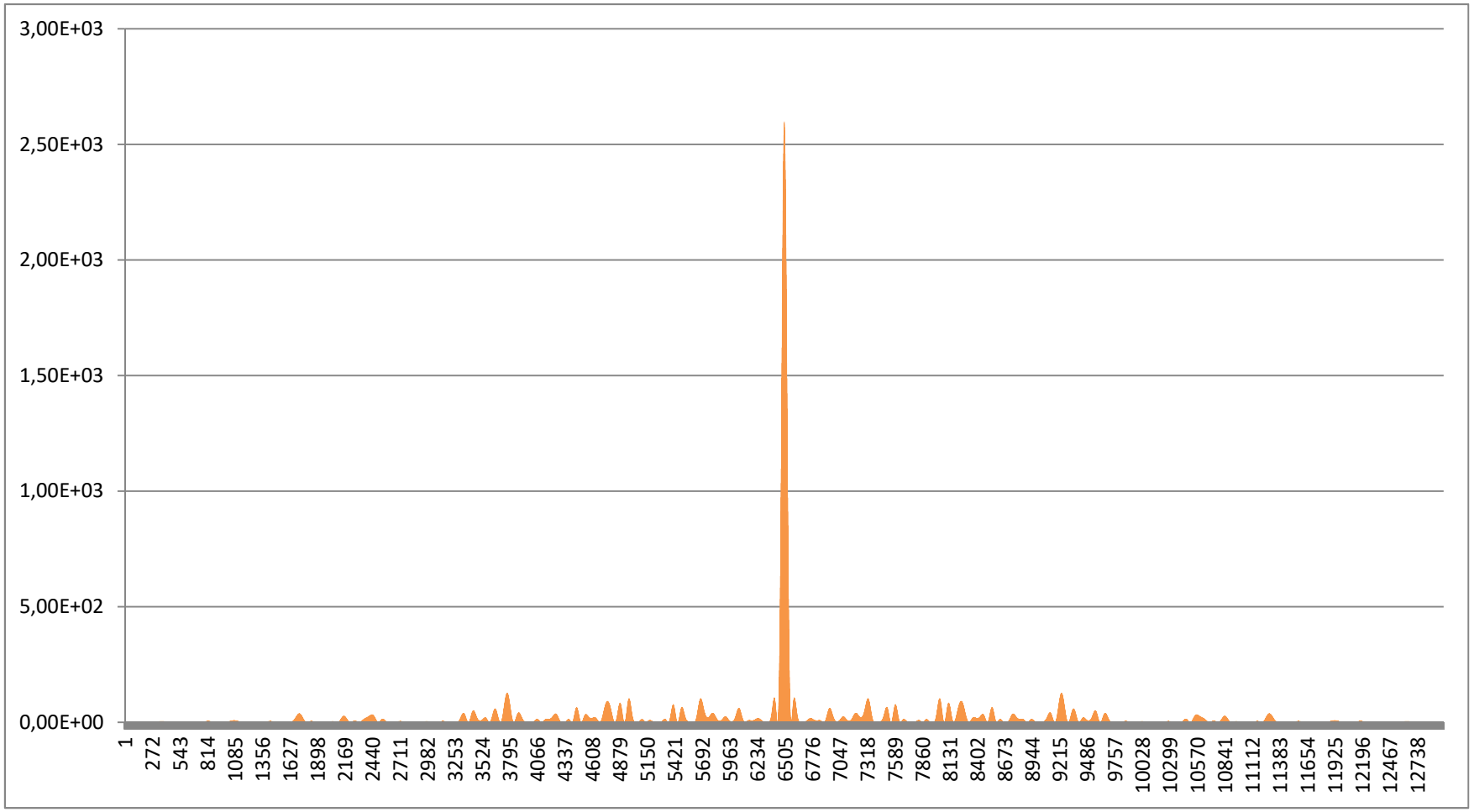

Figure 2-37: Correlation graph of the above signals

Let us consider two correlation scenarios (Fig. 2-38, Fig. 2-39) to test the effectiveness of determining the exact shift:

Scenario 1

$d_1 = 2 * T_s$

$d_2 = 4 * T_s$

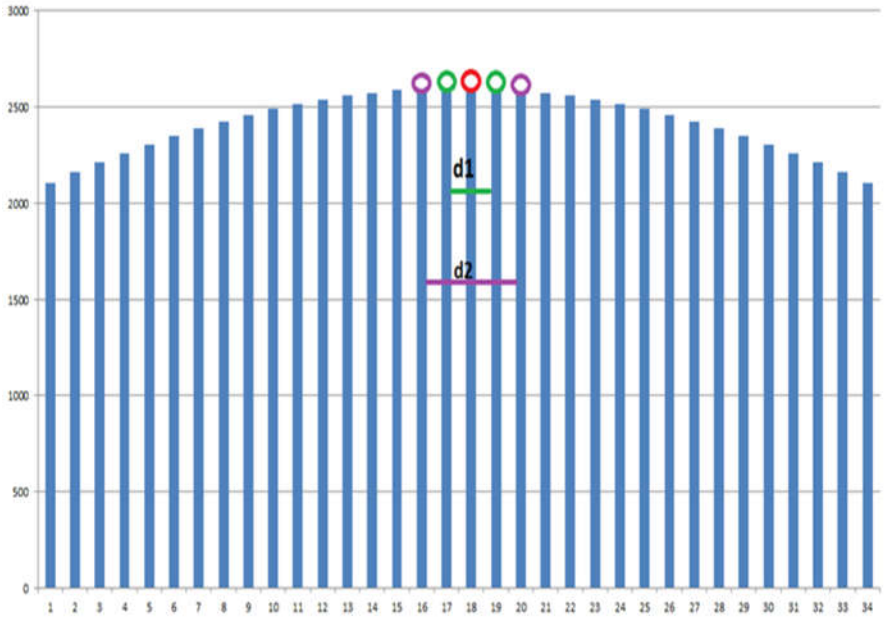

Figure 2-38: Scenario with a smaller spacing of the second pair of samples

Scenario 2

$d_1 = 2 * T_s$

$d_2 = 8 * T_s$

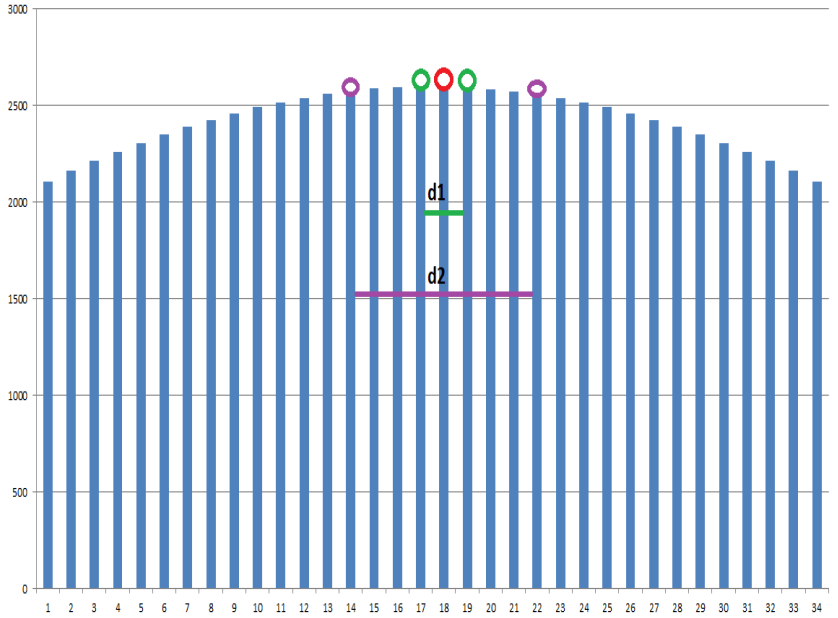

Figure 2-39: Scenario with a larger spacing of the second pair of samples

The efficiencies obtained for various correlator configurations are presented below (Fig. 2-40). It can be seen how the double delta correlator reduces the error in determining the offset of the samples. Compared to the basic correlator, this error is smaller by as much as half the sample.

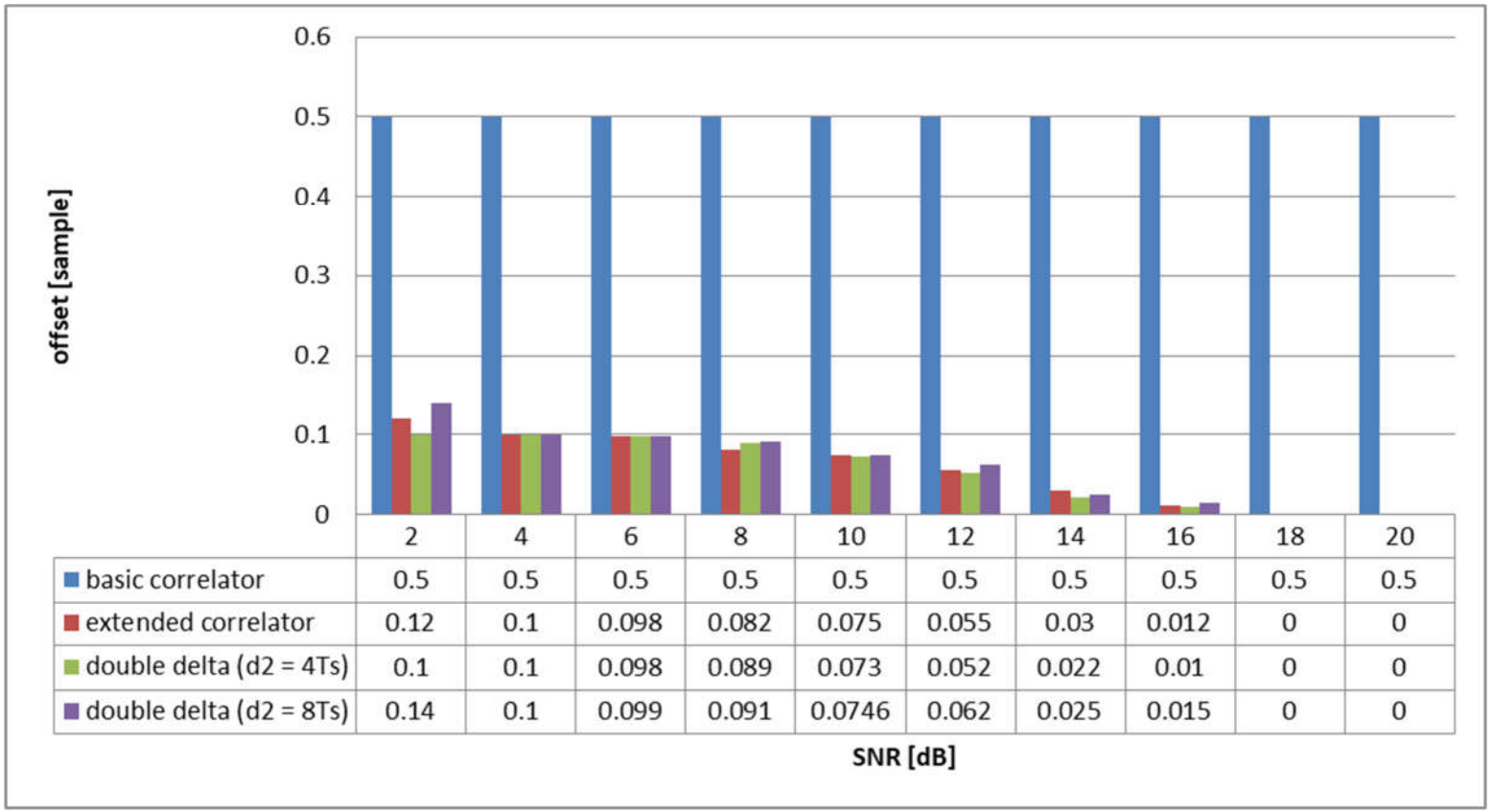

	2	4	6	8	10	12	14	16	18	20
basic correlator	0.5	0.5	0.5	0.5	0.5	0.5	0.5	0.5	0.5	0.5
extended correlator	0.12	0.1	0.098	0.082	0.075	0.055	0.03	0.012	0	0
double delta (d2 = 4Ts)	0.1	0.1	0.098	0.089	0.073	0.052	0.022	0.01	0	0
double delta (d2 = 8Ts)	0.14	0.1	0.099	0.091	0.0746	0.062	0.025	0.015	0	0

Figure 2-40: The obtained efficiencies for various configurations of the correlator

Chapter 'The concept of a multi-correlator and its implementation in the project in order to reduce the multi-path phenomenon' explains what a multicorrelator is and what are its principles of operation. The method of its use and the results that can be obtained thanks to it were presented in a theoretical and practical way. The introductory part of the document focused precisely on the description of the multicorrelator concept - its block diagram and mathematical model in order to better understand the need for its application.

After the theoretical description, it was possible to go to the practical side. Based on the implementation of a simple program, the principle of multi-correlation operation was presented. Two signals were generated shifted from each other by some part of the sampling period. Thanks to this, it was possible to check whether the multicorrelator was correctly implemented and whether it would show exactly such a shift. The simulation study was successful, which additionally showed the advantage of using a multi-correlator over the base correlator based on the sample with the maximum value. Thanks to this solution, it was possible to eliminate the correlation error oscillating around the distance of one sample. This solution is used in GNSS receivers in order to obtain greater accuracy of the distance.

In the next stage of research, the topic of double delta multicorrelator was explored further and deepened. The multicorrelator itself was based on adjacent samples around the main peak, while the double delta multicorrelator still corrects a possible shift on the basis of the second pair of samples separated by a selected value from the main peak. From the conducted simulation studies, it was possible to see how effectively such a solution is suitable, above all, in multi-path scenarios. After an in-depth theoretical analysis, a number of simulation studies were carried out. The tests were carried out on the modulated $\pi/4$ - QPSK signal for different widths of the second pair of the double delta multi-correlator, its influence on the determination of the distance accuracy was checked. Simulations were also carried out on signals with a different number of samples per one symbol.

In order to check the effectiveness of using the multicorrelator in practical situations, its operation was checked on the samples collected during measurement campaigns carried out by the National Institute of Telecommunications in Gdansk. In the application for the correlation of recorded signals, 4 types of correlators have been implemented:

- Basic correlator
- Multicorrelator based on adjacent samples around the peak with the maximum value,
- Double delta multicorrelator which is additionally based on a pair of samples separated from the main peak by 10 samples,
- Double delta multicorrelator which is additionally based on a pair of samples separated from the main peak by 20 samples.

To sum up, this chapter presented research on correlators and multicorrelators that were implemented in the correlator application in the R-Mode project. These studies were aimed at discussing the concept of multicorrelators, including double delta correlators. Their implementation and simulation studies have shown why it is worth using the above solutions. Due to the use of double delta multicorrelators, the error of the determined distance accuracy in practical measurements can be significantly reduced. When using receivers with a low sampling rate, this is of great importance, since a simple basic correlator based on the designated correlation peak alone could determine error distances of up to several hundred kilometers, which in practice would translate into no need for such a solution. The results obtained in the above chapter showed the detailed results that were obtained for the different SNR values.

This helped in selecting an appropriate double delta correlator in the design and further consideration in selecting the spacing between the second pair of samples in the correlator. Further research will be able to show how the tested multicorrelators behave in a multi-path environment and how effective they are in processing real – not simulated – signals.

3 Studies of the impact of a multi-path propagation on the effectiveness of the correlation

Propagation of the signal in the radio channel is a phenomenon that depends on many factors. It depends primarily on the properties of the wave itself, i.e. its length and polarization, as well as on the conditions of the environment in which the wave propagates. The environmental conditions are understood as the topography and the type of its cover - radio waves propagate differently in areas covered with water, in forests, in built-up areas or in open spaces [3-1]. The phenomenon shaping the signal in the radio channel is multipath transmission. The signal transmitted by diffraction and reflections reaches the receiver as a sum of M component signals with different delays, phases and amplitudes. Additionally, in the vicinity of the receiver, each of the components is scattered into N components. If the receiver is in motion, the carrier frequency of each scattering component is shifted by the Doppler pulsation. The graphic below shows the multipath effect (Fig. 3-1):

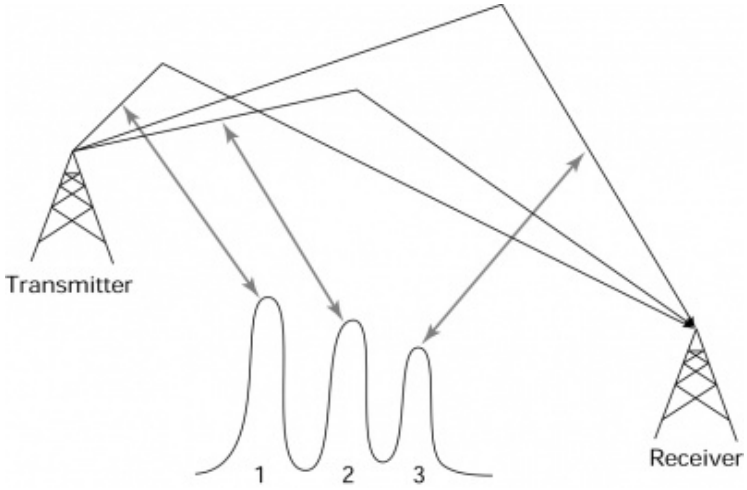

Figure 3-1: The multipath effect

The influence of multipath on the shape of the correlation plot is presented below. Due to numerous signals reaching the receiver, distortions of the correlation function can be observed (Fig. 3-2):

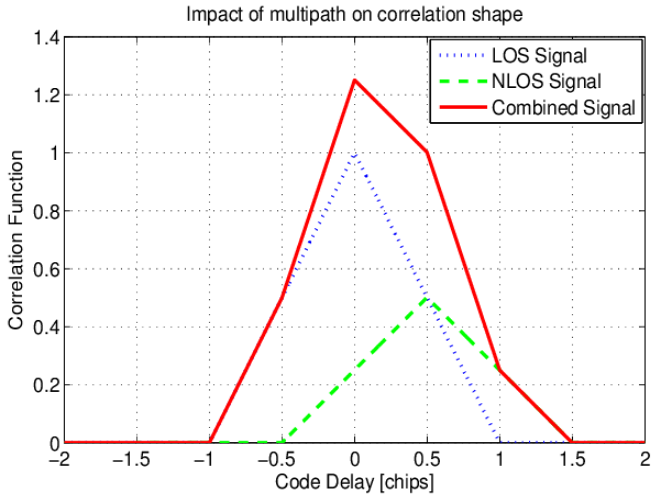

Figure 3-2: The influence of multipath on the shape of the correlation function

3.1 Implementation of measurement scenarios emulating different distances from the transmitter

Three measurement scenarios for different signal replica delay times are presented below. They enable the efficiency of the double delta correlator to be thoroughly investigated. The replica delay times were selected to investigate three cases for the multicorrelator.

In the first scenario, the replica delay is smaller than the selected width of the first sample pair in the double delta correlator (Fig. 3-3).

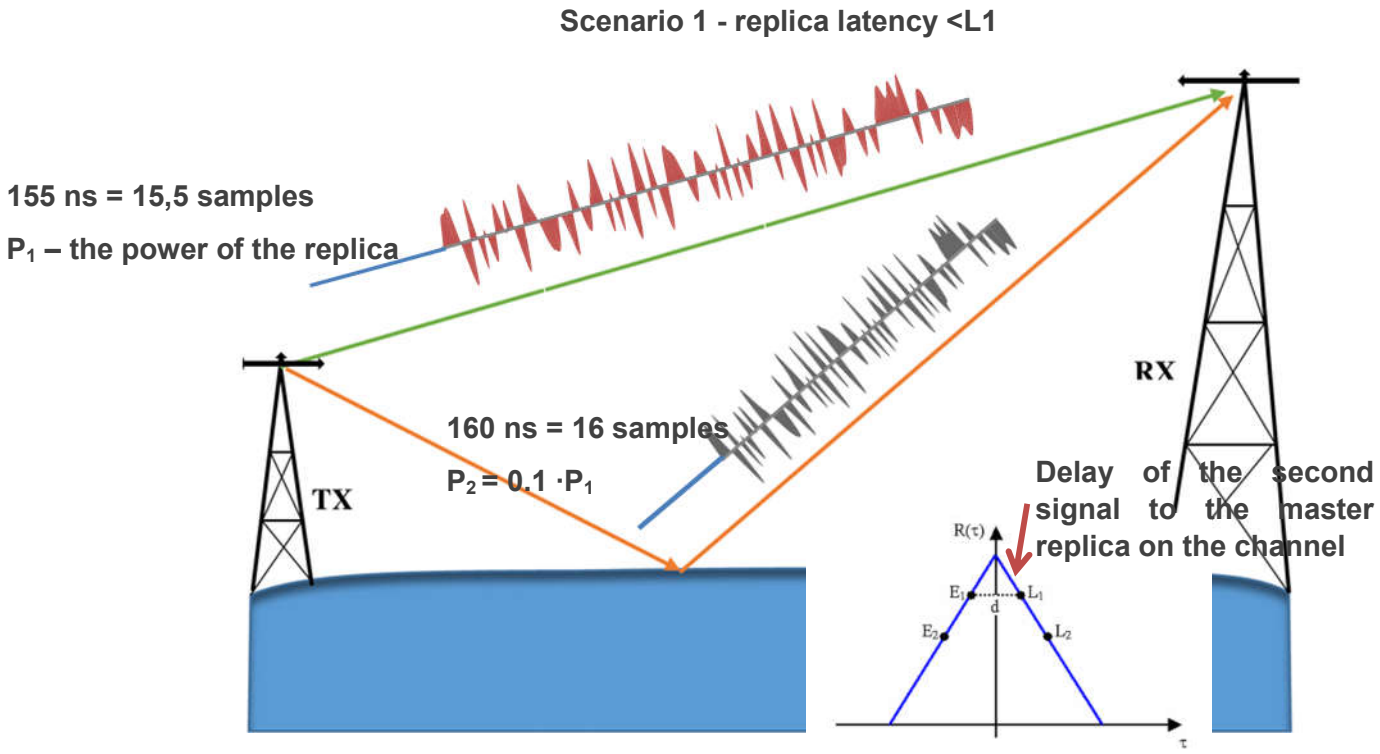

Figure 3-3: First scenario: the replica delay is smaller than the selected width of the first sample pair in the double delta correlator

The graph below shows the error of the determined delay between replicas depending on the type of the used correlator and the signal strength (Fig. 3-4). When replicas are delayed less than the duration of one sample, it can be seen that the best results are obtained by the double delta correlator with a wide spacing of the second pair of samples.

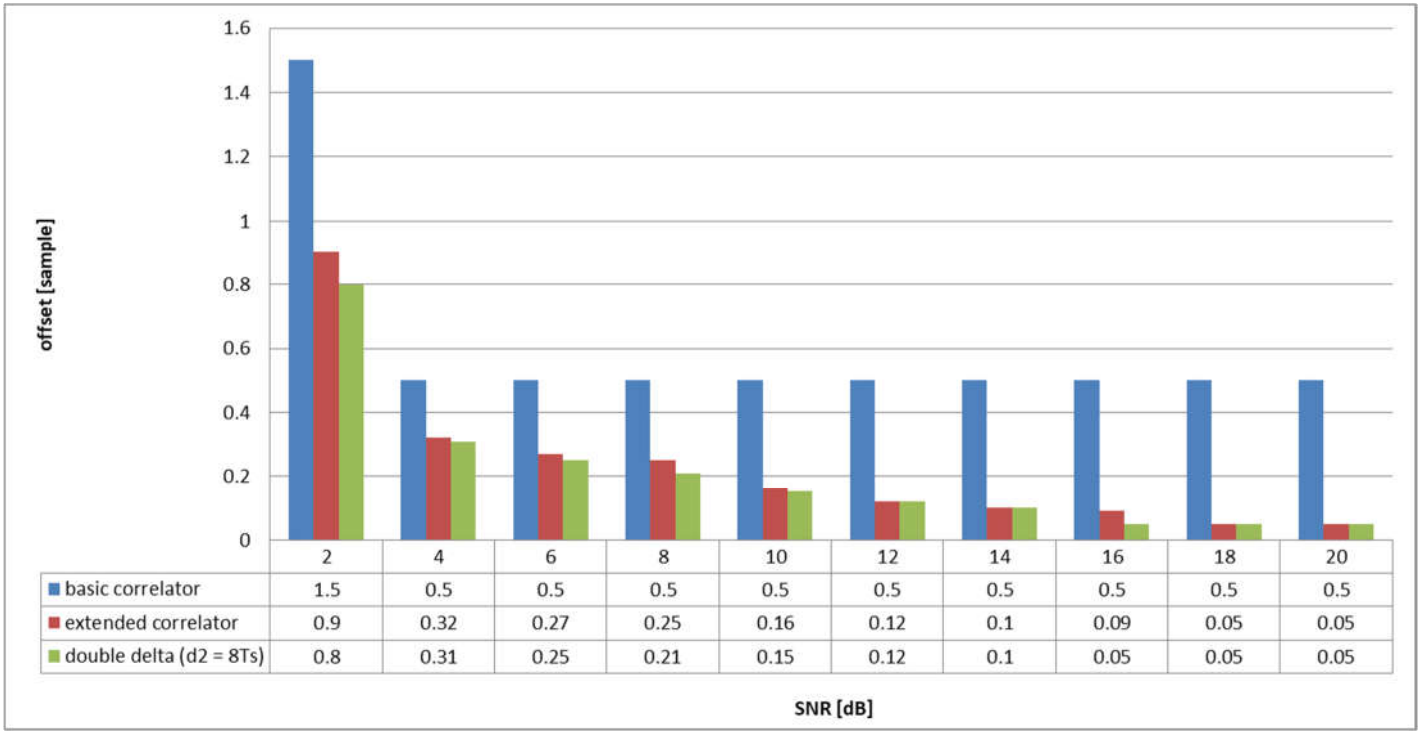

	2	4	6	8	10	12	14	16	18	20
basic correlator	1.5	0.5	0.5	0.5	0.5	0.5	0.5	0.5	0.5	0.5
extended correlator	0.9	0.32	0.27	0.25	0.16	0.12	0.1	0.09	0.05	0.05
double delta (d2 = 8Ts)	0.8	0.31	0.25	0.21	0.15	0.12	0.1	0.05	0.05	0.05

Figure 3-4: The obtained efficiencies for various configurations of the correlator

In the second scenario, the signal replica is delayed with respect to the signal by such a time that the distorted peak of the correlation function is between the first and second pair of double delta correlator samples (Fig. 3-5).

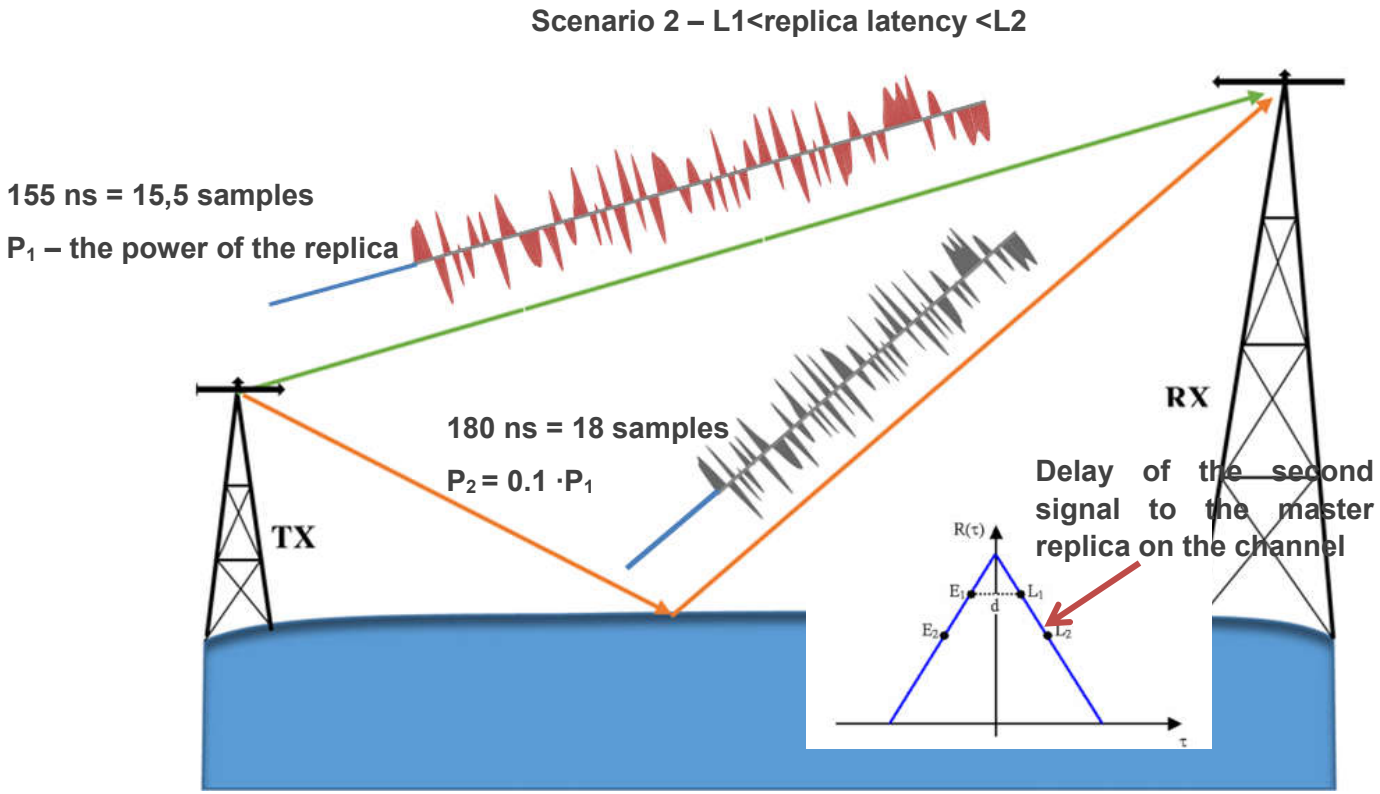

Figure 3-5: The second scenario: the signal replica is delayed with respect to the signal by such a time that the distorted peak of the correlation function is between the first and second pair of double delta correlator samples

Below in the graph (Fig. 3-6), we can see the effectiveness of the different types of correlator. The best results were obtained for the double delta correlator. It takes into account the distortion of the correlation peak due to the delay of the signal replica.

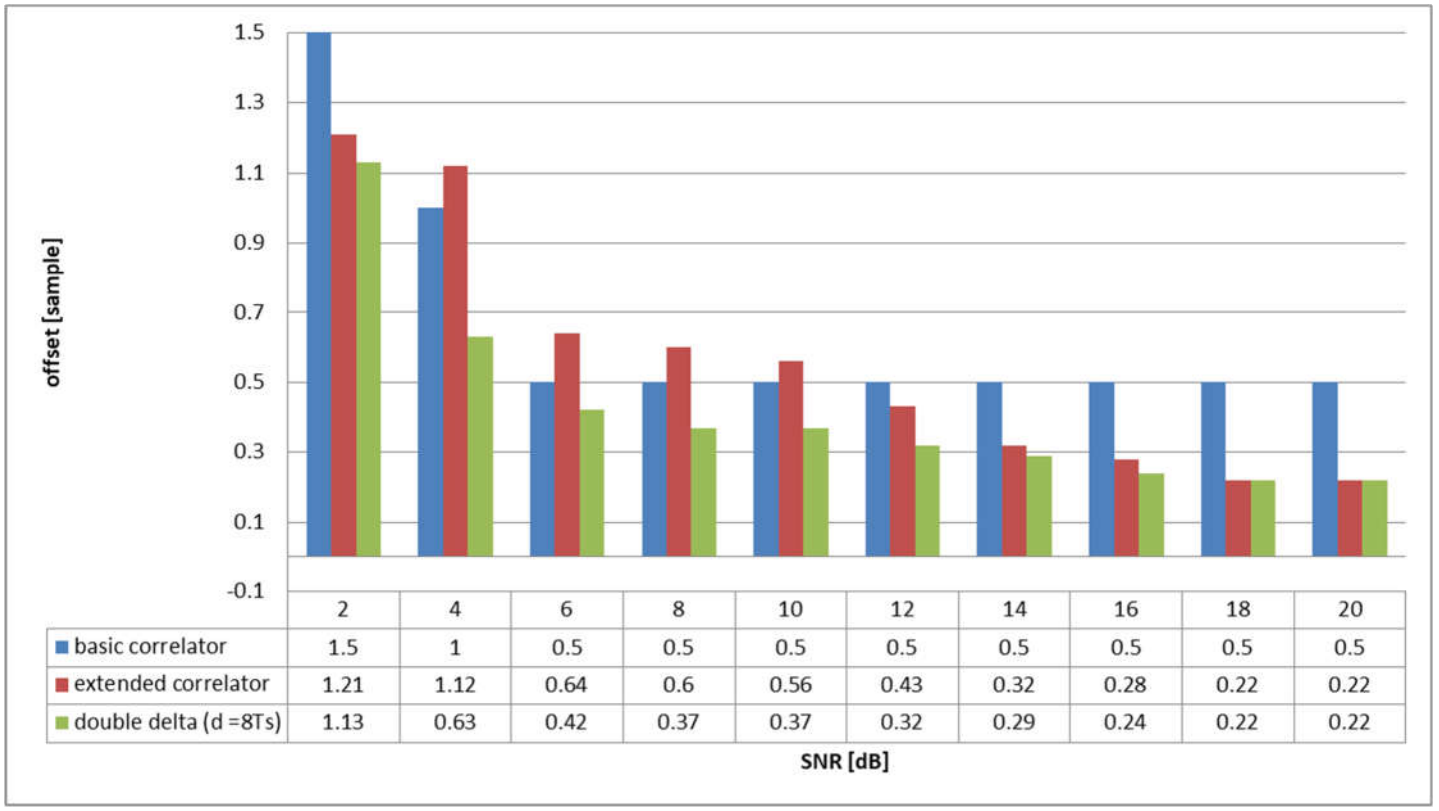

	2	4	6	8	10	12	14	16	18	20
basic correlator	1.5	1	0.5	0.5	0.5	0.5	0.5	0.5	0.5	0.5
extended correlator	1.21	1.12	0.64	0.6	0.56	0.43	0.32	0.28	0.22	0.22
double delta (d =8Ts)	1.13	0.63	0.42	0.37	0.37	0.32	0.29	0.24	0.22	0.22

Figure 3-6: The obtained efficiencies for various configurations of the correlator

In the third scenario, the signal replica is delayed by such a time that the peak distortion of the correlation function is outside the second pair of double delta correlator samples (Fig. 3-7):

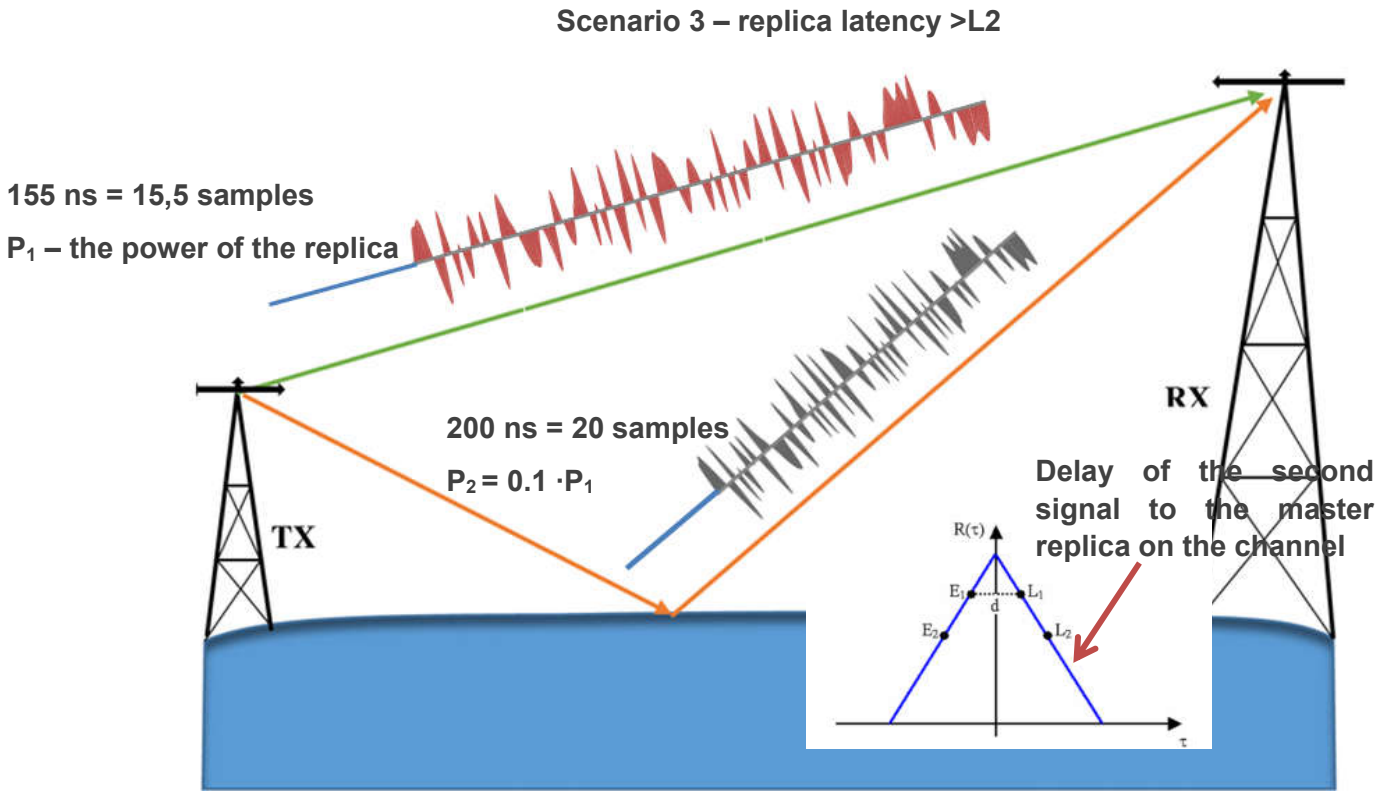

Figure 3-7: Third scenario: the replica of the signal is delayed by such a time that the distortion of the peak of the correlation function is outside the second pair of double delta correlator samples.

For high SNRs in the third scenario (Fig 3-8), the efficiency of the extended and double delta correlator is very similar. On the other hand, for low SNR values, it can be seen that the basic correlator works best.

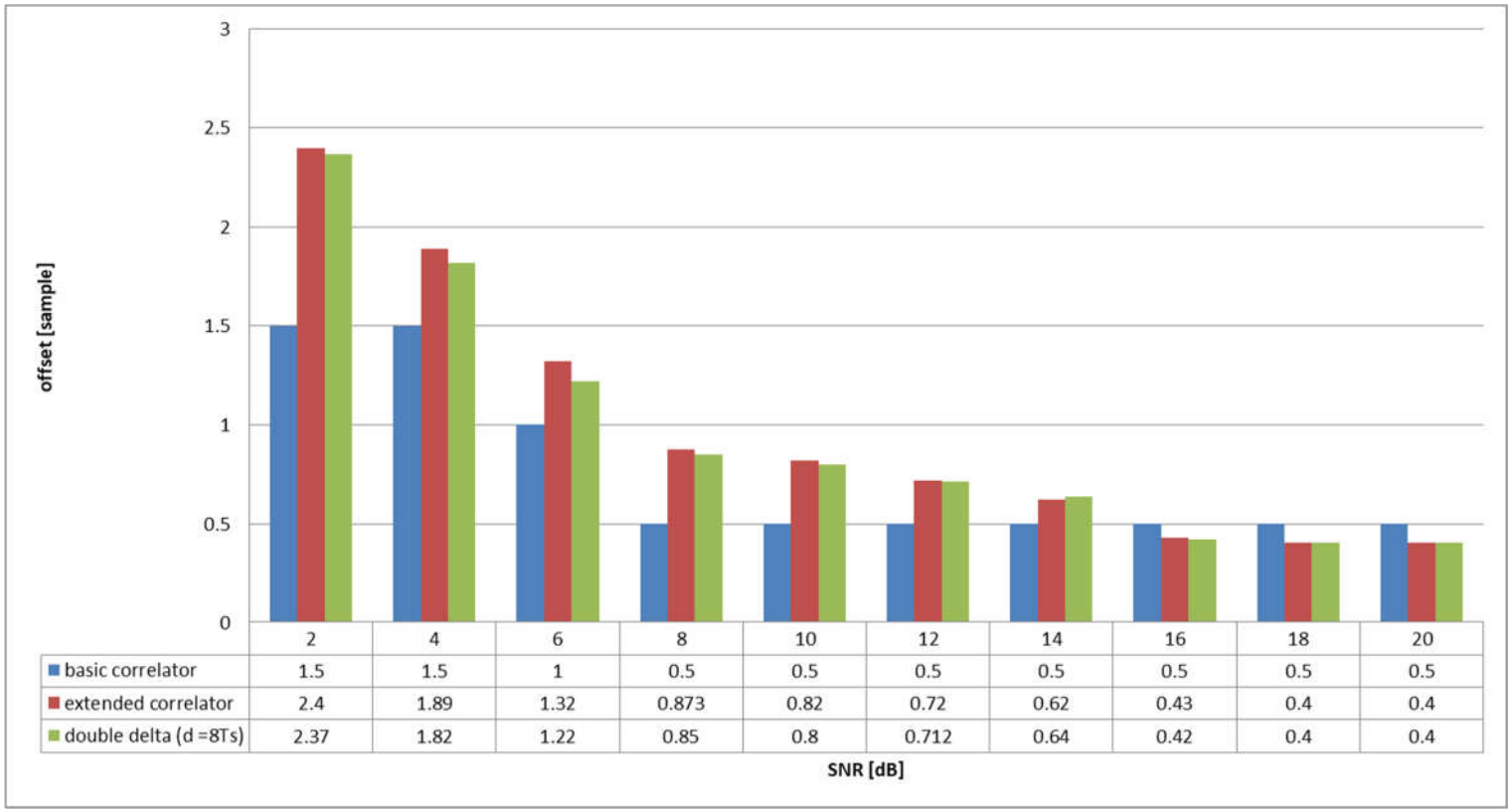

	2	4	6	8	10	12	14	16	18	20
basic correlator	1.5	1.5	1	0.5	0.5	0.5	0.5	0.5	0.5	0.5
extended correlator	2.4	1.89	1.32	0.873	0.82	0.72	0.62	0.43	0.4	0.4
double delta (d =8Ts)	2.37	1.82	1.22	0.85	0.8	0.712	0.64	0.42	0.4	0.4

Figure 3-8: The obtained efficiencies for various configurations of the correlator

The model on the basis of which the multipath (Fig. 3-9) calculations in sea conditions were performed during the measurements aboard the ship are presented below. Using these calculations, it was possible to verify the impact of multipath phenomena on the long measurement route. From the calculations below, it can be concluded that at long distances, the impact of multipath is small. On the other hand, for small distances, such as measurements at the port near the transmitting station, the impact of multipath is much more significant.

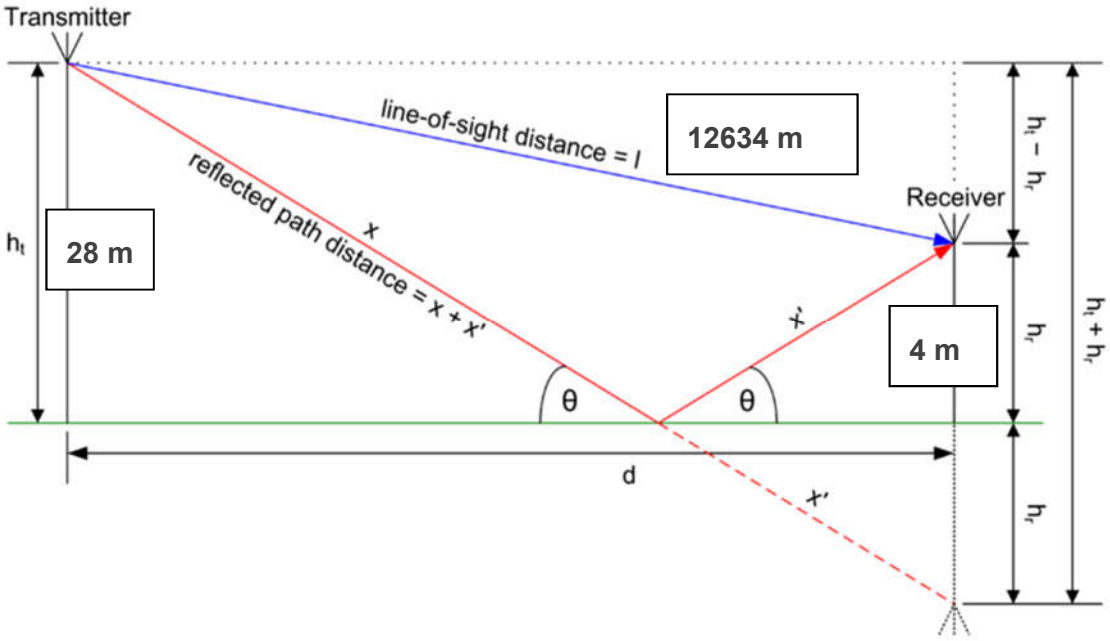

Figure 3-9: Model of multipath during measurements at sea

Below, there are the formulas (25,26) on the basis of which the length of the signal replica's path to the receiving antenna was calculated:

$$d = \sqrt{12634^2 - 24^2} = 12633{,}9772\ m \tag{25}$$

$$x + x' = \sqrt{(h_t + h_r)^2 + d^2} = 12634{,}017\ \text{m} \tag{26}$$

3.2 Implementation of measurement scenarios for different spacing of two pairs of samples in the double-delta correlator

The previous section focused on the study of the double delta correlator, in which the spacing of two pairs of samples was constant, regardless of the scenario under consideration. These studies were to test the effectiveness of the correlator depending on the delay size of the replicas matching the signals to the receiver. In this subchapter, however, it will be possible to investigate how the change of the width span of two pairs of samples in the double delta correlator affects the determination of the accuracy of the distance determination. The main focus was on the detailed study of the main peak of the correlation function. The operation of the correlator on all samples included in this correlation peak was fully analyzed. Cases where the signal was received in the LOS and NLOS zones were considered. It helped to decide which correlator should be used during measurements at sea during the actual measurement campaign.

3.2.1 Sample spread analysis in the double delta correlator for LOS conditions

First, the analysis of the span selection between the second pair of samples in the double delta multicorrelator was carried out in order to obtain the best efficiency in determining the shift of the correlation peak for LOS conditions. The graph (Fig. 3-10) below shows the correlation function for a signal received under LOS conditions. The next graph (Fig. 3-11) presents the correlation peak in a zoomed version.

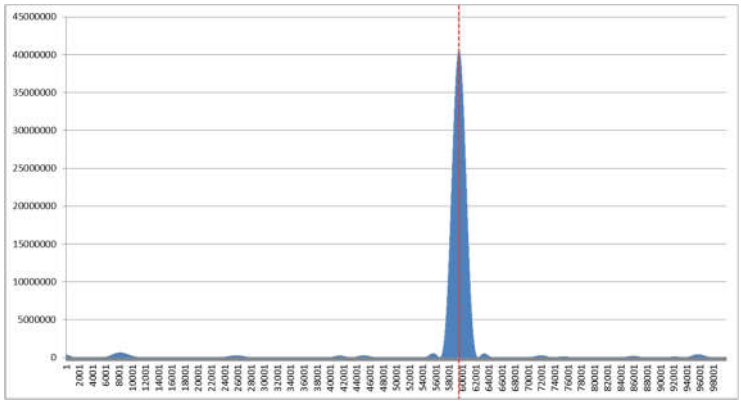

Figure 3-10: Correlation peak for LOS conditions

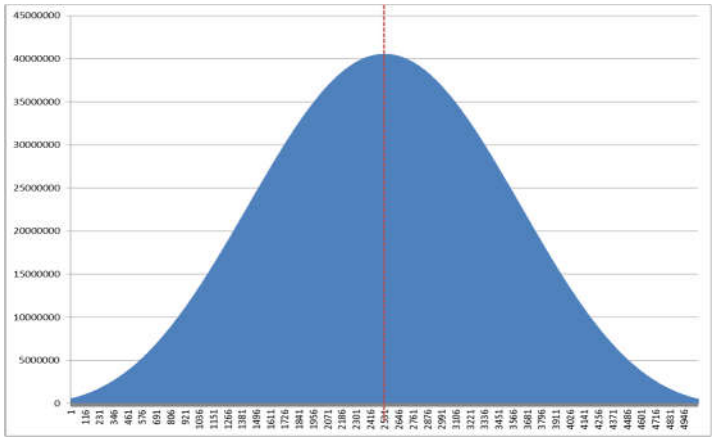

Figure 3-11: Correlation peak for LOS conditions (zoomed)

The graphs below (Fig. 3-12, Fig. 3-13, Fig. 3-14, Fig. 3-15) show how exactly the samples around the peak with the maximum value behave. Thanks to this analysis, it is possible to observe how the remaining pairs of samples behave symmetrically to the maximum peak. We can see that their values are very similar to each other. This shows that for LOS conditions, it is easier to determine the distance from the transmitting station with greater accuracy.

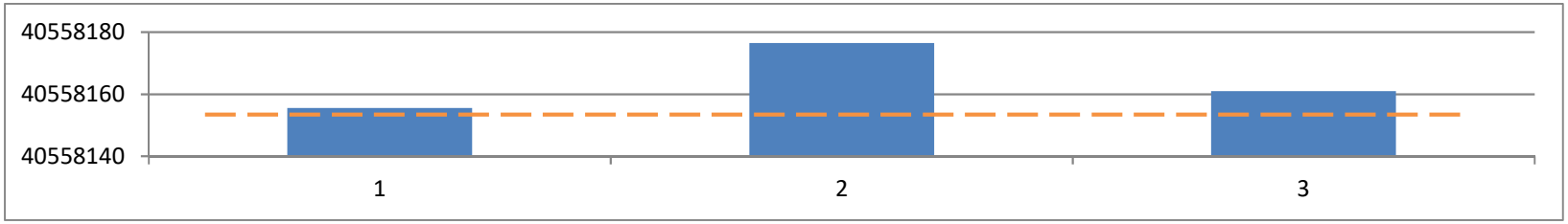

Figure 3-12: Correlation peak analysis for LOS conditions - version a

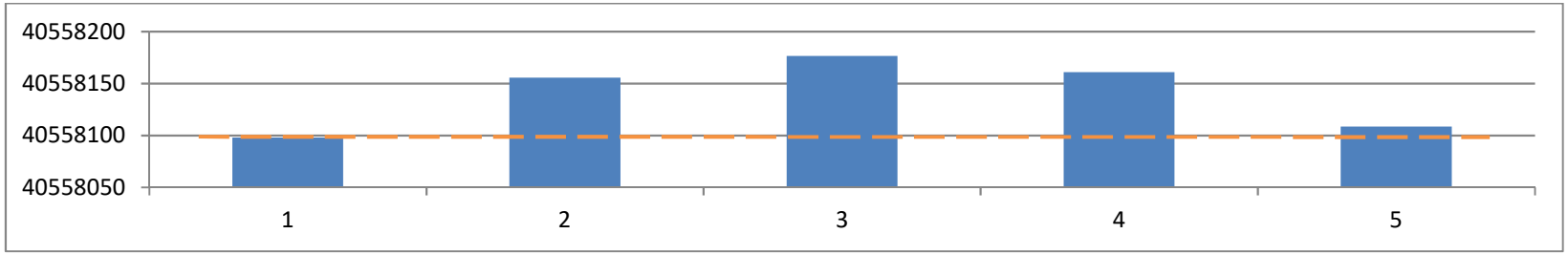

Figure 3-13: Correlation peak analysis for LOS conditions - version b

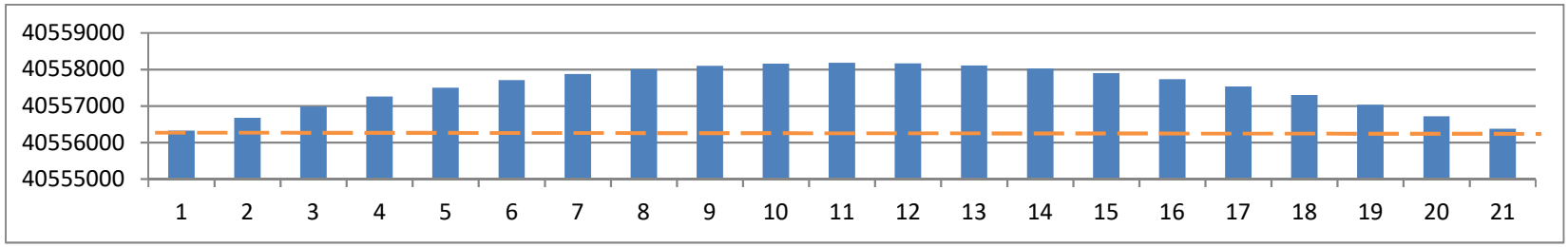

Figure 3-14: Correlation peak analysis for LOS conditions – version c

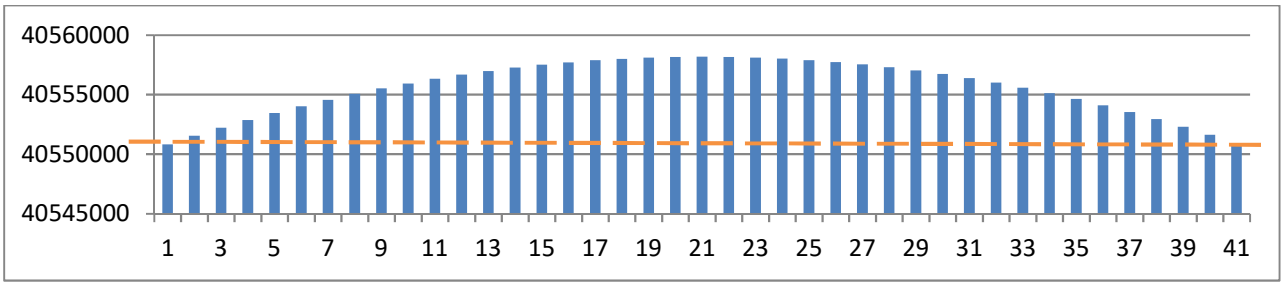

Figure 3-15: Correlation peak analysis for LOS conditions - version d

In the next selected simulation tests for a group of files with high SNRs, the effectiveness of multicorrelators was checked depending on the width of the spacing of the second pair of the correlator samples. By using a low-pass filter through which the samples from the “I” and “Q” tracks with a high ratio of signal power to noise power are processed, it was possible to obtain relatively reliable conclusions as to the results of multi-correlation - that is, an information do they actually improve the determination of the distance accuracy or do they deteriorate this accuracy.

Below (Fig. 3-16), we can see the most representative example of such a correlation peak obtained under very good conditions. When selecting the d2 distance, i.e. the spacing of the second pair of multicorrelator samples, first of all, several factors were taken into account, which were the later target for observation during the simulation. First of all, it was the ratio of the peak values of each pair tested for simulation in the multicorrelator. After performing many simulations, it was possible to estimate the ranges of such distances d2 for which the determination of this distance accuracy was the best, but also the worst.

In the largest number of simulations for the interval in which the distance d2 changed from 17 samples to 45, the determined distance accuracy was the best - about 0.7 m, i.e. less than a tenth of the sample (table 3-1). This may be a slight improvement, but the kind of multi-correlator is there to eliminate the error resulting from the duration of one sample.

With this type of analysis, it is best to get the results from the basic correlator, because all calculations are based on the peak with the maximum value. And it is best to base also on the results obtained for the double delta multicorrelator for d2 = e.g. 20 as the safest value. In this case, we have the position of the sample with the highest value determined as in the basic correlator. We also have a pair of d1 samples that are adjacent to the main peak. The position of the shifted peak of the correlation peak can be determined from the parabola equation method. And based on a pair of samples with a distance d2, based on their power, a correction of the determined vertex by the first pair can be performed and the most reliable result obtained.

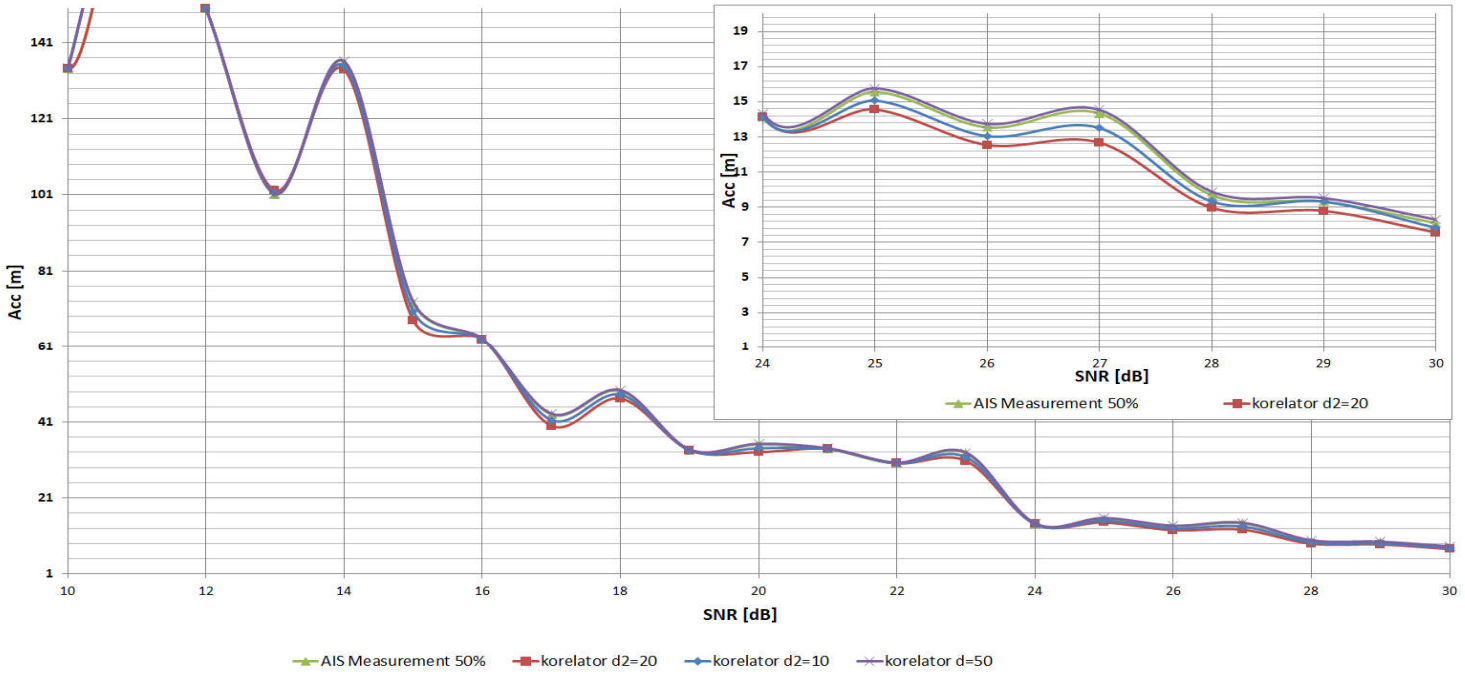

Figure 3-16: Determined distance accuracies in LOS conditions for different types of correlators

SNR	28 dB				
d2	Basic correlator	Extended correlator d2=0	Double delta correlator d2=10	Double delta correlator d2=(~17~-~45)	Double delta correlator d2>=50
RMS Acc [m]	9.6876	9.37	9.251	8.973	10.588

Table 3-1: Determined distance accuracies in LOS conditions for different types of correlators - exact values

3.2.2 Sample spread analysis in the double delta correlator for NLOS conditions - AIS measurement campaign

In this case, the files with the collected samples were analyzed during the AIS measurement campaign (the first measurement campaign that was carried out in June 2019). When analyzing the peak of the correlation function, it is possible to notice the unevenness in the falling of peaks in relation to the peak with the maximum value. This may affect the determination of the distance accuracy, especially when selecting the d2 sample pair for the double delta correlator. It was concluded from the simulation tests that in the worst case, when the correlation was obtained by the base correlator, an error of about 6 samples in relation to the determination of the main peak can be observed. Of course, the number of samples per symbol has a big influence here. Due to large sampling, the influence of noise has a destructive effect on the shape of the correlation peak - it is not smoothed out.

First, the correlation peak for the signal received at a distance of about 30 km from the transmitting station during the measurement campaign was considered (Fig. 3-17).

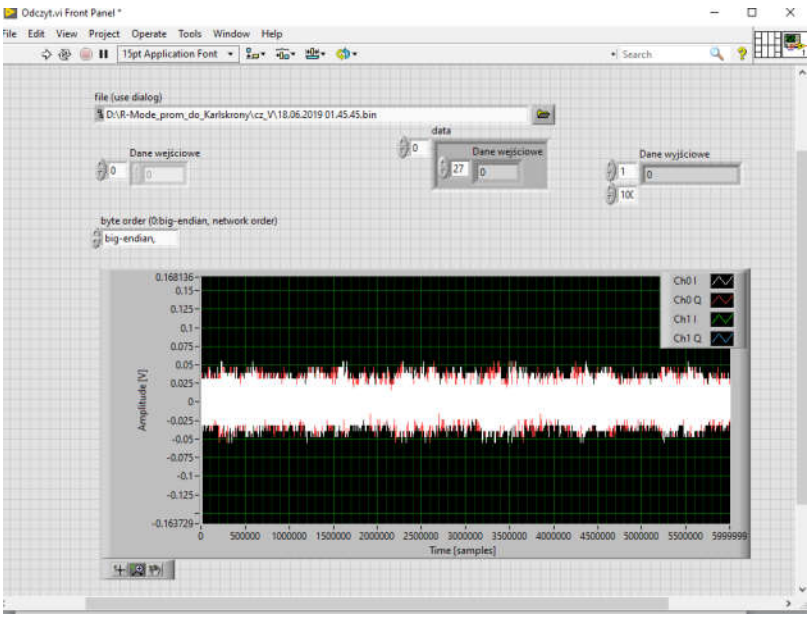

Figure 3-17: Time characteristics of the received signal

It can be seen that compared to the LOS scenario, the correlation peak is no longer symmetrical to the main peak. The detailed analysis of the obtained correlation peak for the NLOS scenario is presented below (Fig. 3-18, Fig. 3-19, Fig. 3-20, Fig. 3-21).

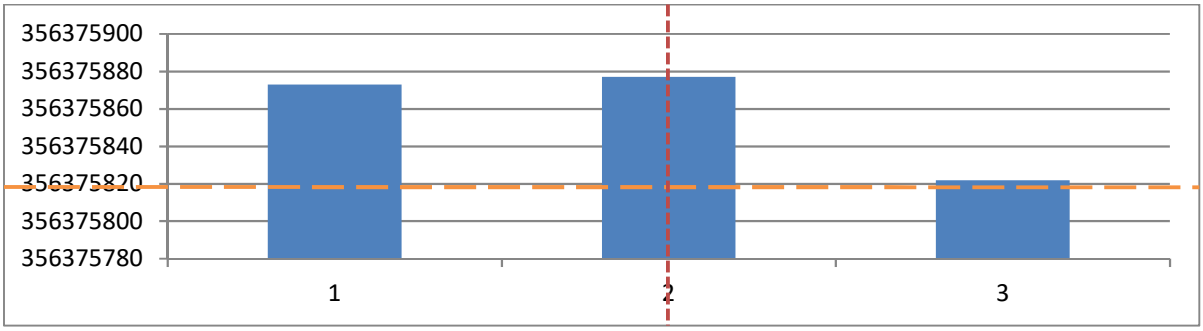

Figure 3-18: Correlation peak analysis for NLOS conditions - version a

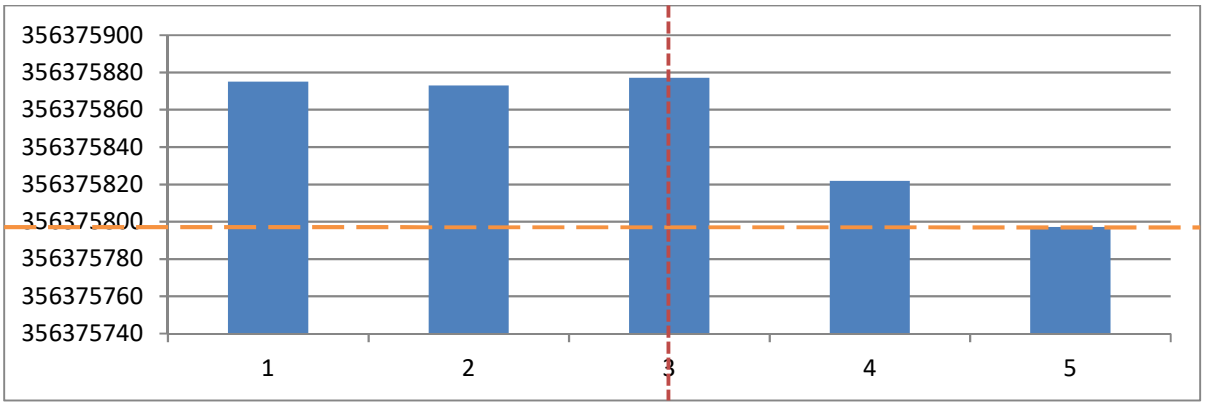

Figure 3-19: Correlation peak analysis for NLOS conditions - version b

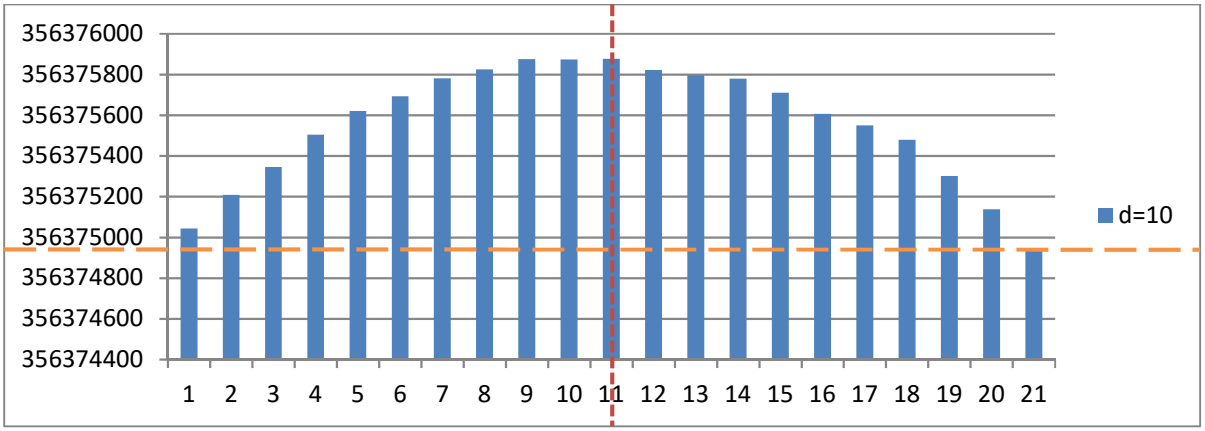

Figure 3-20: Correlation peak analysis for NLOS conditions - version c

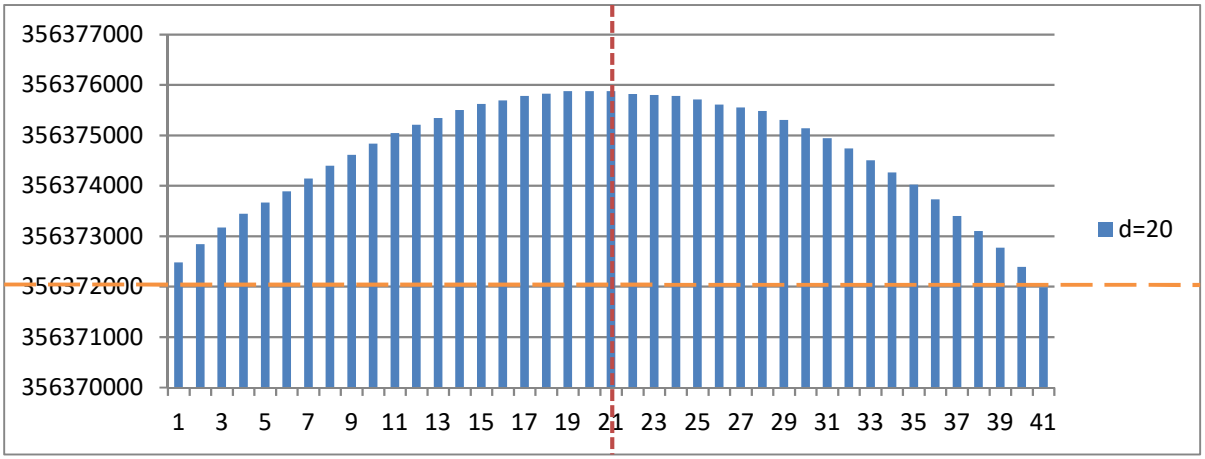

Figure 3-21: Correlation peak analysis for NLOS conditions - version d

In the next case, the correlation peak for the signal received at a distance of about 40 km from the transmitting station during the measurement campaign is presented (Fig. 3-22).

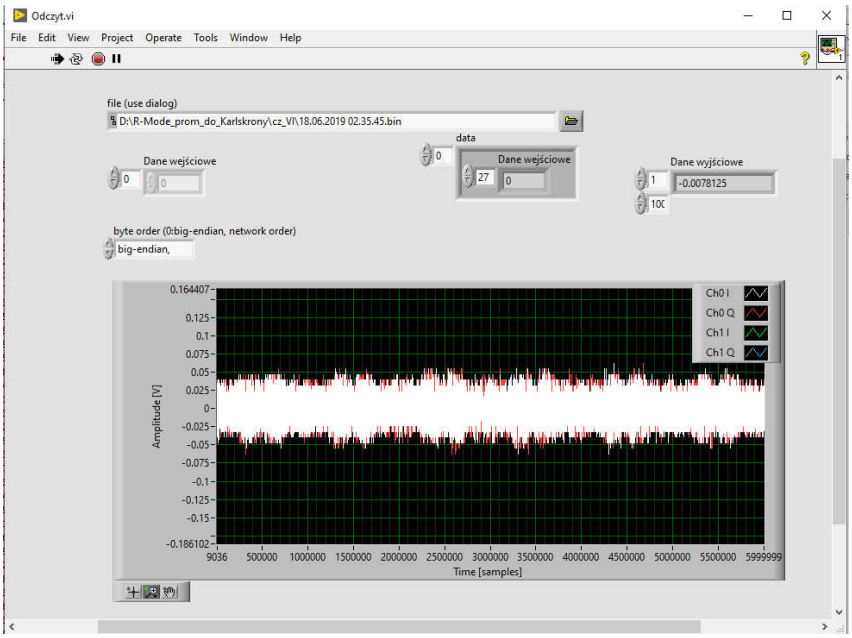

Figure 3-22: Time characteristics of the received signal

The nature of the correlation peak is shown below. It is similar to the previous case. Due to the distance and high noise level of the received signal, the correlation peak is not symmetrical to the maximum peak. The correlation peak for a signal received approximately 40 km from the transmitting station is shown below (Fig. 3-23, Fig. 3-24, Fig. 3-25, Fig. 3-26).

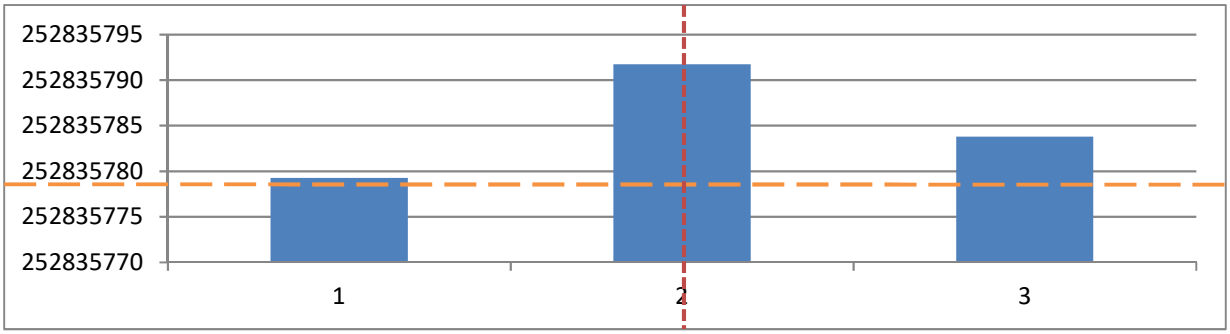

Figure 3-23: Correlation peak analysis for NLOS conditions - version a

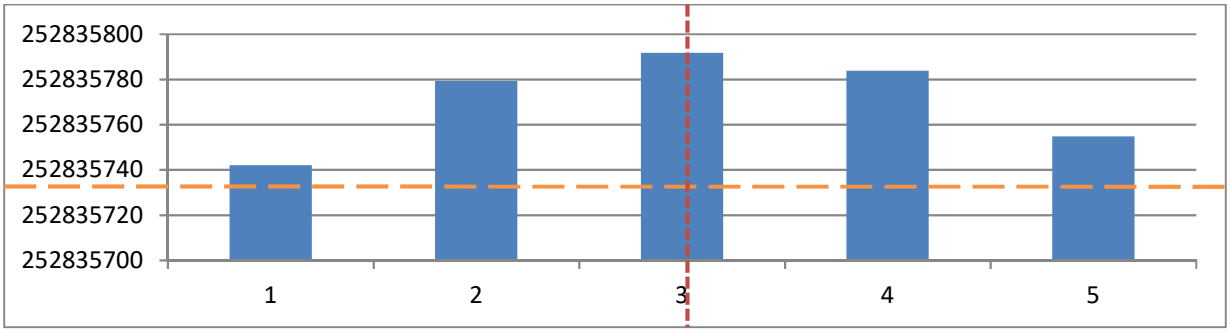

Figure 3-24: Correlation peak analysis for NLOS conditions - version b

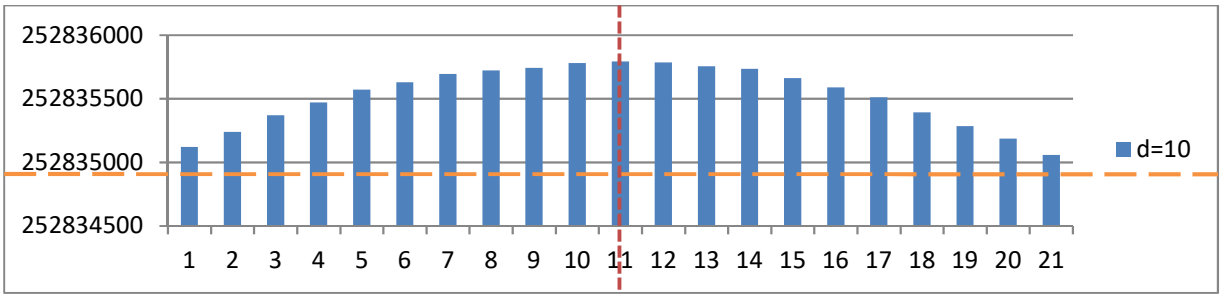

Figure 3-25: Correlation peak analysis for NLOS conditions - version c

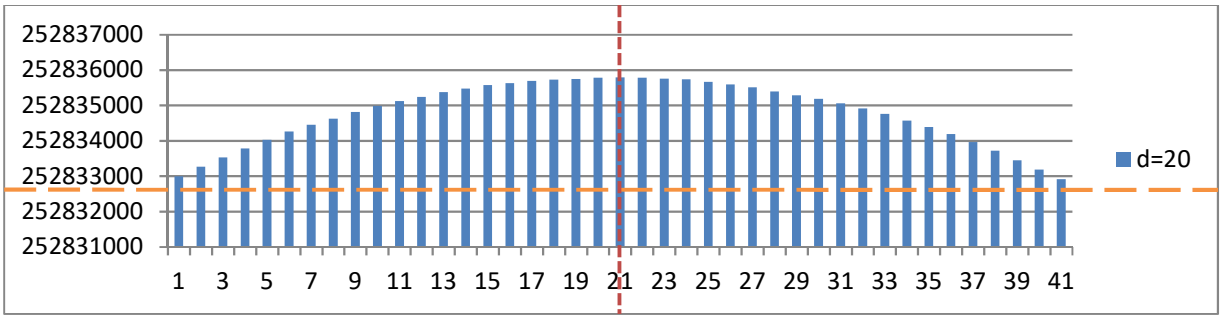

Figure 3-26: Correlation peak analysis for NLOS conditions - version d

3.2.3 Sample spread analysis in the double delta correlator for NLOS conditions - VDES measurement campaign

In the case of the VDES campaign, for sampling reduced two times compared to the AIS campaign, a less destructive effect of noise on the shape of the correlation peak can be noticed. Of course, in these cases we can also see some degradation - to about 5 samples - in determining the accuracy of the distance, but after converting this into meters, it results in a much smaller error than for the AIS. Examples of the shapes of the correlation peaks at a distance of about 40 km from the transmitting station in Gdynia are presented below (Fig. 3-27).

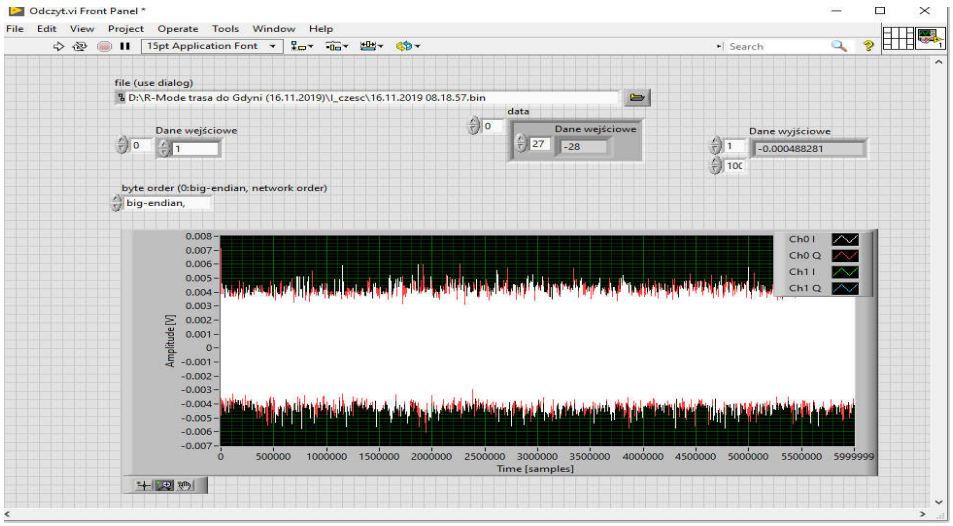

Figure 3-27: Time characteristics of the received signal

Graphs with the shape of the correlation peak are shown below. Its shape and nature are similar to those for the correlation peak for the AIS measurements. This is due to the distance at which the signal was received and the noise level (Fig. 3-28, Fig. 3-29, Fig. 3-30, Fig. 3-31).

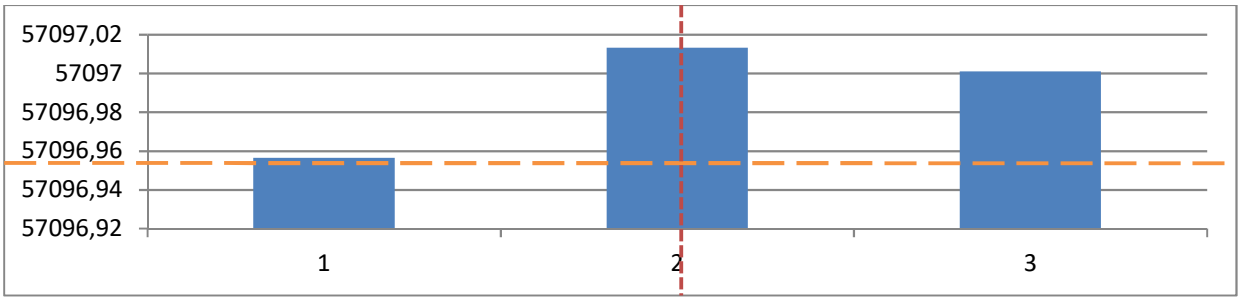

Figure 3-28: Correlation peak analysis for NLOS conditions - version a

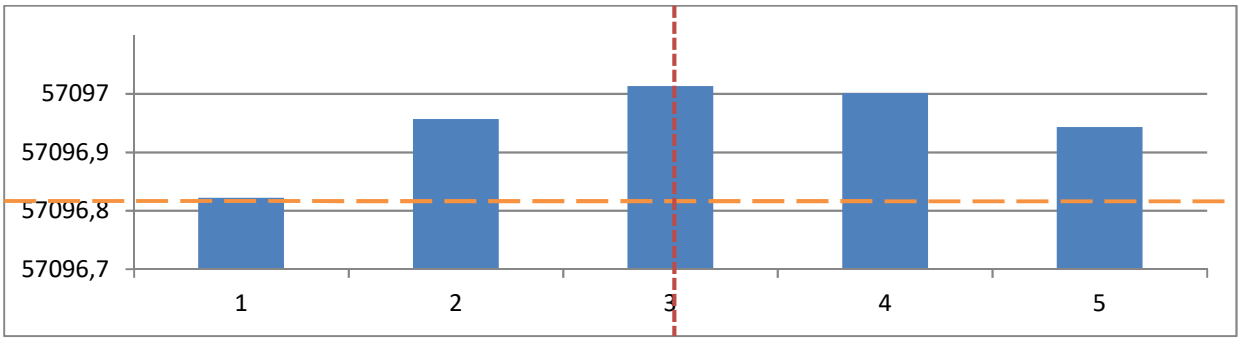

Figure 3-29: Correlation peak analysis for NLOS conditions - version b

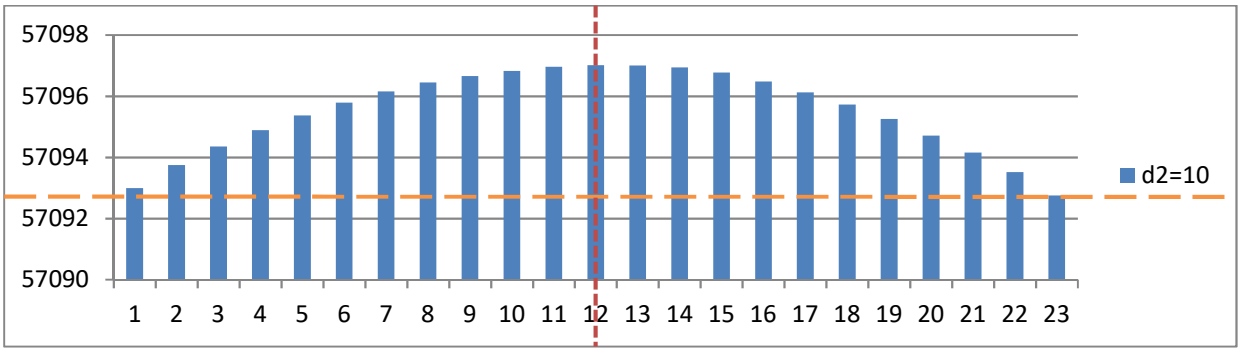

Figure 3-30: Correlation peak analysis for NLOS conditions - version c

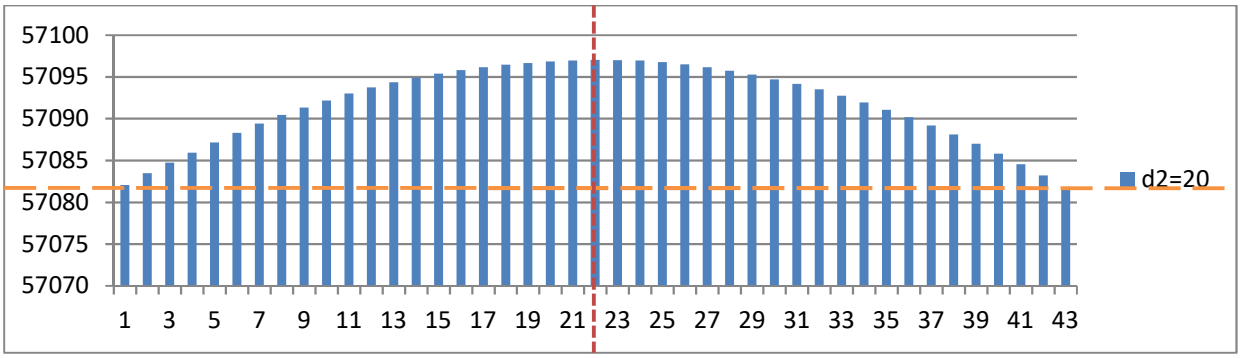

Figure 3-31: Correlation peak analysis for NLOS conditions - version d

Another example for a VDES campaign is a signal received at a distance of 50 km from the broadcasting station. As expected, the nature of the peak is similar to the previous case and is presented below (Fig. 3-32, Fig. 3-33, Fig. 3-34, Fig. 3-35, Fig. 3-36).

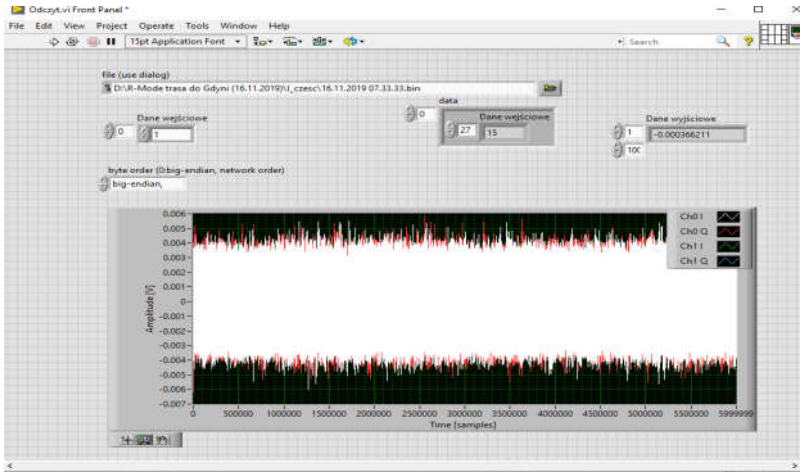

Figure 3-32: Time characteristics of the received signal

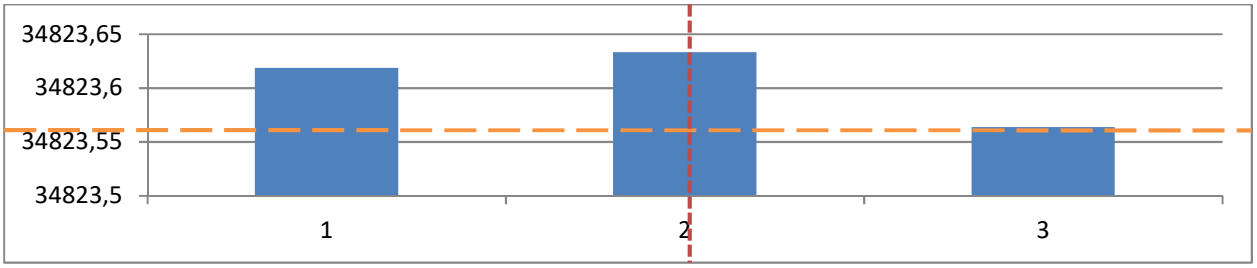

Figure 3-33: Correlation peak analysis for NLOS conditions - version a

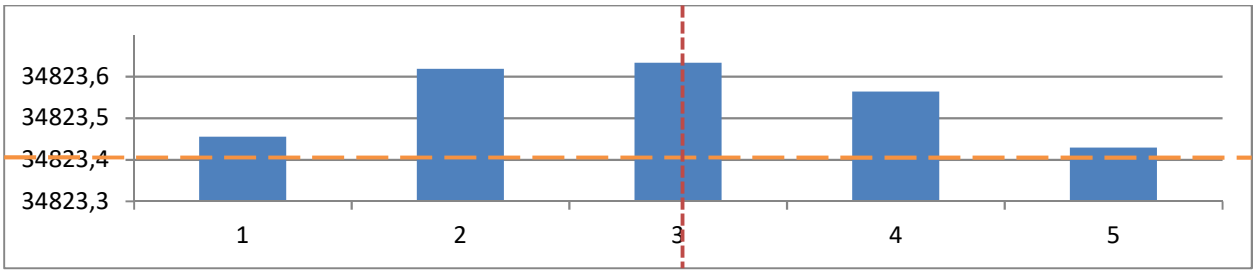

Figure 3-34: Correlation peak analysis for NLOS conditions - version b

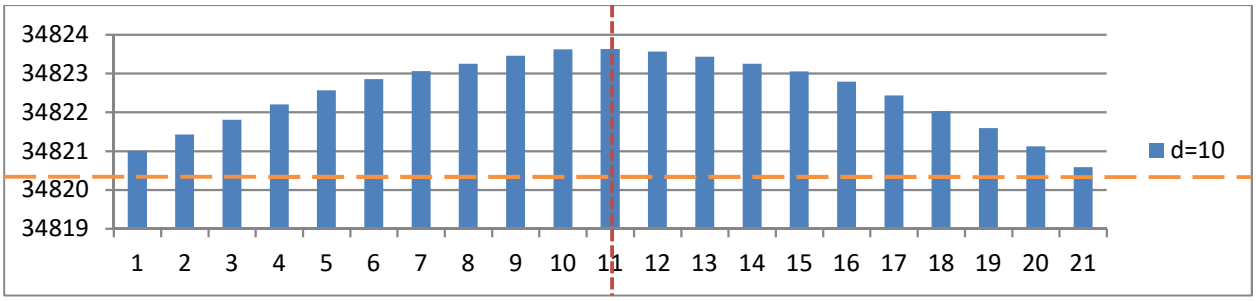

Figure 3-35: Correlation peak analysis for NLOS conditions - version c

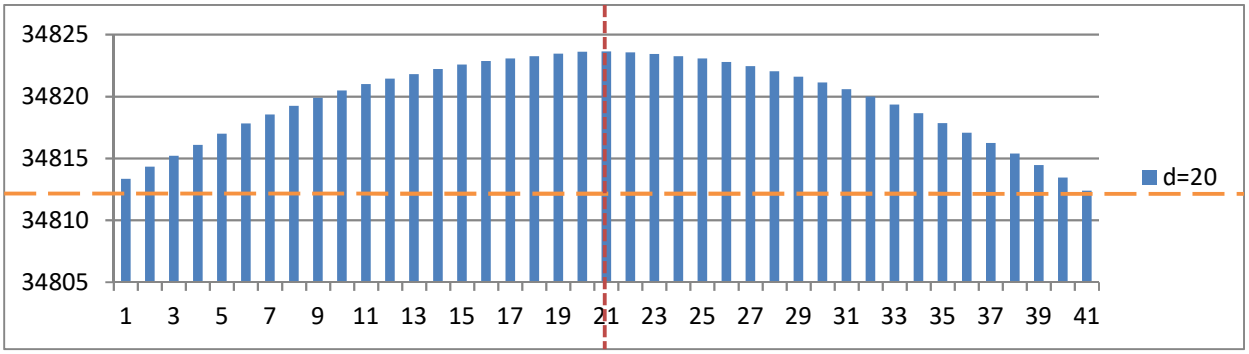

Figure 3-36: Correlation peak analysis for NLOS conditions - version d

All analyzes were performed for the AIS and VDES campaigns, where it should be emphasized that for the first campaign the correlators worked on samples of signals with GMSK modulation, and for the second campaign on samples of signals with π/4-QPSK modulation.

From the previously discussed results, it can be concluded that the biggest improvement of the obtained results was obtained with the use of a double delta multi-correlator with a width of d2 = 20. Of course, it should be added that this is a conventional value, because in the range of width d2 between approximately 18 and 40 samples, these results were very similar to each other. Therefore, d2 = 20 was considered as the conventional and most representative value. For the data from both measurement campaigns, for the LOS scenario, the improvement in the determination of the distance accuracy was noticeable for a part of the sampling period. Thanks to this, e.g. for the AIS campaign, it was possible to correct the distance errors by up to about 4 meters. However, for the VDES campaign, this result was

even around 1 meter. It should also be taken into account that for the AIS campaign, one sample corresponded to 6 meters of distance, while for the VDES campaign, one sample corresponded to 1.5 meters.

In a situation where the measurements took place beyond the Hel Peninsula, i.e. for the NLOS environment (in this case, the aquatic environment), no significant improvement was noticed. Due to the effect of noise on the received signals, the correlation peak was not always of a shape that would allow the distance accuracy to be reliably determined. For such cases, the determined error in the worst cases counted up to 8 samples in relation to the distance determined by the basic or extended correlator based on the adjacent samples to the main peak. This means that if the double delta multicorrelator also took samples separated by d2 = 20 for analysis, it could take samples which were dominated by noise. In such a situation, the determined distance accuracy may be incorrect.

On the basis of the data analyzes and simulation tests performed, it was possible to see the influence of multicorrelators on the determination of the accuracy of the distance between the transmitting antenna and the receiving antenna.

In the next measurement campaign, it is best to use three correlators for processing and detailed data analysis:

- Basic correlator,
- Extended correlator based on a pair of adjacent samples,
- Extended correlator with the double delta concept additionally based on the second pair of samples d2 = 20.

By recording the results for the three types of correlators, we are able to obtain the most reliable data. For the LOS situation, in our case to the Hel Peninsula, for later analysis it will be possible to take into account the data from the double delta multicorrelator d2 = 20, because these results will be the most accurate and burdened with the lowest error. On the other hand, beyond the Hel Peninsula, data from the basic and extended correlators can be used for analysis. Such an addition to the overall analysis of the results will help to obtain distances that will not be affected by additional error caused propagation phenomenon

3.3 Research on the effectiveness of a multicorrelator in a measurement campaign

The research was carried out using the results obtained during the June 2019 measurement campaign. The sample registration took about 4 hours at that time, which allowed us to collect over a thousand useful files for analysis. The route from Gdynia to Karlskrona was analyzed (Fig. 3-37).

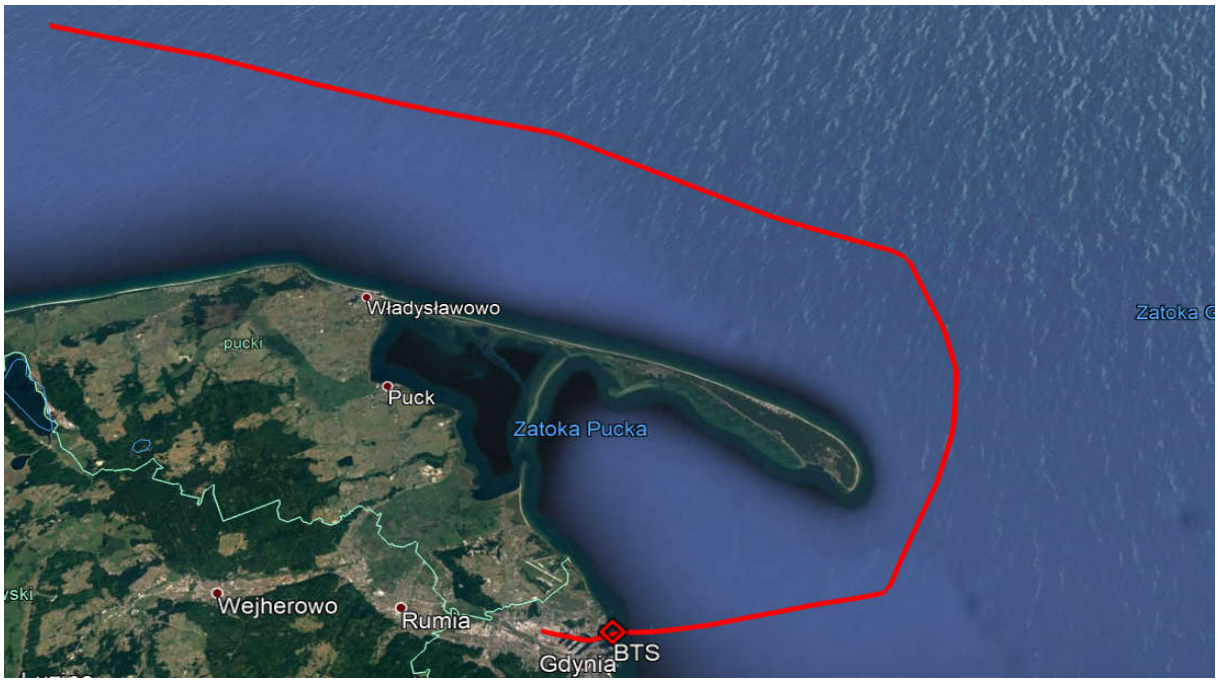

Figure 3-37: The analyzed Gdynia - Karlskrona measurement route from the 2019 measurement campaign

In order to check whether the multicorrelator can improve the obtained results, four correlation scenarios (Fig. 3-38, Fig. 3-39, Fig. 3-40, Fig. 3-41) were considered for the purposes of the analysis. In the first scenario, the very top of the correlation peak was simply analyzed looking for samples with the maximum value. In the second analysis, the peak and its adjacent samples were analyzed. In the third, the analysis of the peak, adjacent samples and samples separated by 10 samples from the peak with the maximum value were analyzed. Finally, for the fourth scenario, the distance between these samples was set at 20.

Scenario 1

$d_1 = Sample\_MAX$

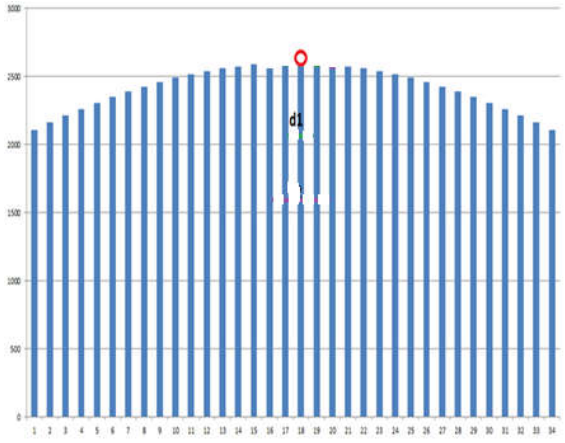

Figure 3-38: Measurement scenario a)

Scenario 2

$d_1 = 2 * T_s$

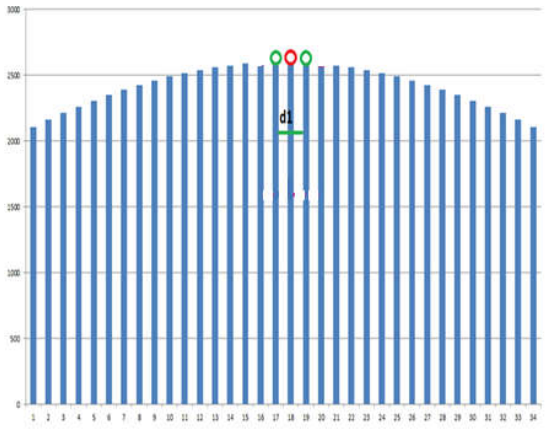

Figure 3-39: Measurement scenario b)

Scenario 3

$d_1 = 2 * T_s$

$d_2 = 10 * T_s$

Scenario 4

$d_1 = 2 * T_s$

$d_2 = 20 * T_s$

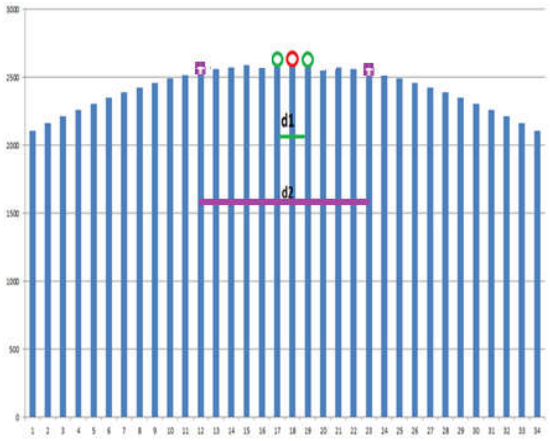

Figure 3-40: Measurement scenario c)

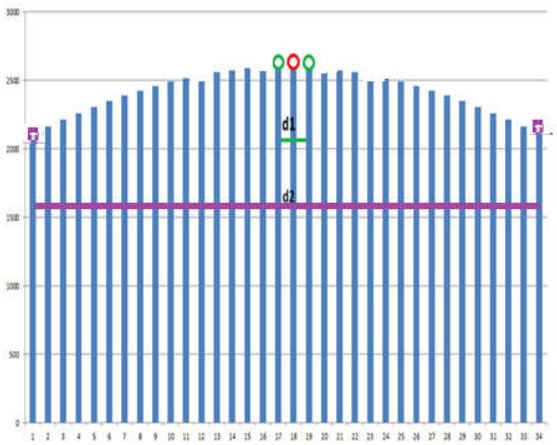

Figure 3-41: Measurement scenario d)

The results for the double delta correlator with span d2 = 20 samples are shown below. The chart shows only the best result due to the fact that the results of the rest of the correlators closely corresponded to the results for the basic correlator (AIS campaign, Fig. 3-42). The results obtained for the base correlator, which was used in data processing in 2019, are also shown below (Fig. 3-43).

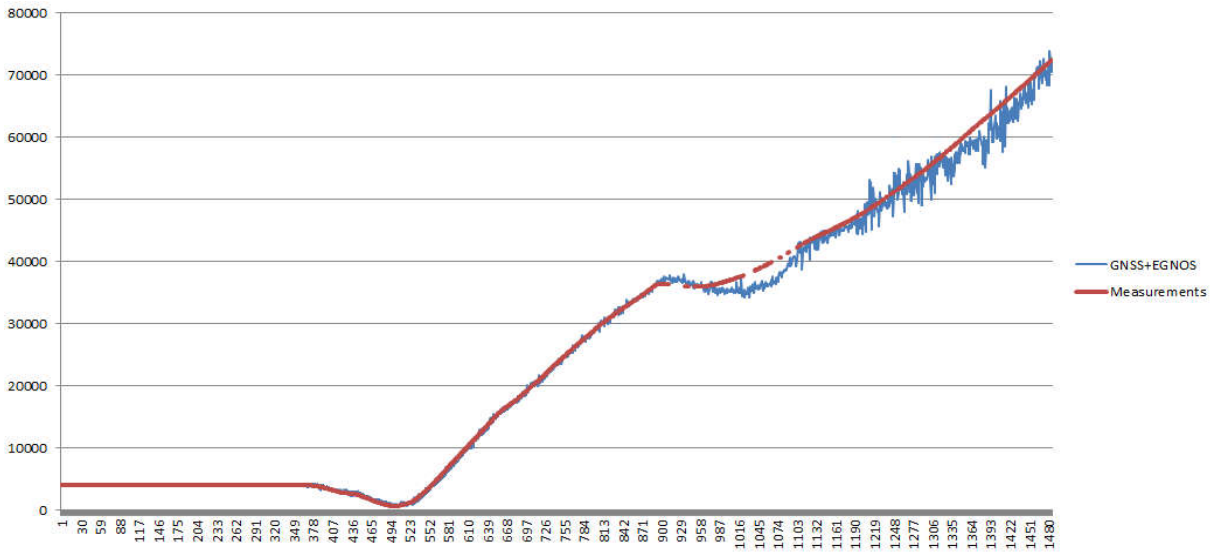

Figure 3-42: Data processed with an extended correlator

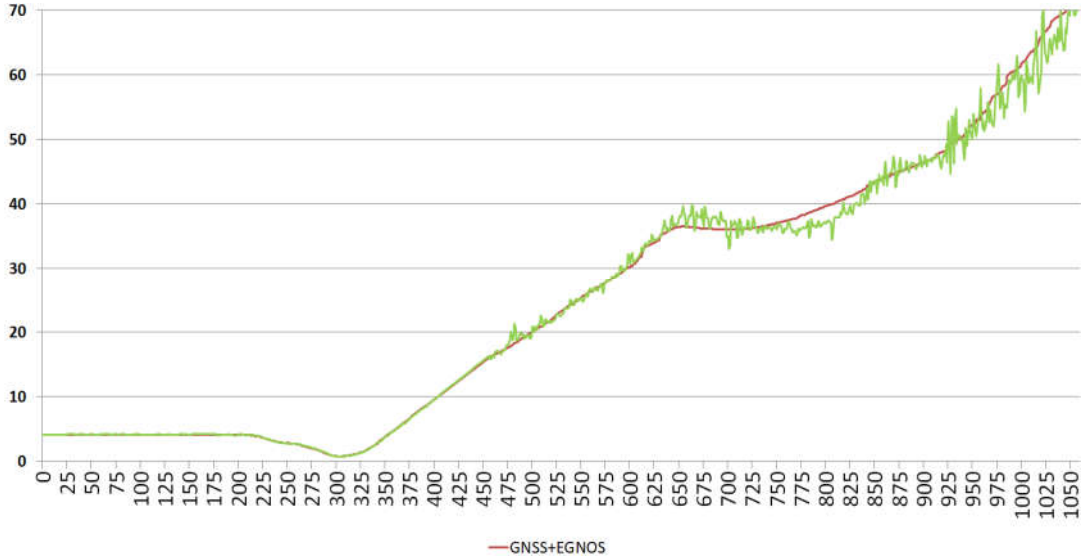

Figure 3-43: Data processed with the primary correlator

At first glance, it's hard to draw any conclusions. A detailed analysis of the AIS campaign conducted in 2019 was included in the previous report. After processing the same data with a double delta correlator, it was possible to see a slight improvement of the determined distance accuracies.

Below is a demonstration photo showing the measurement methodology in the port of Gdynia (Fig. 3-44). The waveforms of the signals in the time course with different disturbances are also presented below (Fig. 3-45, Fig. 3-46).

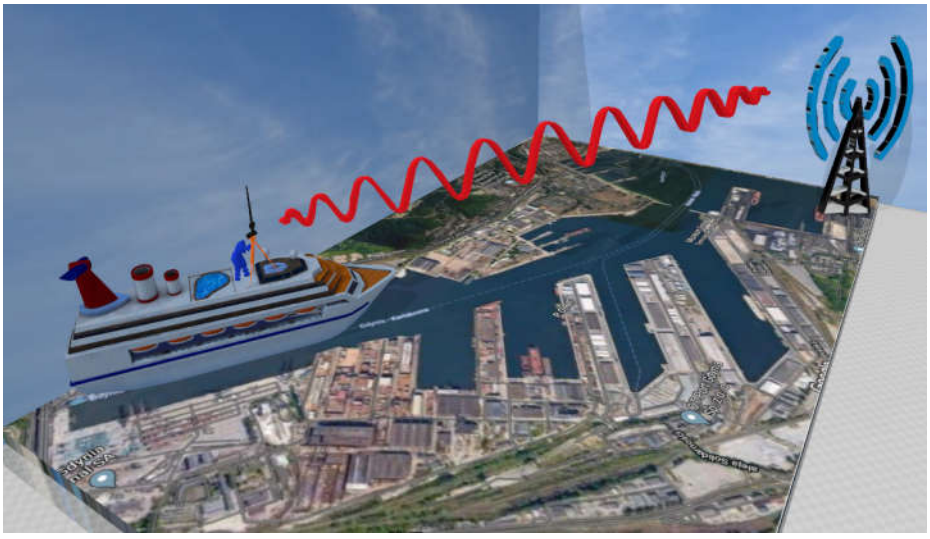

Figure 3-44: Measurement scenario in the port of Gdynia

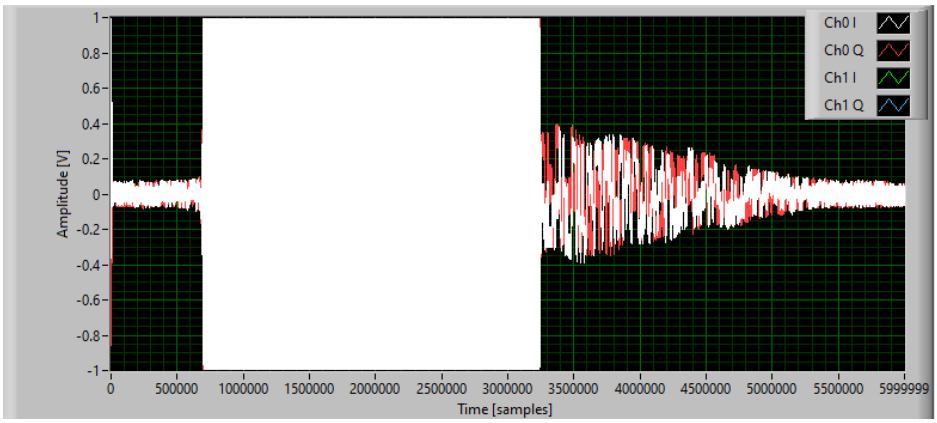

Figure 3-45: A significant part of the useful signal is disrupted

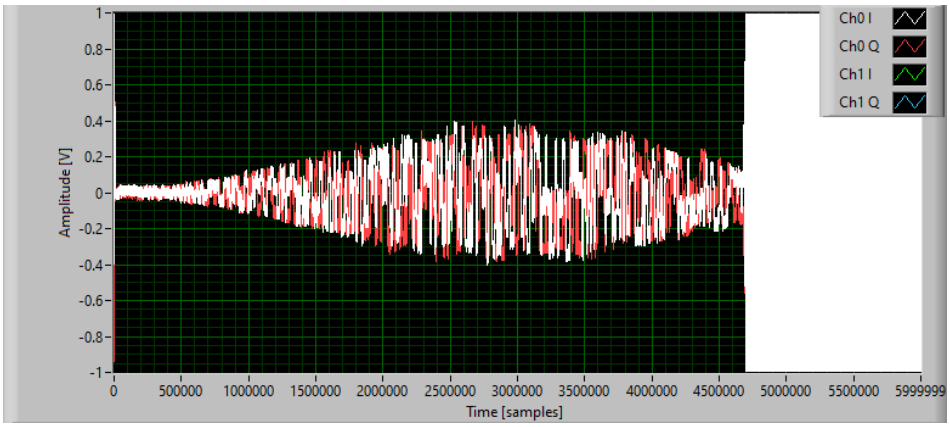

Figure 3-46: End part of useful signal disrupted

The picture below shows the measurement methodology for LOS measurements (Fig. 3-47), i.e. from the Bay of Gdansk to the Hel Peninsula. In the next figure, we can see a graph showing how the double delta correlator improved the distance accuracy results compared to the fundamental correlator (Fig. 3-48).

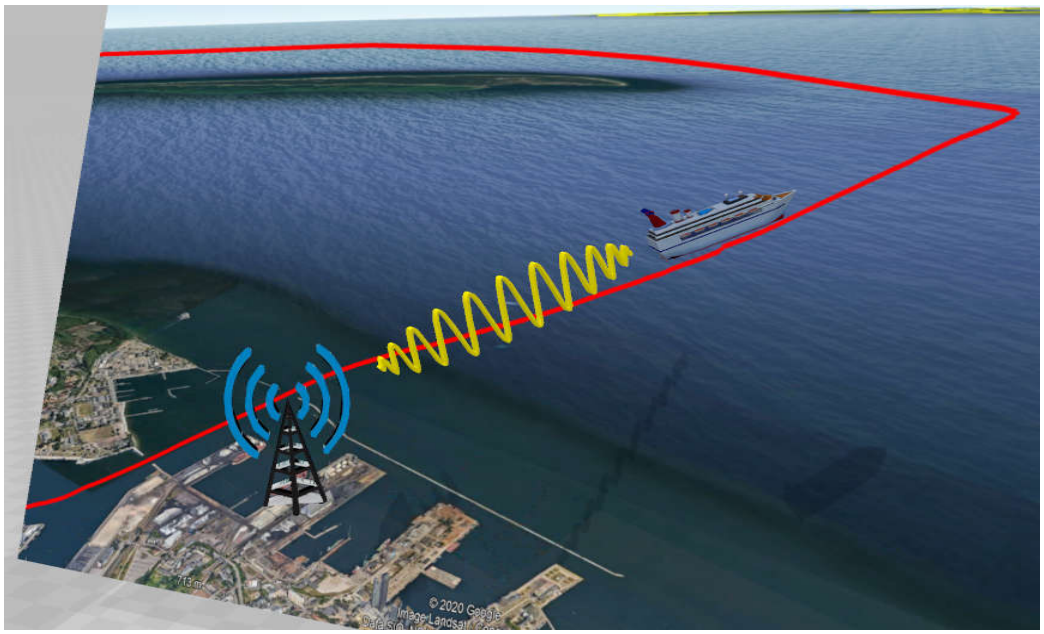

Figure 3-47: Scenario with dynamic measurements

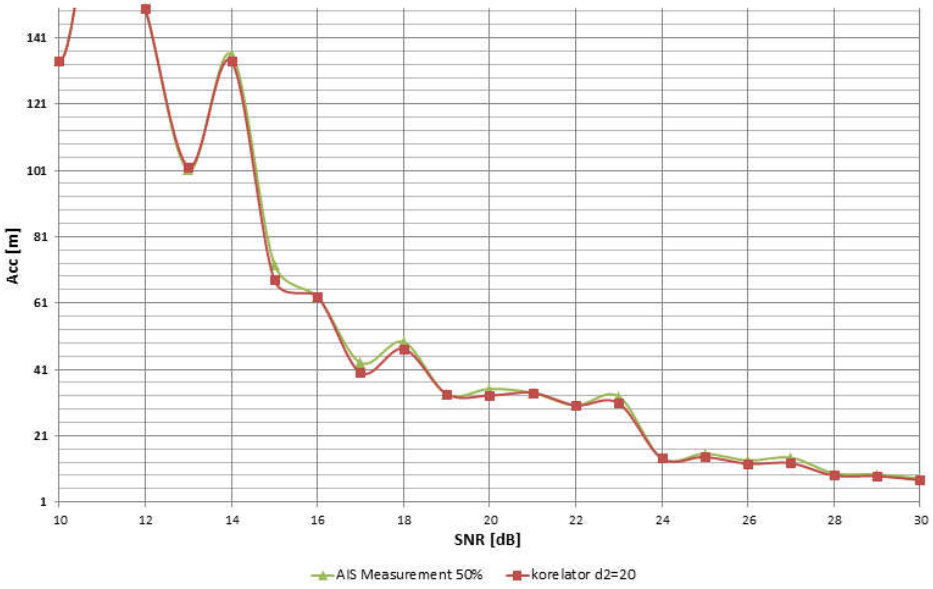

Figure 3-48: Graph of the obtained RMS depending on the correlator used

The results for the double delta correlator with span d2 = 20 samples are shown below (Fig. 3-49, Fig. 3-50). The chart (Fig. 3-51) shows only the best result due to the fact that the results of the rest of the correlators closely corresponded to the results for the basic correlator (VDES campaign).

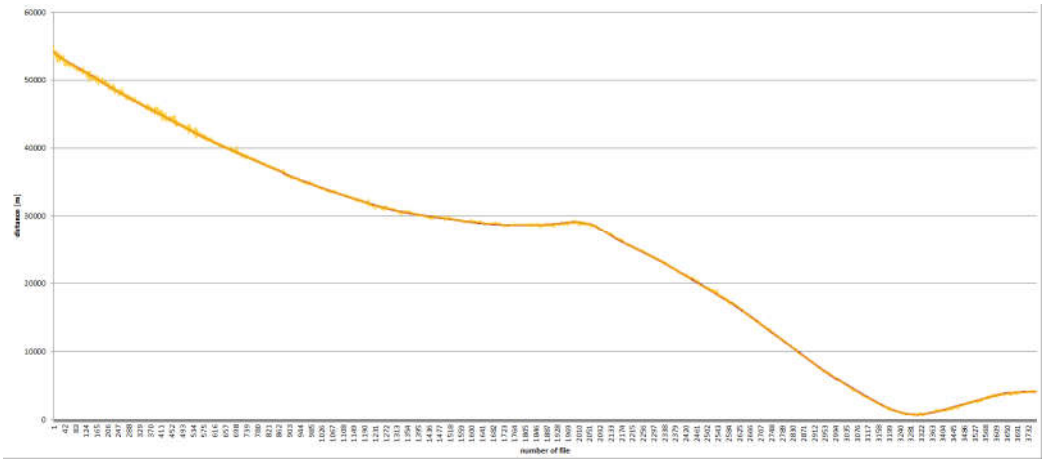

Figure 3-49: Results for VDES campaigns processed with an extended correlator

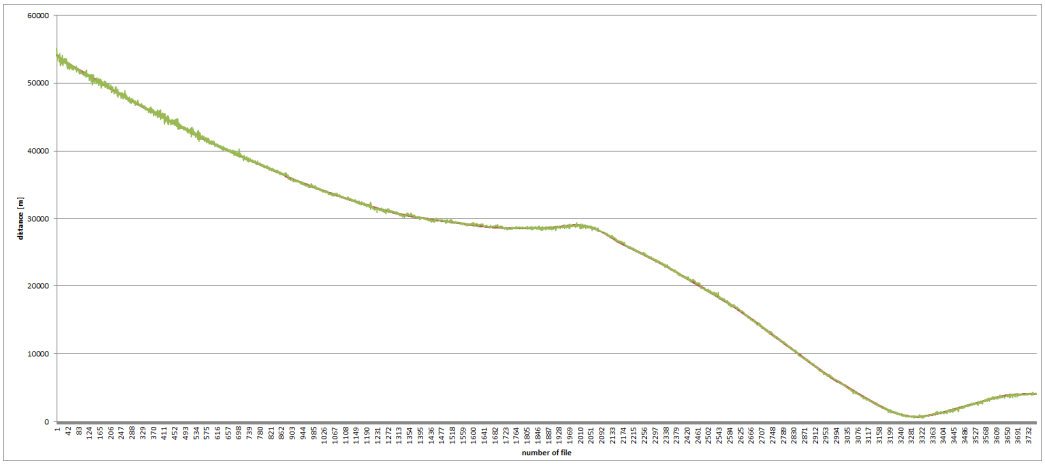

Figure 3-50: Results for VDES campaigns processed with the basic correlator

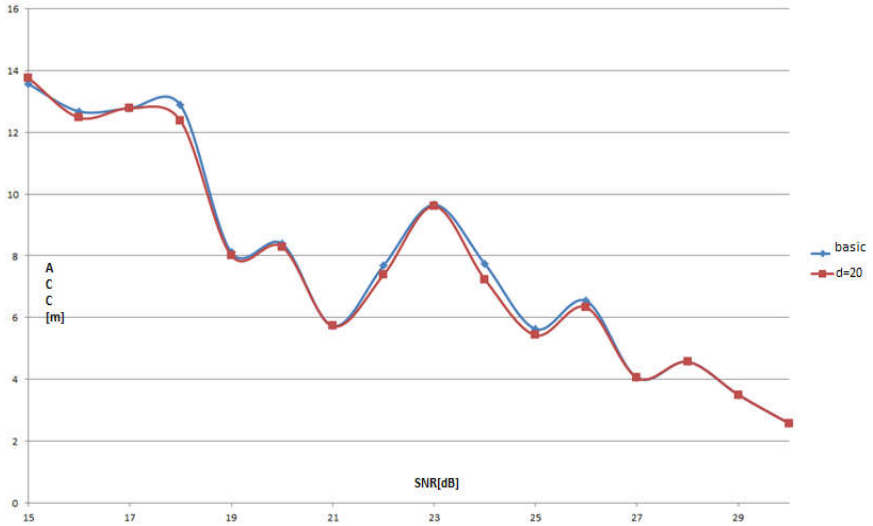

Figure 3-51: RMS chart for VDES campaigns

One of the most important features of the double delta multicorrelator in these cases is its capability of analyzing the peak shape changes not only within the next two samples relative to the main peak but also for greater ranges.

The chart above shows only the best result for the correlator d2 = 20 because the results of the rest of the correlators closely matched the results for the base correlator. The main attention was devoted to the analysis of static data recorded on the ferry during the hour when the ferry was in the port. Data was recorded here from 22:40 to 23:50, thanks to which a solid portion of samples ready for analysis was obtained. Measurements were made at a distance of 4068 meters from the broadcasting station.

At this point, very high SNR was obtained, where the received signal power was very high in relation to the low noise power, which did not have a destructive effect on the received signal. In this case, for all mean errors subtracted, the best result was obtained for the double delta correlator with a sample spacing of 20 samples. The correlator in this case lived up to its task. Of course, during these measurements, some incorrectly determined distances were also found, but this is also due to other signals that we received. For such cases, the correlator may yield a false result. Likewise, the signal or noise power can be miscalculated due to the highly subtle power coming from another signal received on the same frequency at the same time.

To check the credible impact of the multicorrelator application, its effectiveness was tested during the LOS measurements between the port and Hel, i.e. up to about 20 km. After subtracting all the mean errors, the improvement in the determination of the distance accuracy by the multicorrelator in this area, it can be seen that the improvement was from one meter to even 4 meters at some occasions. The analysis of the rest of the correlators was omitted here due to very little improvement or deterioration of the results on the order of 0.01 meters. For the d2 correlator, the improvement in results was sometimes at the level of 2 m, but it occurred in very few cases.

The second data analysis was carried out for the data from the VDES measurement campaign, which was carried out in November 2019. In the same way, for the different types of correlators as for the AIS data, the analysis was performed for the VDES data. Also in this case, the correlator d2 = 20 gave the best results. The improvement of the determined distance at some points was in the order of 1 meter. These are lower results than for the AIS data, but in that campaign, one sample corresponded to an accuracy of 6 meters, while in the VDES campaign, one sample corresponded to a distance of 1.5 m.

4 R-Mode system – implementation

This section presents a description of all the modules forming the R-Mode positioning system. Our implemented solution consists of four cooperating modules - two hardware and two software modules.

They are presented in the diagram (Fig. 4-1) and their functions are as follows:

- RF module - periodically receives radio transmissions from the R-Mode stations and stores IQ samples,
- Signal correlation application - reads files with IQ samples, correlates them, and then, having information about the coordinates of the stations, determines the pseudoranges,
- GNSS receiver - records UTC time, GNSS position, speed and track angle. The first two parameters are used for accuracy comparison purposes, while the other two are fed to the input of the Kalman filter,
- R-Mode real-time positioning application - determines the position based on the calculated pseudo-ranges to the R-Mode stations and additionally using Kalman filtration. It also determines positioning errors with respect to GNSS position.

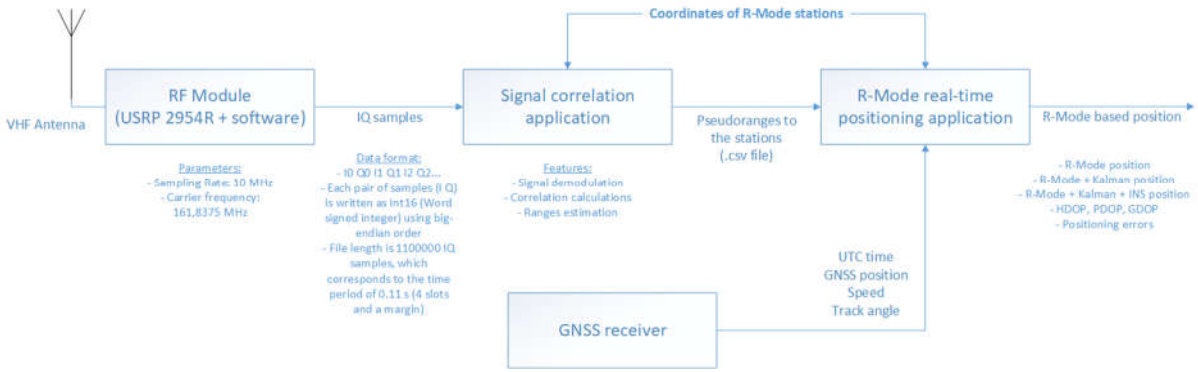

Figure 4-1: A diagram of the implementation of the R-Mode system

All system components are described in the following sections.

4.1 Test-bed for the VDES transmission

To improve performance and accuracy of distance determination, new USRP modules and new software (described in the next subchapter) were used. The diagrams of the transmitting and receiving parts of the test-bed for VDES transmission are illustrated in Figures 4-2 and 4-3, respectively.

The main components of the R-Mode test system are the NI USRP 2954 programmable radios responsible for transmitting and receiving test signals, as well as the Quartzlock E80 GPS rubidium oscillators, which provide a stable source of time and frequency. It is particularly important for the measurements of the radio signal propagation time. In addition to the above-mentioned elements, the measuring stations were built with the use of appropriate filters, power amplifiers and antennas, as well as the GNSS receiver u-blox EVK-M8 [4-1], necessary to record the reference values: UTC time, coordinates, speed, course and DOP values.

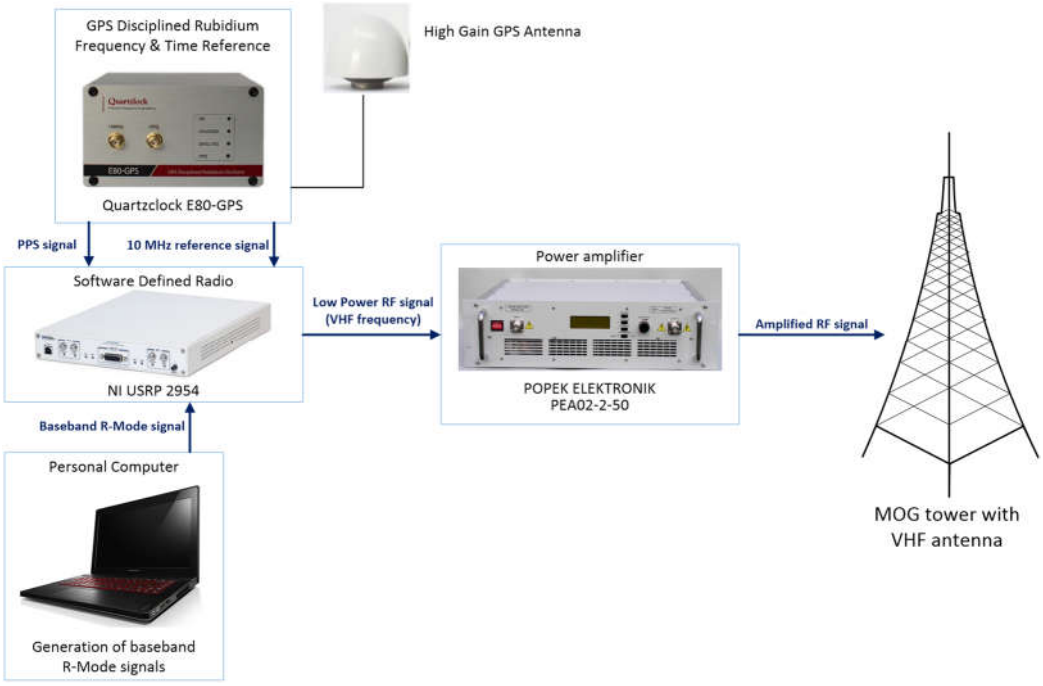

Figure 4-2: Test-bed transmitter diagram for the VDES transmission

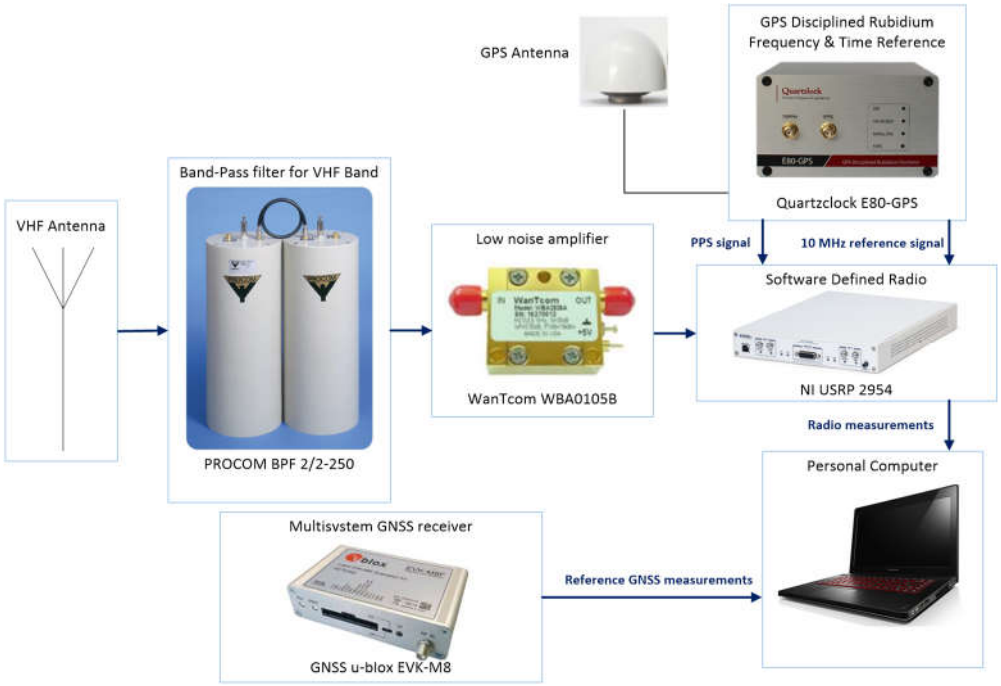

Figure 4-3: Test-bed receiver diagram for the VDES transmission

The R-Mode demonstration stand uses a highly-accurate GNSS-M1G2 receiver (Fig. 4-4,4-5), [4-2]:

Figure 4-4: New GNSS receiver used in the R-Mode project (1/2)

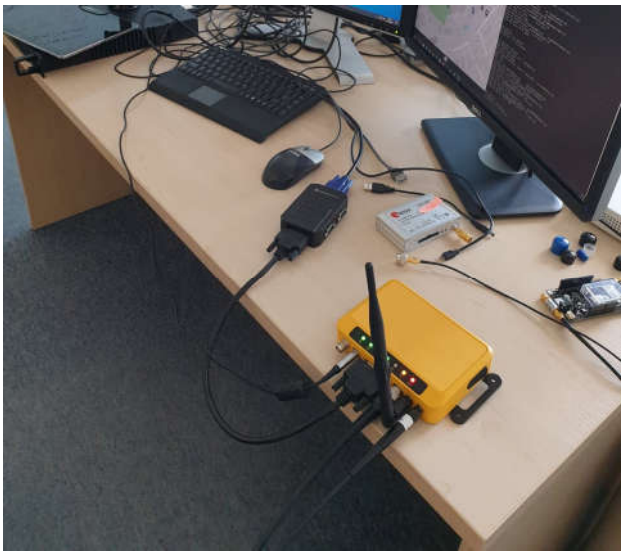

Figure 4-5: New GNSS receiver used in the R-Mode project (2/2)

The new algorithm for calculating the reference distance between the transmitter and receiver has been implemented based on GNSS navigation data; it utilizes the so-called Vincenty's formulae method. The Vincenty's formulae are two related iterative methods used in geodesy to calculate the distance between two points on the surface of a spheroid, developed by Thaddeus Vincenty. They are based on the assumption that the figure of the Earth is an oblate spheroid, and hence are more accurate than methods that assume a spherical Earth, such as great-circle distance.

The most important parameters of the new USRP 2954 model are specified below.

USRP 2954 transmitter parameters [4-3]:

• Frequency range: 10 MHz to 6 GHz,
• Frequency step: <1 kHz,
• Maximum output power: 50 mW to 100 mW (17 dBm to 20 dBm),
• Gain range: 0 dB to 31.5 dB,
• Gain step: 0.5 dB,
• Frequency accuracy:
  - 25 ppb (not locked to GPS),
  - 5 ppb (locked to GPS),
• Maximum instantaneous real-time bandwidth: 160 MHz,
• Maximum I / Q sample rate: 200 MS / s,
• Digital-to-analog converter (DAC):
  - 2 channels
  - Resolution: 16 bit,
  - Spurious-free dynamic range (sFDR): 80 dB.

USRP 2954 receiver parameters [4-3]:

• Frequency range: 10 MHz to 6 GHz,
• Frequency step: <1 kHz,
• Gain range: 0 dB to 37.5 dB,
• Gain step: 0.5 dB,
• Maximum input power: -15 dBm,
• Noise figure: 5 dB to 7 dB,
• Frequency accuracy:
  - 25 ppb (not locked to GPS),
  - 5 ppb (locked to GPS),
• Maximum instantaneous real-time bandwidth: 160 MHz,
• Maximum I / Q sample rate: 200 MS / s,
• Analog-to-digital converter (ADC):
  - 2 channels
  - Resolution: 14 bit,
  - Spurious-free dynamic range (sFDR): 88 dB.

The most important parameters of the POPEK PEA02-2-50 broadband power amplifier:

- Frequency range: 20 ÷ 1000 MHz, 1000 ÷ 2000 MHz
- Output power: ≥ 60 W typ. ; ≥ 50 W min.
- Output power @ 1 dB compression gain: ≥ 60 W typ. ; ≥ 50 W min.
- Gain for small signals: 47 dB min., 50 dB max
- Small Signal Gain Wave: <± 1.5 dB typ., <± 2 dB max.
- Waveform with ALC on ≤ ± 0.8 dB.

The characteristics of the filter used are presented below (Fig. 4-6), [4-4]:

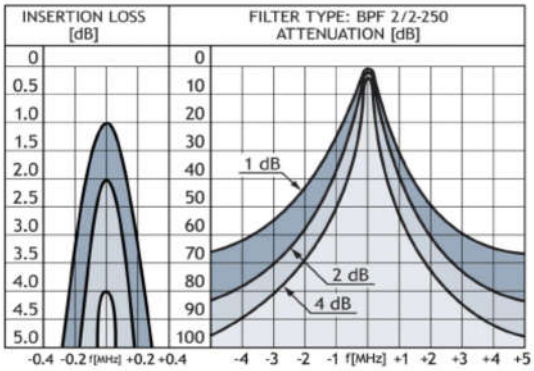

Figure 4-6: Characteristics of the filter used

Parameters of the transmitting antenna Radmor 32812/1:

- Frequency range: 146 ÷ 174 MHz,
- Nominal input impedance: 50 Ω,
- WFS in the antenna operating band: <1.6,
- Vertical polarization,
- Energy gain in relation to the λ/2 dipole: 0 dBd (2.15 dBi),
- The radiation pattern in the horizontal plane: omnidirectional,
- The radiation pattern in the vertical plane: octal,
- Half power angle in the vertical plane (E vector): 70°.

Receiving antenna parameters APS 40 VHF 156 H - 5/8 L:

- Frequency range: 155 ÷ 165 MHz,
- Energy gain: 5.5 dBi,
- VSWR: <1.5: 1
- Impedance: 50 Ω,
- Polarization: vertical.

4.2 USRP application

In the R-Mode system, the distance between base station and mobile station aboard the ship is determined using the TOA method which is based on the measurement of radio signal propagation time. Therefore, the key issue is to ensure transmission and reception start of R-Mode messages in precisely defined moments of time. For this purpose, the triggers are utilized in the USRP modules. They are used for generation and acquisition synchronization to the timestamp specified by the 'Start Trigger Time' properties. The 'Start Trigger' occurs when the onboard device timer reaches the timestamp specified by the user. Therefore, the operation of setting the trigger and data transmission/reception must be performed periodically - in a loop.

Applications have the following features:

- full configurability of radio parameters,
- reading/writing signals from/to the file in the form of IQ samples,
- possibility of graphical signal presentation,
- automation of measurements,
- monitoring of application's operation and logging of its configuration and possible errors.

In the report "AIS and VDES Ranging – measurements results" the flowcharts of the transmitting and receiving applications are illustrated. The schemes of the measurement applications for the VDES transmission has not changed, only some modifications were necessary:

- A new 64-bit version of LabView and a new USRP Driver,
- AIS signal covered 5 time slots, while VDES - one slot,
- The single VDES transmission measurement file has 22.8 MB (due to the higher IQ rate and better resolution), while the AIS transmission measurement file was 11.4 MB in size,
- Different frequency of receiving messages. Due to the higher performance of the USRP 2954, the recording of samples for VDES transmission was performed every second (for the AIS transmission - every 4 seconds). In both cases, the measuring signal was transmitted every 3 seconds. So, for VDES the useful signal was recorded in 1 of 3 samples, whereas for AIS – in 1 of 12 samples.

4.3 Signal correlation application

As part of the implementation work, the software application responsible for the AIS and VDES signals correlation (in order to determine the distance between the transmitting and receiving antennas) has been extended with additional functional modules, which gave much greater possibilities of data analysis compared to the previous version of the application. One of the major changes was the implementation of an advanced double delta multicorrelator. The multicorelator itself was based on adjacent samples around the main peak, while the double delta multicorrelator also performed a possible delay correction on the basis of a second pair of samples separated by a predetermined value from the main peak (see chapter 2). From the simulation tests performed, it was possible to observe how the distance determination accuracy works with the use of a multi-correlator in the conditions of multipath,

but also in the scenario when the distance was determined for low sampling rates. Based on the research, three types of correlators have been implemented in the application:

- basic correlator based on the sample with the maximum value;
- extended multicorrelator based on a pair of adjacent samples;
- extended multicorrelator with the concept of double delta, additionally based on the second pair of samples.

Such an advanced correlator is able to analyze the entire correlation peak (which may be distorted under the influence of noise, reduced signal strength and multipath) and calculates the distance with greater accuracy. Another extension in the application was the implementation of the module with an automatic detection of the type of file selected for analysis (which is very useful when recording files with different sampling rates and different correlation sequences). The possibility of selecting the correlation sequence used to determine the distance (Gold sequence / training sequence / alternating sequence), the ability to select the sampling frequency, the ability to select the type of message processed (AIS / VDES / 1 slot message / 2 slot message) and the ability to activate the Hann window have also been added. The application also includes a module for analyzing the effectiveness of the double delta multicorrelator. Additionally, a graphical visualization mode of the processed data has been introduced (graph of calculated distances, graph of averaged distances, graph of the average calculated distance for the stationary measurement mode). One of the main changes to the application was the addition of a module for stationary research (algorithm for long-term data processing / data processing from a specific location on the disk / option of making the application wait for new data to arrive).

All the details of the signal correlation application were described in the previous report. The screenshots (Fig. 4-7, 4-8, 4-9) below show the modified (extended) version of the application.

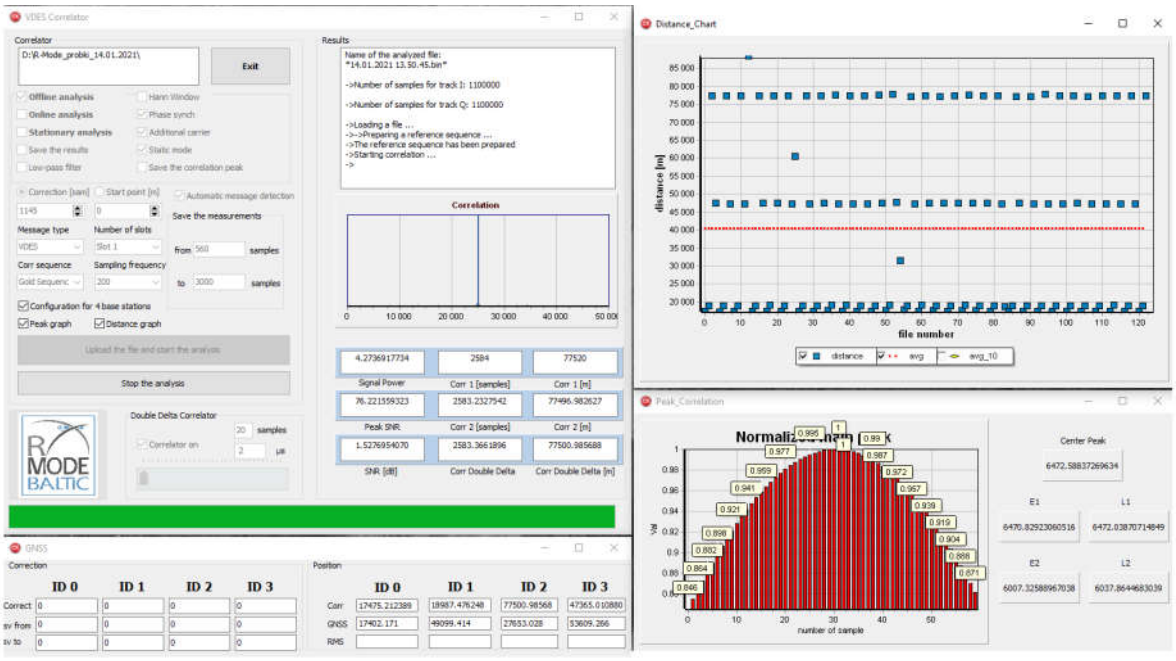

Figure 4-7: Signal correlation application for 4-slot message a)

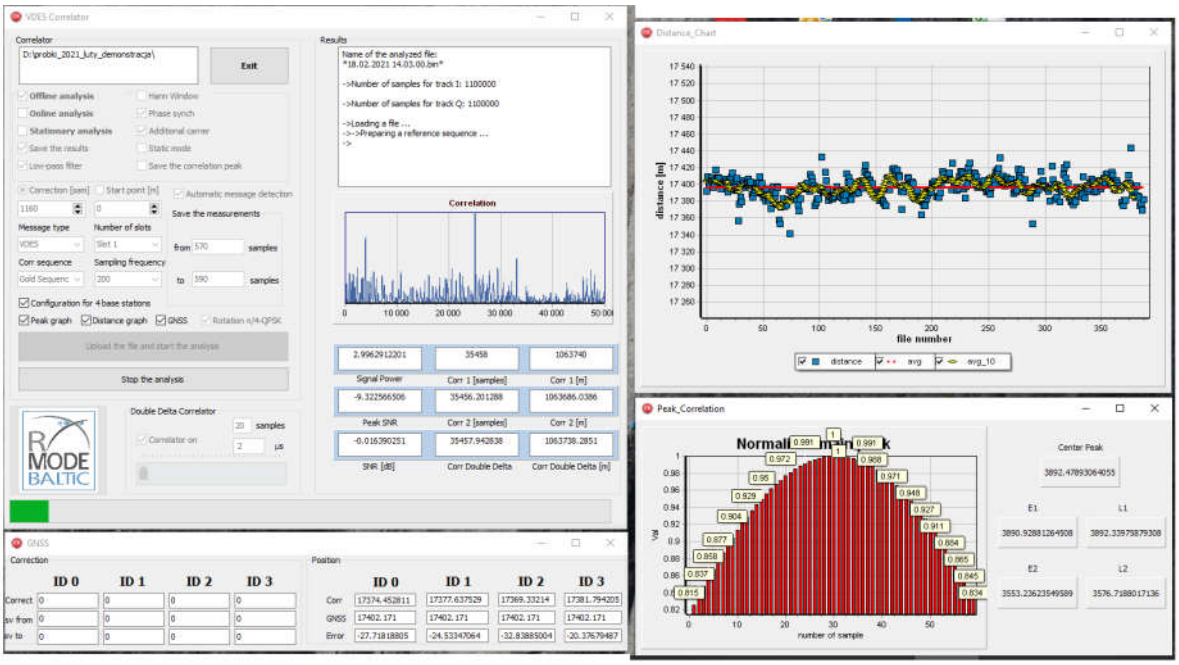

Figure 4-8: Signal correlation application for 4-slot message b)

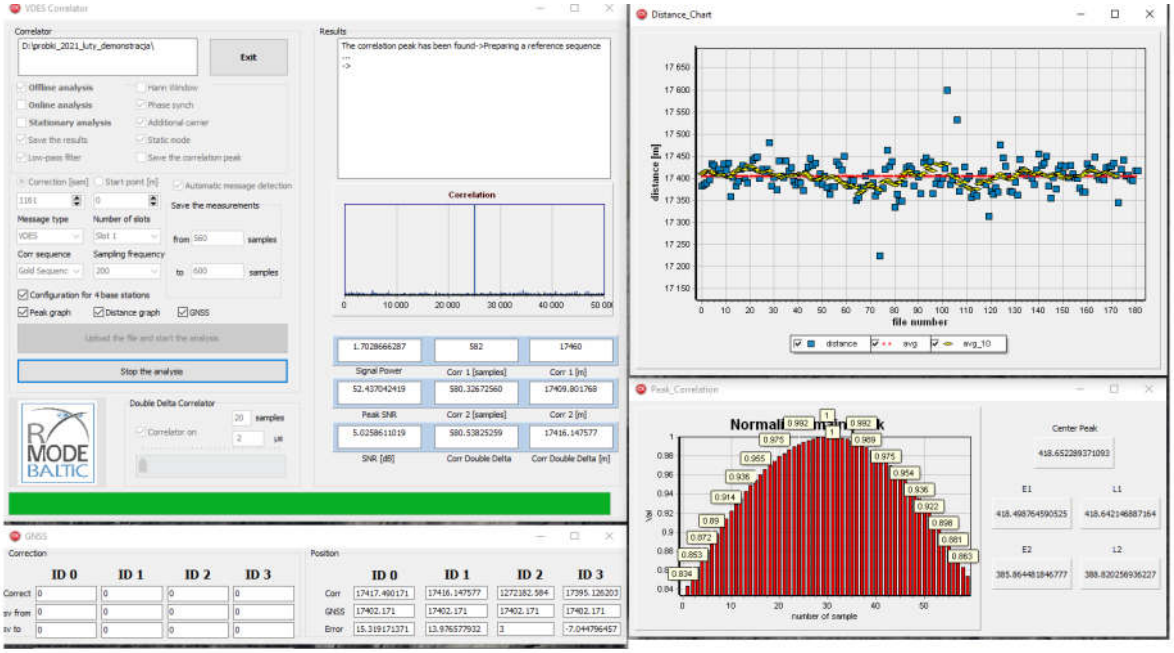

Figure 4-9: Parallel correlation for four signals in different time slots

For the purposes of the project, measurement scenarios emulating the presence of four base stations were also created. This has been implemented in the signal correlation application. This allowed for a parallel correlation for the four time slots. The picture above shows just such an example (Fig. 4-9).

4.4 R-Mode positioning application

As part of one of the tasks of the R-Mode Baltic project, a prototype reference station for the terrestrial location system was built at the Z-8 premises. This station, based on the decision of the President of the Office of Electronic Communications and in cooperation with the Maritime Office in Gdynia, was launched and is currently operating in the Port of Gdynia. Due to the Institute's budget constraints, only one such station could be built in the project. As part of the measurement campaign of the National Institute of Telecommunications, the project made it possible to collect data based only on this single reference station. This allowed for measurement verification of errors as a function of the distance from the station, as well as the range within which measurements of the signal propagation time can be performed with the accuracy required in the project. It is therefore necessary to use simulations for the implementation of the Institute's tasks under R-Mode Baltic.

The use of the prepared simulator with the integrating module allowed for the simulation of the operation of the entire complete location system. The simulator was supplied with measurement data that came from the constructed reference station and was collected as part of the measurement campaign in the Baltic Sea. In simple terms, the use of the simulator in the R-Mode project will allow to estimate the mobile terminal location based on (a) the measured propagation time of the reference signal coming from the real base station and (b) simulated measurement results from at least three virtual reference stations. The quality of the system operation will be verified on the basis of a comparison of the estimated position with the known, real position of the terminal.

The location simulator designed for the analysis of measurement results consists of modules that provide the following functionalities:

- location of the terminal using the TOA method,
- determination of the HDOP (Horizontal Dilution of Precision) and PDOP (Position Dilution of Precision) coefficients,
- simulation of measurement errors' sources resulting from various factors (drift and offset of reference station clocks, drift and offset of terminal clock, noise impact from the SNR level of the reference signal, influence of the propagation environment),
- calculation of position estimation errors and determination of error values for the confidence levels of 50%, 80%, 90%, 95% and 99%,
- graphical user interface for static, dynamic and measured scenarios,
- a module that allows to enter measurement data from the R-Mode Baltic project and their integration with the existing part of the software,
- results visualization module with the possibility of drawing 3D charts for static scenarios,
- automatic generation of .kml files that allow to visualize on the map (in Google Earth) the real and estimated locations of the mobile terminal and its position in relation to reference stations,
- scenario visualization module with measurement data with the ability to analyze the results using four different types of graphs: positioning error and distance measurement error, positioning error and HDOP and PDOP (Position Dilution of Precision) coefficients, errors in determining the distance from the terminal for each reference station and the function RMS (Root Mean Square) of the positioning error depending on the SNR (Signal to Noise Ratio) of the measured station signal,

- Kalman filtration module.

In order to add the measurement results to the simulator, complete information on the location of the reference stations is required. It is necessary to provide its exact latitude and longitude in degrees and the height of the antenna suspension above sea level in meters. The Browse button opens a dialog box, allowing the user to select a file containing the measurement data. The measurement data must be placed in a *.txt* file with a specific structure. The subsequent lines in the file correspond to the subsequent measurements. The file should contain the following columns:

- Real latitude of the terminal, in degrees (from GNSS data),
- Real longitude of the terminal, in degrees (from GNSS data),
- Measured distance from the reference station, in meters,
- SNR value of the reference station signal for which the measurements are being made,
- Terminal speed, in kilometres per hour (from GNSS data),
- Terminal course, in degrees (from GNSS data),
- Measurement time, date and time (from GNSS data).

The application window where the measurement data can be added is shown in figure 4-10.

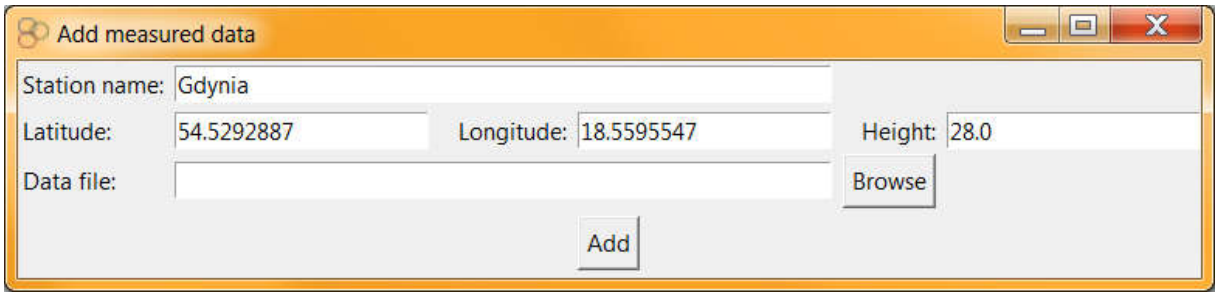

Figure 4-10:Measurement data adding window

In order to perform the simulations, it is necessary to add simulated reference stations, on the basis of which - together with the measurement results - the estimated location of the terminal will be determined. The minimum number of simulated reference stations in the measured scenario is two. However, in the case of an unfavorable geometry of the reference stations arrangement in relation to the terminal, this number may be insufficient due to the occurrence of irreversibility of the matrix in the TOA algorithm.

Measured scenarios, both static and dynamic, can be saved by the user. The data containing the saved scenario configurations are stored in files with the *.json* extension.

The appearance of the main window of the positioning simulator is shown in figure 4-11.

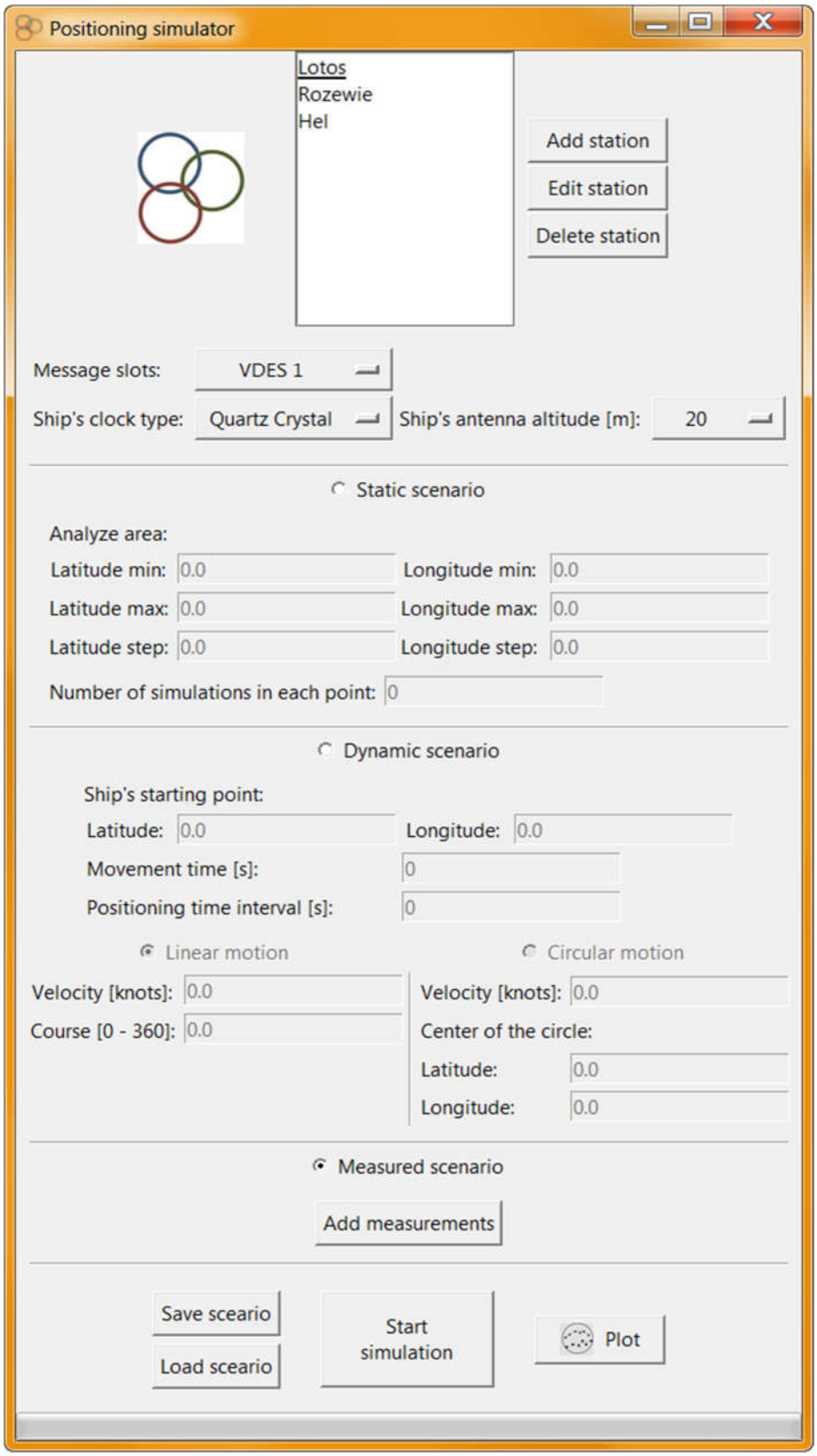

Figure 4-11: The main window of the positioning simulator

The data obtained at a distance of up to 75 km from the prototype reference station in Gdynia was used for the simulation. The remaining reference stations are fully simulated using the developed software. The use of rubidium oscillators was simulated; it was assumed that for each of the stations,100 seconds elapsed since the last synchronization. The EIRP power of the signal transmitted by all simulated reference stations was 46 dBm. The height of the receiving terminal suspension is 25 m above sea level. Reference stations with actual locations (shown in Figure 4-12) and actual antenna suspension heights are as follows:

- Gdynia (real station) – 28 m.a.s.l.,
- Lotos (oil rig station) – 41 m.a.s.l.,
- Rozewie – 80 m.a.s.l.,
- Hel – 70 m.a.s.l.

Figure 4-13 shows a map with marked locations of:

- the reference stations - red color,
- the actual location of the terminal on the ferry route at the time of taking subsequent measurements – orange color,
- the terminal positions estimated by the TOA method on the basis of the obtained measurement results and simulated data - white color.

Figure 4-14 shows the values of errors in measuring the distance to the station in Gdynia and the values of errors in estimating the location of the terminal calculated on the basis of measurement and simulated data, as well as the actual distance to the station in Gdynia.

Figure 4-15 shows the values of the HDOP and PDOP coefficients resulting from the current geometry of the location of the reference stations in relation to the terminal. The obtained position estimation errors, also visible in the previous graph, are plotted as well.

Figure 4-16 is a visualization of the error values in determining the distance from individual stations. For the station in Gdynia (top) it is the measurement error, for the others - these are simulated errors from various sources. Also marked is the actual distance from the terminal for each station.

The last graph, in Figure 4-17, shows the dependence of the RMS value of the position estimation error on the measured SNR value of the R-Mode station reference signal. RMS values were determined independently for the 1 dB SNR intervals.

Figure 4-12: Location of reference stations (red) alongside the actual (orange) and estimated (white) terminal positions.

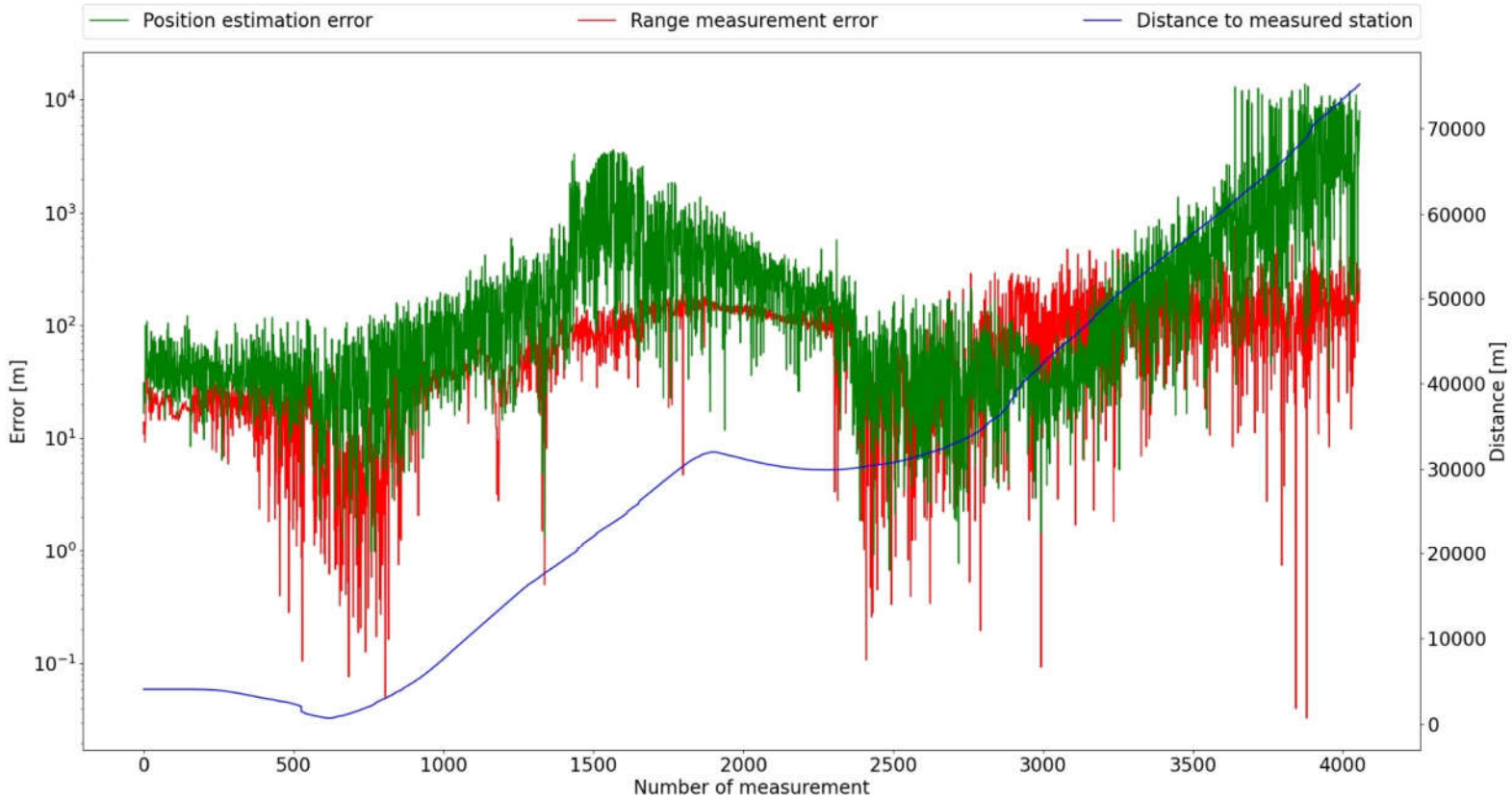

Figure 4-13: Error values for distance measurement and position estimation

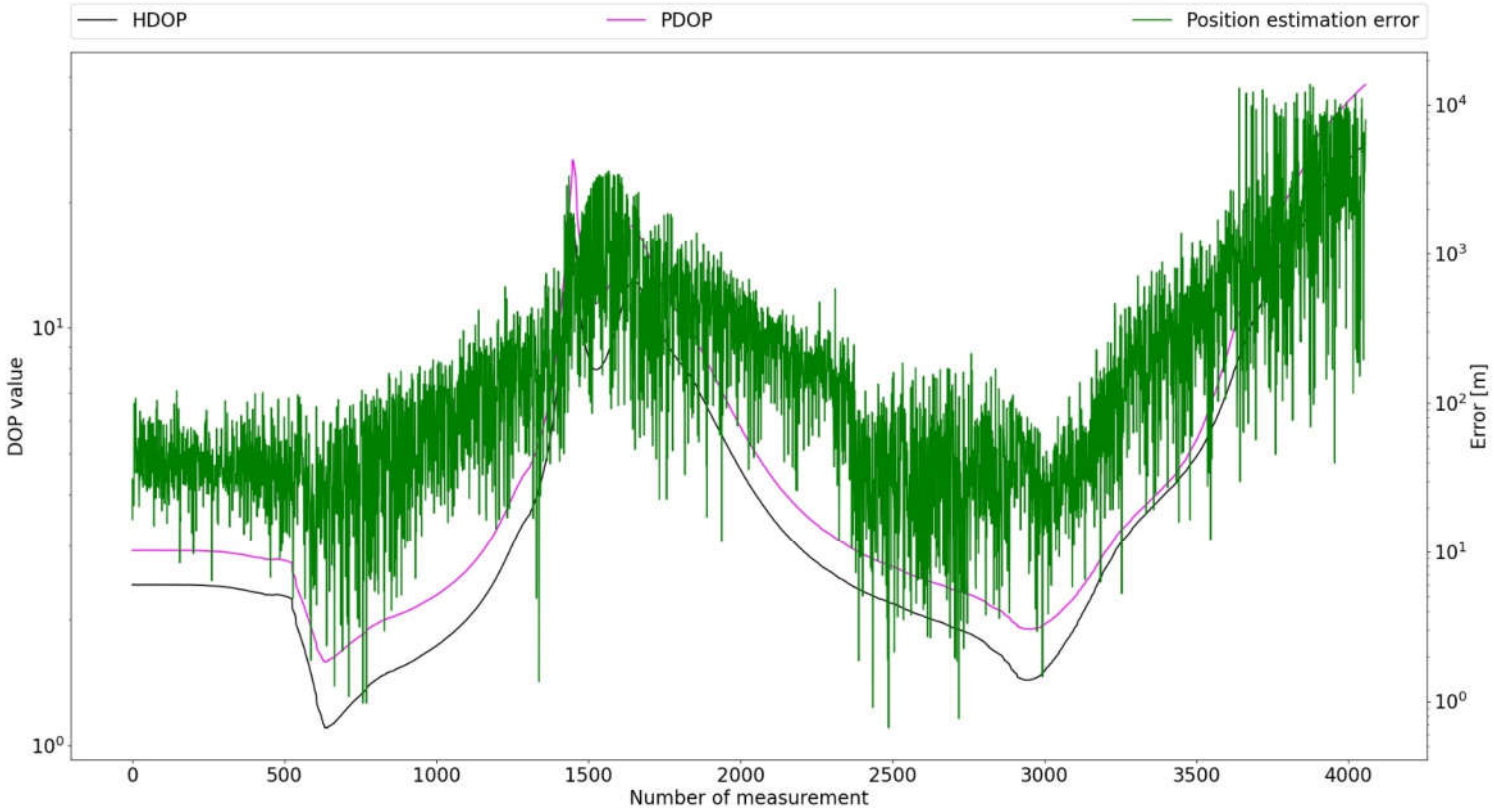

Figure 4-14: Values of HDOP and PDOP coefficients

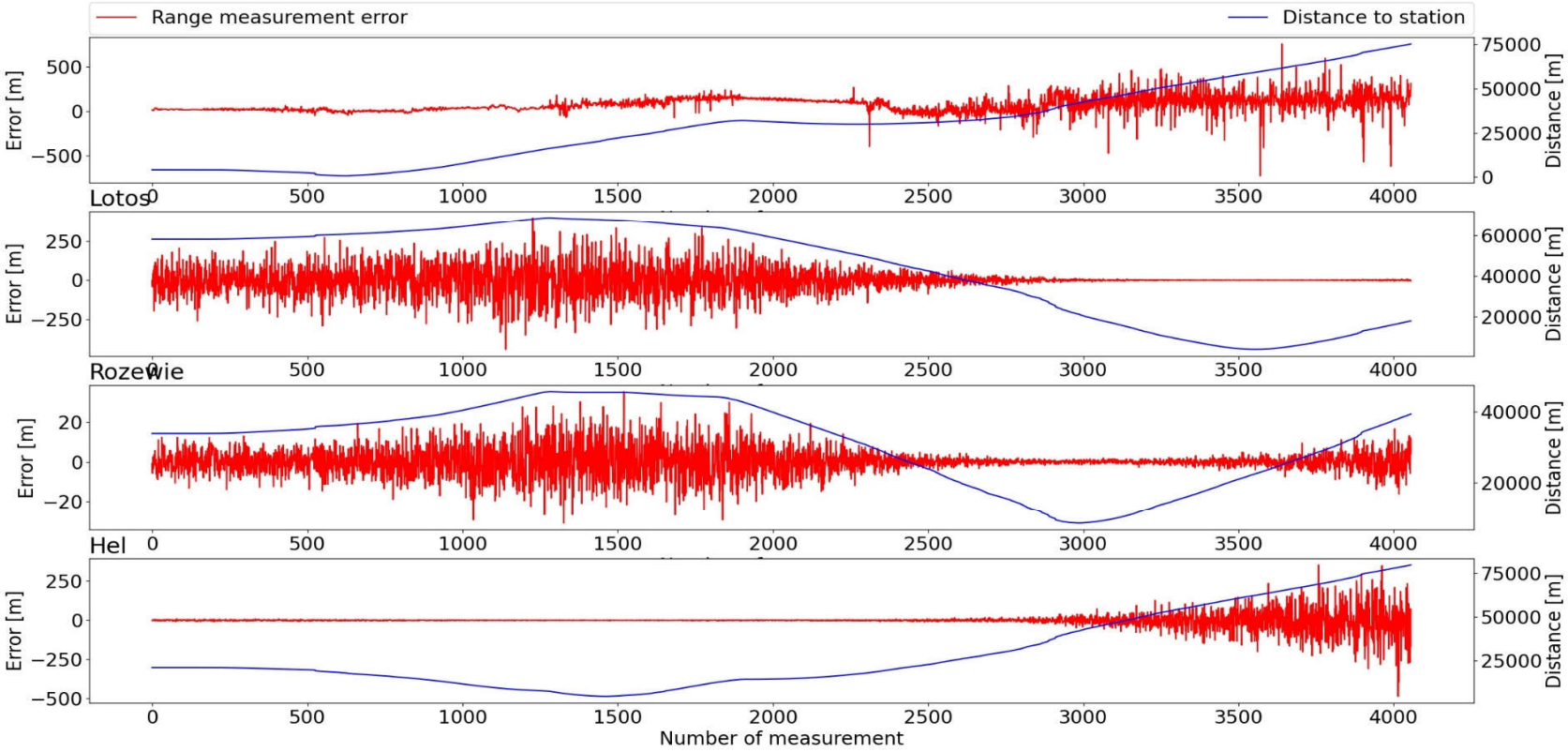

Figure 4-15: Error values of the distance from individual stations (top to bottom: Gdynia, Lotos, Rozewie, Hel)

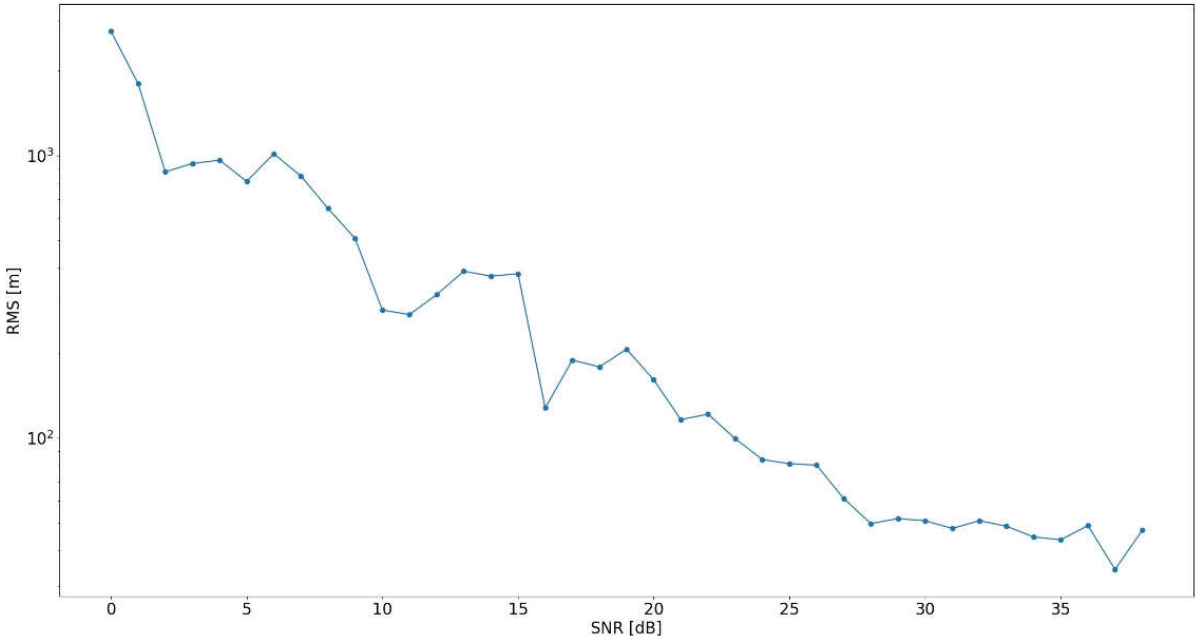

Figure 4-16: Dependence of the RMS value of the position estimation error on the value of the measured SNR of the R-Mode station.

As can be seen by analyzing the above graphs, the size of error in measuring the distance between the terminal and the reference station depends primarily on the distance to this station. This error is directly related to the decrease of the SNR value which results from the increase in propagation attenuation.
The value of the position estimation error depends largely on the distance to the individual reference stations and is generally slightly larger than the distance measurement errors. However, attention should be paid to the great importance of the geometry of the location of the reference stations. The position estimation error increases proportionally to the increase of the HDOP and PDOP coefficients values, which is particularly visible in areas with unfavorable geometry. In the vicinity of the “end” of the Hel Peninsula, a clear increase in position estimation errors can be observed, despite the short distance to the reference station.
As part of the tests, a similar simulation was carried out for the time from the last synchronization, amounting to 20,000 seconds (about 5.5 hours), where we obtained a similar accuracy of the terminal location estimation. This is because the errors caused by the loss of synchronization of the rubidium oscillator after a predetermined time are two orders of magnitude smaller than the errors caused by the power decrease of the reference signal.

For the purpose of the last measurement campaign carried out as part of the R-Mode Baltic project, a module for visualizing the results of the receiving terminal (ship) positioning in real time was developed. The window shown in Figure 4-17 shows the real-time positioning from the GNSS data and the positioning results from (a) the R-Mode system, (b) from the R-Mode system using Kalman filtration, and (c) from the R-Mode system using Kalman filtration and the INS module.

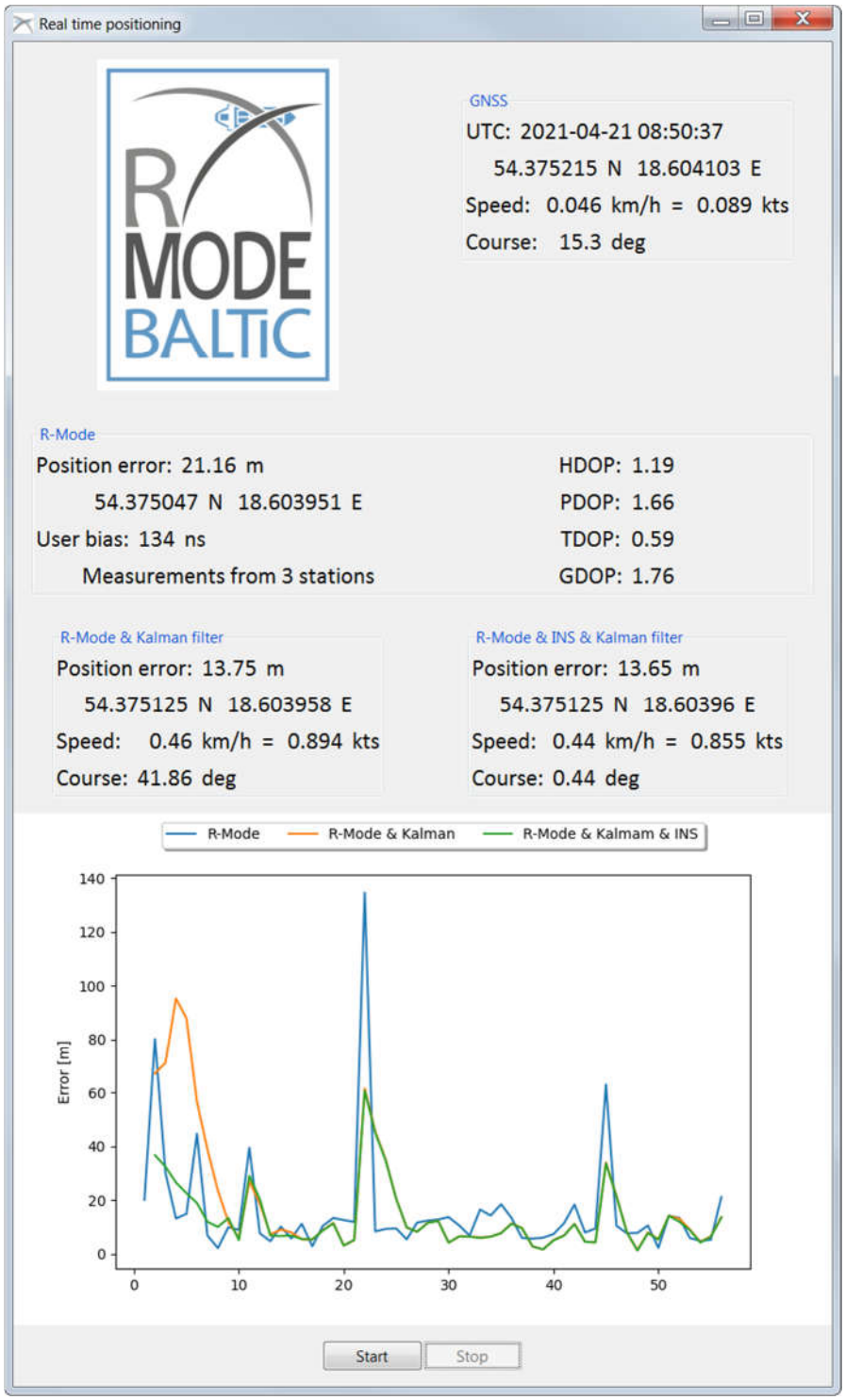

Figure 4-17: Real time visualisation window

Figure 4-18 shows a map with real-time visualization of positioning results. Orange color represents the actual position (based on GNSS), blue is the R-Mode position, black is the R-Mode position with Kalman filtration, and green is the R-Mode & Kalman & INS position.

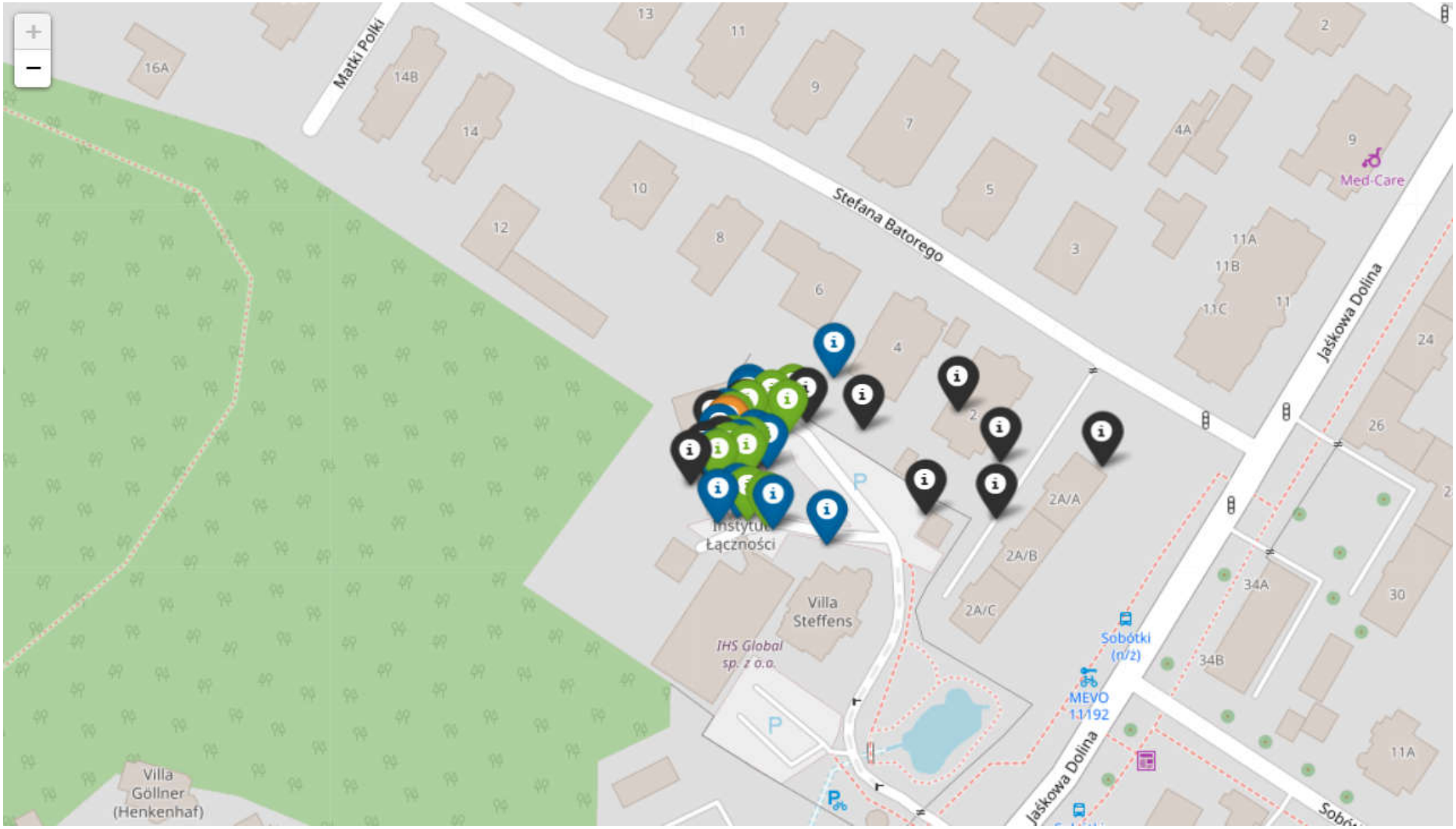

Figure 4-18: Map with real-time visualization of positioning result

5 Analysis of the measurement campaign results

This chapter focuses on the analysis of the results of the VDES measurement campaign that took place in 2020. This was the third measurement campaign during the R-Mode project. As part of detailed analyzes, the following charts were obtained, thanks to which it was possible to explain and understand many interesting phenomena along the measurement route:

- measurement chart for the route to Karlskrona,
- measurement chart for the route to Gdynia,
- SNR measurement chart,
- graph of measurements of the main-peak-to-side-peaks ratio,
- accuracy error graph,
- RMS curves for all measurements,
- RMS curves for the water environment,
- RMS curves for the terrestrial environment,
- impact of the width of the Hel peninsula on the RMS,
- map with accuracy errors in the measurement campaign,
- comparison of results from the AIS campaign with the VDES campaign.

5.1 VDES R-Mode campaign preparations

National Institute of Telecommunications (NIT) organized two measurement campaigns of the VDES R-mode System. Both took place on the Baltic Sea waters, i.e. in the target environment of the future system.

For the purpose of the measurements, the Maritime Office in Gdynia (MOG) provided its VHF antenna installation located on the tower near the entrance to the port in Gdynia. It was the localization of the R-Mode testbed's transmitter (Tx) which was designed, built and installed by the NIT.

The testbed receiver (Rx) – also built by the NIT – was located aboard the Stena Line ferry operating between Gdynia and Karlskrona

The main goal of the measurements was the analysis of the impact of the maritime radio VHF channel on the ranging accuracy when using time-based methods (this analysis will be performed for different weather conditions).

In order to eliminate some sources of errors, the rubidium oscillators were installed on both ends of the radio link. Additionally, the exact locations of the transmitting/receiving stations were determined via RTK measurements and using GNSS+EGNOS.

The configuration for which the measurements were performed is shown below:

- Modulation: π/4-QPSK
- RRC filter and 100 kHz bandwidth,
- Data rate: 76,8 ksym/s,
- New USRP modules (higher sampling rate and better A/D converter resolution),
- Gold Code length: 1877 symbols,

- compared to the second measurement campaign, the Hann Window was not used this time,
- VDES physical layer will allow to achieve 8-fold increase of the data rate (consequently, the correlation's peak width will decrease 8 times). Additionally, VDE-TER modulation schemes and filtering mechanisms make the signal more suitable for both correlation and, consequently, also for navigation purposes,
- No filter on the transmitting side,
- Amplifier with higher output power levels (greater range of the station!),
- Different LNA and filter configuration on receiver side.

One week before the planned measurement campaign, calibration measurements were carried out. They were aimed at thorough preparation of the measuring equipment and checking all measuring modules. The table 5-1 contains information on the number of recorded files, which were later processed in the signal correlation application and during the validation of data reception.

Table 5-1: List of the number of files recorded during calibration

Route	Number of files	File size
The first point is 30 meters from the broadcasting station	1790	39,9 GB
The second point is located 450 meters from the broadcasting station	1690	39,2 GB
The NiT building is 17450 meters away from the broadcasting station	1908	42,2 GB

The graph below shows the results for the processed part of the files (Fig. 5-1):

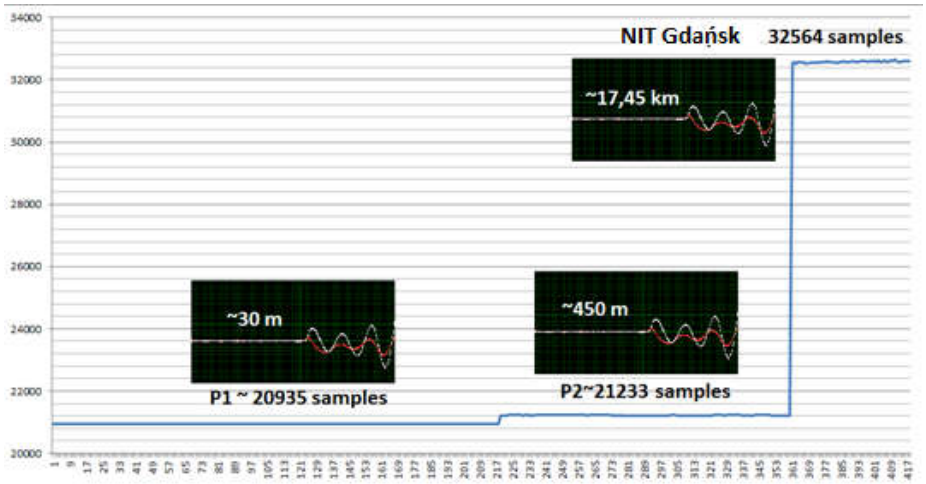

Figure 5-1: Processed calibration files

From the graph above, we can see that the calibration measurements ended with a positive result. The recorded sample files have been processed in the signal correlation application. All signals were correctly received and correlated. The obtained results allowed for the selection of a constant value of the number of samples that should be subtracted during the measurements. This correcting factor takes into account all cable delays and all other delays introduced by the samples' recording application. By subtracting the correctly calculated delay, the exact distances that are the result of a signal correlation application can be obtained.

Pictures from the calibration measurements that took place in the port of Gdynia are presented below (Fig 5-2, Fig. 5-3, Fig. 5-4, Fig. 5-5, Fig. 5-6, Fig. 5-7).

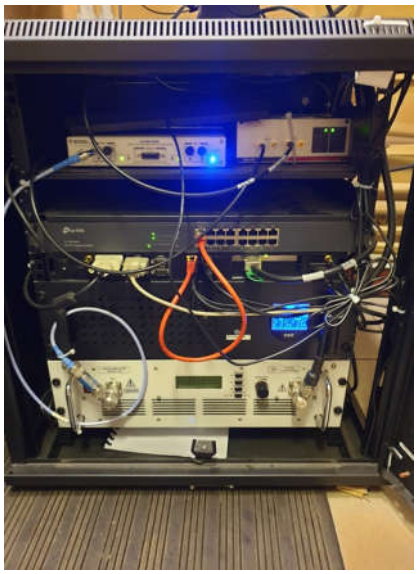

Figure 5-2: Photo from calibration a)

Figure 5-3: Photo from calibration b)

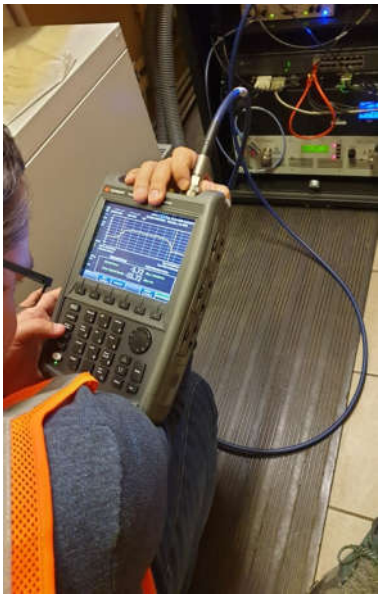

Figure 5-4: Photo from calibration c)

Figure 5-5: Photo from calibration d)

Figure 5-6: Photo from calibration e)

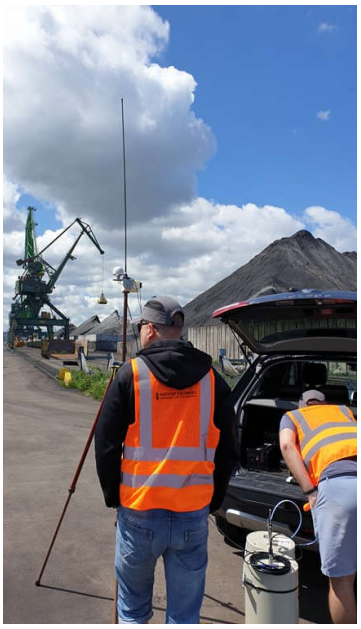

Figure 5-7: Photo from calibration f)

In the pictures below, we can see the signals recorded during calibration measurements in the NIT building. The recorded samples of I and Q are shown in Fig. 5-8. The next screenshot shows a calibration measurement scenario for receiving signals from the NIT building. The preview picture shows a map with the marked place of sending and receiving samples. We can also preview the recorded signal and show the signal correlation application that determined the distance based on the recorded signal (Fig. 5-9).

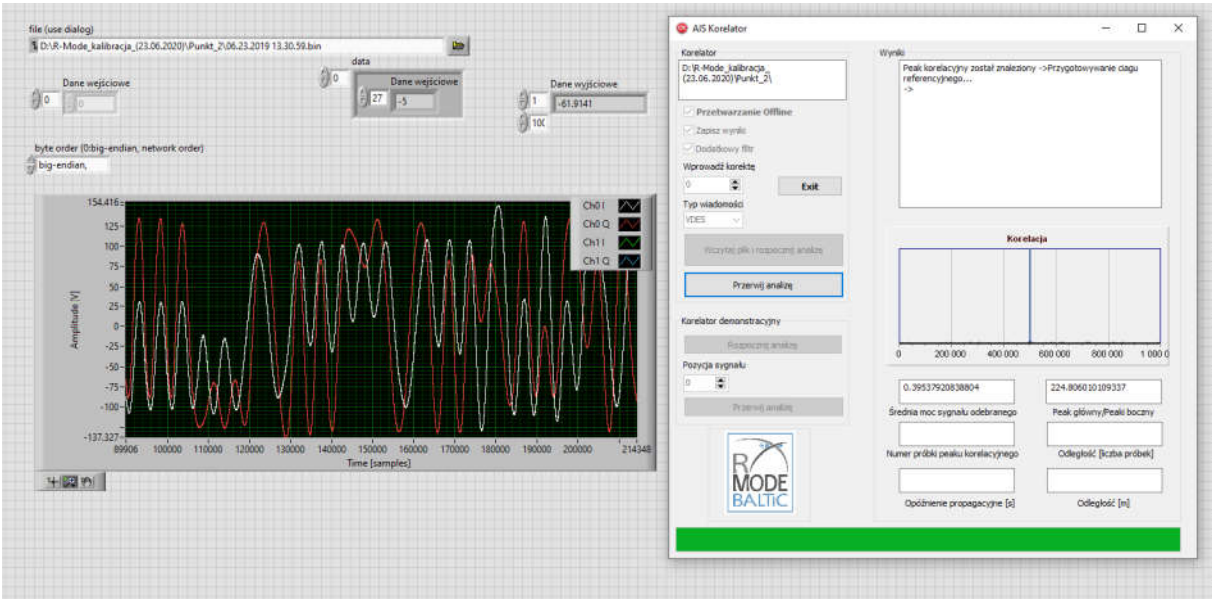

Figure 5-8: Application with recorded samples I and Q

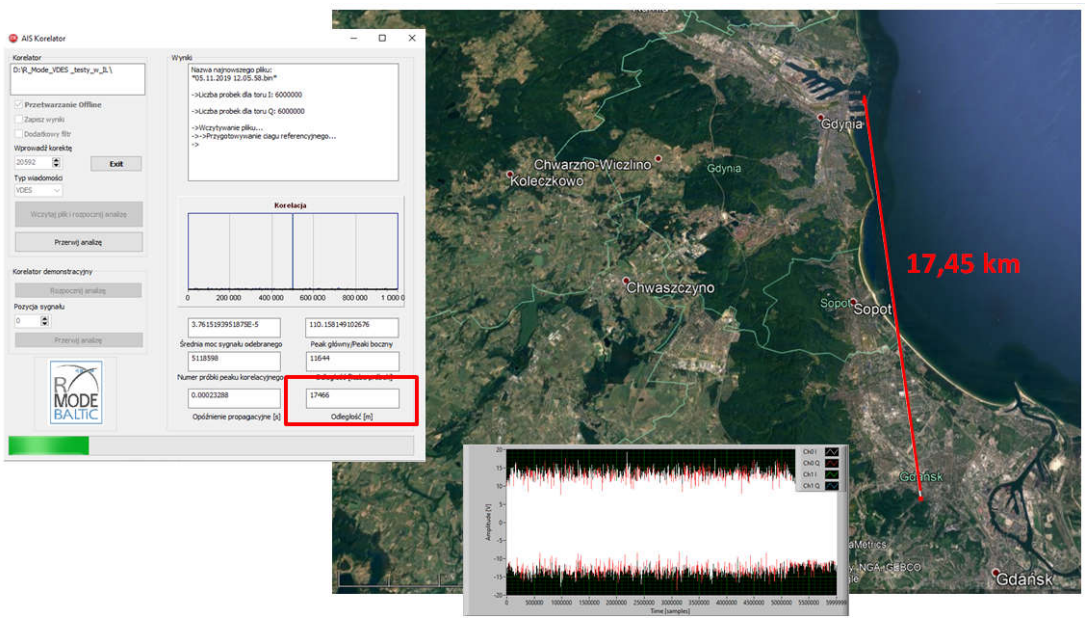

Figure 5-9: Application for the correlation of signals

5.2 Analysis of results from the VDES measurement campaign

The measurements took place on 29-30 June 2020. The table 5-2 below shows the number and size of the files which have been processed by the application for signal correlation.

Table 5-2: Number and size of processed files for VDES

Route	Number of files	File size
Gdynia – Karlskrona	20830	494 GB
Karlskrona - Gdynia	20700	470 GB

The table 5-3 gives the exact start and end times of the measurements.

Table 5-3: Time of processed files for VDES

Route	Start time	End time
Gdynia – Karlskrona	02:04:44	06:04:17
Karlskrona - Gdynia	16:16:32	22:10:33

Compared to the previous measurement campaigns, many more measurements records were collected during this campaign. The reason for that was the expected increase in the range of the received signal caused, among others, by removing the Hann window from the transmitted signal and by removing the VHF filter on the transmitting side.

Pictures from the measurement campaign are presented below (Fig. 5-10, Fig. 5-11, Fig. 5-12, Fig. 5-13):

Figure 5-10: Photo from measurements a)

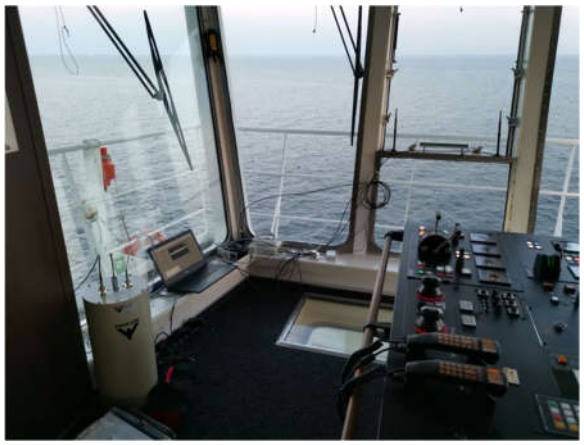

Figure 5-11: Photo from measurements b)

Figure 5-12: Photo from measurements c)

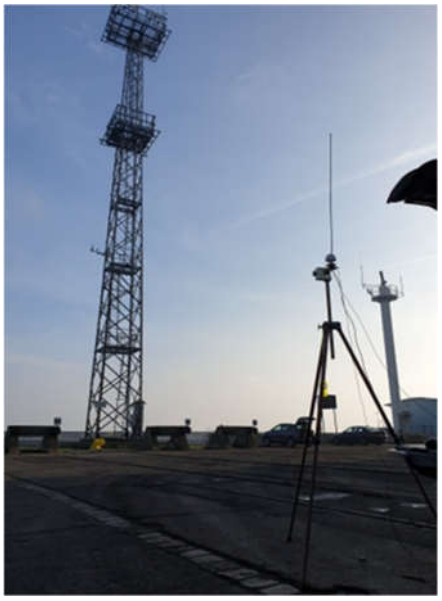

Figure 5-13: Photo from measurements d)

5.2.1 Analysis on the Gdynia - Karlskrona route

Below, two graphs present the distance depending on the number of the recorded file containing samples. The first graph (Fig. 5-14) shows the results that have been calculated by the signal correlation application. It was possible to obtain the correct correlation up to about 150 km. This range is twice as large compared to the value obtained in the 2019 measurement campaign. The second graph (Fig 5-15) shows the results recorded by the GNSS receiver.

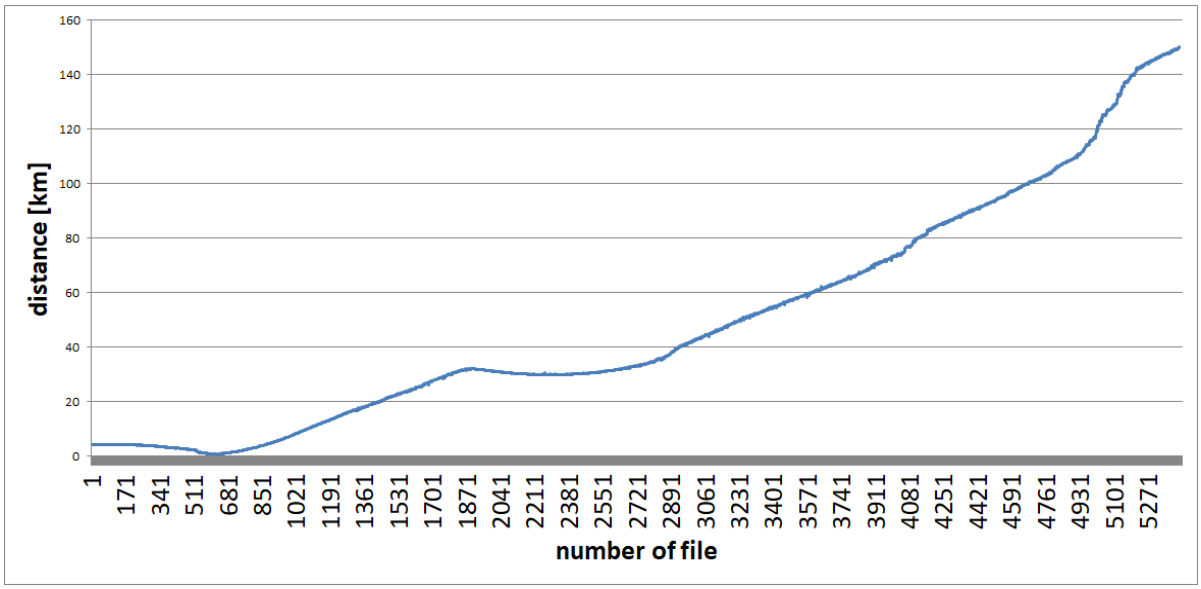

Figure 5-14: Distance measurements from the application for the correlation of signals on the Gdynia-Karlskrona route

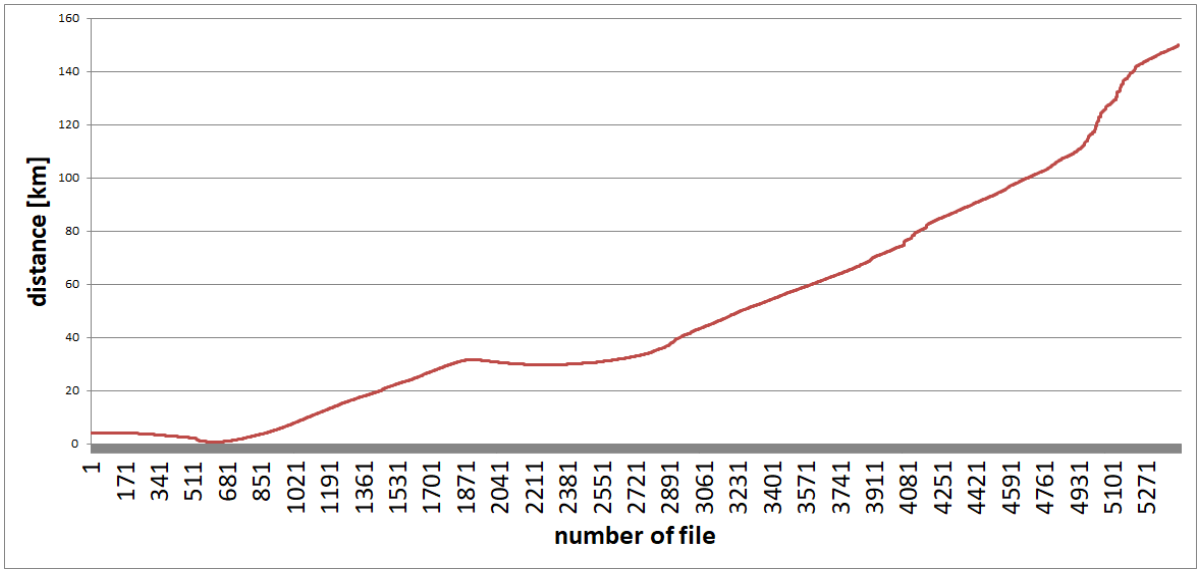

Figure 5-15: Distance measurements from the GNSS + EGNOS receiver on the Gdynia-Karlskrona route

On the basis of the results presented above, in the next steps it was possible to calculate the error of the determined distances and at the same time to calculate the RMS depending on the signal strength. By visually superimposing the results obtained from the correlator and the GNSS receiver for this campaign (Fig. 5-16) and comparing these results with the AIS campaign (Fig. 5-17) that took place in 2019, we can see a huge difference in the distance indicated. It is noticeable from the 20 km mark. This analysis is more for illustrative purposes. More detailed cases will be discussed in the following sections.

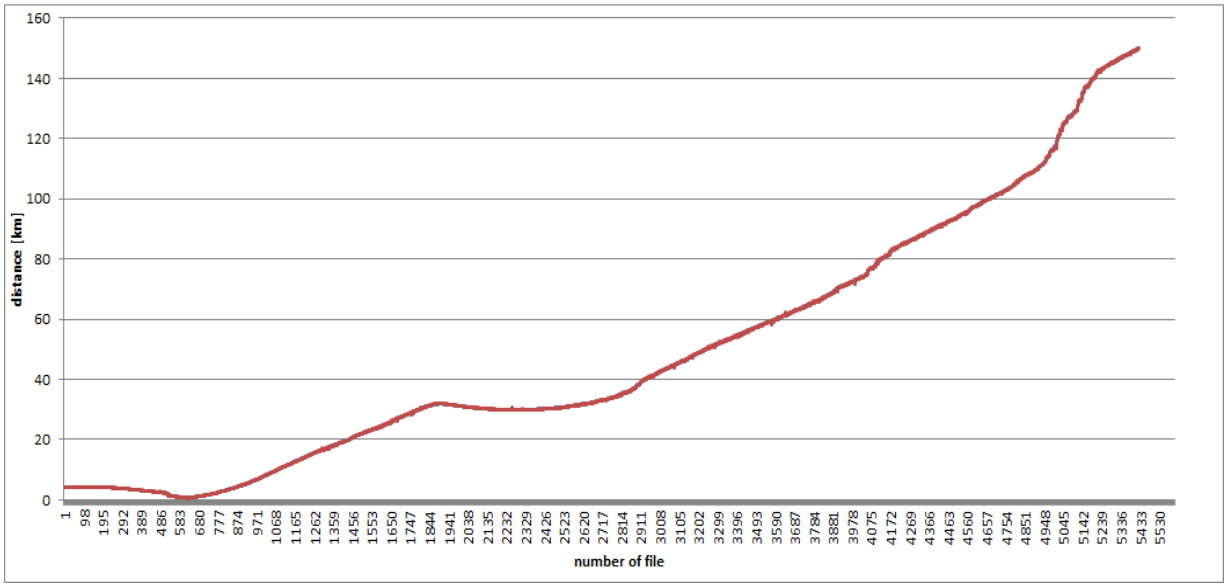

Figure 5-16: Superimposed results from the correlator and GNSS + EGNOS receiver for the VDES measurement campaign on the Gdynia-Karlskrona route

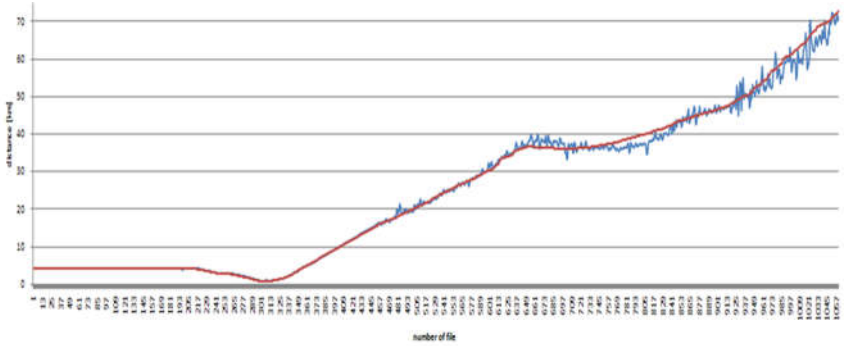

Figure 5-17: Superimposed results from the correlator and GNSS + EGNOS receiver for the AIS measurement campaign on the Gdynia-Karlskrona route

The next step presents the SNR values obtained on the Gdynia-Karlskrona route (Fig. 5-18). This graph shows how the ratio of signal power to noise power was changing throughout the entire route. In the first part up to the file number 900, we can see that the survey vessel was in and in the vicinity of the port. The signal strength in this case is very high. As we got closer to the Hel Peninsula, the signal strength decreased proportionally. The next part of the chart shows the SNR value increases above the file number 1900. This is due to the fact that the ship in this section was parallel to the Hel Peninsula and the distance between the transmitting and receiving antennas was smaller than in the area where the ship had to circumnavigate Hel. By using a filter on the receiving side, it was possible to increase the signal power to noise power ratio.

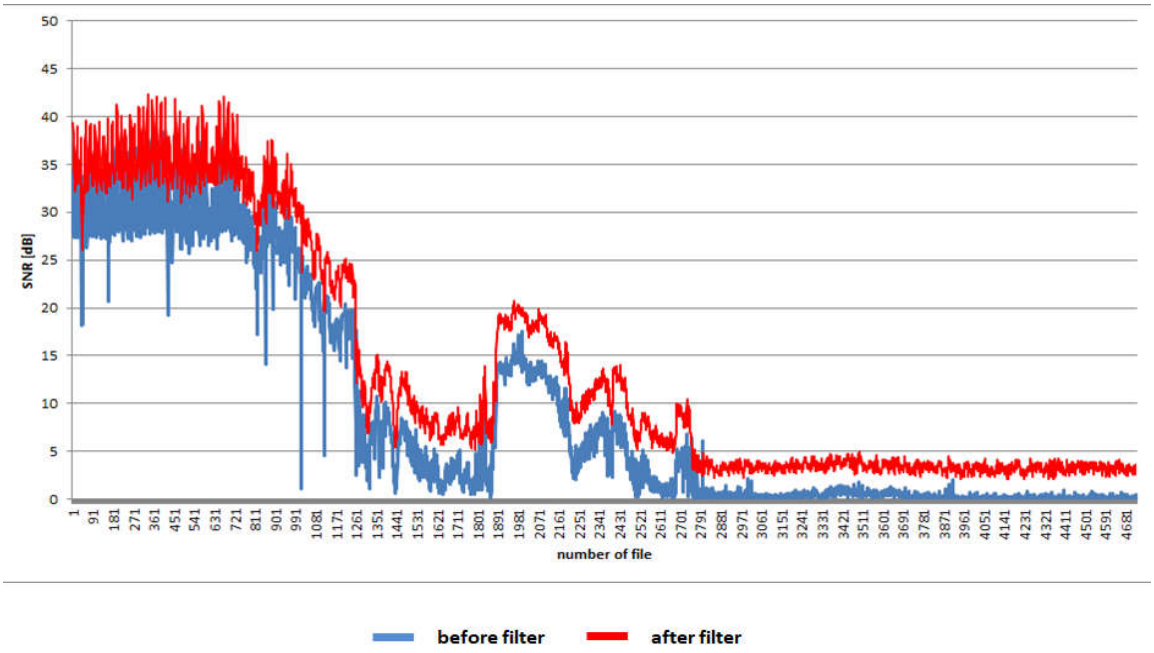

Figure 5-18: Measured SNR on the Gdynia-Karlskrona route

A plot of the correlation peak to adjacent peaks is shown below. This plot (Fig. 5-19) allows us to find out at which times the correlation was the most effective. This factor is important because when its value is high, a better accuracy of the calculated distances can be observed. This means that the mean value of the main peak is much greater than the mean value of the adjacent peaks. It indicates very good correlation properties of the signal.

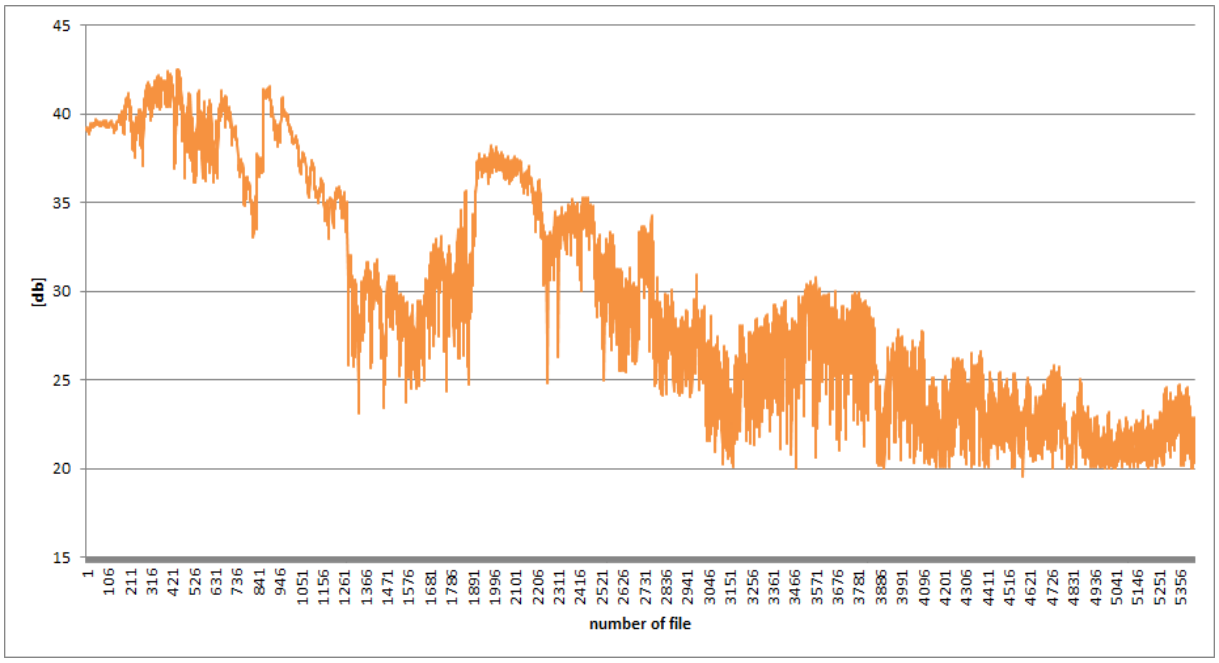

Figure 5-19: Measurements of the 'highest peak/ side peaks' ratio at the Gdynia – Karlskrona route

On the basis of many studies on the received samples and their processing in the correlation application, it was possible to establish correlation value thresholds. By using such a

solution, the R-Mode positioning system is protected against false results from the correlation application. This applies to files where it is difficult to distinguish the useful signal from noise with low SNR. On the basis of many studies, it is possible to estimate the threshold of the correlation value, below which we can assume that a given signal was noise, and not a useful signal. As a result, the correlation result for the uncorrelated data file is not saved and is not passed on to the next application, which is used to compute the position. This way we can avoid a false position results.

In Fig. 5-20, Fig. 5-21, Fig. 5-22, there are three graphs that show the efficiencies obtained by the correlators. During the processing of measurement files, the signal correlation application recorded the calculated distance accuracy for several types of correlators in order to later analyze their effectiveness in real conditions. In the graphs below, the samples indicate by how many meters the determination of the accuracy of the distance per sample was improved = 1.5 meters (for the sampling frequency of 200 MHz). The efficiency of a given correlator means its ability to better optimize the determined distance errors.

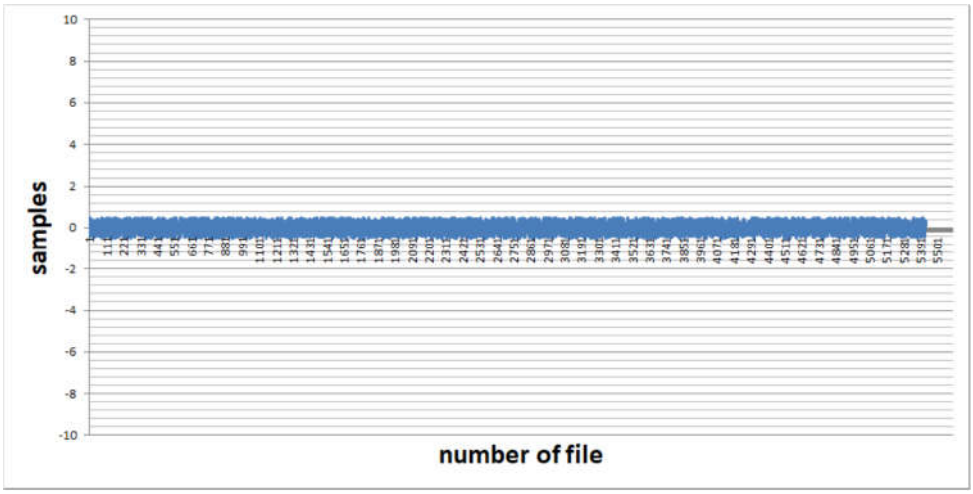

Figure 5-20: Effectiveness of using multicorrelation - Extended correlator d1=d2=1

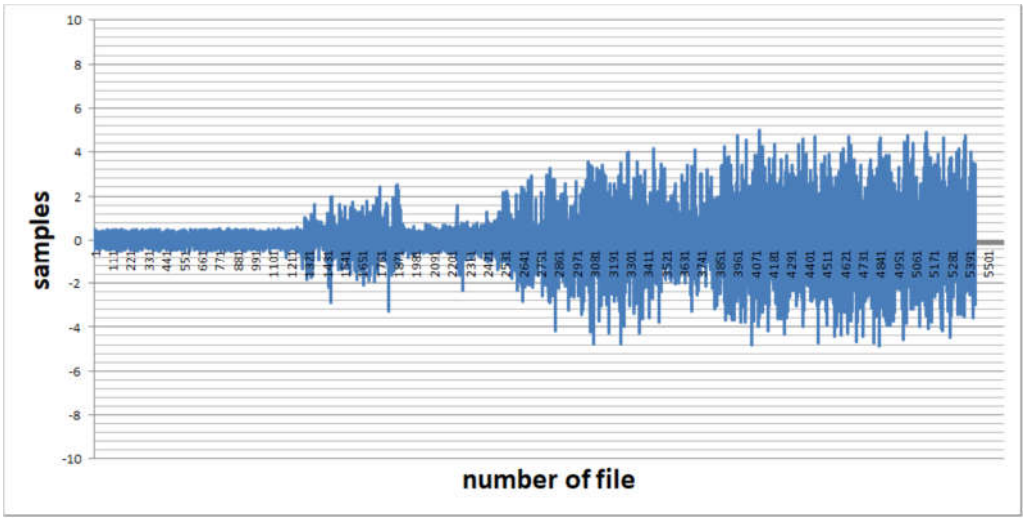

Figure 5-21: Effectiveness of using multicorrelation – Double-delta correlator d1=d2=10

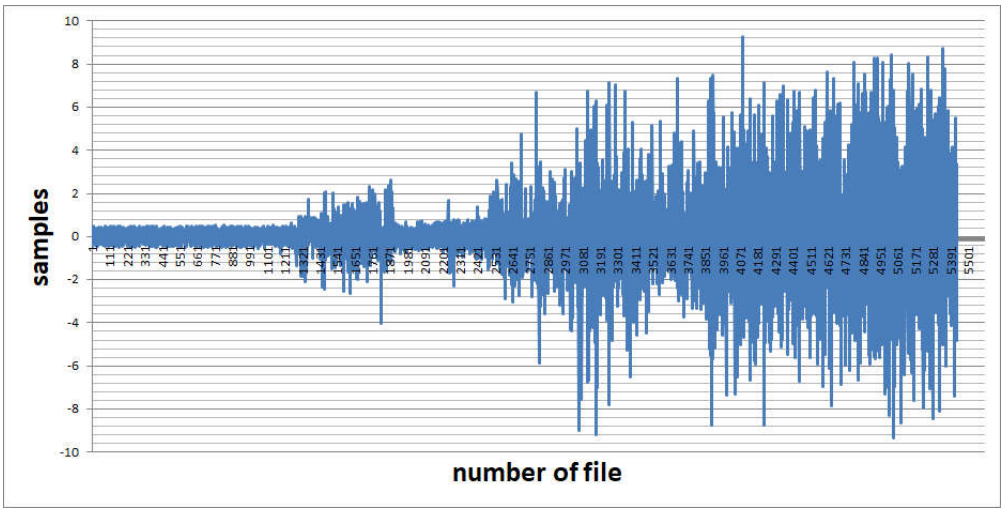

Figure 5-22: Effectiveness of using multicorrelation - Double-delta correlator d1=d2=20

The above graphs show the efficiency of the applied correlator depending on the width of the sample spacing of the second pair of this correlator. Three cases of this sample spacing have been studied in particular. In the first case, it was an extended correlator, where the analysis was focused between the peak with the maximum value and a pair of samples around this main peak. This solution only improves the determination of the accuracy of the distance by approx. one sample, which translates into a maximum improvement of 1.5 m in this case, where the sampling frequency on the receiving side is 200 MHz. In the next case, the spacing of the second pair of samples is 10 samples between the main peak and the sample coming from the second pair of correlator. Such a configuration already improves the determination of the distance accuracy by 5 samples, which in practice amounts to 7.5 meters. In the third case, with a sample spacing of 20, we have an improvement in the determination of the distance by about 13 meters. This is the best result obtained. It seems that if the next time the sample spacing in the correlator was increased, we would have obtained a better result. But this is not the case as we can see in the chart below (Fig. 5-23):

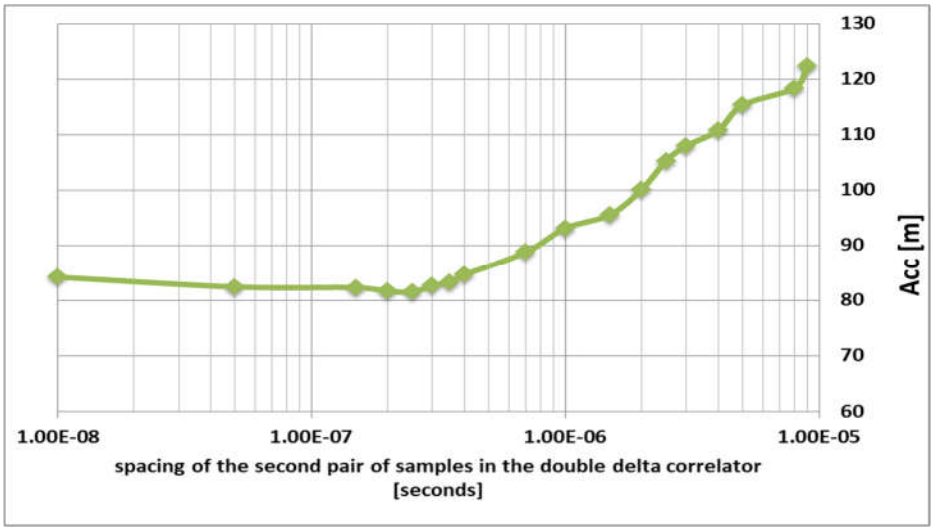

Figure 5-23: The accuracy of the distance as a function of the spacing of the pair of samples in the correlator

Fig. 5-23 shows a chart with tests of the selection of the samples spacing in the correlator for determining the distance. These tests were performed on files obtained from calibration in the port of Gdynia. On this basis, a simulation was performed to apply different sample pair delays. With the selection exceeding 20 samples, the determination of the accuracy starts to deteriorate more and more. It needs to be added that VDES measurement campaign was carried out with the sampling frequency on the receiving side equal to 200 MHz. To see the best efficiency of a multicorrelator – we have to work with signals of lower frequencies. Such research will be presented in the next chapter.

For illustrative purposes, a graph (Fig. 5-24) with the calculated distances by a signal correlation application superimposed on a graph of the efficiency of the correlator for the optimal sample spacing of the second pair (i.e. 20) is shown.

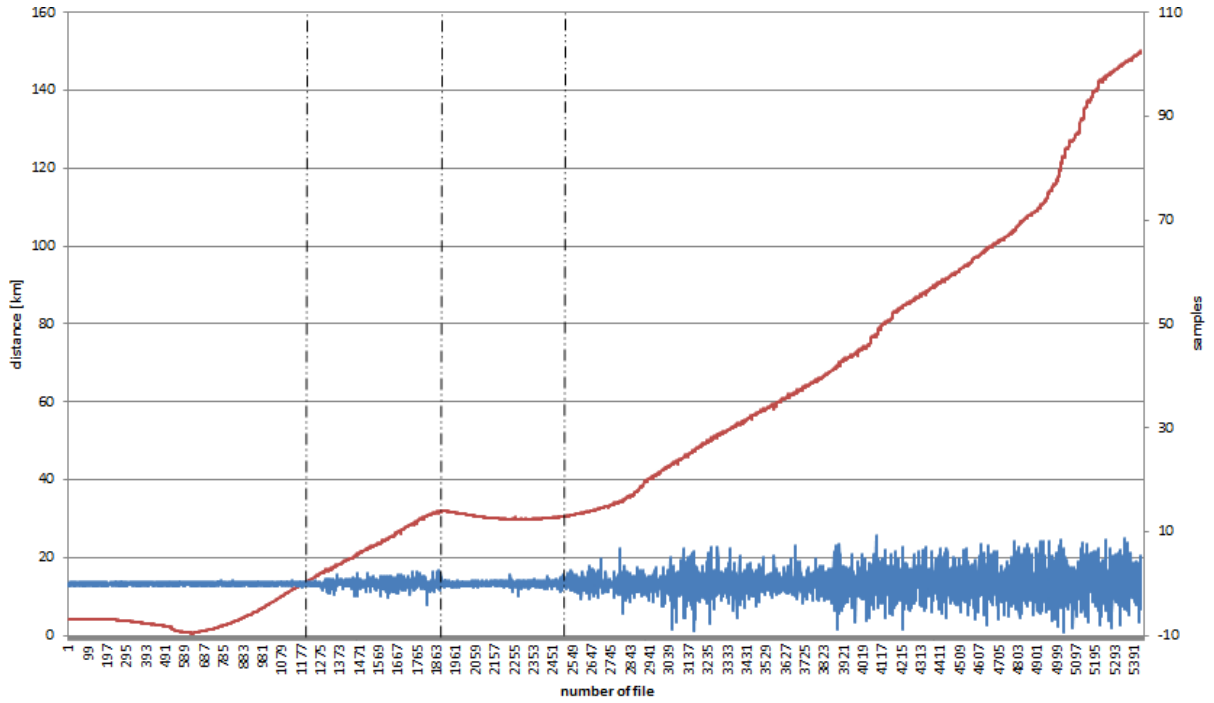

Figure 5-24: Ranges where the multicorrelator d2 = 20 operated most effectively

The accuracies obtained at the calculated distances for selected places are presented below (Fig. 5-25). These accuracies are much better than in the previous measurement campaign. For the short distances from the transmitting antenna, it can be seen that the distances from the GNSS receiver almost coincide with the results that were calculated by the signal correlation application. Such results allow for their subsequent transfer to the positioning application and the calculation of the exact position of the receiving station. This is very important, especially in the port where accurate navigation is critical. For long distances over a distance of 66 km, this error is 180 meters. This is a very good result compared to previous measurement campaigns. It should also be added that at a distance of about 120 km, these accuracies were in the order of 300 meters, which is still a satisfactory result.

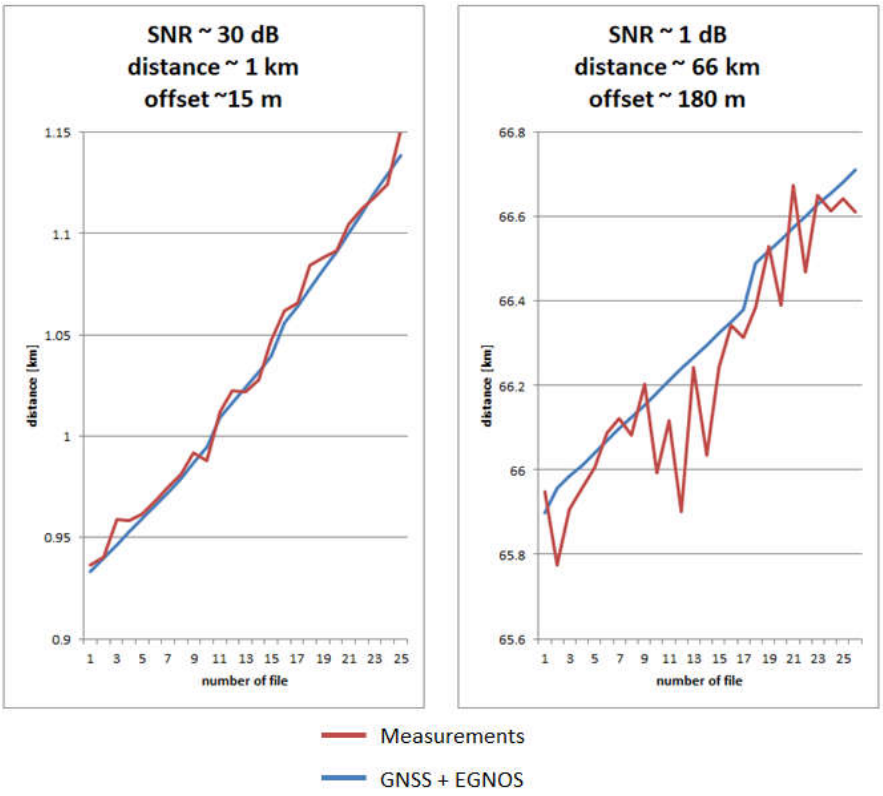

Figure 5-25: Accuracy obtained on measurements at the Gdynia – Karlskrona route

The characteristics of the error in determining the distance depending on the file number is presented below (Fig. 5-26). It can be noticed that along the entire route, the errors here reach about 400 meters at the edge of the correlation. A more detailed discussion of this graph can be found in the next section when we will compare it with the errors obtained in the previous campaign.

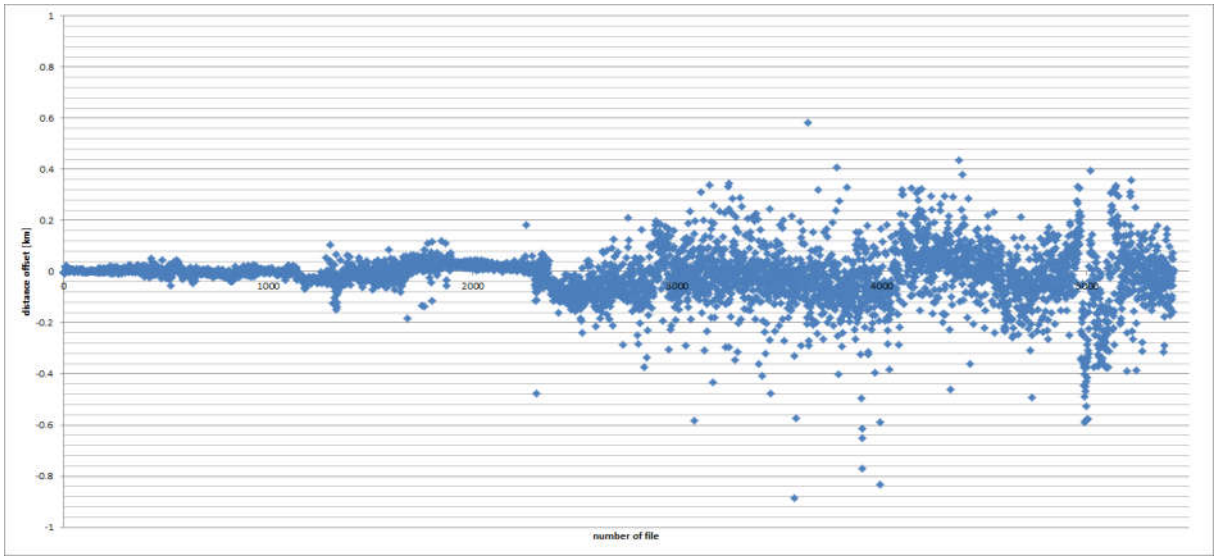

Figure 5-26: Distance error accuracy at the Gdynia – Karlskrona route

5.2.2 Analysis on the Karlskrona – Gdynia route

Unfortunately, some problems on the Karlskrona-Gdynia route occurred. At a distance of 50 km from the transmitting antenna, the oscillator became unsynchronized. The consequence of that was that the previously calculated correction value was no longer valid at that moment. During the desynchronization of the oscillator, there was a jump by 1000 samples, which in practice translates into 1.5 km. With each subsequent measurement, the delay value of one sample was added to the sample file. The next big fault occurred near the port of Gdynia. There, the value of 8,000 samples was added.

After analyzing the problems that occurred, correction values for fault points were applied manually, and additional delays were added in the form of one sample with each subsequent measurement.

Of course, for further analysis of the effectiveness of the positioning system, its RMS calculations and accuracy, only the route from Gdynia to Karlskrona – where no such problems occurred – was taken into account. For the experimental purposes, on the Karlskrona-Gdynia route, a manual delay correction was added and the accuracy of the distance after this correction was also analyzed, which is included in this subsection. Below is the graph before the correction (Fig. 5-27):

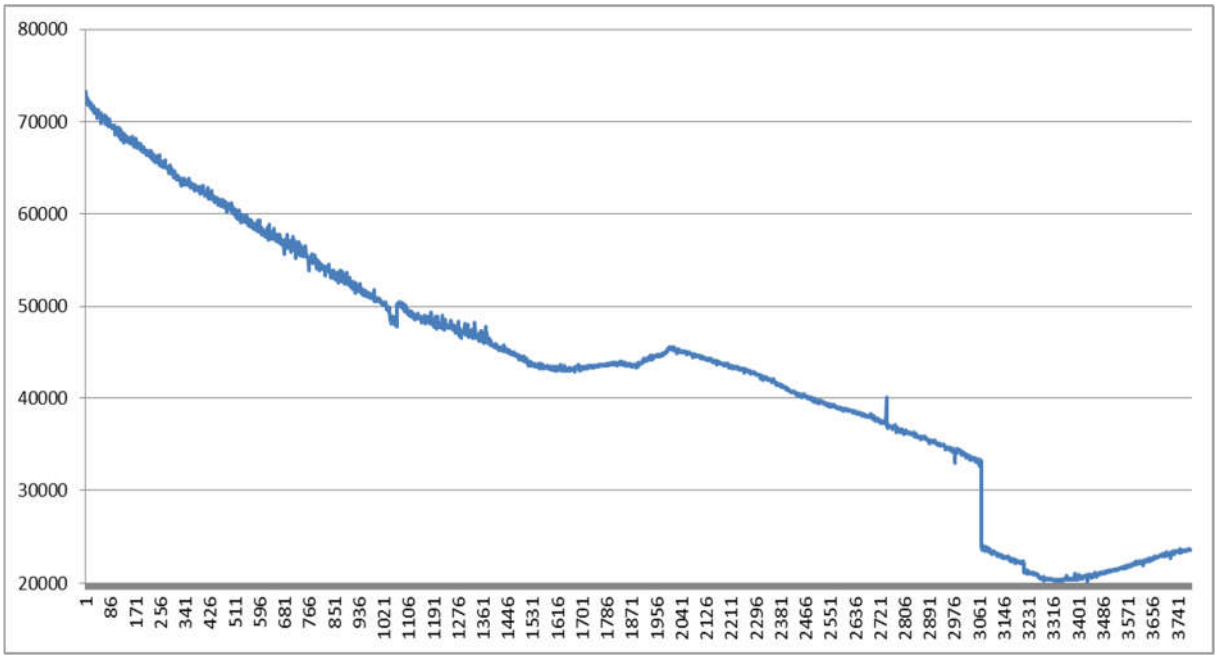

Figure 5-27: Karlskrona - Gdynia route with problems during measurements

Below are two graphs showing the distance depending on the number of the recorded file with samples. The first graph (Fig. 5-28) shows the results that have been calculated by the signal correlation application. It was possible to obtain the correct correlation up to about 80 km. The second graph (Fig 5-29) shows the results recorded by the GNSS receiver.

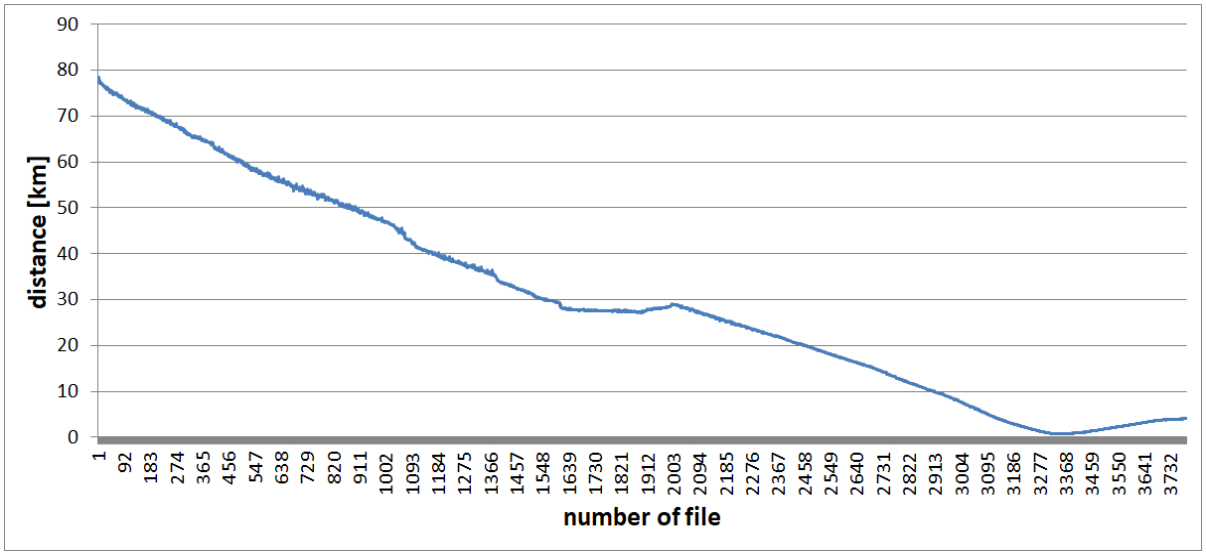

Figure 5-28: Distance measurements from the application for the correlation of signals on the Karlskrona-Gdynia route

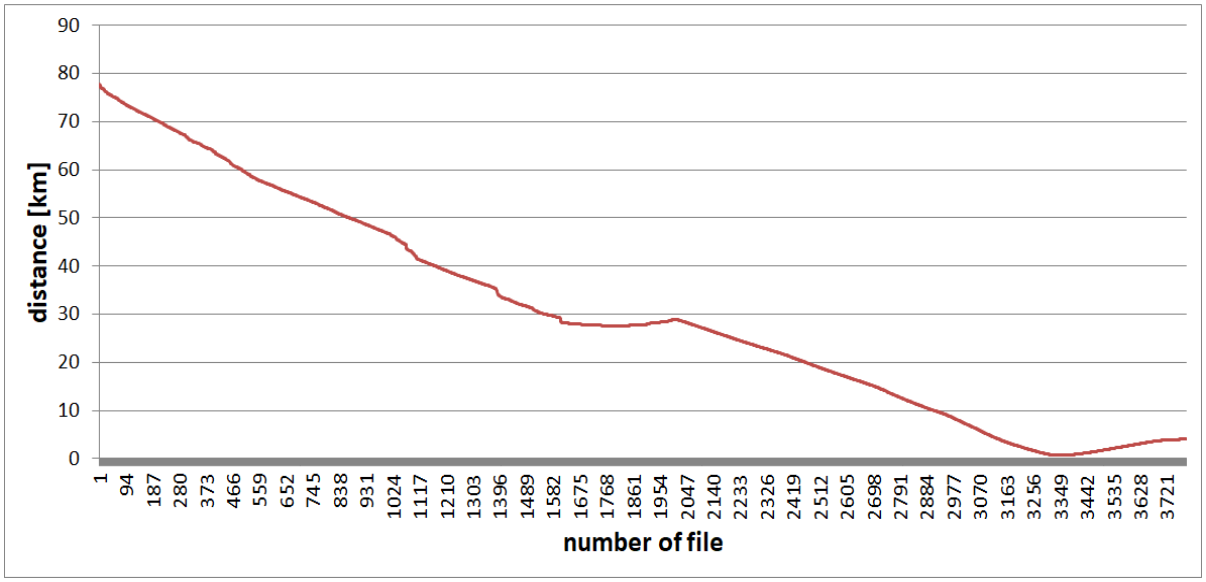

Figure 5-29: Distance measurements from the GNSS + EGNOS receiver on the Karlskrona-Gdynia route.

Thanks to the results obtained above, in the next steps it was possible to calculate the error of the determined distances and at the same time to calculate the RMS as a function of the signal strength. By visually superimposing (Fig. 5-30) the results obtained from the correlator and the GNSS receiver for this campaign and comparing these results with the AIS campaign (Fig. 5-31) that took place in 2019, we can see a huge difference in the distance indicated. It is noticeable from 16 km. This analysis is more for illustrative purposes. More detailed cases will be shown in the following sections.

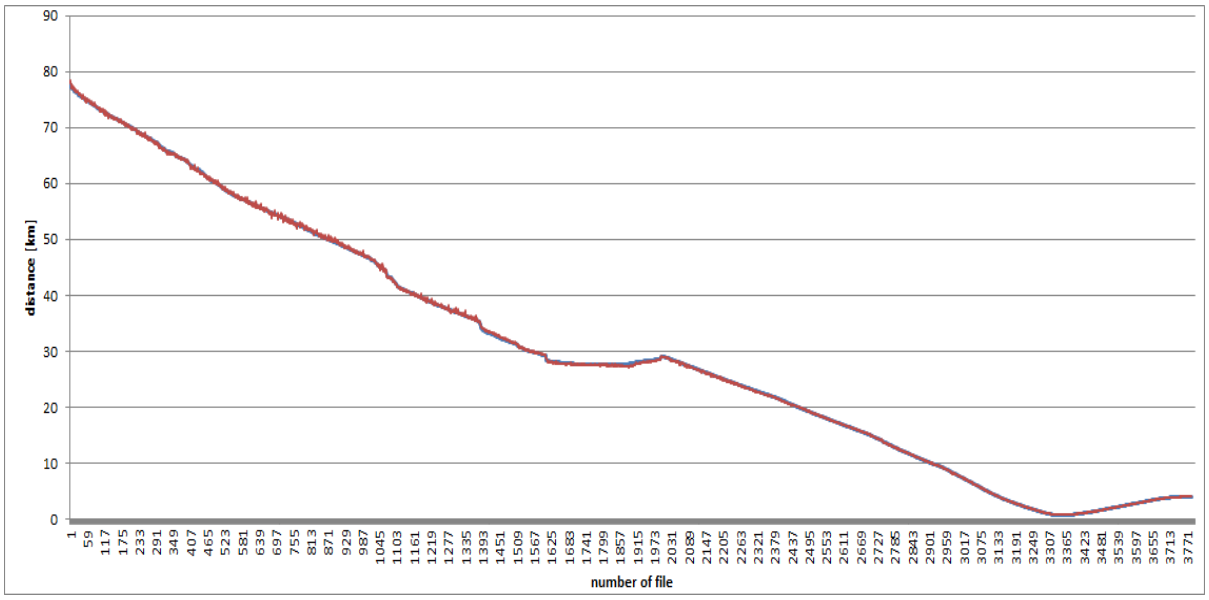

Figure 5-30: Superimposed results from the correlator and GNSS + EGNOS receiver for the VDES measurement campaign on the Karlskrona-Gdynia route

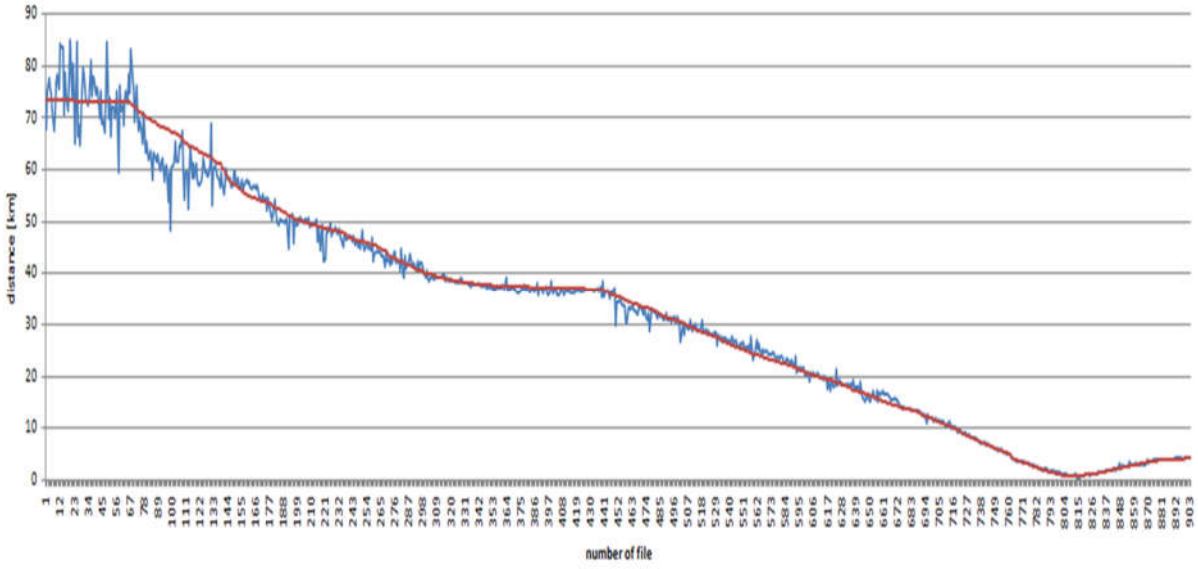

Figure 5-31: Distance measurements from the GNSS + EGNOS receiver on the AIS measurement campaign on the Gdynia-Karlskrona route

The next step presents the obtained SNR values on the Karlskrona-Gdynia route. Below is a graph of this relation (Fig. 5-32). The graph shows how the ratio of signal power to noise power has changed throughout the entire route. In the first part, the files up to the number 1700 represent the low SNR case; they were recorded beyond the Hel Peninsula. Files from number 1700 to 2300 represent the period when the ship began to sail along the peninsula. Starting from the file number 2300, the ship begins to sail around the tip of the Hel Peninsula and from that moment on, the SNR starts to increase significantly until the end of the chart, i.e. until reaching the port in Gdynia.

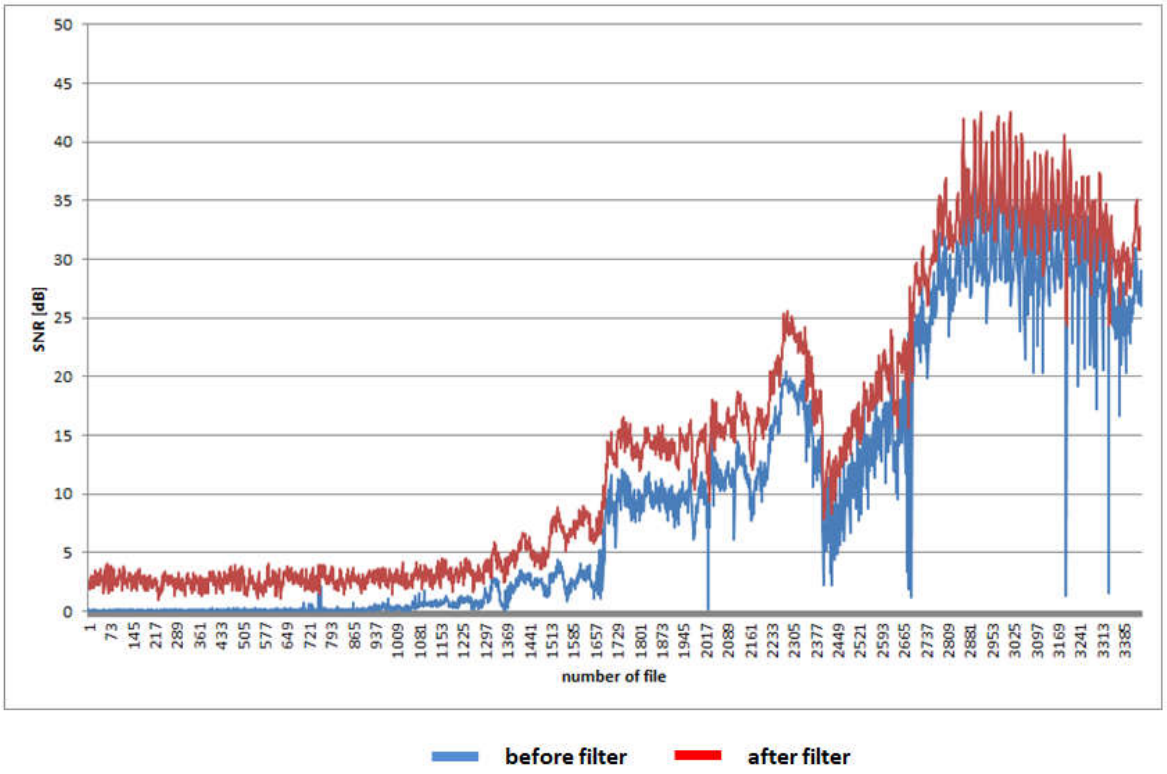

Figure 5-32: Measured SNR on the Karlskrona-Gdynia route

A plot of the correlation peak to adjacent peaks is shown below (Fig. 5-33). This plot allows us to see at which times the correlation was the most effective.

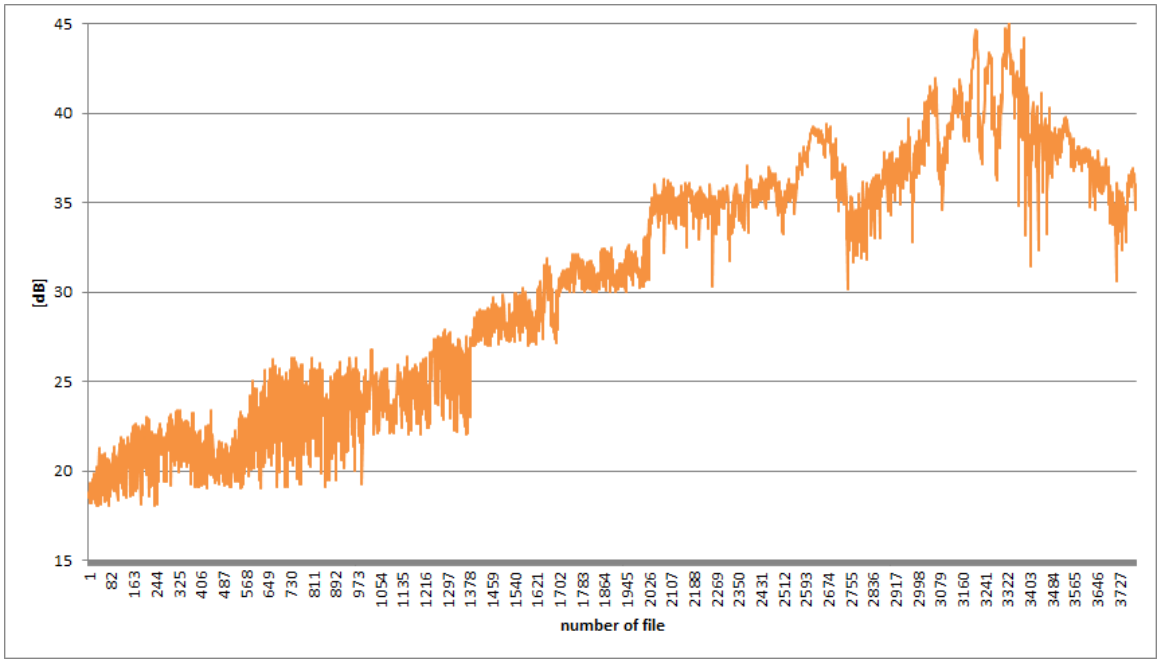

Figure 5-33: Measurements of the 'highest peak/ side peaks' ratio on the Karlskrona-Gdynia route

On the basis of many studies on the received samples and their processing in the correlation application, it was possible to establish correlation value thresholds. By using such a

solution, the R-Mode positioning system is protected against false results obtained from the correlation application. This applies to files where it is difficult to distinguish the useful signal from noise with low SNR. On the basis of many studies, it is possible to estimate the threshold of the correlation value, below which we can assume that a given signal was noise, and not a useful signal. As a result, the correlation result for the uncorrelated data file is not saved and is not passed on to the next application, which is used to compute the position. This way we can avoid a false position results.

In Fig. 5-34, Fig. 5-35, Fig. 5-36, there are three graphs showing the efficiencies achieved by the correlators. During the processing of the measurement files, the signal correlation application recorded the calculated distance accuracy for several types of correlators in order to later analyze their effectiveness in real conditions.

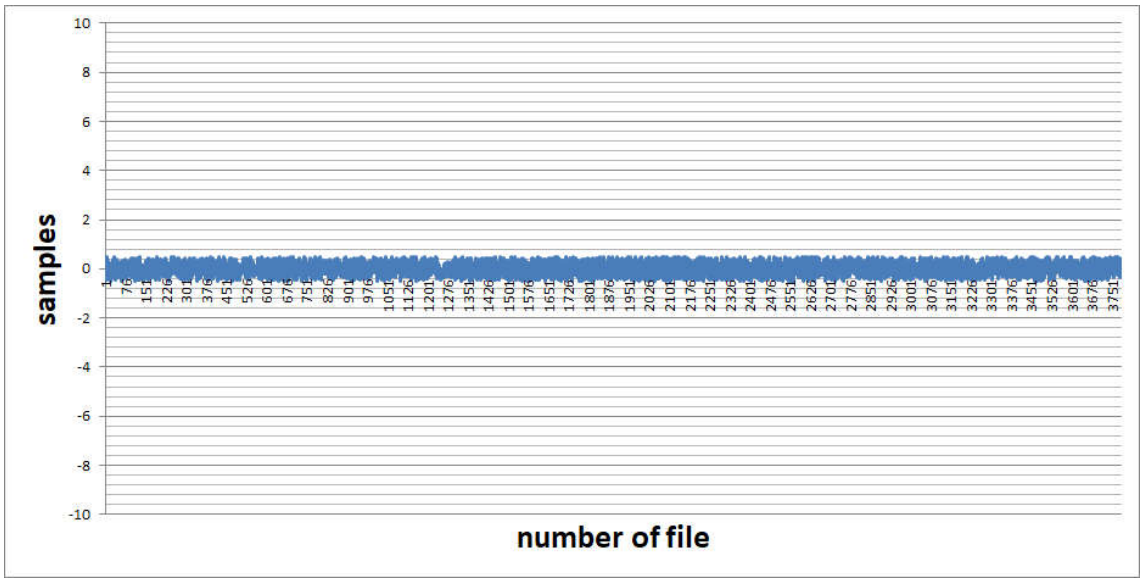

Figure 5-34: Effectiveness of using multicorrelation - Extended correlator d1=d2=1

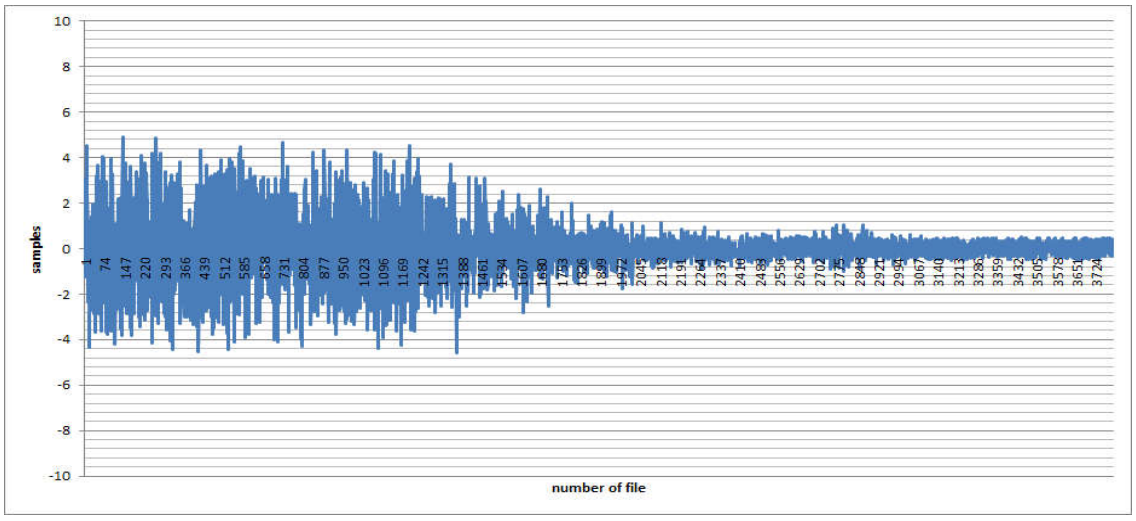

Figure 5-35: Effectiveness of using multicorrelation - Double-delta d1=d2=10

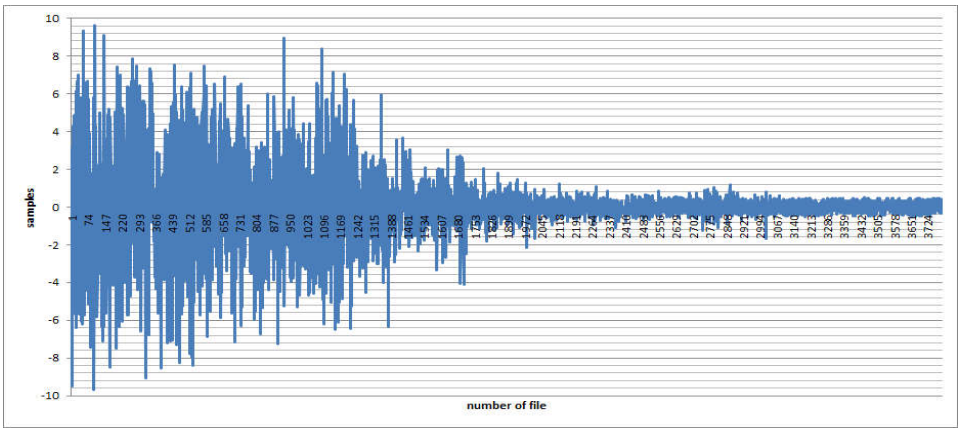

Figure 5-36: Effectiveness of using multicorrelation - Double-delta d1=d2=20

The above graphs show the efficiency of the applied correlator depending on the width of the sample spacing of the second pair of this correlator. Three cases of this sample spacing have been studied in particular. In the first case, it was an extended correlator, where the analysis was focused between the peak with the maximum value and a pair of samples around this main peak. This solution only improves the determination of the accuracy of the distance by approx. one sample, which translates into a maximum improvement of 1.5 m in this case, where the sampling frequency on the receiving side is 200 MHz. In the next case, the spacing of the second pair of samples is already 10 samples between the main peak and the sample coming from the second pair of correlator. Such a configuration already improves the determination of the distance accuracy by 5 samples, which in practice amounts to 7.5 meters. In the third case, with a sample spacing of 20, we have an improvement in the determination of the distance by about 13 meters. This is the best result obtained. For illustrative purposes, a graph (Fig. 5-37) we can see the distances calculated by a signal correlation application superimposed on a graph of the correlator's efficiency for the best sample spacing of the second pair (i.e. 20).

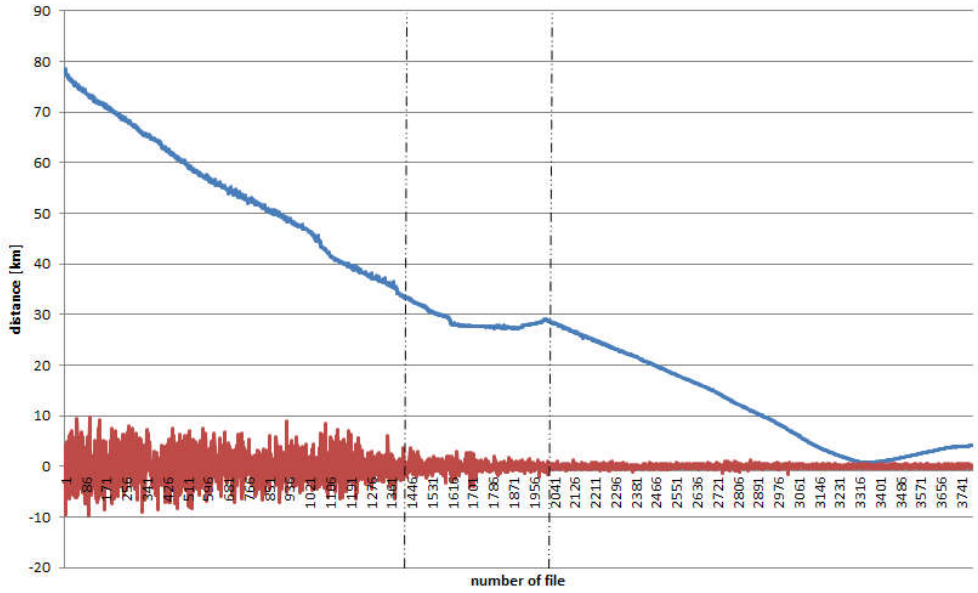

Figure 5-37: Ranges where the multicorrelator d2 = 20 operated most effectively

Fig. 5-38 depicts the error in determining the distance depending on the file number. It can be noticed that along the entire route, the errors here reach up to 500 meters at the edge of the correlation. A more detailed discussion of this graph will be in the next section when we will compare it with the errors obtained in the previous campaign.

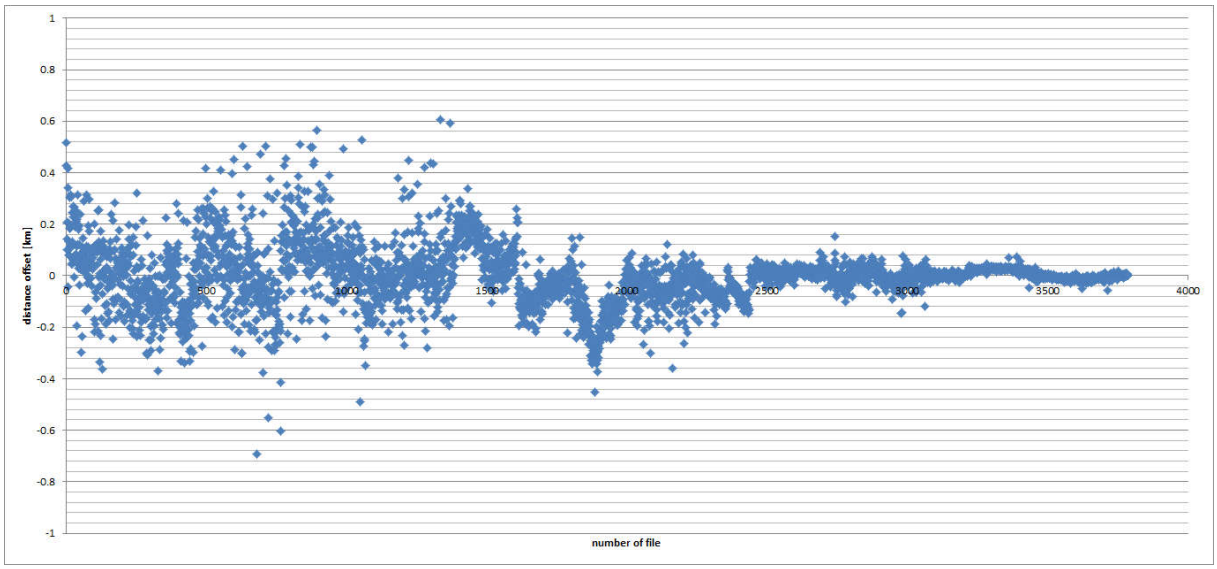

Figure 5-38: Distance error accuracy on the Gdynia – Karlskrona route

5.3 The obtained results of the accuracy of the measured distances from two VDES campaigns

In this section, graphs will be shown that illustrate the difference in measurement errors between the 2019 VDES measurement campaign and the VDES campaign that took place in 2020. In addition, the results will also be shown where the correlation sequence used to determine the distance is not the Gold sequence but a training sequence normally used to synchronize the signal in the receiver. For illustrative purposes, a graph with the influence of the Hel Peninsula on the determination of the distance accuracy is also presented.

The 2020 VDES measurement campaign also uses the same sampling frequency on the receiving end so the results can be reliably compared. After calculating the difference between the indications of the GNSS receiver and the signal correlation application, it was possible to generate the RMS plot. It clearly shows the ratio of the distance accuracy error to the SNR. Thanks to this data, it was possible to compare the results obtained for all measurement campaigns in a meaningful way.

Some changes were made in the 2020 measurement campaign in relation to the 2019 campaign:

• in order to improve the power of the transmitted signal, changes were made to the filtration of the transmitted signal: Hann windows were turned off and the physical VHF filter was removed,

• the transmitted sequence has been modified in accordance with the IALA Guideline VDES guidelines,

• application on the receiving side of the physical VHF PROCOM BPF 2 / 2-250 filter with a narrower passband (previously installed on the transmitting side),

• in order to eliminate the need to use an attenuator at the USRP input, a low-noise amplifier with lower gain than before was used,

• in order to maximize the number of used GPS and Galileo satellites, the reference GNSS receiver was reconfigured.

With the second VDES 2020 campaign, the ERP power was increased to 14.8 dBW

The chart (Fig. 5-39) shows the distance accuracy of the results obtained in both measurement campaigns. The next graph (Fig. 5-40) shows the determined distances for the correlation of the training sequence compared against the results obtained using the Gold sequence correlation. Then on the next graph (Fig. 5-41), it is possible to see the obtained RMS results and finally, in Fig. 5-42, the errors obtained in the presence of the Hel Peninsula are shown.

1st measurement campaign: 15-16 November 2019

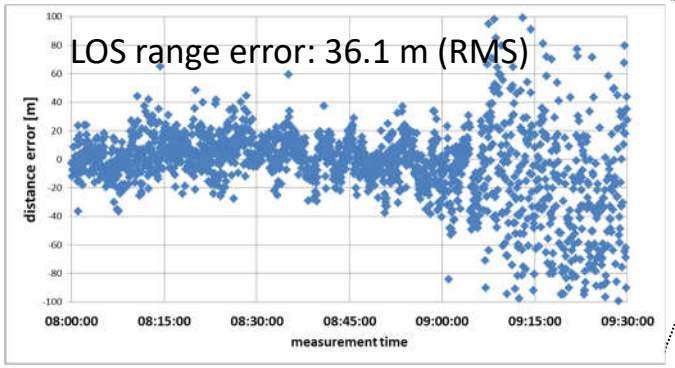

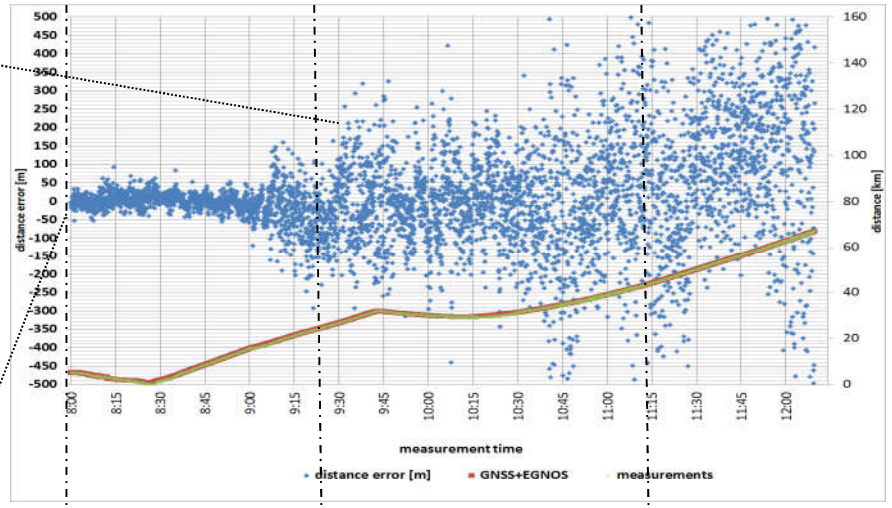

<-- Range up to 65 km

Range much greater than 150 km !!

2nd measurement campaign: 29-30 June 2020.

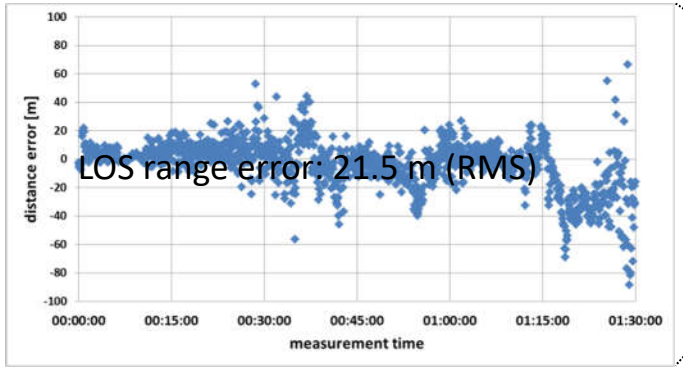

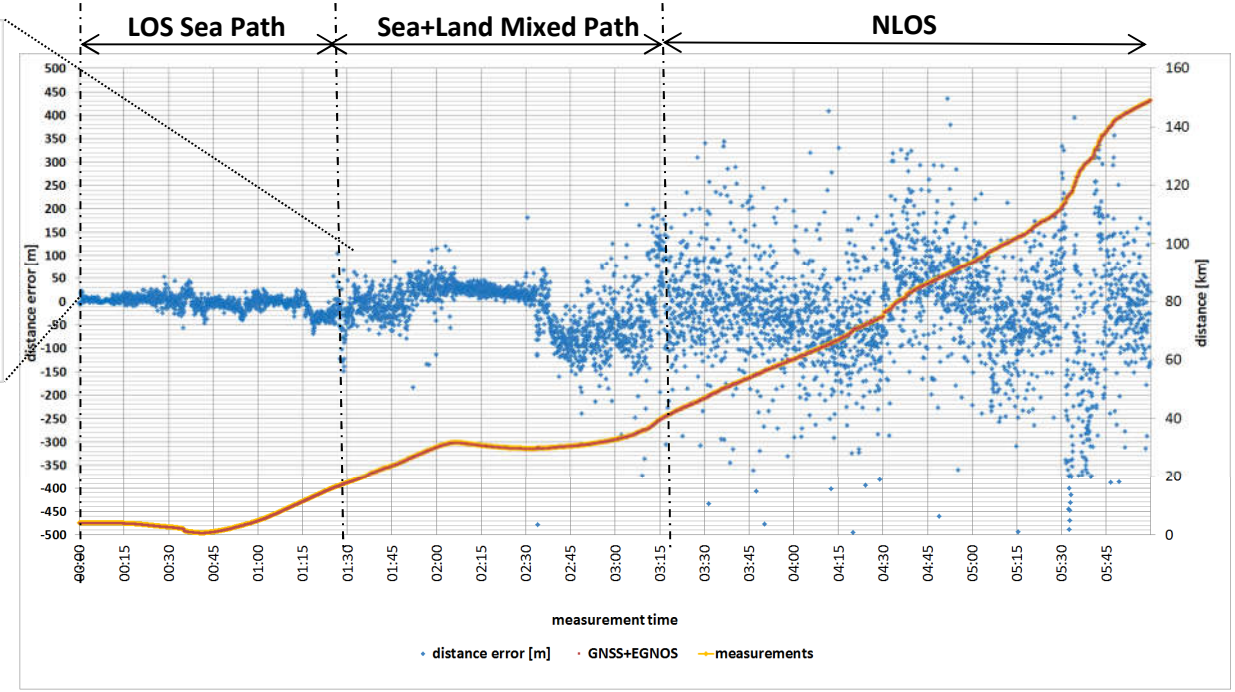

Figure 5-39: Obtained measurement results – ranging accuracy

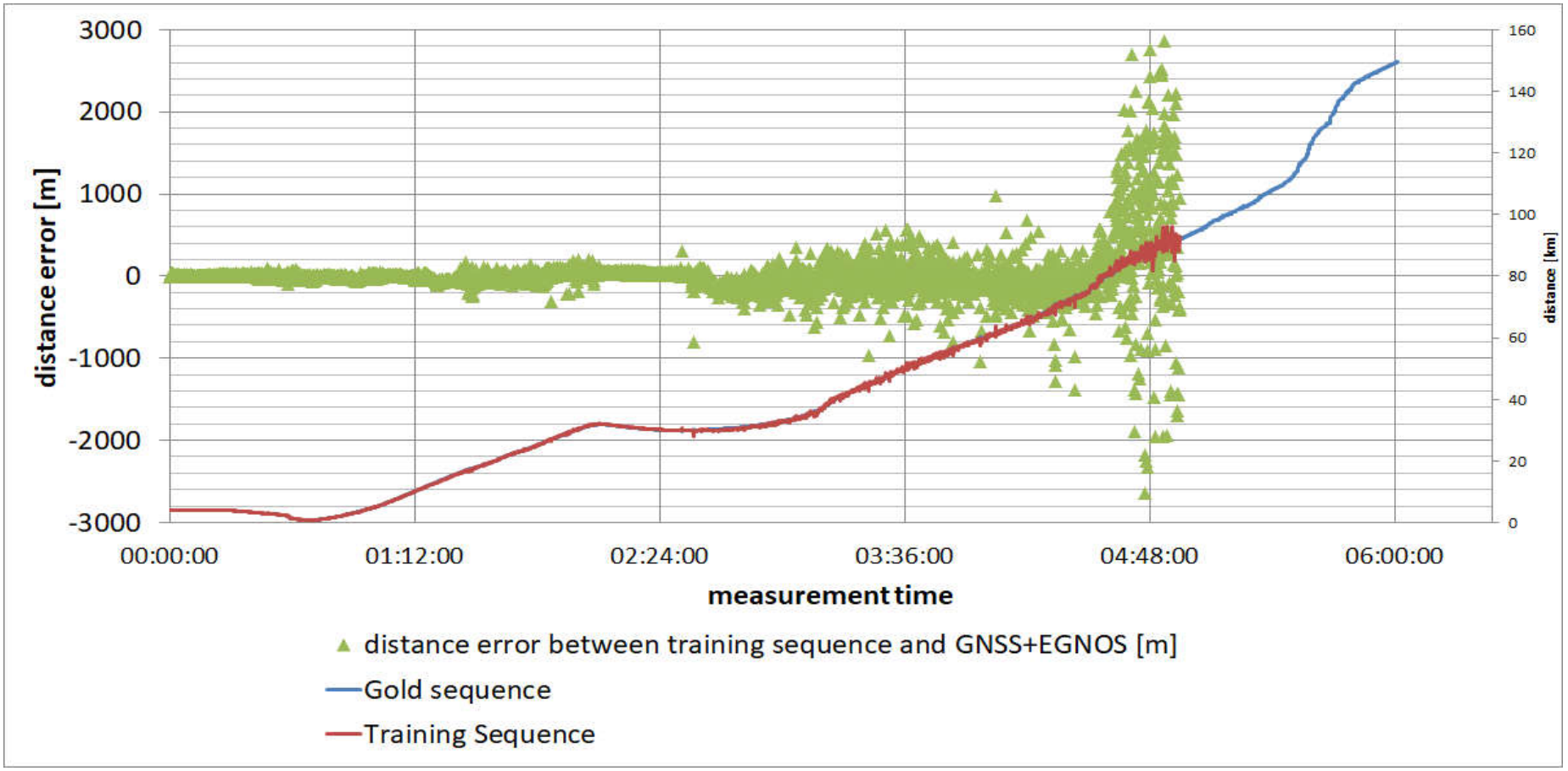

Figure 5-40: Comparison of the correlation effectiveness for the training and Gold sequences

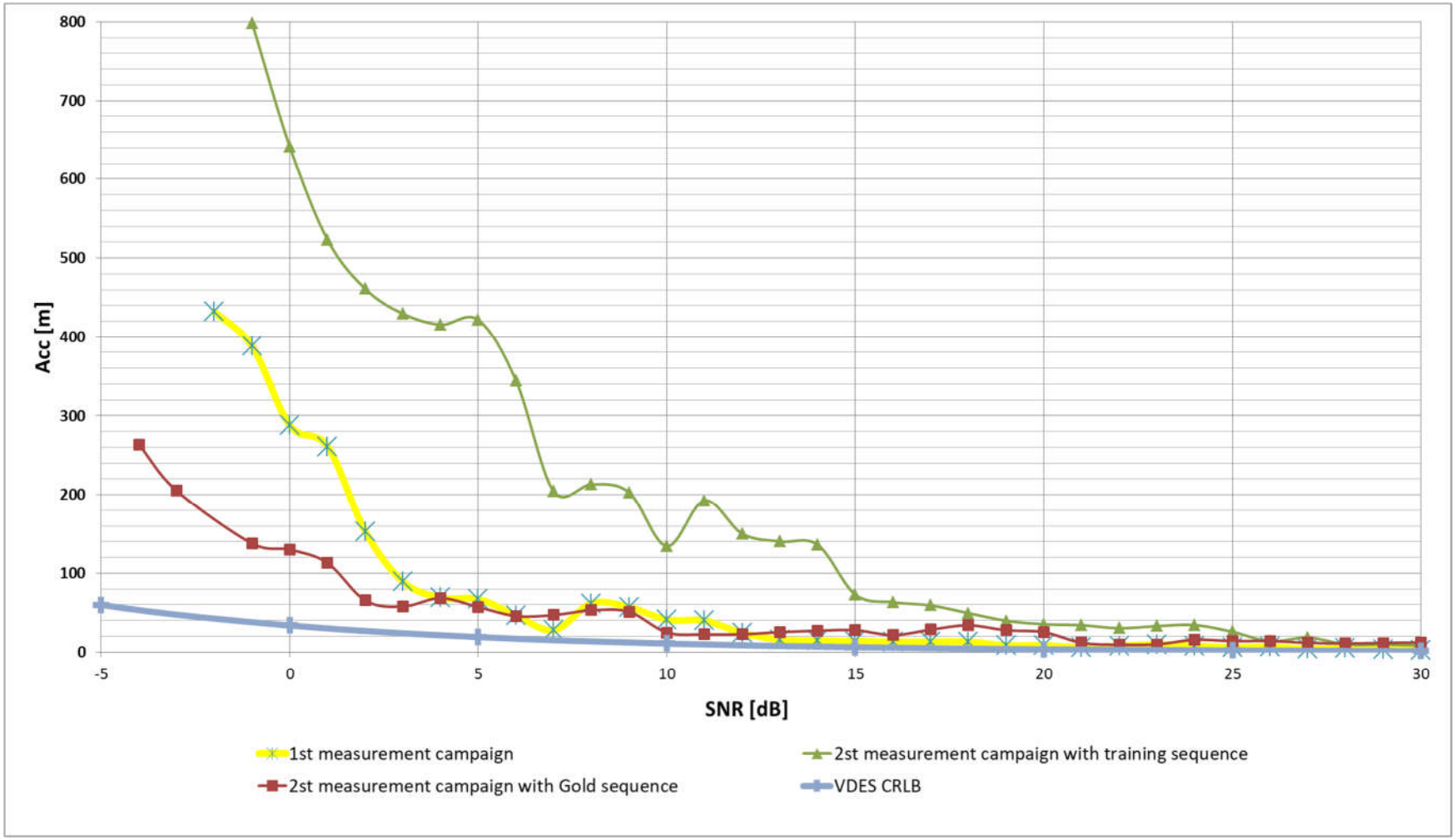

Figure 5-41: Accuracy obtained – as a function of SNR

The results of the first measurement campaign on the Stena Line ferry showed that the configuration changes made both on the transmitter and receiver sides of the system allowed, first of all, to significantly extend the operating range of the system - from approx. 70 km obtained as part of the measurement campaign carried out in 2019 to approx. 150 km obtained in the June 2020 campaign (Fig. 5-39).

The results presented in fig. 5-39 show that due to the introduced changes and optimization of transmitting and receiving stations, not only was it possible to more than double the range of the R-Mode VDES system, but also the accuracy of the determined distance was improved. In the frame structure of the VDES system, in addition to the Gold sequence sent as part of the data packet, there is also a training sequence (Fig. 5-40) that is used to synchronize the receiver. As part of the analyzes, the possibility of using this sequence to determine the distance from the base station was also compared. Fig. 5-41 shows the accuracy of the determined distance based on data from the 2019 measurement campaign and on the basis of the Gold sequence and training sequence obtained as part of the measurement campaign of June 2020. This comparison shows that although the training sequence of the VDES frame can be used for ranging, the accuracy obtained in this case does not meet the assumptions of the R-Mode system even for high SNR values. The comparison also shows an increase in the accuracy of the determined position due to the applied modifications.

The results obtained in the measurement campaigns were compared with theoretical curves calculated on the basis of the Cramer-Rao Lower Bound (CRLB) method. As can be seen in fig. 5-41, for very low SNR values the discrepancy between the theory and the measurements was initially very significant but it was going down as the SNR increased. The fact that for lower SNR values the accuracy of the determined distance was not satisfactory for both analyzed systems, confirms the well-known limitation of the Cramer-Rao method that it is more suitable for high SNR scenarios. On the other hand, the results obtained for high SNR values almost coincided with the theoretical curves generated for the AIS and VDES systems, with the exception of the nearly constant, about 10 m difference of the RMS error. On the basis of the results, it can be stated that much better accuracy of the determined distance was obtained for the VDES system. In the second measurement campaign for the VDES system, for low SNR values, a clear improvement in the determination of the distance accuracy can be seen.

Other possible sources of errors resulting in a behavior observed in fig. 5-41 which caused some deviation between theory and measurements, have been identified and are listed in table 5-4. It should be noted that some of these errors only apply to the low-SNR region, while others are valid for the entire SNR range in fig. 5-41.

Below in the table, the '+' sign indicates problems that may have occurred on the measurement route and affected the measurement results. Problems which in the given case did not occur and did not have any influence on the problems were marked with the '-' sign.

Table 5-4: Source of error

Source of error	low SNR region	high SNR region
Possible impact of residual clock errors	+	+
Errors caused by the presence of the Hel Peninsula	+	-
Errors that can be caused by lack of EGNOS and/or high HDOP	+	+
Ship's speed too high	+	+
Weather conditions	+	+
Error resulting from passing the line of sight distance (beyond the 42.4 km mark)	+	-
Sampling rate	+	+

The chart below (Fig. 5-42) shows the influence of the Hel Peninsula terrain on the determined distance accuracy during the measurement campaign.

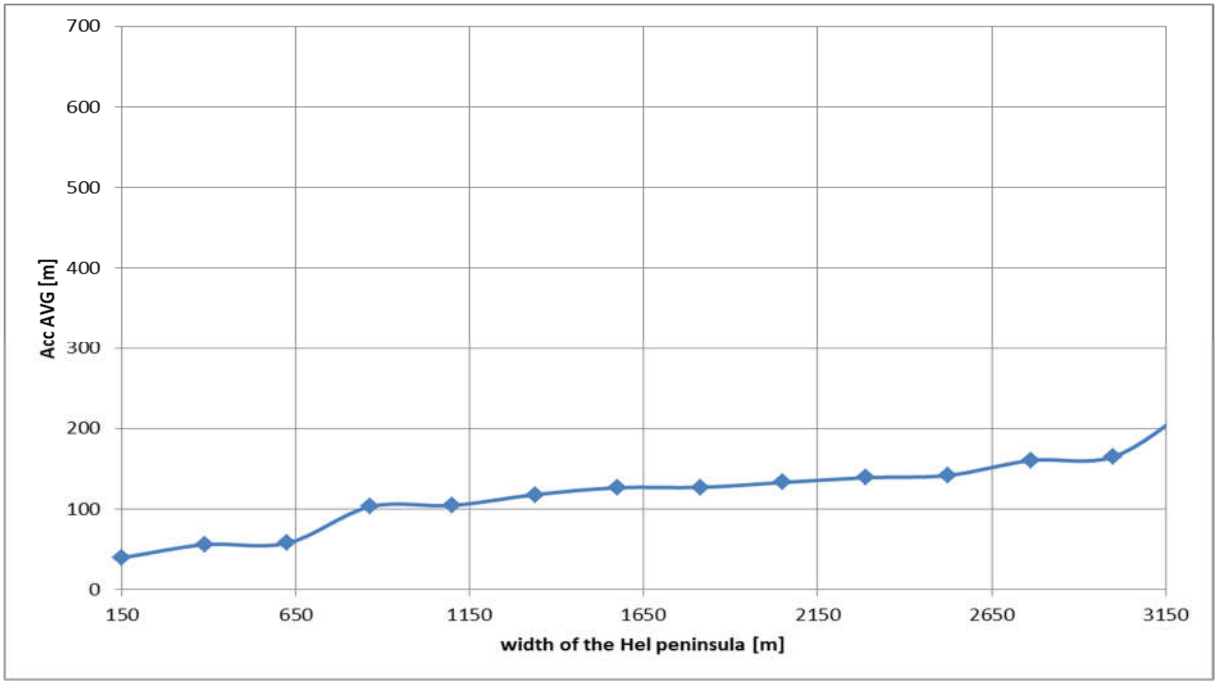

Figure 5-42: Hel peninsula influence for VDES

It can be clearly seen that in places where the width of the land on the Hel Peninsula was greater, the accuracy of the distance determination deteriorated. It was also related to the existing forest areas.

Below is a map from the second measurement campaign on the Gdynia-Karlskrona route, where the magnitude of the errors was marked (Fig 5-43).

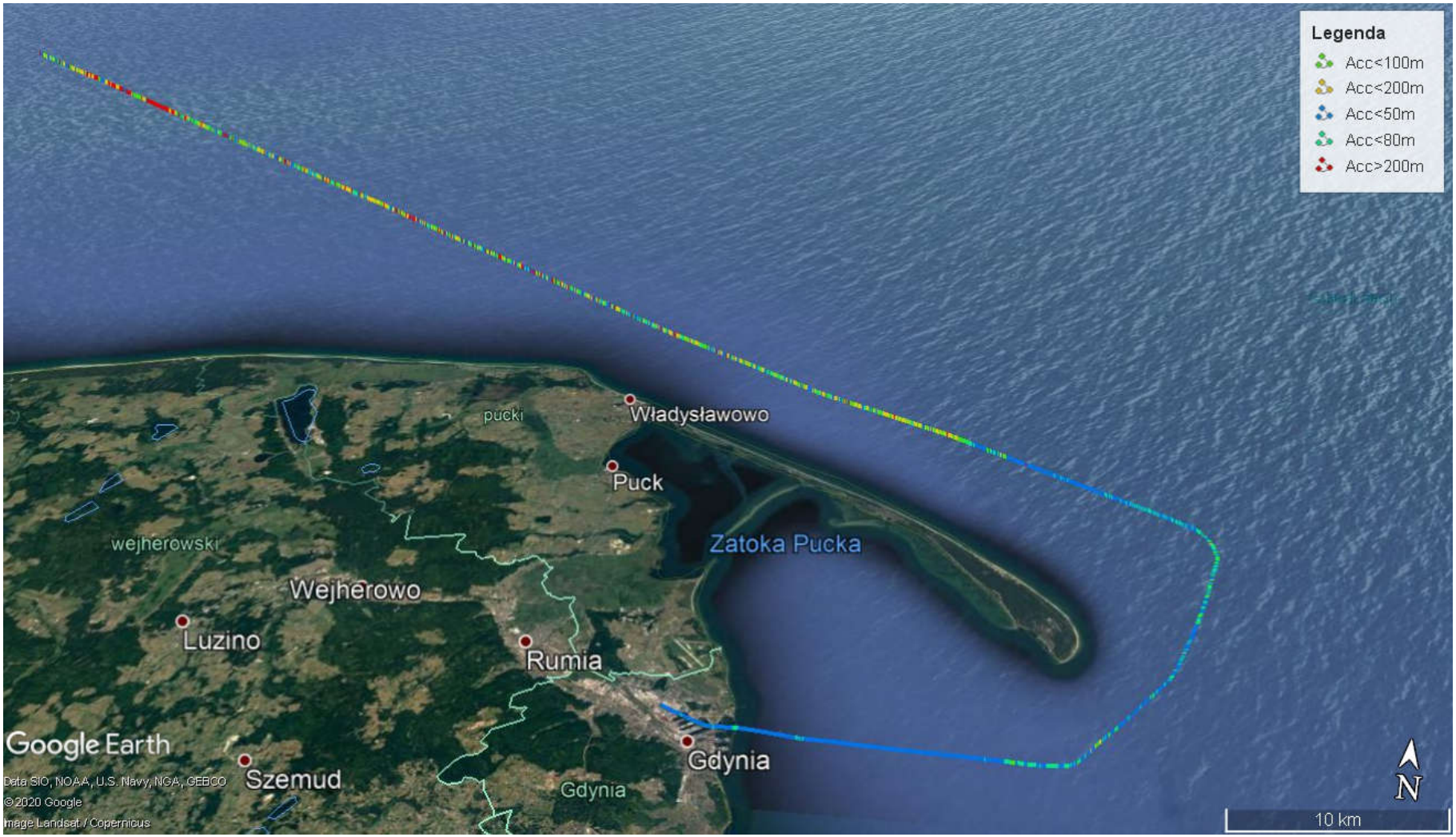

Figure 5-43: Measurement route and accuracy – 2nd campaign

Below are brief conclusions from the measurement campaigns:

- Lack of line-of-sight (LOS) and potentially high noise at the Rx are the main accuracy limiting factors,
- Theoretical analysis fits quite well with measurements for high SNRs,
- Mixed paths introducing additional (almost constant) range error / delay,
- System is still usable in deep non-line-of-sight (NLOS) conditions (for rough position estimation) – even much below communication sensitivity level / range,
- VDES training sequence has limited applications only,
- Quite sophisticated filters and LNA used at the Rx – minimizing noise needed.

6 Ranging accuracy tests based on the reception of a multi-slot message (emulation of the multiple R-mode stations - based on one physical station in Gdynia)

This chapter presents the results of the research that was carried out in the NIT building. The receiving part was located in Gdańsk (NIT premises), and the transmitting part was located in the port of Gdynia, 17.4 km from the receiver antenna in Gdańsk. The following subsections present the results obtained for the application of different sampling frequencies on the receiving end. Using the calculated RMS, it was possible to objectively compare all the obtained results. Various measurement scenarios were also used in the research. By introducing an additional delay, the presence of up to four transmitting stations was simulated. For the simulated different distances of the transmitting stations, the powers of the transmitted signals were also simulated: they were proportionally changed depending on the artificially introduced delay in a given slot. This solution allowed to conduct the research for one-slot, two-slot and 4-slot messages. All these studies helped to optimally select the sampling frequency on the receiving side and the appropriate correlation sequence, which gave the best results (i.e. the highest accuracy of the calculated distance).

6.1 Performing tests to calculate the accuracy of the distance based on the change of the sampling frequency of the received signal

As part of further activities carried out under the R-Mode Baltic project, the correlators operating on the receiving side were modified, which, on the one hand, would allow to increase the accuracy of the determined distance, and on the other hand, would make it possible to reduce the sampling frequency of the received signal. The latter aspect is particularly important due to the possibility of building the R-Mode VDES target receiver in the programmable radio technology using commercially available electronic components (as opposed to the expensive laboratory equipment that was used during system tests). As part of subsequent measurement campaigns carried out in the point-to-point relation, i.e. the VDES R-Mode base station in the port of Gdynia - the premises of the NIT in Gdansk, a number of solutions were tested. The results of the conducted analyzes allowed for a significant reduction of the sampling frequency from the initially used 200 MS / s, down to 2 MS / s, with a simultaneous reduction of the error level, as shown in Fig. 6-1.

The reduction of the sampling frequency had yet another colossal significance - the computational complexity of the algorithms used decreased, as did the amount of the measurement data processed in real time. It is worth mentioning here that so far all measurement data was first recorded and then analyzed in post-processing.

A series of measurements was made for the following frequencies:

- 200 MHz,
- 100 MHz,
- 50 MHz,
- 10 MHz,
- 5 MHz,
- 2 MHz,
- 1 MHz.

For each series of measurements for different frequencies, 100 files were recorded. This was a sufficient number for which reliable results could be calculated.

Until now, all measurements in the measurement campaign were conducted the receiving frequency of 200 MHz. This resulted in a large size of the files with the recorded samples. Thanks to tests with lower frequencies and testing the effectiveness of multi-correlators, it will be possible to select a lower frequency that will allow to reduce the size of the recorded files with samples.

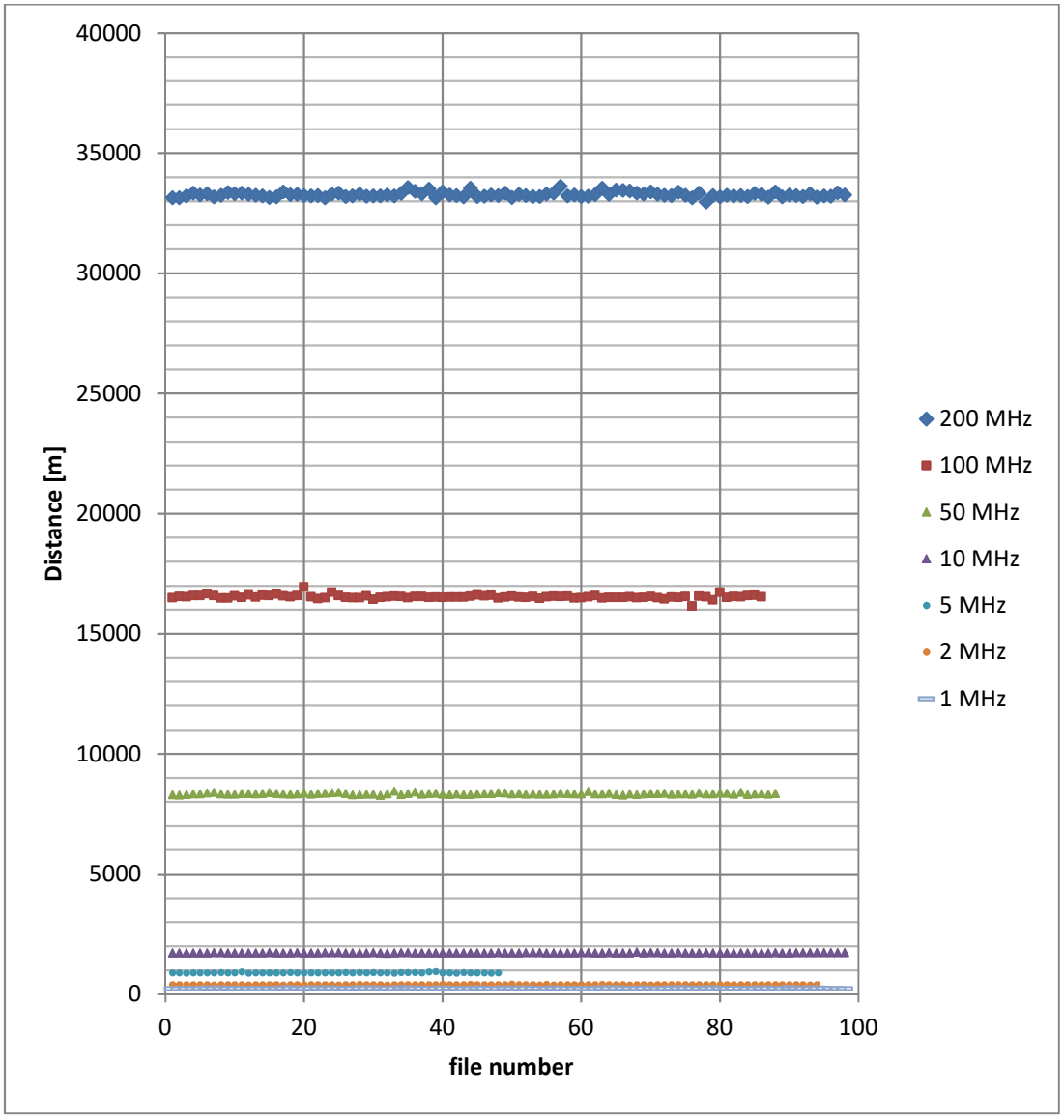

Figure 6-1: Analysis of the calculated distance accuracy depending on the sampling frequency

The figures 6-2, 6-3, 6-4, 6-5, 6-6, 6-7, 6-8 below show the exact results for each of the tested sampling frequencies on the receiving side.

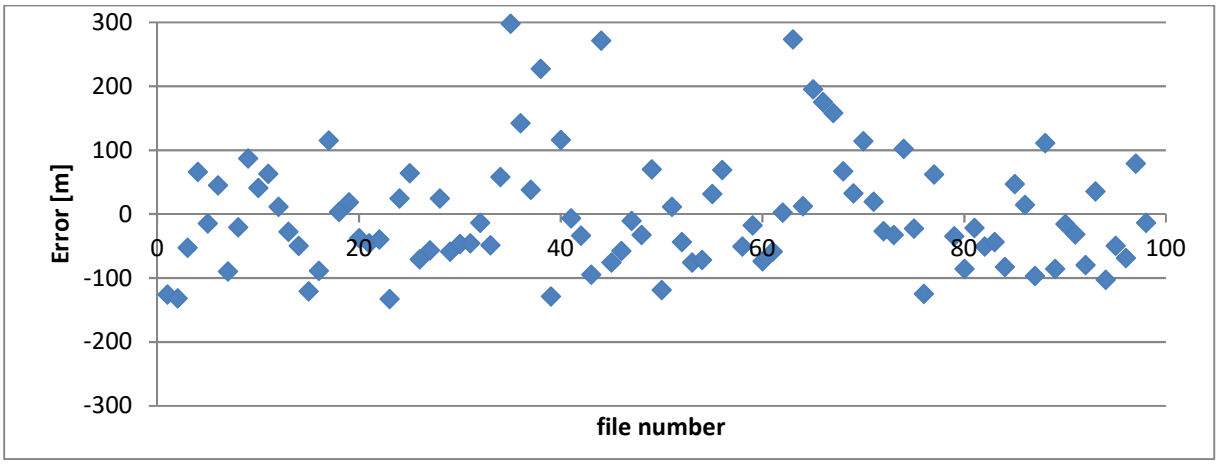

Figure 6-2: Measurement results for 200 MHz sampling frequency

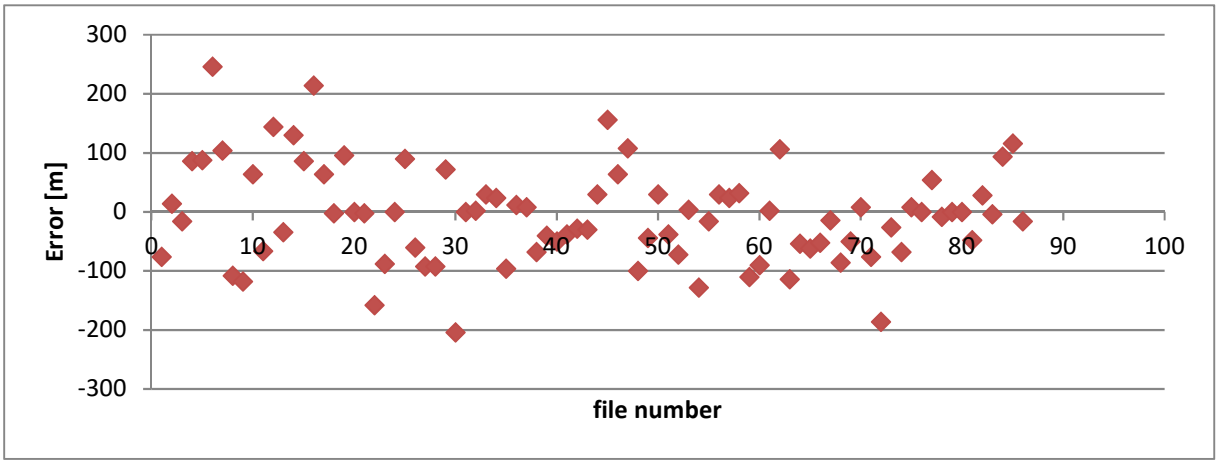

Figure 6-3: Measurement results for 100 MHz sampling frequency

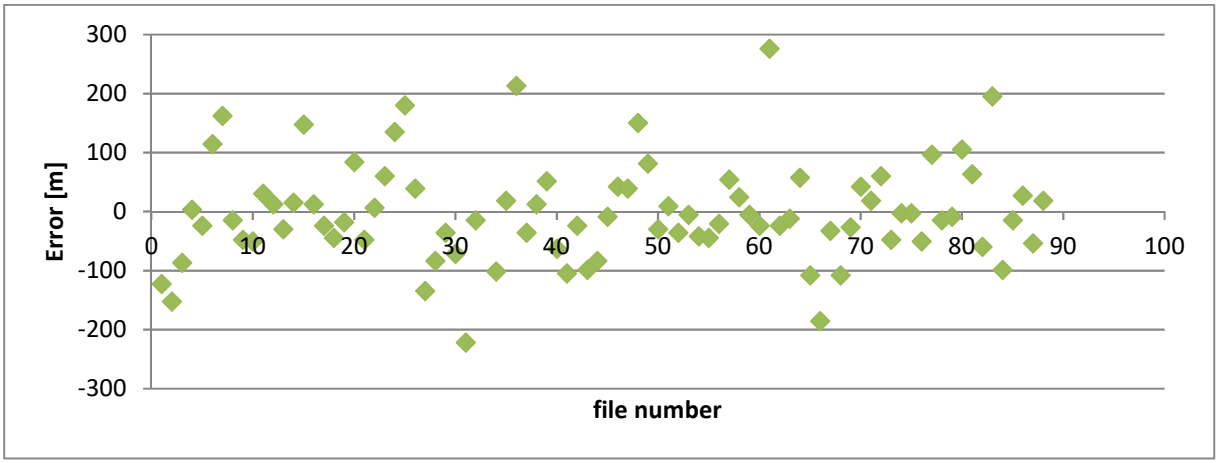

Figure 6-4: Measurement results for 50 MHz sampling frequency

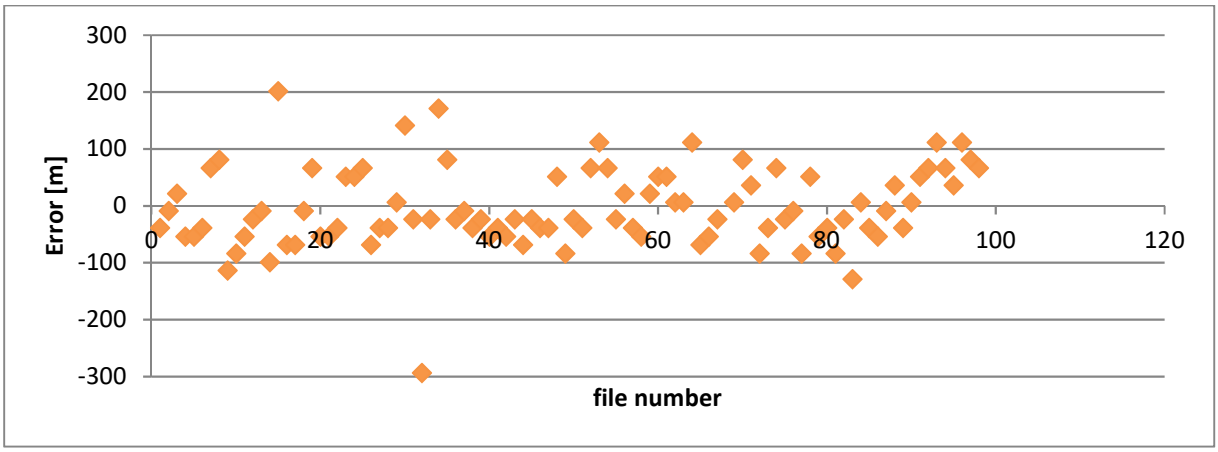

Figure 6-5: Measurement results for 10 MHz sampling frequency

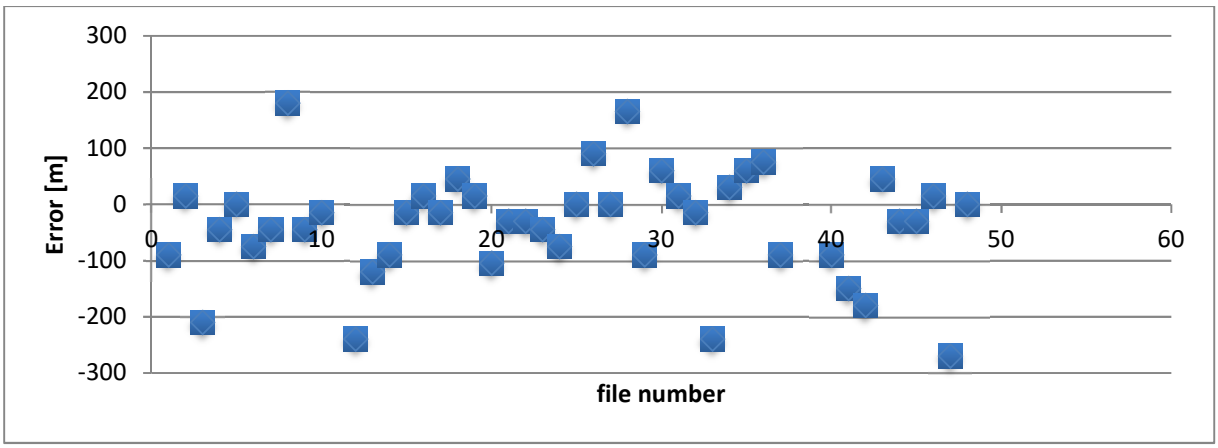

Figure 6-6: Measurement results for 5 MHz sampling frequency

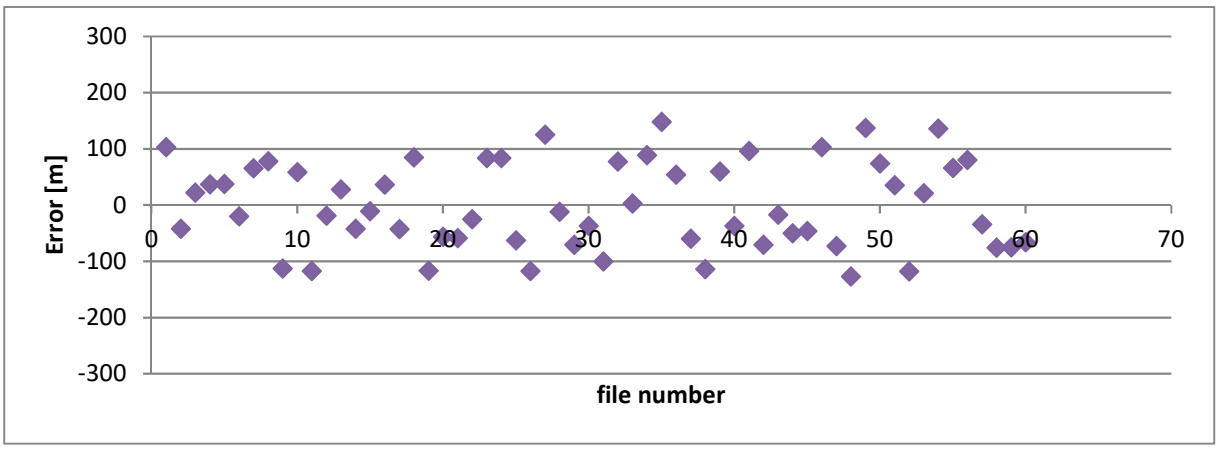

Figure 6-7: Measurement results for 2 MHz sampling frequency

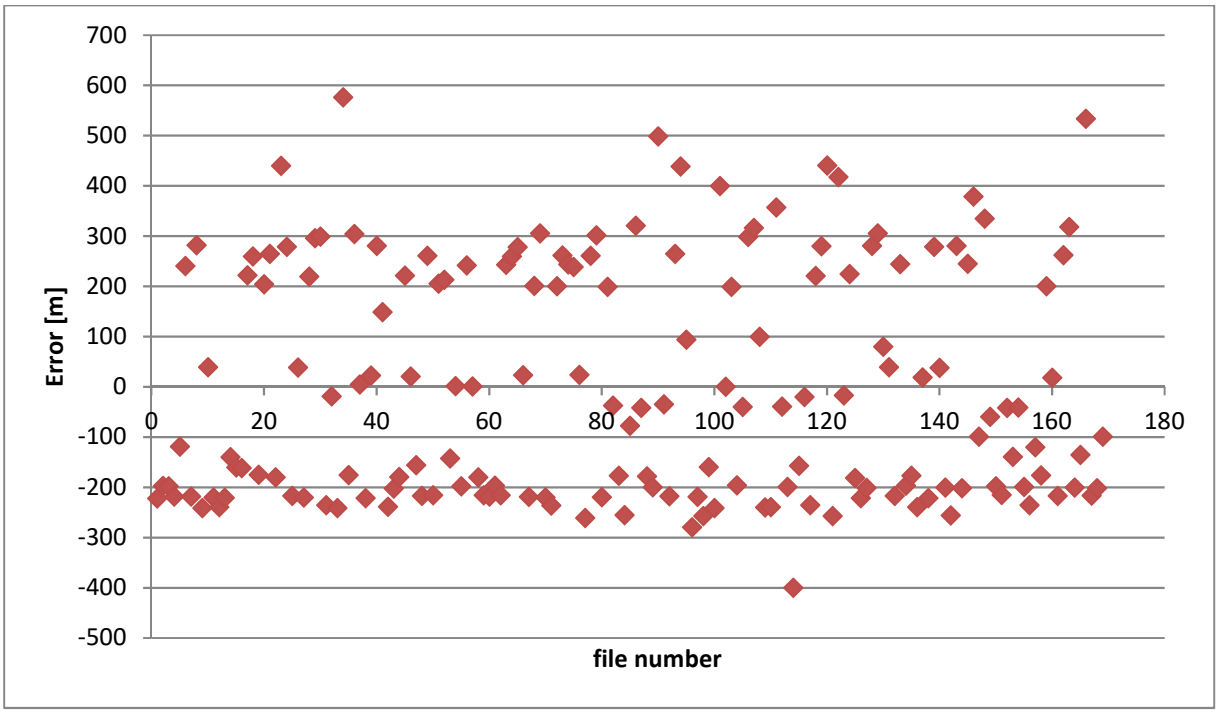

Figure 6-8: Measurement results for 1 MHz sampling frequency

The table 6-1 below shows all the RMS results that were computed in the signal correlation application.

Table 6-1: Correlation of the signal received at the NIT location in Gdańsk at different sampling frequencies

Sampling frequency [MHz]	RMS for the extended correlator [m]	RMS for the double delta correlator [m]
200	97.31	97.22
100	88.81	88.19
50	91.12	91.54
10	82.25	82.41
5	92.3	90.8
2	98.2	96.65

For selected frequencies, the results for a set containing more than 1000 files are presented below (Fig. 6-9, Fig. 6-10).

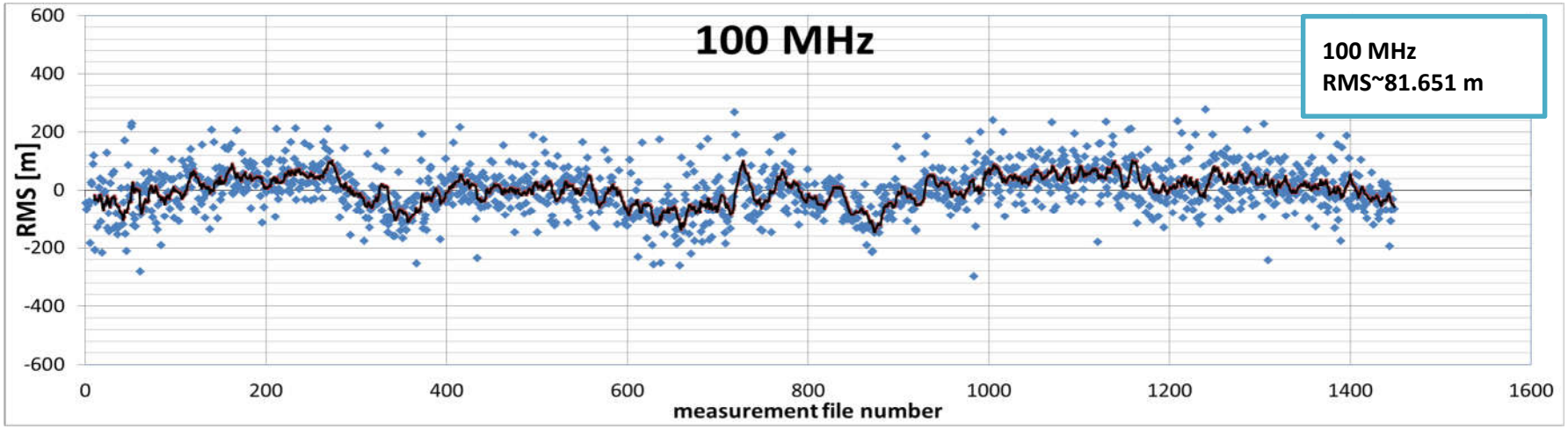

Figure 6-9: Results for a sampling frequency of 100 MHz

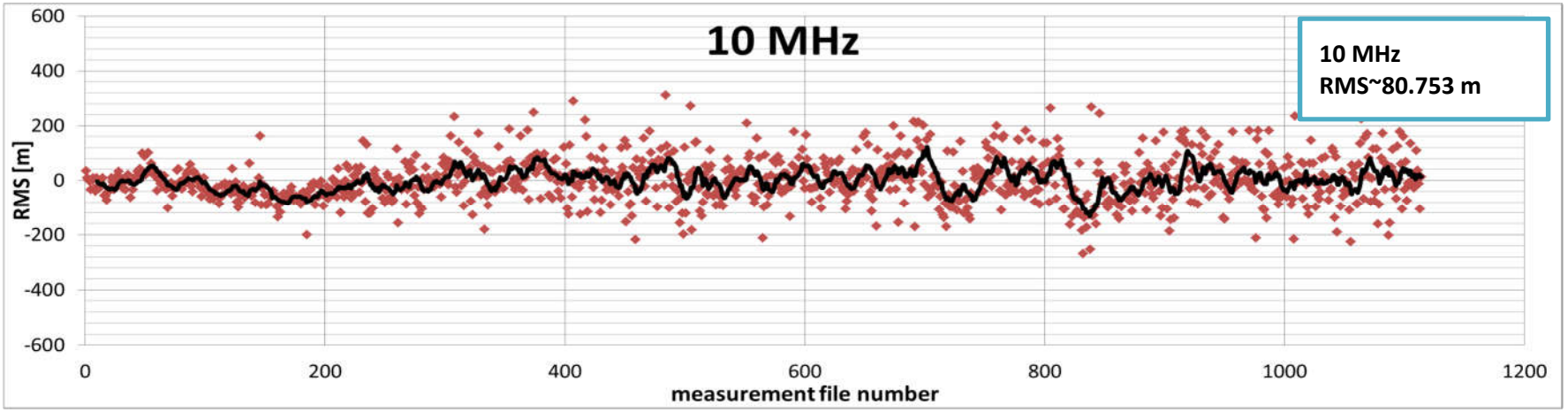

Figure 6-10: Results for a sampling frequency of 10 MHz

A series of graphs showing the results of the research conducted in NIT are presented above. First, a series of tests was performed for different sampling rates on the receiving end. Based on these studies, the frequencies of 100 MHz and 10 MHz were selected for further measurements due to their better stability over time. After conducting research on a large sample of files, it was decided to use the 10 MHz frequency for further measurements, which gave the best and most stable results.

The average RMS obtained here is about 80 meters. It should also be emphasized that this was a study for a signal using 1877 Gold sequence symbols, used for correlation and determination of distance accuracy.

6.2 Two-slot message composed of a Gold sequence and an alternating sequence.

In this case, the signal was broadcast in two time slots. The first slot broadcasts a stream containing Gold's sequence consisting of 1877 symbols (Fig. 6-11) [6-1].

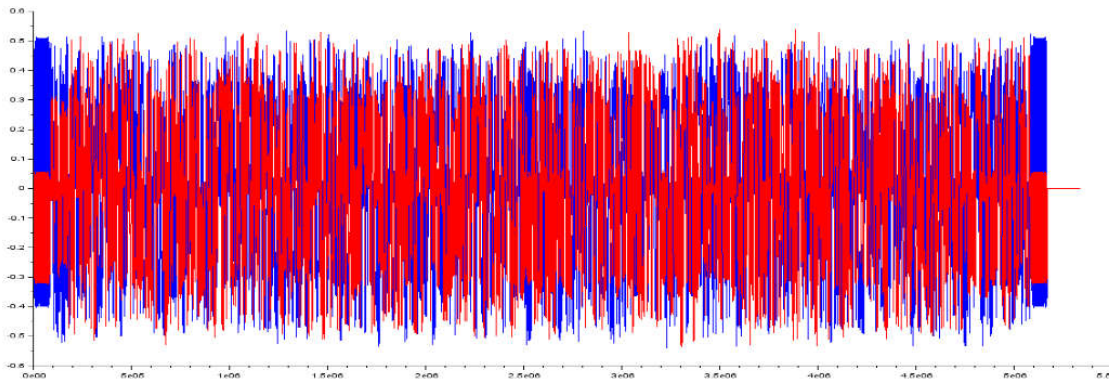

Figure 6-11: VDES signal transmitted with Gold sequence

For the second slot, a new correlation sequence was transmitted - containing an alternating sequence (Fig. 6-12). The alternating sequence – as the name suggests – contains an alternating stream of „0”s and „1”s; it provides more correlation peaks than the Gold code-based sequences. The station transmitting such a signal has already been established. The measurements will allow to compare the performance of these types of ranging sequences in real maritime environment.

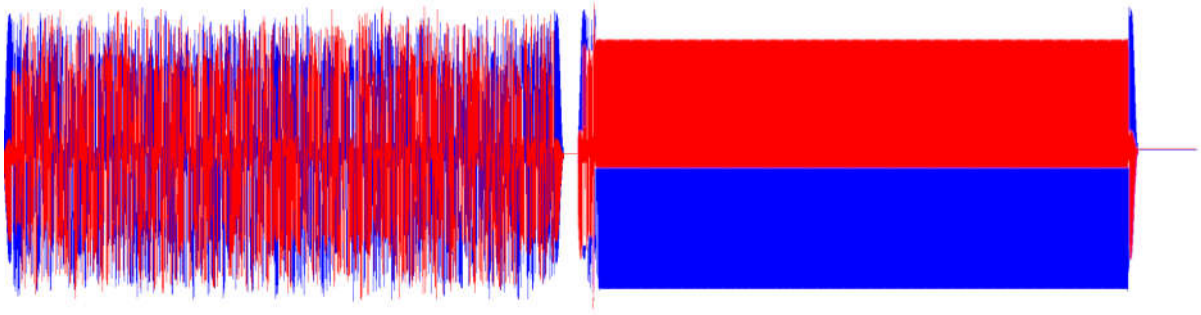

Figure 6-12: VDES signal transmitted in two time slots. In the first slot, the Gold sequence is transmitted, in the second slot the alternating sequence is transmitted.

.

The shape of the correlation function for the alternating sequence is shown below (Fig. 6-13). At a first glance, it can be seen that it contains a large number of correlation peaks compared to the Gold correlated sequence.

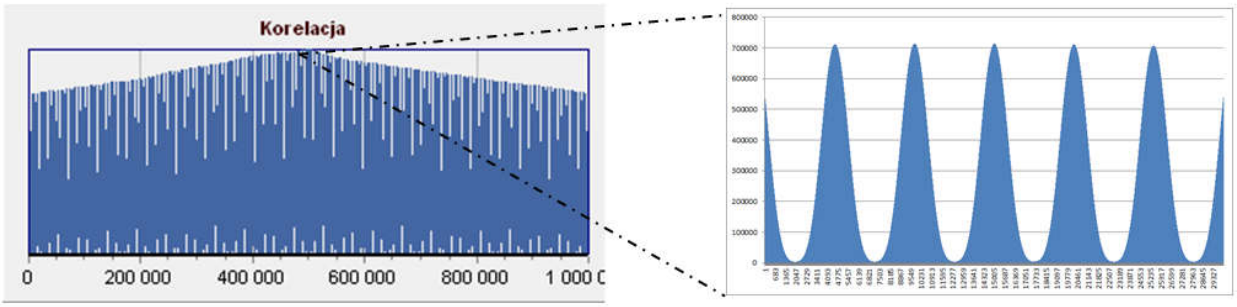

Figure 6-13: New shape of the correlation peak for analysis – alternating sequence

Studies by the NIT were performed for both sequences. Assuming that the two-slot sequence will be transmitted continuously, where the correlation will be performed first for the Gold sequence - the exact position of the correlation peak for the alternating sequence can be determined. By determining the correlation peak for the Gold sequence, knowing the sizes of the slots and signals - we can calculate where the correlation peak for the alternating sequence should be. Why did we choose this approach? It was due to the fact that for the SNR with smaller values, if we correlated the message only for the alternating sequence - we would get correlation peaks with unequal heights. It would be difficult to estimate which of the correlation peaks is the peak from which the distance has to be determined. Sending an alternating sequence would make more sense if the SNR is high.

6.3 Four-slot message - emulation of four base stations - for the Gold sequence

In the next research measurements, the signal was sent in four slots. This was to simulate the presence of four transmitting stations and prepare the system for measurements in a real environment with the presence of several base stations. The four-slot message was created by combining four signals with a Gold sequence with a frequency of 10 MHz. In order to simulate different distances of the transmitting stations from the receiver, additional delays were added and the powers were proportionally adjusted.

The research was carried out on a group of 1500 offline files. Each of the slots simulated a separate broadcasting station. The transmitted signal is presented below (Fig. 6-14):

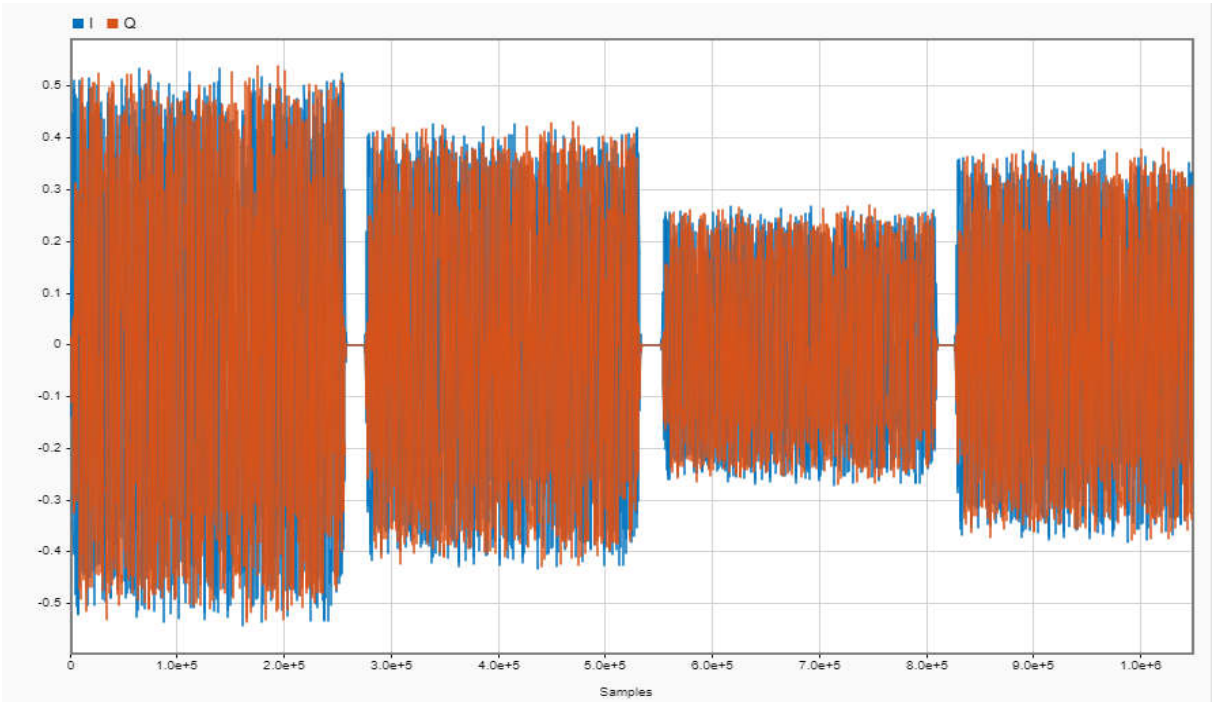

Figure 6-14:A four-slot message

Shown below are graphs showing the frequency domain (Fig. 6-15) and time domain characteristics (Fig. 6-16) of the received signal.

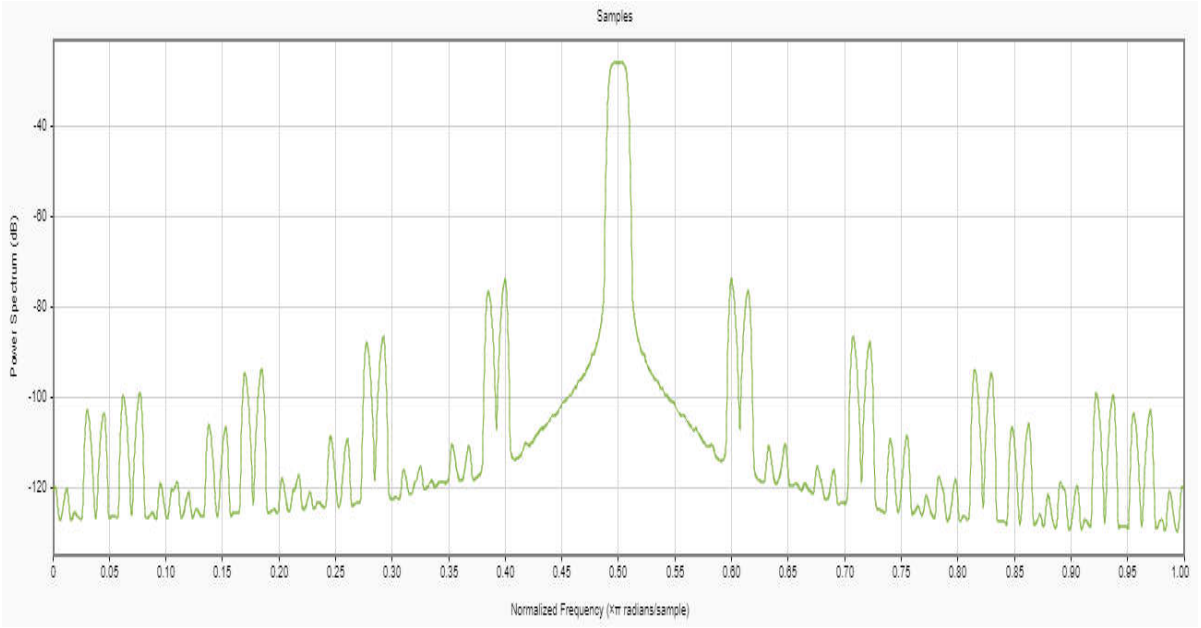

Figure 6-15: Frequency domain signal

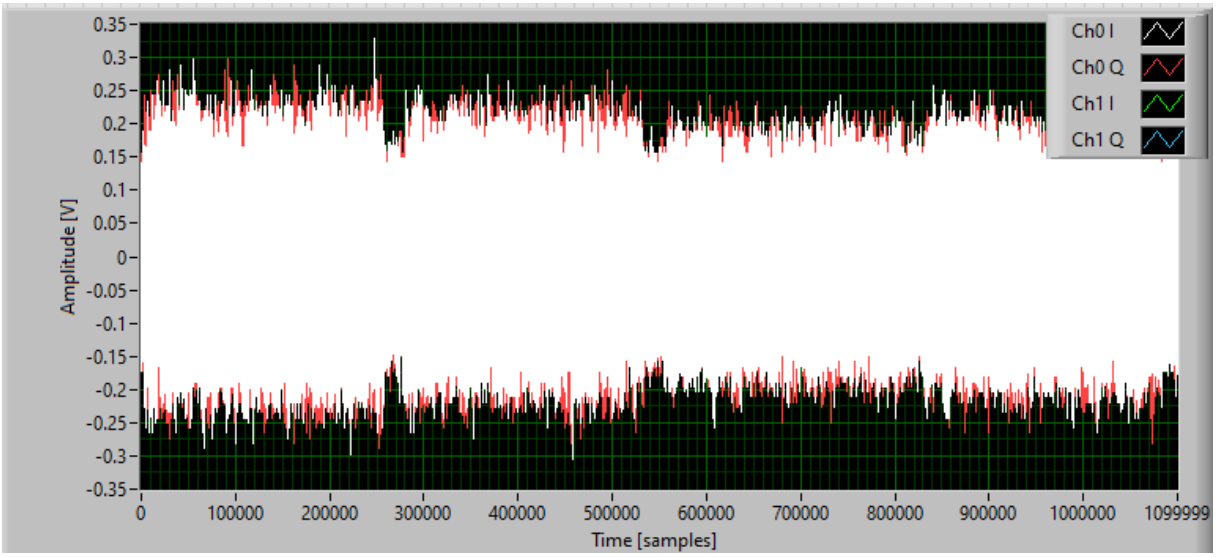

Figure 6-16: Time domain signal

The fig. 6-17 below shows the results obtained from the signal correlation application. It is clear from the graph that the distances for the four stations at different distances have been calculated.

Figure 6-17: Signal correlation application - scenario for four stations

Above is a screenshot of some of the processed data. All the results were saved to a csv file and then detailed distance accuracy results for each of the four stations were generated. On the basis of the results, we can conclude that for the transmitting station at the distance of 17.4 km, ranging accuracy with respect to the GNSS receiver was around 20 m. We may assume that for shorter distance between the transmitter and receiver, the accuracy will significantly improve – to just a few meters.

The determined distances for each of the slots that represent the base station are shown below (Fig. 6-18).

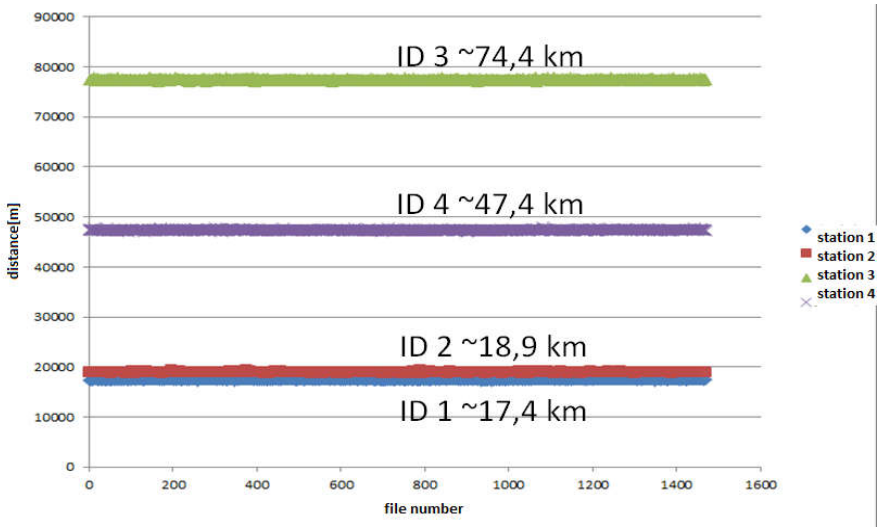

Figure 6-18: Designated distances for four base stations

The values of the correlation peaks depending on the signal strength and the distance from the receiver are presented below (Fig. 6-19):

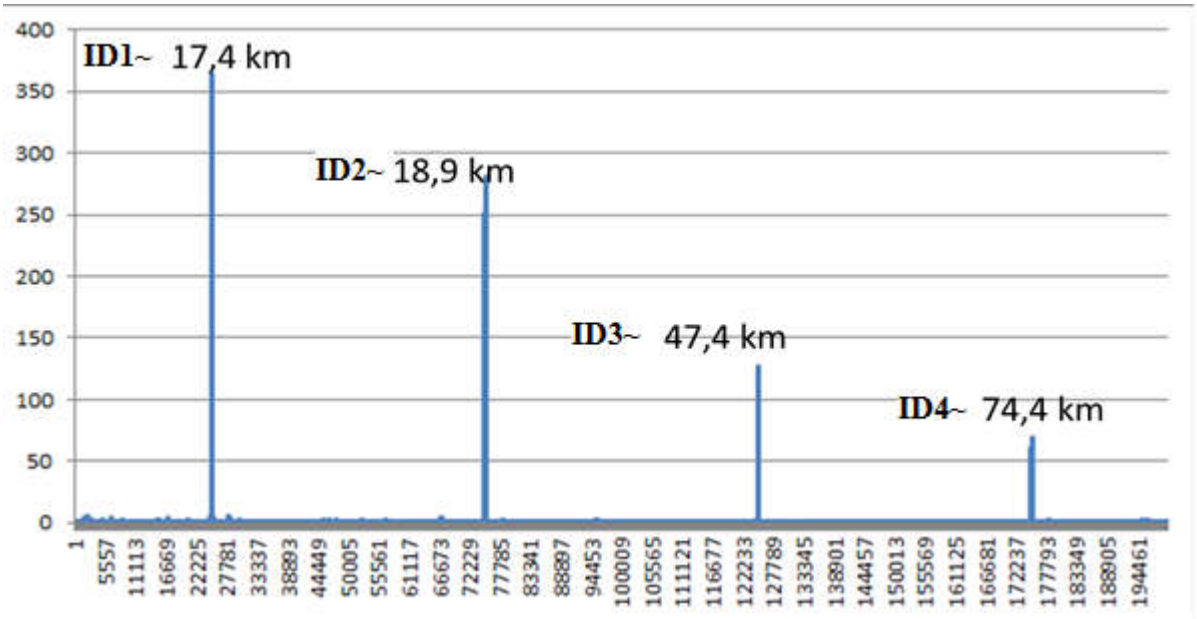

Figure 6-19: Correlation peaks for each of the slots

During the reception, the signals from other transmitters were received simultaneously, which caused the calculated SNR of the target signal to be false. The calculated SNR for each slot is listed below. By manually changing the value of the transmitted signal depending on its simulated distance, it was possible to obtain different SNR values (Fig. 6-20)

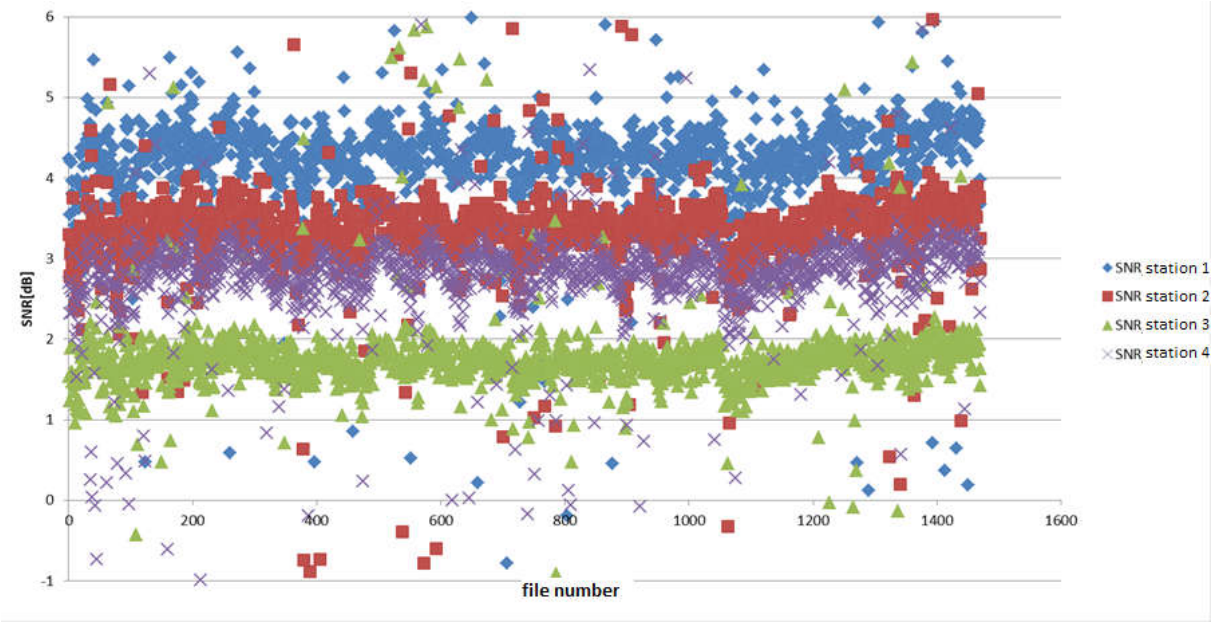

Figure 6-20: Calculated SNR for all slots

SNR values do not exceed 5 dB due to the fact that the transmitting station was actually about 17 km from the NIT building. The other simulated signals had even lower powers, which, as we can see, reached a minimum of 1 dB.

The exact results for the first station are presented below (Fig. 6-21). The chart shows the calculated distance accuracy and the table 6-2 shows the calculated RMS.

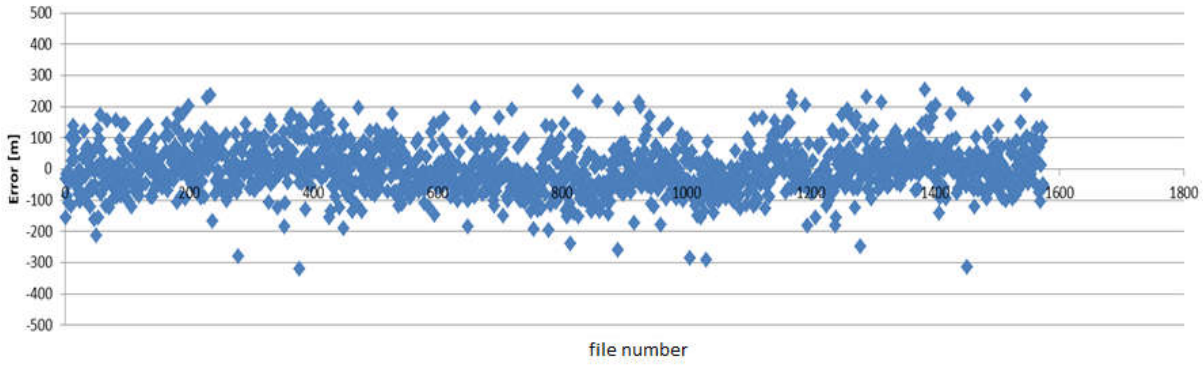

Figure 6-21: Calculated distance accuracy for the first station

Table 6-2: Calculated distance accuracy for the first station

Station number	Average distance from transmitter	Sampling frequency [MHz]	RMS for the double delta correlator [m]
1	17437 m	10	75.314 m

The calculated accuracies for the second station are presented below (Fig. 6-22). The table 6-3 shows the calculated RMS.

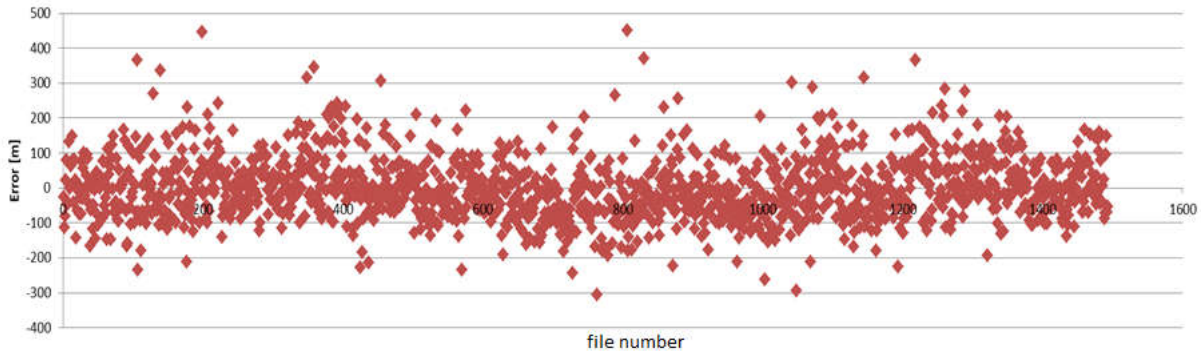

Figure 6-22: Calculated accuracy for the second station

It can be seen that the results for the second station are already worse than for the first station. This station was 1500 meters farther away from the first station. The power of the signal transmitted for the second slot was also reduced proportionally, which can be seen from the value of the correlation peak. These conditions translated into the calculated RMS, which, as we can see, is about 15 meters worse than for the first slot.

Table 6-3: Calculated distance accuracy for the second station

Station number	Average distance from transmitter	Sampling frequency [MHz]	RMS for the double delta correlator [m]
2	18931 m	10	89.549 m

The distance accuracy graph for the third slot is shown below (Fig. 6-23):

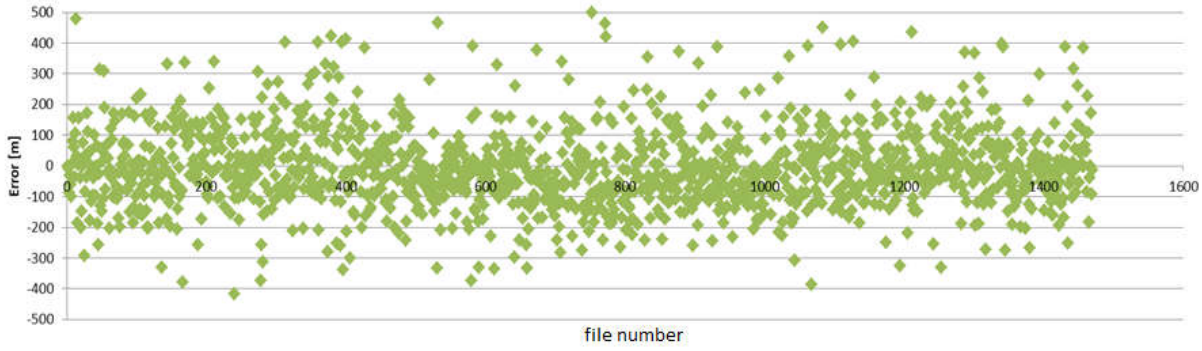

Figure 6-23: Calculated accuracy for the third station

The table 6-4 below shows the exact RMS results calculated for the third slot:

Table 6-4: Calculated distance accuracy for the third station

Station number	Average distance from transmitter	Sampling frequency [MHz]	RMS for the double delta correlator [m]
3	77427 m	10	135.263 m

The case for the third slot had the highest delay introduced and the lowest signal strength. This is especially seen in the calculated RMS, which is much greater than the rest. The error is at the level of 130 meters, which is significant.

The distance accuracy graph for the fourth slot is shown below (Fig. 6-24):

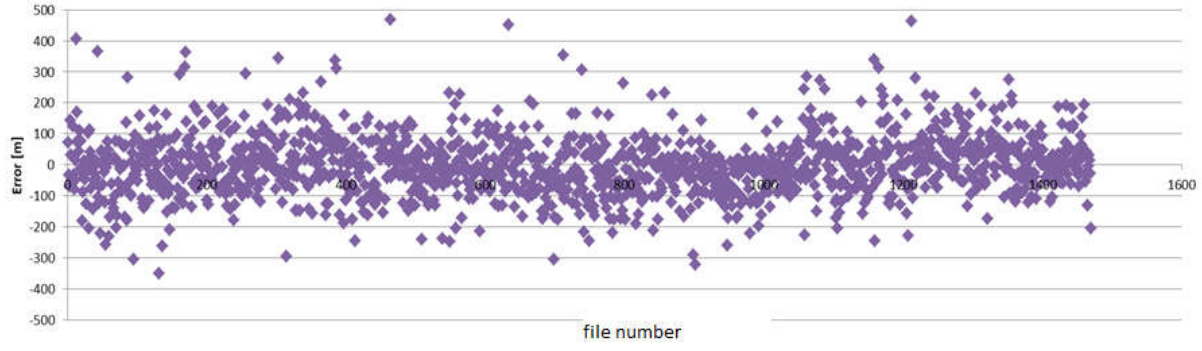

Figure 6-24: Calculated accuracy for the fourth station

The table 6-5 below shows the RMS obtained for the results for the fourth slot.

Table 6-5: Calculated distance accuracy for the fourth station

Station number	Average distance from transmitter	Sampling frequency [MHz]	RMS for the double delta correlator [m]
4	47388 m	10	98.499 m

The table 6-6 shows a summary of all the results obtained for the four slots:

Table 6-6: A summary of all the results obtained for the four slots

Station number	Average distance from transmitter	RMS for the double delta correlator [m]
1	17437 m	75.314 m
2	18931 m	89.549 m
3	77427 m	135.263 m
4	47388 m	98.499 m

As we can see above, all the results obtained for the four slots have been compiled. Thanks to this, it was possible to check the correctness of the implementation of all modules in the system until the distance accuracy was determined. In the scenario for four base stations, their presence was simulated as separate time slots. In a signal correlation application, each slot has been correlated with a reference signal. After numerous mathematical operations, the calculated distance was obtained. The tests confirm the correctness of the implemented modules for determining the signal distance from the transmitting station based on the signal delay.

6.4 Measurement scenario with ranging accuracy studies for four slots with gamma = 0.7

In this research scenario, a signal consisting of a Gold sequence and an alternative sequence was used [6-2].

The ranging sequence is known and it is a part of the data payload. Each shore station shall send out the ranging sequence once per second.

The ranging sequence is a combination of two sequences to customize the required performance based on the given scenarios. The scenarios are:

- Shorter distances between shore station and vessel
- Longer distances between shore station and vessel

The first sequence is based on the $\pi/4$-QPSK modulation alphabet and alternates its constellation points. The second part of the ranging sequence is a Gold code.

Both sequences are weighted and then added together. The alternating sequence is multiplied by a weighting factor $\gamma(short) = 0.7$ for short distances (higher SNR) and $\gamma(large) = 0.3$ for larger distances (lower SNR). The Gold code is multiplied by a weighting factor $1 - \gamma(short) = 0.3$ for short distances and $1 - \gamma(large) = 0.7$ for large distances.

The signal for γ= 0.7 is shown below (Fig. 6-25)

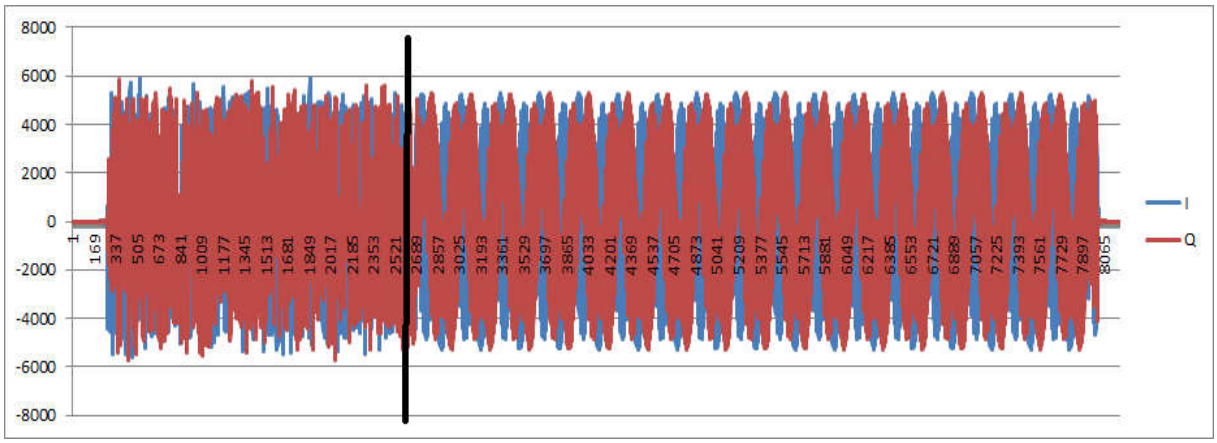

Figure 6-25: Signal for γ= 0.7

Correlation plots for this signal are shown below. The first graph shows the correlation for the part with the Gold signal (Fig. 6-26). In the second plot (Fig. 6-27), there is a correlation of the part with the alternating sequence. The last graph (Fig. 6-28) shows what the autocorrelation function of this signal looks like.

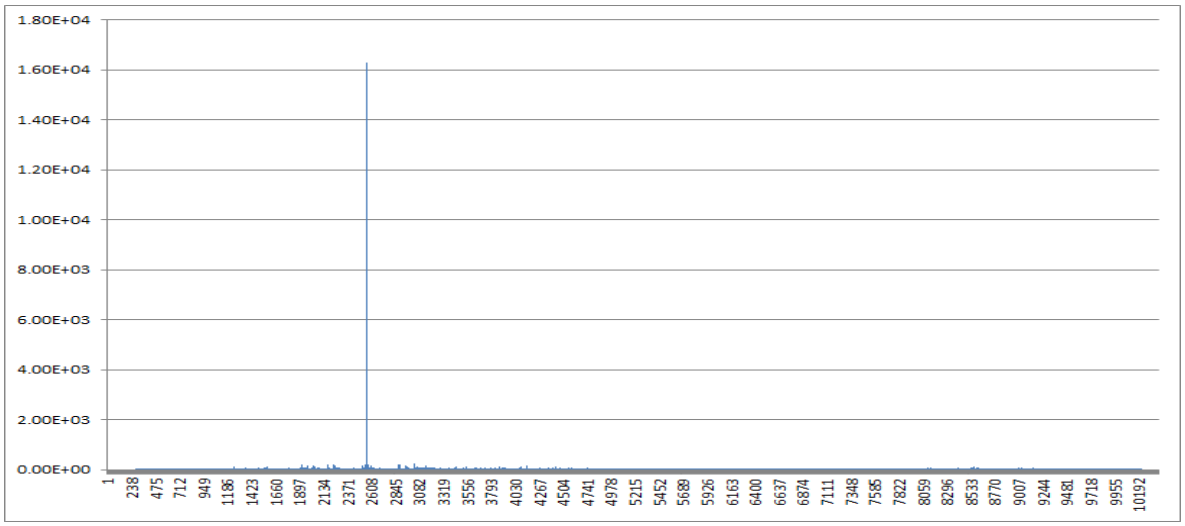

Figure 6-26: Correlation of parts of the Gold sequence

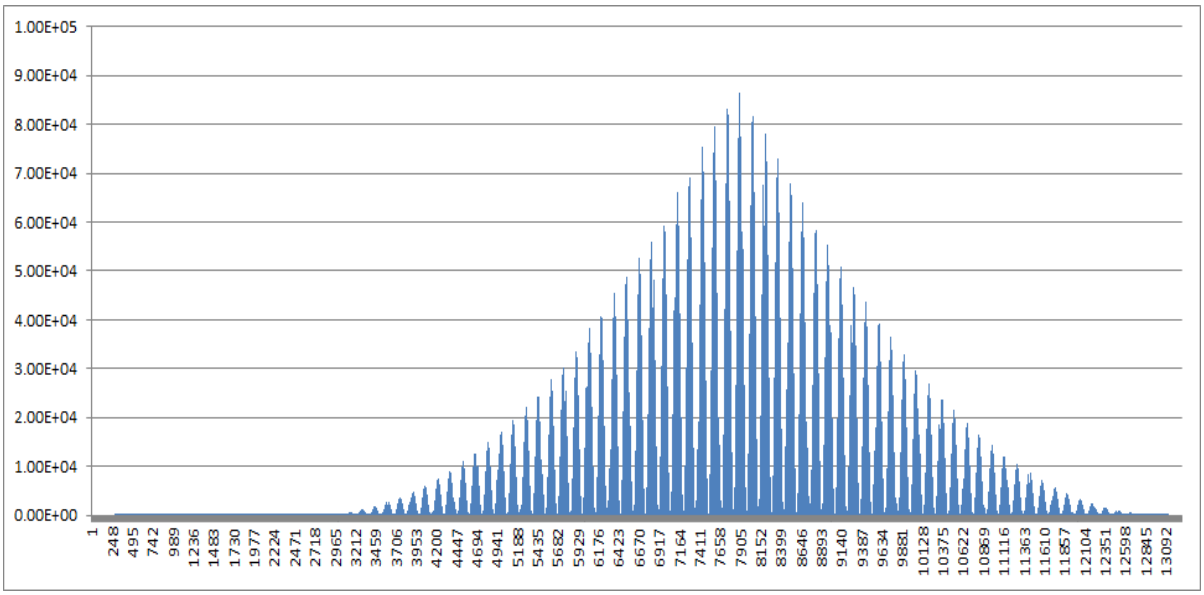

Figure 6-27: Correlation part of the string alternative sequence

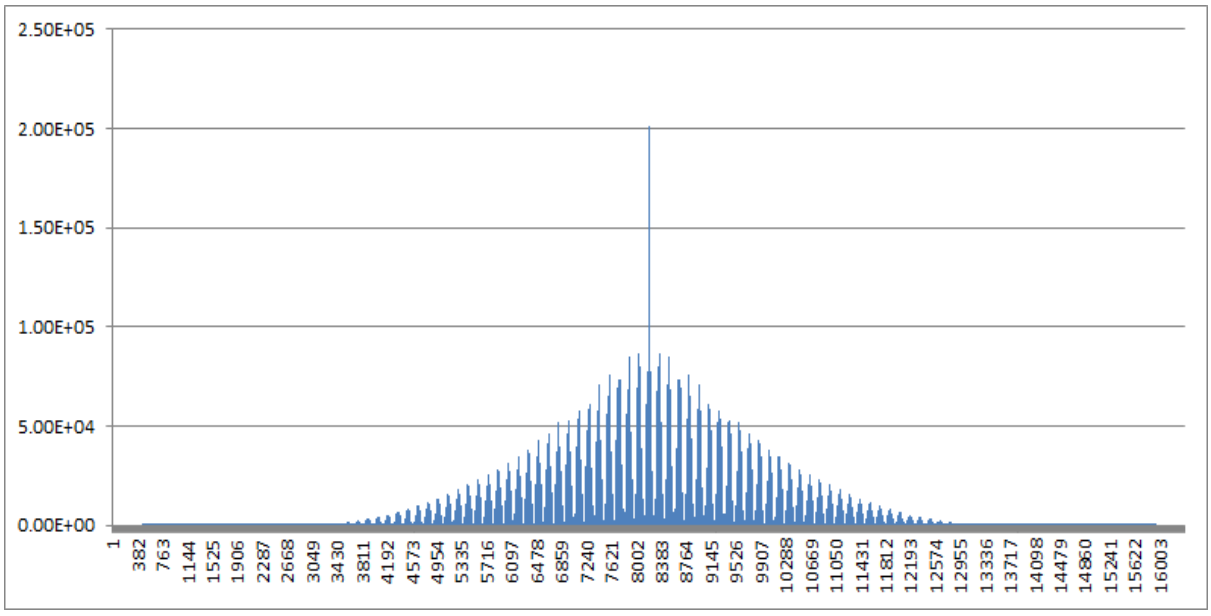

Figure 6-28: Autocorrelation for the entire signal

The above shows the correlations for this type of signals. Thanks to the combined sequence in the measurement tests, even better distance accuracy was obtained, which greatly influenced the obtained results. The screenshot below (Fig. 6-29) shows a signal correlation application that processes recorded samples from a transmitting station located in Gdynia, 17 km from the receiving antenna. With the correlation of signals for the $\gamma = 0.7$, distance accuracy of an average of 20 meters was obtained.

Figure 6-29: Processing samples with γ = 0.7

The screenshot also shows the signal correlation application, which determines the accuracy of distances up to 20 meters. In this case, the sample file was saved as a four-slot message, i.e. the presence of four base stations located at equal distances from the receiver was simulated. In addition, measurements were read from the GNSS module in order to calculate the accuracy of the determined distance in real time.

First, the correlation of the signal set to γ = 0.7 was dealt with. In the first analysis, it was correlated with the γ = 0 signal, i.e. the full Gold sequence, to compare it with the correlation for γ = 0.7 to see how the obtained distance accuracy changes.

With the correlation (Fig. 6-30) of the γ = 0.7 signal with the γ = 0 signal, RMS = 44.68 m was obtained, which is still very accurate compared to the previous analyzes. However, for the same signal with γ = 0.7 (Fig. 6-31), which was also correlated with the γ = 0.7 signal, the result was RMS = 17.58 m for about 5400 files, which is a really good result.

Below are graphs on the same scale for comparison:

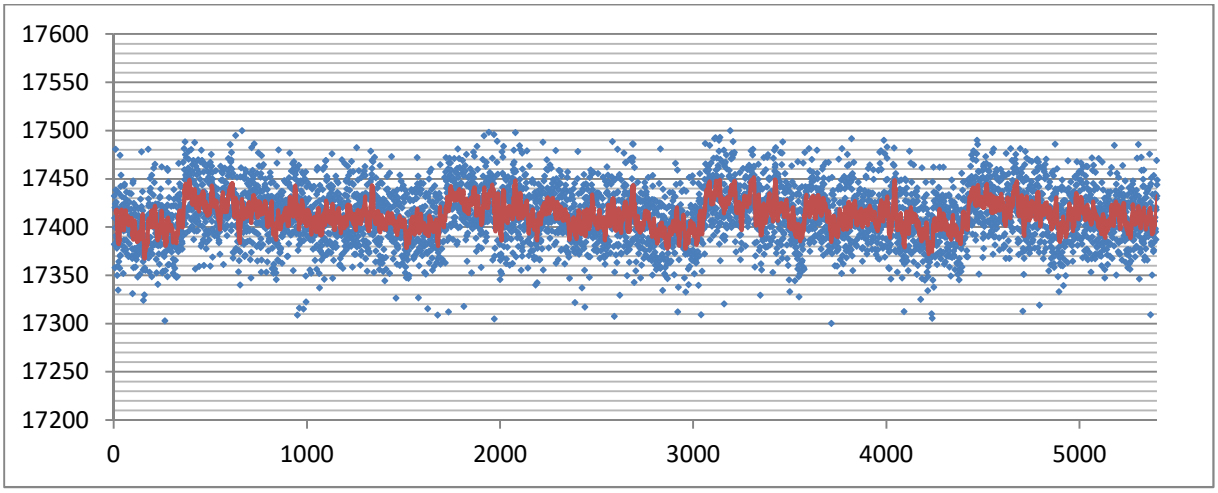

Figure 6-30: GAMMA (γ) signal = 0.7 correlated with GAMMA (γ) signal = 0

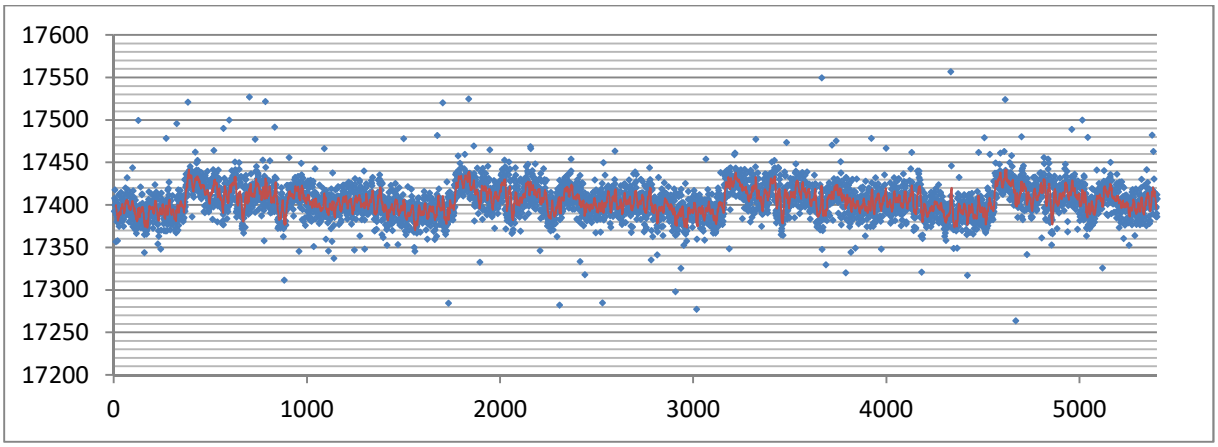

Figure 6-31: GAMMA (γ) signal = 0.7 correlated with GAMMA (γ) signal = 0.7

Almost the same results were observed for the transmitted signal γ = 0.3. Here, the RMS for that signal correlated with the γ = 0 signal (Fig. 6-32) is RMS = 44.52 m and the RMS for that signal correlated with the γ = 0.3 signal (Fig. 6-33) is RMS = 20.54 m.

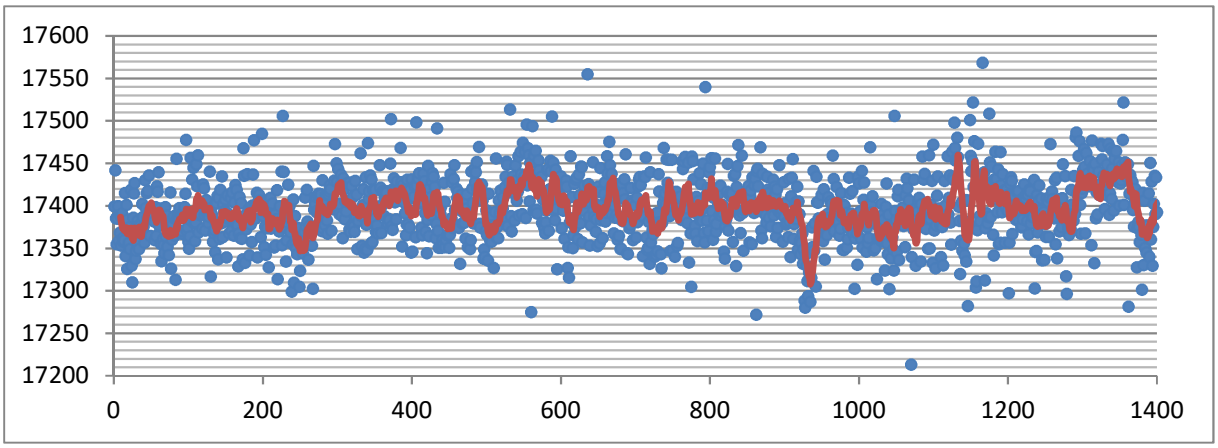

Figure 6-32: GAMMA (γ) signal = 0.3 correlated with GAMMA (γ) signal = 0

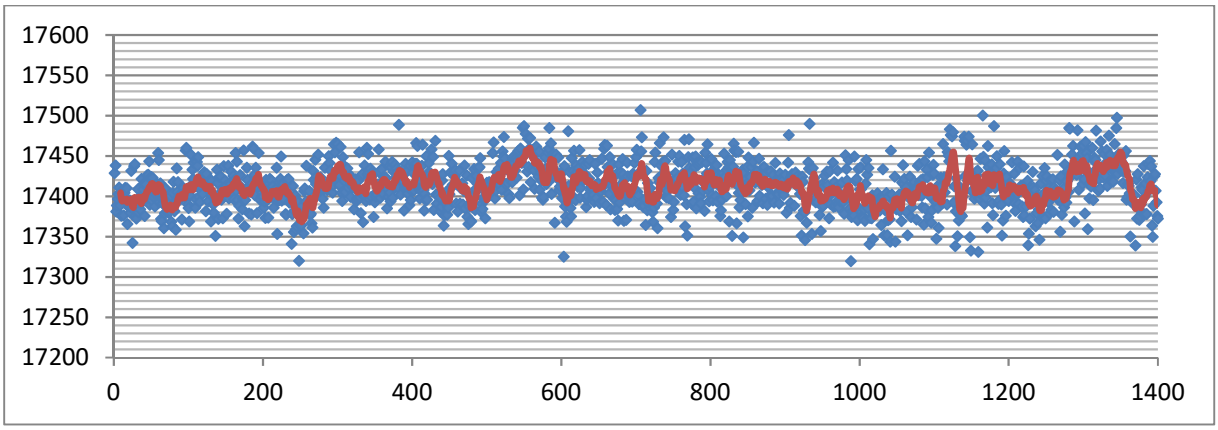

Figure 6-33: GAMMA (γ) signal = 0.3 correlated with GAMMA (γ) signal = 0.3

7 R-Mode positioning demonstration

In March 2021, the R-Mode system for real-time positioning was tested under laboratory conditions. The research consisted in integrating all hardware and software modules, thanks to which a demonstration stand of the R-Mode system was created.

In the first stage, the part in which the USRP and u-blox recorded all the necessary data was integrated, and then that data were transferred to the second module with the signal correlation application.

The integration was successful and its effects are presented below (Fig. 7-1, 7-2, 7-3, 7-4, 7-5, 7-6).

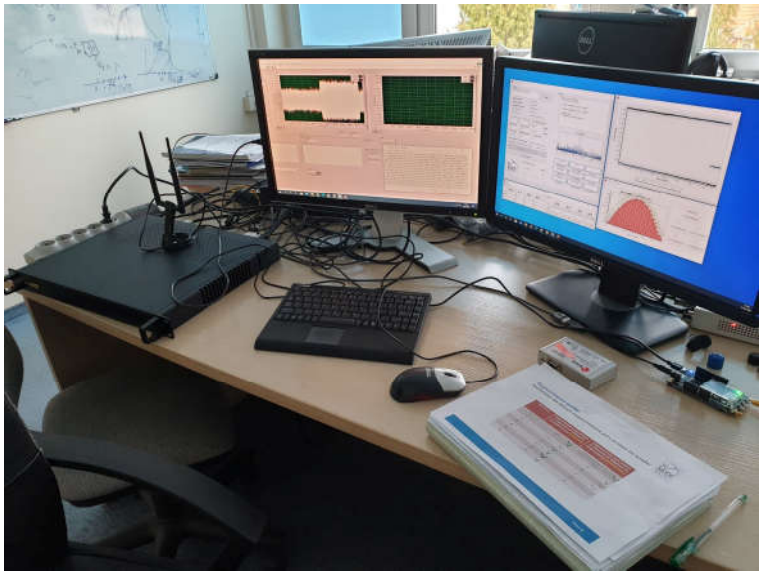

Figure 7-1: Integration of a sample recording module with a signal correlation module that determines pseudoranges a)

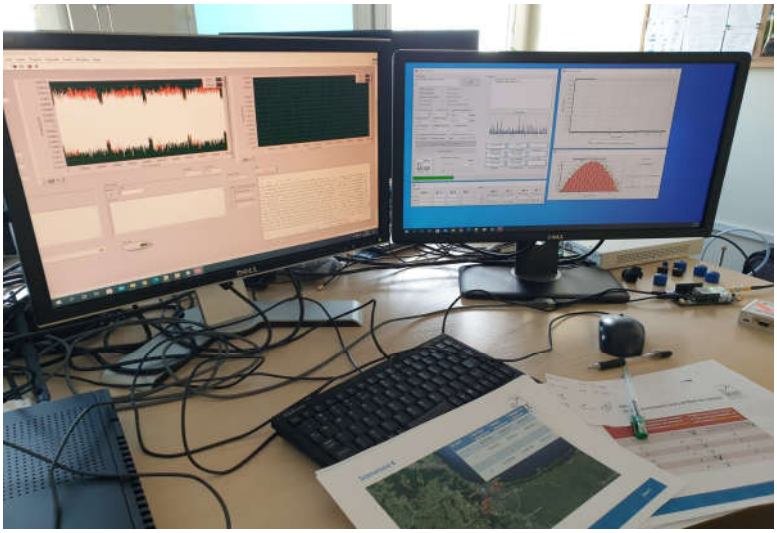

Figure 7-2: Integration of a sample recording module with a signal correlation module that determines pseudoranges b)

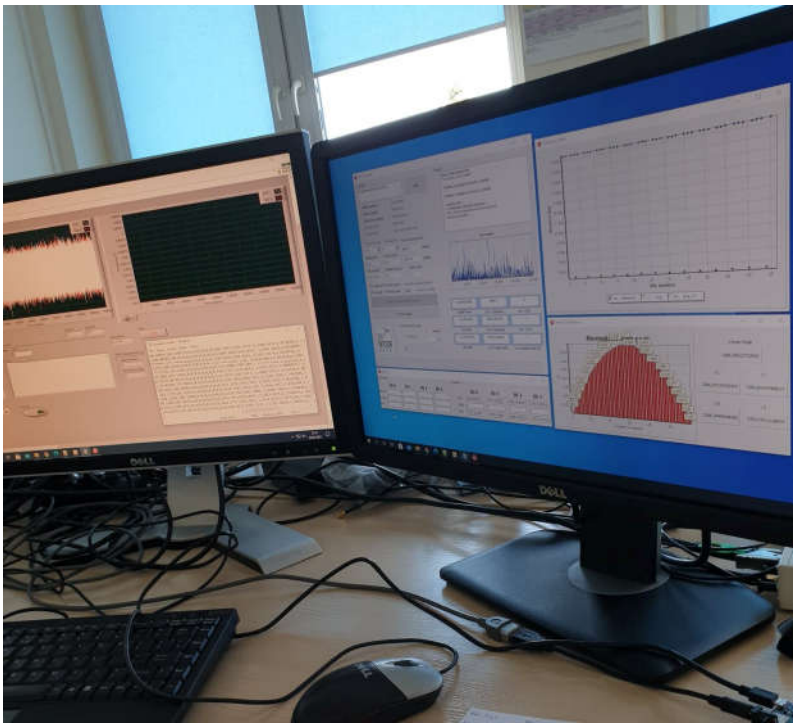

Figure 7-3: Integration of a sample recording module with a signal correlation module that determines pseudoranges c)

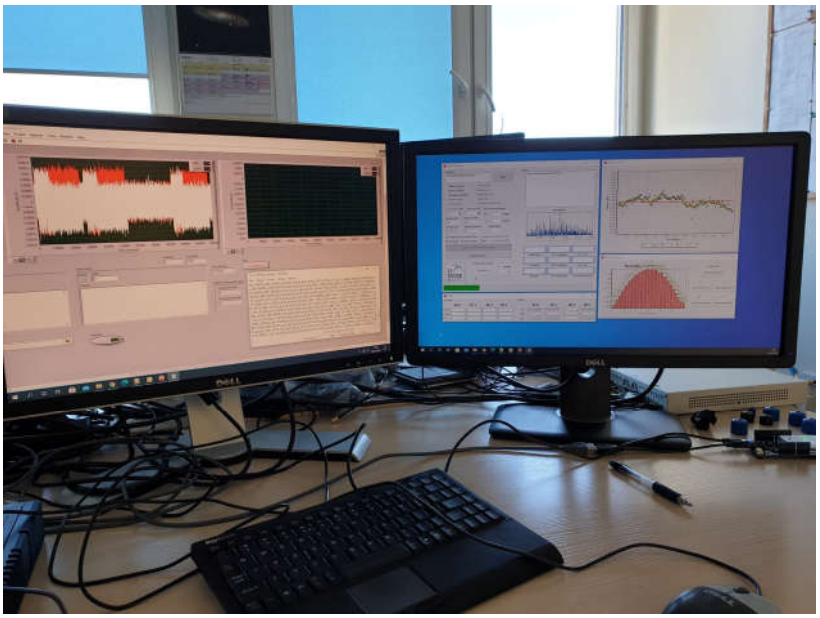

Figure 7-4: Integration of a sample recording module with a signal correlation module that determines pseudoranges d)

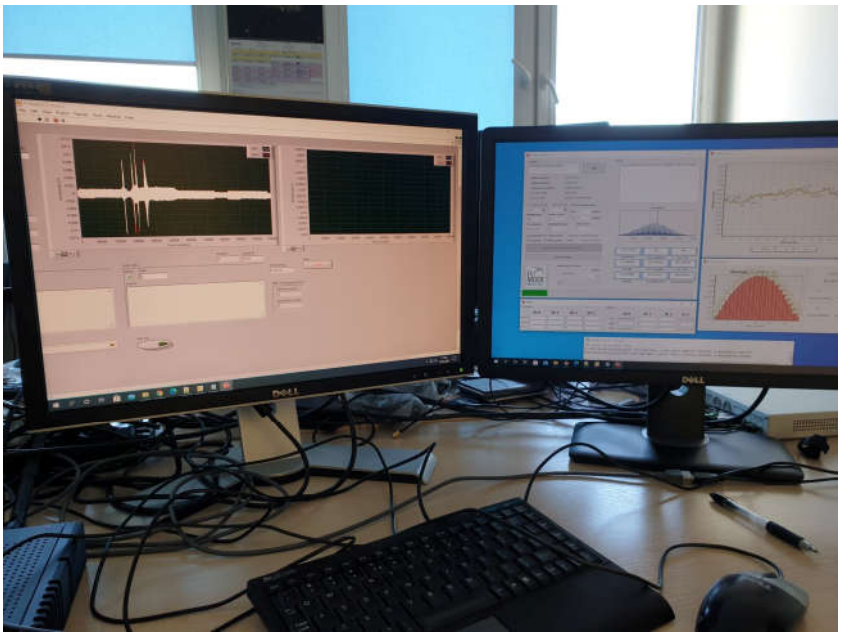

Figure 7-5: Integration of a sample recording module with a signal correlation module that determines pseudoranges e)

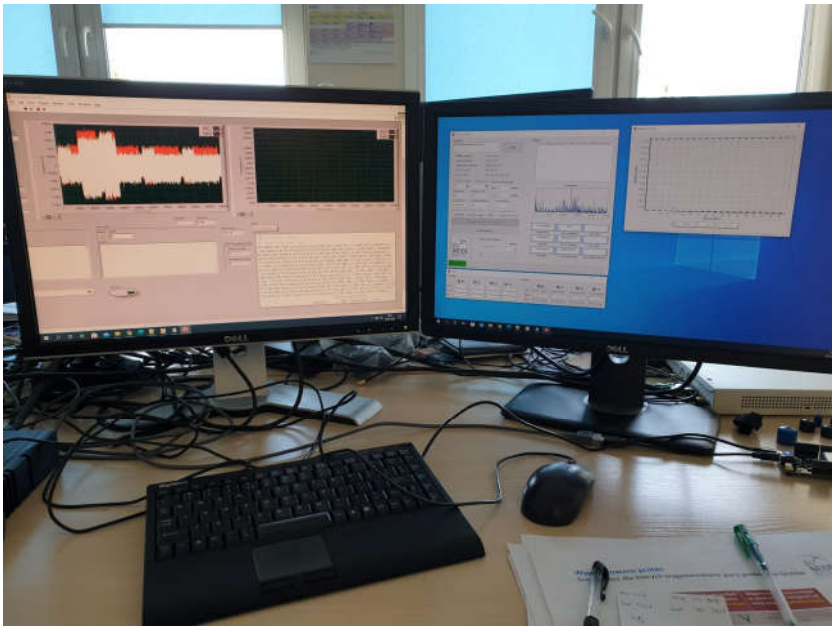

Figure 7-6: Integration of a sample recording module with a signal correlation module that determines pseudoranges f)

In the second stage, the integration of all modules was completed, i.e. the module with samples from USRP together with the module for correlation of signals were integrated with the application for determining the position based on the obtained pseudoranges.

As part of the tests, the influence of different positioning of the R-Mode base stations in relation to the receiver and the influence of various factors on the errors of the determined position was examined.

The 6 scenarios based on which all tests were performed are presented below (Fig. 7-7, 7-8, 7-9, 7-10, 7-11, 7-12):

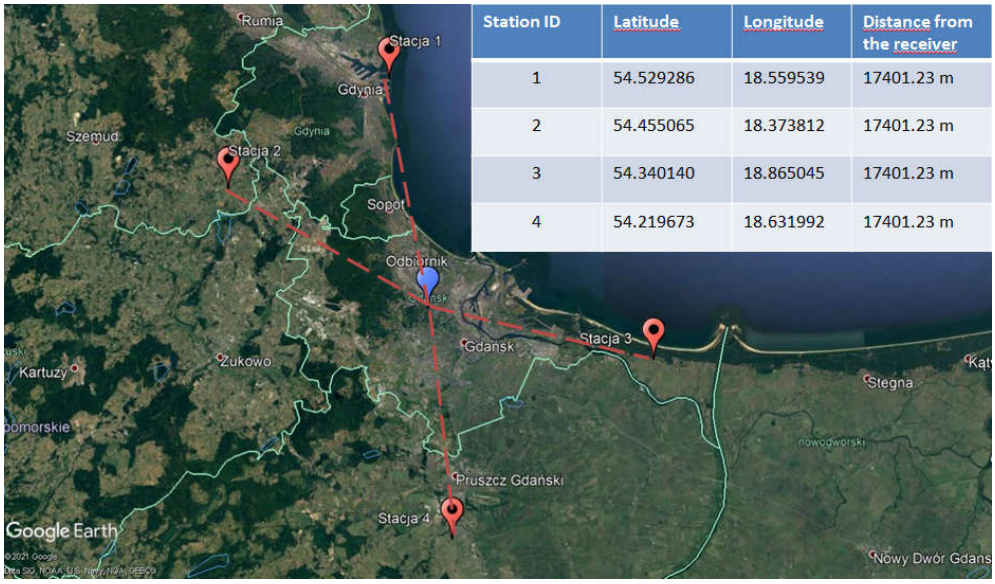

Station ID	Latitude	Longitude	Distance from the receiver
1	54.529286	18.559539	17401.23 m
2	54.455065	18.373812	17401.23 m
3	54.340140	18.865045	17401.23 m
4	54.219673	18.631992	17401.23 m

Figure 7-7: The first measurement scenario for testing the positioning R-Mode demonstrator in real time

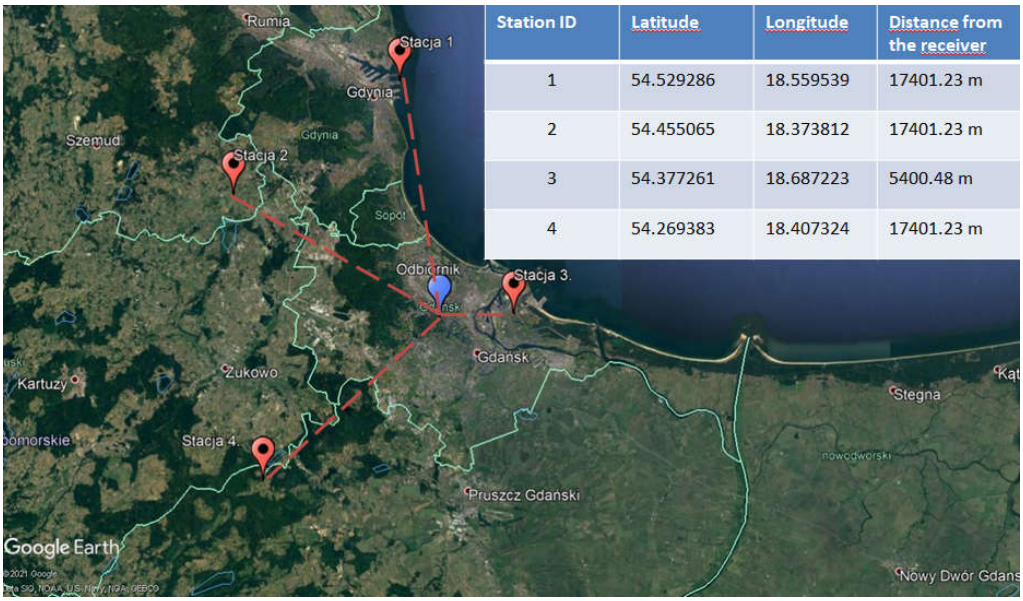

Station ID	Latitude	Longitude	Distance from the receiver
1	54.529286	18.559539	17401.23 m
2	54.455065	18.373812	17401.23 m
3	54.377261	18.687223	5400.48 m
4	54.269383	18.407324	17401.23 m

Figure 7-8: The second measurement scenario for testing the positioning R-Mode demonstrator in real time

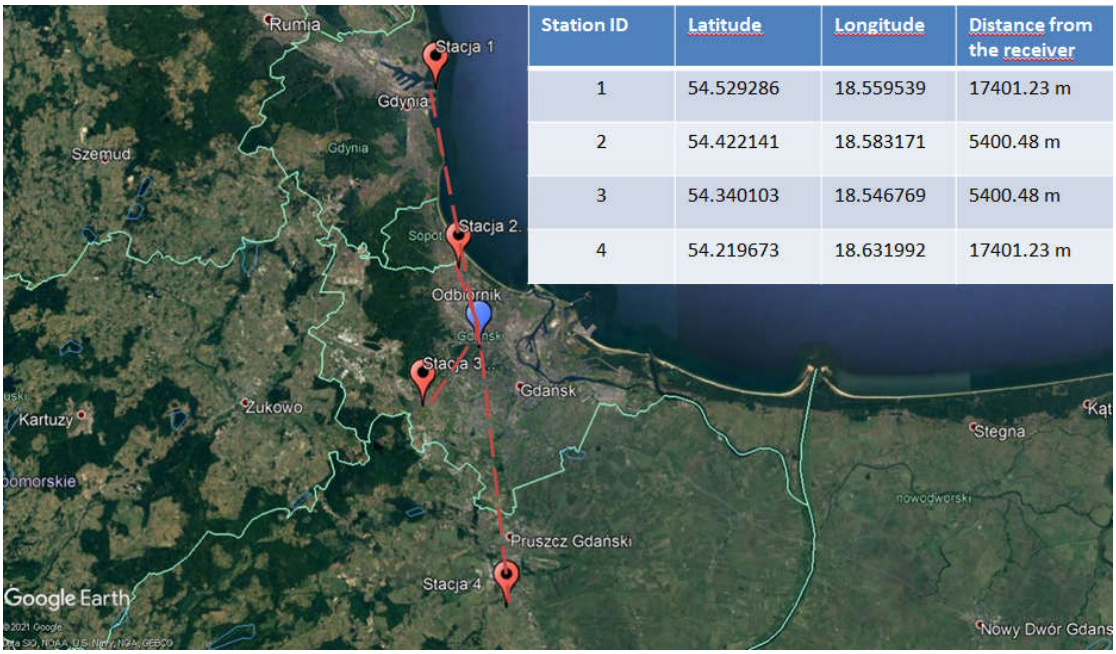

Station ID	Latitude	Longitude	Distance from the receiver
1	54.529286	18.559539	17401.23 m
2	54.422141	18.583171	5400.48 m
3	54.340103	18.546769	5400.48 m
4	54.219673	18.631992	17401.23 m

Figure 7-9: The third measurement scenario for testing the R-Mode positioning system demonstrator in real time

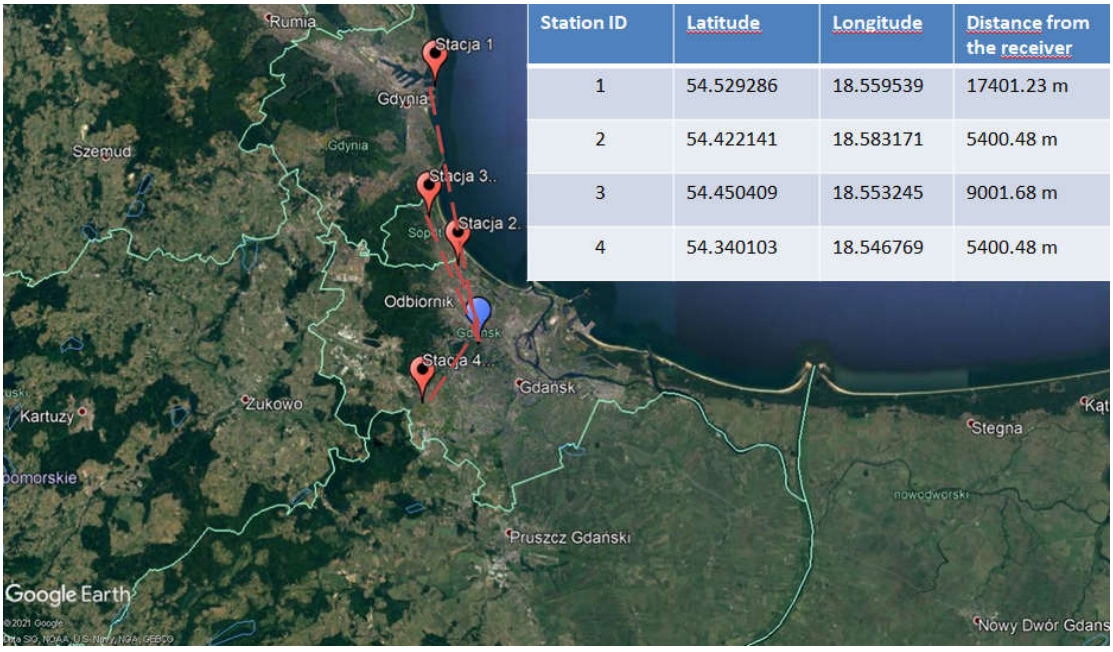

Station ID	Latitude	Longitude	Distance from the receiver
1	54.529286	18.559539	17401.23 m
2	54.422141	18.583171	5400.48 m
3	54.450409	18.553245	9001.68 m
4	54.340103	18.546769	5400.48 m

Figure 7-10: The fourth measurement scenario for testing the R-Mode system demonstrator that determines the position in real time

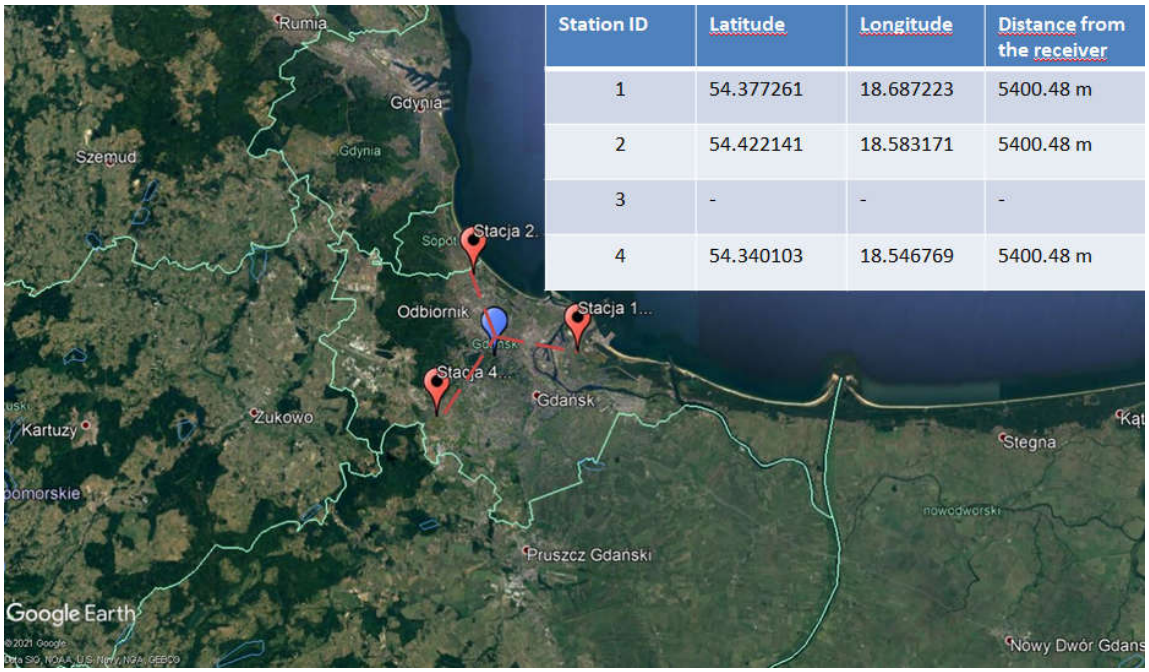

Station ID	Latitude	Longitude	Distance from the receiver
1	54.377261	18.687223	5400.48 m
2	54.422141	18.583171	5400.48 m
3	-	-	-
4	54.340103	18.546769	5400.48 m

Figure 7-11: The fifth measurement scenario for testing the R-Mode positioning system demonstrator in real time

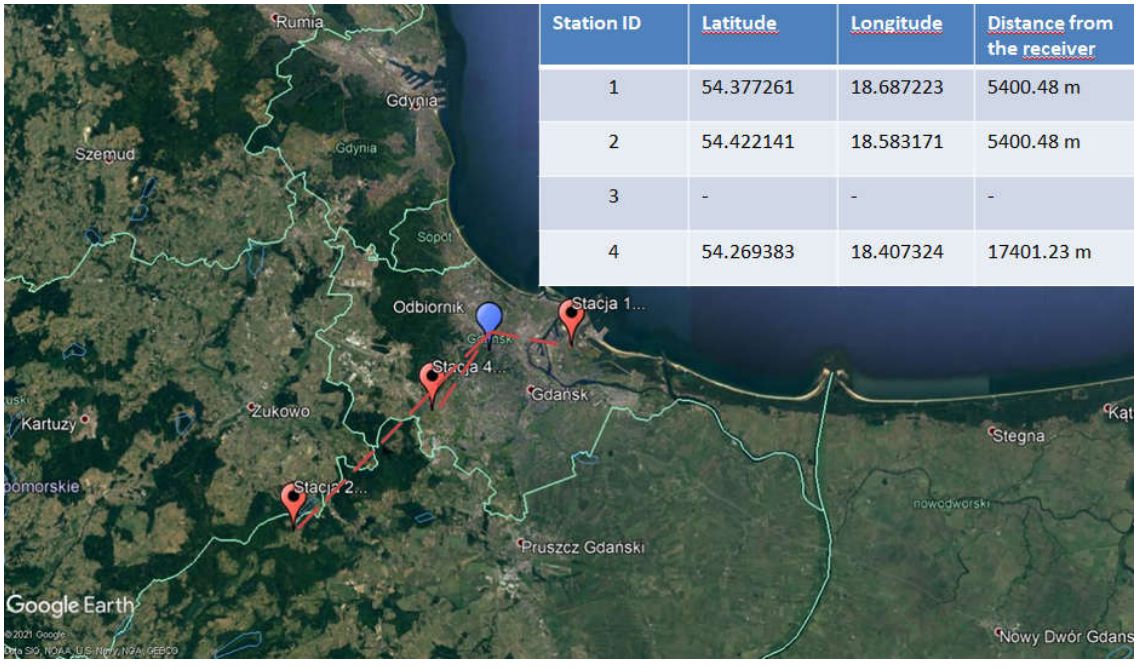

Station ID	Latitude	Longitude	Distance from the receiver
1	54.377261	18.687223	5400.48 m
2	54.422141	18.583171	5400.48 m
3	-	-	-
4	54.269383	18.407324	17401.23 m

Figure 7-12: The sixth measurement scenario for testing the R-Mode positioning system demonstrator in real time

Measurement studies were carried out for the above scenarios. Pictures from the R-Mode system demonstrator are shown below (Fig. 7-13, 7-14, 7-15, 7-16, 7-17, 7-18).

Figure 7-13: R-Mode demonstration stand a)

Figure 7-14: R-Mode demonstration stand b)

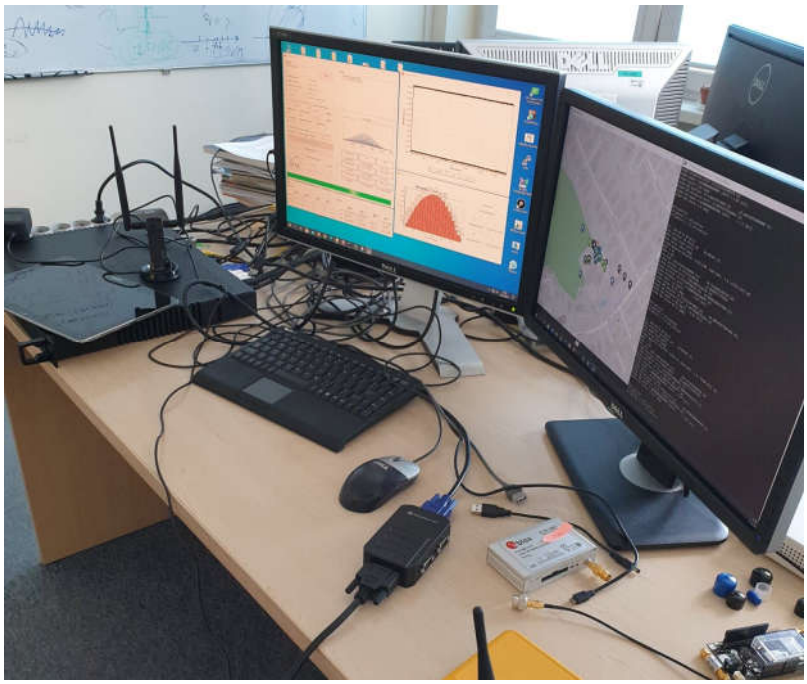

Figure 7-15: R-Mode demonstration stand c)

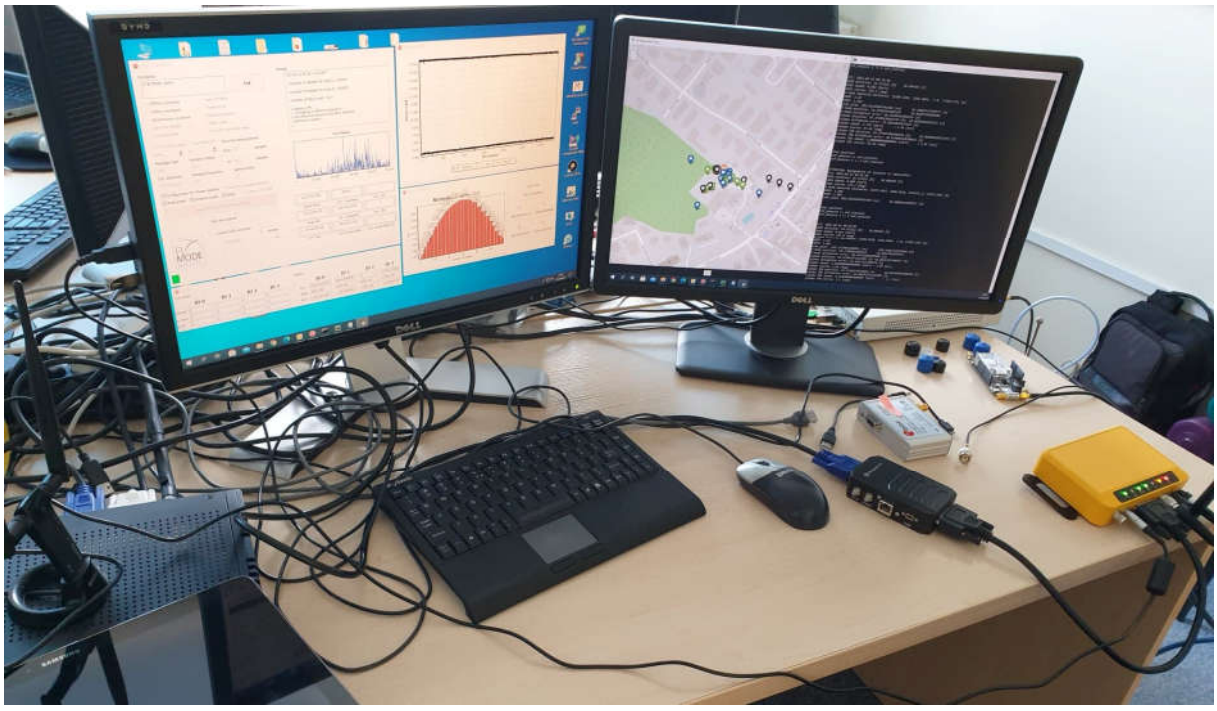

Figure 7-16: R-Mode demonstration stand d)

Figure 7-17: R-Mode demonstration stand e)

Figure 7-18: R-Mode demonstration stand f)

The table 7-1 below shows the results for all measurement scenarios. Fixed power scenarios mean that the signals from the simulated transmitting stations have the same power regardless of their distance from the receiver. On the other hand, scenarios with variable strengths mean that the signal strength changes proportionally to the distance from a given transmitting station.

Table 7-1: Results of measurement scenarios

scenario	rmode_avg	kalman_avg	ins_avg	nof_measurements	hdop_avg	pdop_avg
Scenario 1 - constant power	15.7753	118.5524	8.696161	186	1.146	1.603
Scenario 1 - variable power	17.04171	18408.79	86.48589	120	1.146	1.603
Scenario 2 - constant power	12.67883	92.52741	7.210433	228	1.063	1.559
Scenario 2 - variable power	13.57581	71.22065	5.979512	144	1.063	1.559
Scenario 3 - constant power	22.21149	80.1648	16.91396	155	1.833	2.194
Scenario 3 - variable power	29.49874	31.41097	24.53933	128	1.833	2.194
Scenario 4 - constant power	79.20474	54.13518	38.23067	243	7.836	8.819
Scenario 4 - variable power	109.6123	74.98872	62.74601	277	7.836	8.82
Scenario 5 - constant power	13.00927	12.91655	12.73657	112	1.182	1.654
Scenario 5 - variable power	15.79613	13.91848	13.78193	197	1.183	1.655
Scenario 6 - constant power	15.12704	11.66721	11.5944	220	1.189	1.66
Scenario 6 - variable power	14.07674	10.22931	10.16125	323	1.189	1.66

The second column of the table shows the results calculated for the R-Mode system itself. The next column shows the results for the R-Mode system along with the Kalman filter. The next column shows the results for the additional inertial module.

As can be seen for the emulated broadcasting stations, where the only broadcasting station was the station in Gdynia - 17.4 km away, very high accuracy of the determined position was obtained: about 15 meters. After a more detailed analysis, it can be seen that for the poor geometry of the distribution of transmitting stations, the determined position accuracy has significantly deteriorated. Of course, it should also be added that the R-Mode demonstrator worked in static mode without any movement.

The screenshot below (Fig. 7-19) shows how the signal correlating application processes the samples recorded by the USRP and then the positioning application processes the determined pseudoranges (Fig. 7-20).

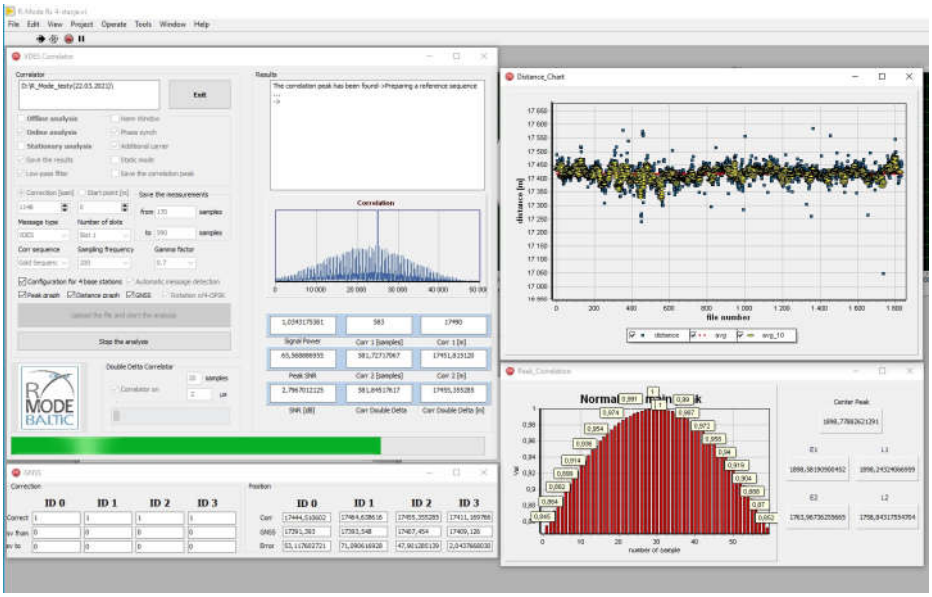

Figure 7-19: A signal correlation application that determines pseudoranges

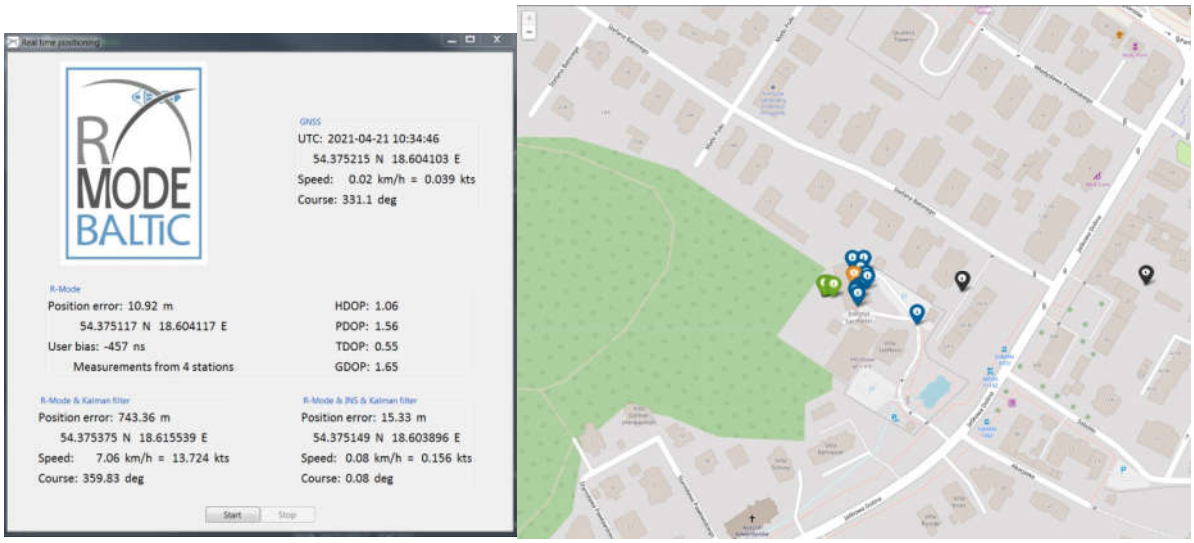

Figure 7-20: Real-time positioning application

8 Summary and conclusions for the next measurement campaign

The above report shows a comprehensive list of steps to create a complete real-time R-Mode positioning system demonstrator. The obtained results showed the correctness of the operation of the VDES R-Mode system demonstrator receiver designed and performed by NIT in R-Mode Baltic project, and confirmed that the design assumptions were met. For the purposes of the project, a measurement campaign was carried out in June 2020. It was preceded by calibration measurements in the field to verify the correct operation of the system.

National Institute of Telecommunications (NIT) organized two measurement campaigns of the VDES R-mode System. Both took place on the Baltic Sea waters.

The created VDES R-Mode station was the first station of this type in the Baltic Sea, which determined the position in real time.

The saved files with samples during the several-hour measurement campaign allowed for the later calculation of the pseudoranges and determination of the accuracy error between the distances calculated between the transmitter and the GNSS receiver. The observed accuracy was around 20 meters for the LOS environment. In the last measurement campaign, the system easily reached a range of approximately 150 km and was still usable in NLOS.

Several studies on the advanced double delta correlator were conducted for the purposes of the project. Its use allowed to limit the impact of multipath phenomena on the obtained distance accuracy.

Work is now also underway to integrate the Kalman filter and the GNSS-based INS module, which will guarantee even more accurate positioning.

Further work also focused on the selection of the signal with the best correlation properties. In cooperation with partners from DLR, we were able to check the quality of the correlation depending on the correlation sequence used. After a series of simulation tests and tests with the received signal, the best correlation properties were shown by a signal consisting of a combined Gold sequence and an alternative sequence. The use of this signal allowed for a large reduction of the error of the calculated accuracy of the distance.

Based on the research on the design of multicorrelators and the possibility of using them in the R-Mode project, a fully functional application for signal correlation was created. Through the calculated pseudo-distances, in the next stage - these data were transferred to the application determining the position. By connecting the modules for recording the sequence of samples through the USRP device, then transferring them in the form of a saved binary file to the application correlating the signals and finally connecting the module to calculate the exact position of the receiver - a station for determining the position of the receiving station in real time was created.

As previously mentioned, the obtained results showed the correctness of the operation of the R-Mode VDES system demonstration stand designed and performed by NIT and confirmed the fulfillment of the design assumptions. The R-Mode Baltic project ended on 03/31/2021, but on 04/01/2021 its continuation began in the form of the Ranging Mode Baltic Sea test bed evaluation project under the acronym R-Mode Baltic 2. Further campaigns are being planned this project's framework.

A receiving station will be installed in Jastarnia in the near future. It will be used for long-term stationary measurements. This will allow very accurate results to be obtained throughout the

Bay of Gdansk in the LOS marine environment at a distance of 18 km. Thanks to this, it will be possible to monitor the accuracy of the position determined in the R-Mode system. In Summer/Autumn 2021 (at the R-Mode test-bed area), another measurement campaign is planned to verify the R-Mode system's capabilities of real-time positioning in dynamic conditions. In addition, it is planned to create a VDES R-Mode monitoring system for long-term observation of positioning results in the Gdańsk Bay.

References

[1-1] R-Mode Baltic - Baseline and Priorities

[2-1] GMV, Multicorrelator,2011,https://gssc.esa.int/navipedia/index.php/Multicorrelator

[2-2] Betz, J. W., Klodziejski, K. R., “Extended Theory of Early-Late CodeTracking for a Bandlimited GPS Receiver,” Submitted to: Journal of the Institute of Navigation

[2-3] Robert Eric Phelts, MULTICORRELATOR TECHNIQUES FOR ROBUST MITIGATION OF THREATS TO GPS SIGNAL QUALITY

[2-4] A. Iliopoulos; C. Enneking; O. G Crespillo; T. Jost; S. Thoelert; F. Antreich,IEEE 10.1109/AERO.2017.7943579, Multicorrelator signal tracking and signal quality monitoring for GNSS with extended Kalman filter

[3-1] Braasch, M. S., “Multipath Effects,” in Global Positioning System:Theory and Applications, B. W. Parkinson and J. J. Spilker (eds.), , American Institute of Aeronautics and Astronautics, Washington DC

[4-1] Quartzlock E80-GPS Specification: GPS Disciplined Rubidium Frequency & Time Reference

[4-2] M1G2, https://geo-matching.com/gnss-receivers/m1g2

[4-3] National Instruments, “NI USRP™-USRP 2954, https://www.ni.com/pl-pl/support/model.usrp-2954.html

[4-4] PROCOM BPF 2/2-250, https://amphenolprocom.com/products/filters/654-bpf-2-250

[6-1] R M.2092-0, 2015, "Technical characteristics for a VHF data exchange system in the VHF maritime mobile band"

[6-2] IALA GUIDELINE, G1139-ANNEX-R-MODE, VDES R-MODE 2019 ITU

Appendix A Detailed analysis of the results from the AIS and VDES measurement campaign

This appendix provides detailed analytical analyzes of the pseudo-ranges obtained during the measurement campaigns.

Analysis for AIS signals:

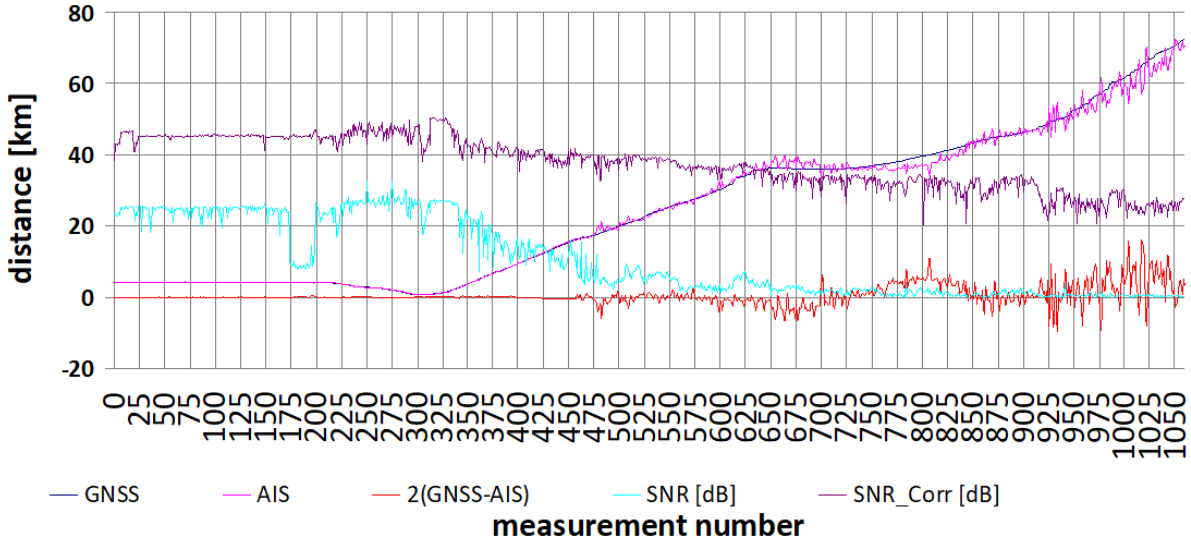

Figure 1: Analysis of the results from the measurement campaign depending on the distance

The figure 1 shows the following signals: GNSS (reference), AIS (measured distances in the R-mode), 2(GNSS-AIS) (distance measurement errors), SNR of the AIS signal and the SNR of the signal from the correlator (SNR_Corr) in the order of their occurrence (0 - 1059).

The entire range of measurements is divided into five sub-ranges:

1. (0 - 169) - very small changes in distance, maneuvers in the port channel,

2. (170 - 456) - route with small errors,

3. (457 - 649) - route with increasing errors,

4. (650 - 923) - route with increasing errors and a significant decrease in SNR_Corr, and

5. (924 - 1059) - a route with increasing errors and a significant decrease in SNR_Corr in the range of distances over 50 km.

Distances from the AIS transmitting station in the specified sub-ranges (table 1) (the minus sign at the given distance, e.g. -4.066, means that the measuring point was to the west of the transmitting station):

Table 1: Distances from the AIS transmitting station in the specified sub-ranges

Sub-ranges:	Item No .:	Distance to the transmitting station [km]:	Item No .:	Distance to the transmitting station [km]:
whole	0	-4,06662	1059	72,481637
1	0	-4,06662	169	-4,066524
2	170	-4,066893	456	16,033374
3	457	16,121657	649	36,423312
4	650	36,433425	923	48,627494
5	924	48,696175	1059	72,481637

Analysis of the errors as well as the corrections of distance measurements in R-Mode based on the AIS system are shown below:

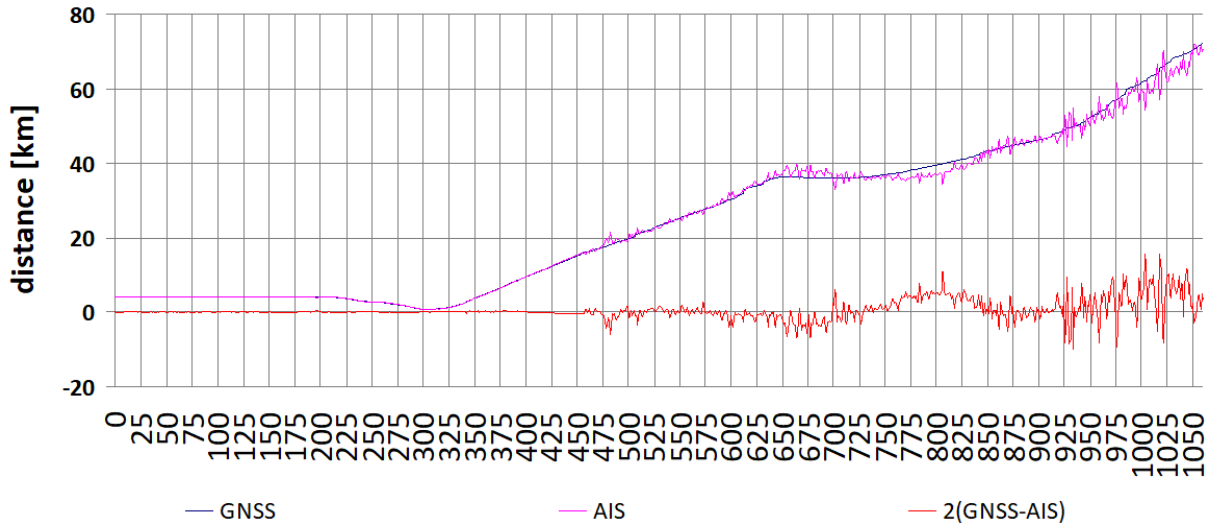

Figure 2: Analysis of the errors and the corrections of distance measurements in R-Mode based on the AIS system

The above figure 2 shows the primary measurement results obtained during the measuring campaign. In order to determine the correction of distance measurements in the R-Mode based on the AIS system, the trend line analysis determined by the moving average method was used.

The moving average trend analysis predicts an error value based on the average of the *n* previous distance measurement's error results. The predicted value of the measurement error in the i-th step calculated in this way is added or subtracted (depending on the sign of the error) from the measured distance value. The following figures show the results of the improvement of measurements for n = 2, 3 and 9. Moreover, the table below shows the results of the mean error and standard deviation calculations in the entire range as well as in the assumed individual sub-ranges of the measurements.

The results after adjusting for the moving average n = 2 (fig. 3):

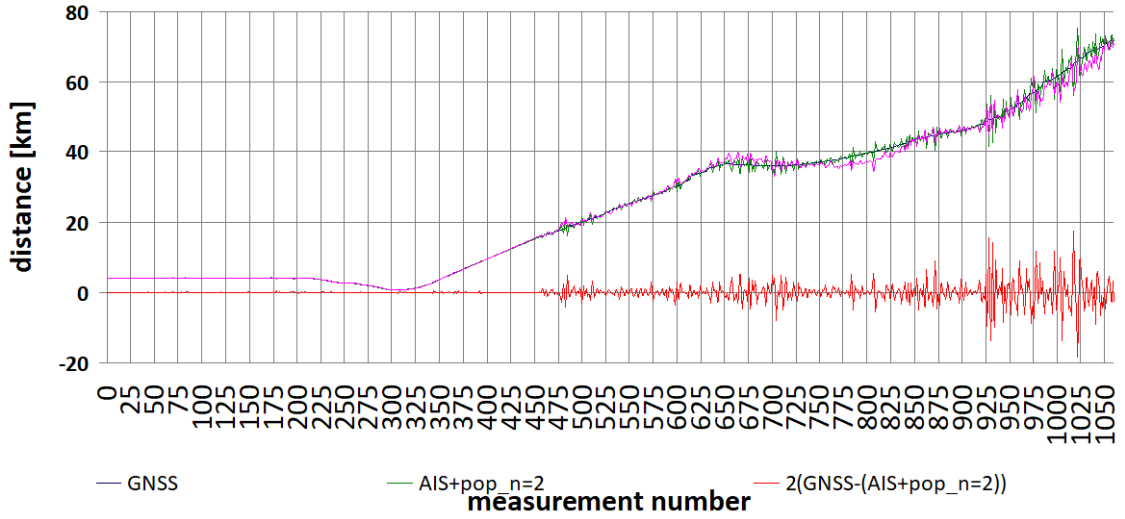

Figure 3: The results after adjusting for the moving average n = 2

The results after adjusting for the moving average n = 3 (fig. 4):

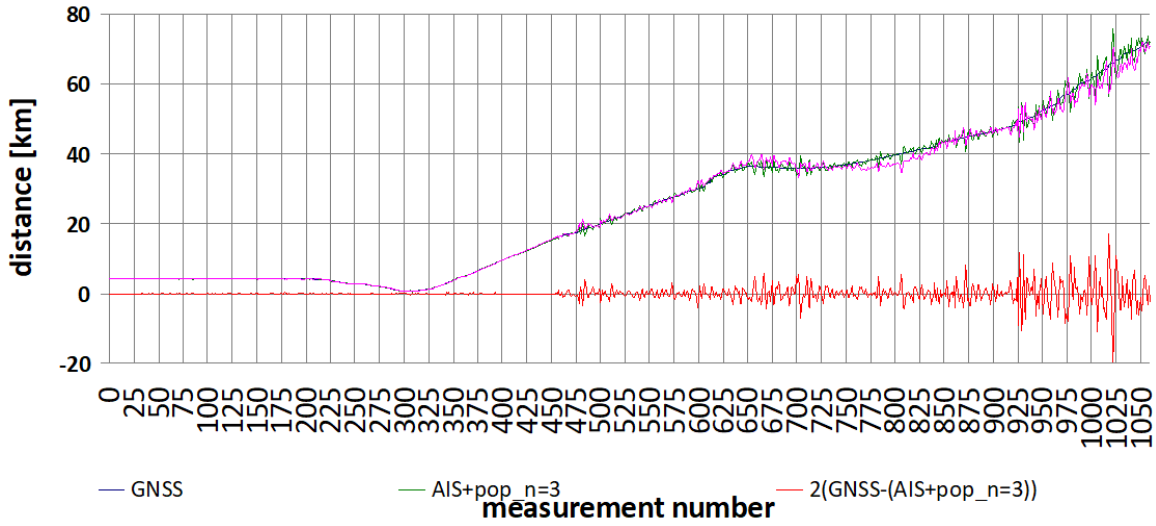

Figure 4: The results after adjusting for the moving average n = 3

The results after adjusting for the moving average n = 9 (fig. 5):

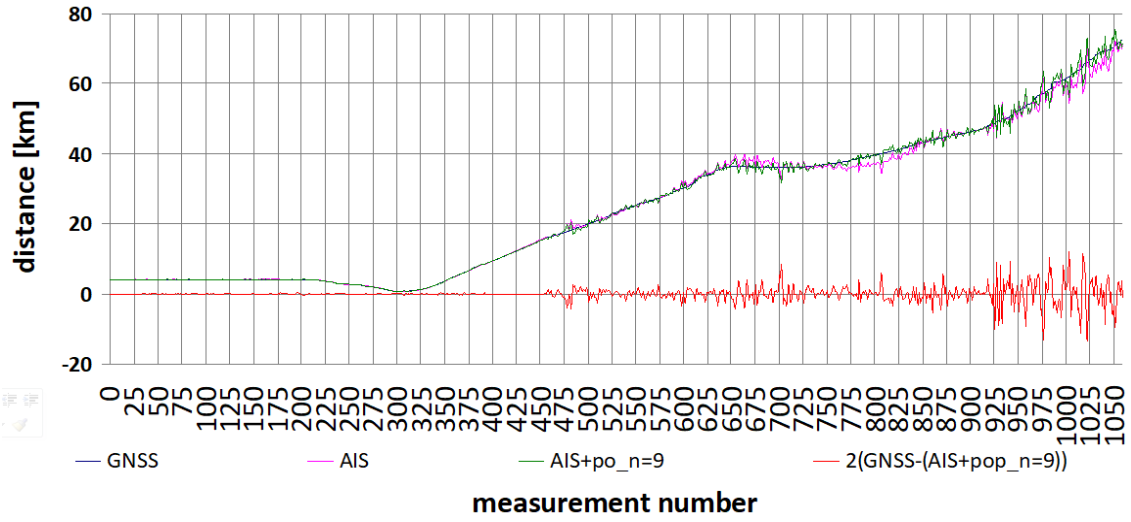

Figure 5: The results after adjusting for the moving average n = 9

Comparison of the corrections for n = 2, 3 and 9 (fig. 6):

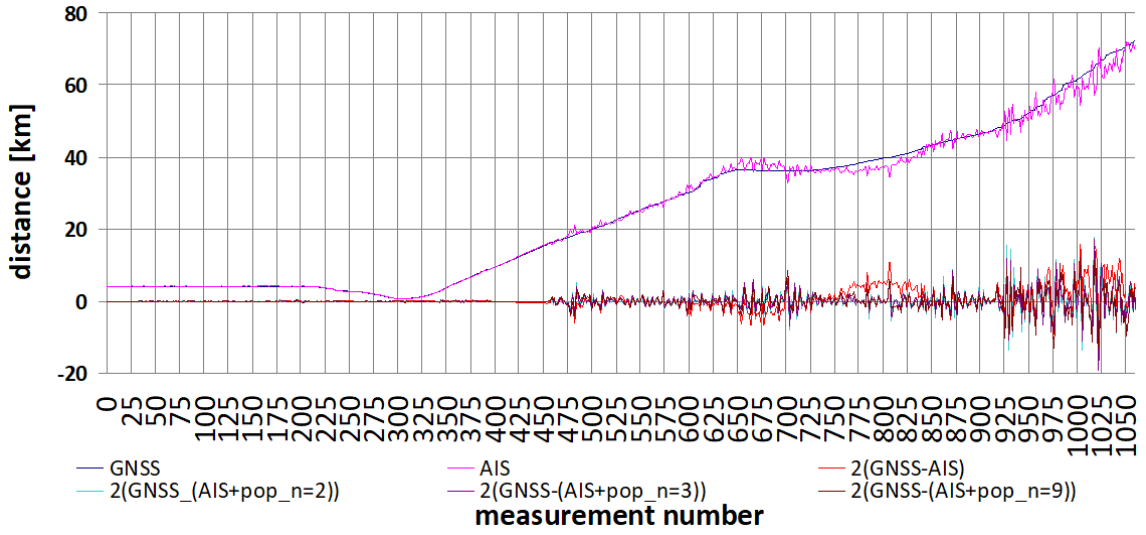

Figure 6: The results after adjusting for the moving average n = 2,3 and 9

The calculation results of the mean and standard deviation of the GNSS distance difference and the distance calculated from the R-mode measurements in the AIS mode are summarized in the table 2 below for the following cases (in meters):

• Results obtained in the measurement campaign,

• The obtained results after taking into account the error correction using the moving average n = 2,

• The obtained results after taking into account the error correction using the moving average n = 3,

• The obtained results after taking into account the error correction using the moving average n = 9.

Table 2: The results of the error distance depending on the moving average

Sub-ranges analisys	(GNSS-(AIS+pop_n=0))		(GNSS-(AIS+pop_n=2))		(GNSS-(AIS+pop_n=3))		(GNSS-(AIS+pop_n=9))	
	average	standard deviation	average	standard deviation	average	standard deviation	average	standard deviation
0:1059 (all)	267,197	1397,592	1,133565566	1158,922607	1,61969717	1139,970062	5,08734046	1076,735882
0:169	-20,907	30,98799	-0,77579118	27,87217903	-0,964860784	28,54409011	-2,53164641	29,0098938
170:456	-15,744	100,2063	-0,70292683	50,83409629	-0,942254355	50,53171624	-2,69533682	56,51950247
0:456	-17,665	81,60855	-0,73003173	43,68808298	-0,950663749	43,62879944	-2,63444542	48,11906709
457:649	-247,14	649,4163	-2,39896632	614,2783608	-2,921865285	604,0376341	-10,4165826	597,4816764
650:923	408,038	1579,127	0,737255474	1050,065614	1,926066667	1032,079622	23,0733856	950,6747897
924:1059	1680,96	2646,279	13,20732721	2786,184701	15,10629412	2739,839119	16,8001119	2598,079055

Moreover, the mean value and standard deviation of the SNR of the AIS signal and the SNR_Corr of the correlator signal were calculated for the the same sub-ranges as previously. These results are summarized in the table 3 below.

Table 3: Mean value and standard deviation of SNR

Sub-ranges analysis	(GNSS-(AIS+pop_n=0))		(GNSS-(AIS+pop_n=2))		SNR signal AIS [dB]		SNR_Corr [dB]	
	average	standard deviation	average	standard deviation	average	standard deviation	average	standard deviation
0:1059 (all)	267,197	1397,592	1,133565566	1158,922607	10,50062684	10,46983084	37,5314753	7,111364419
0:169	-20,907	30,98799	-0,77579118	27,87217903	24,29627412	1,413412097	45,1348459	1,014036525
170:456	-15,744	100,2063	-0,70292683	50,83409629	19,7951476	7,024704709	43,8411547	3,449863294
0:456	-17,665	81,60855	-0,73003173	43,68808298	21,46952726	6,03602342	44,3223965	2,870105611
457:649	-247,14	649,4163	-2,39896632	614,2783608	4,597879508	2,167631216	37,3882269	1,793278421
650:923	408,038	1579,127	0,737255474	1050,065614	1,346600906	0,789741571	31,9146854	2,284400955
924:1059	1680,96	2646,279	13,20732721	2786,184701	0,461258031	0,40240834	26,2314485	2,22346756

On the basis of the above table 3, it can be seen that the mean value of the SNR_Corr signal, due to the small value of the standard deviation, can be used as an estimate of the quality criterion for the distance calculation. For example, for SNR_Corr> 40 dB, the distance can be estimated with an average of approx. 1 m and a standard deviation below approx. 50 m.

The aim is to establish the method of determining corrections for distance measurements in R-mode in the AIS system for the purpose of monitoring measurement errors caused by variable propagation condition.

Analysis for VDES system signals:

The figure 7 shows the original results of distance measurements in R-Mode for VDES signals without taking into account the possible corrections.

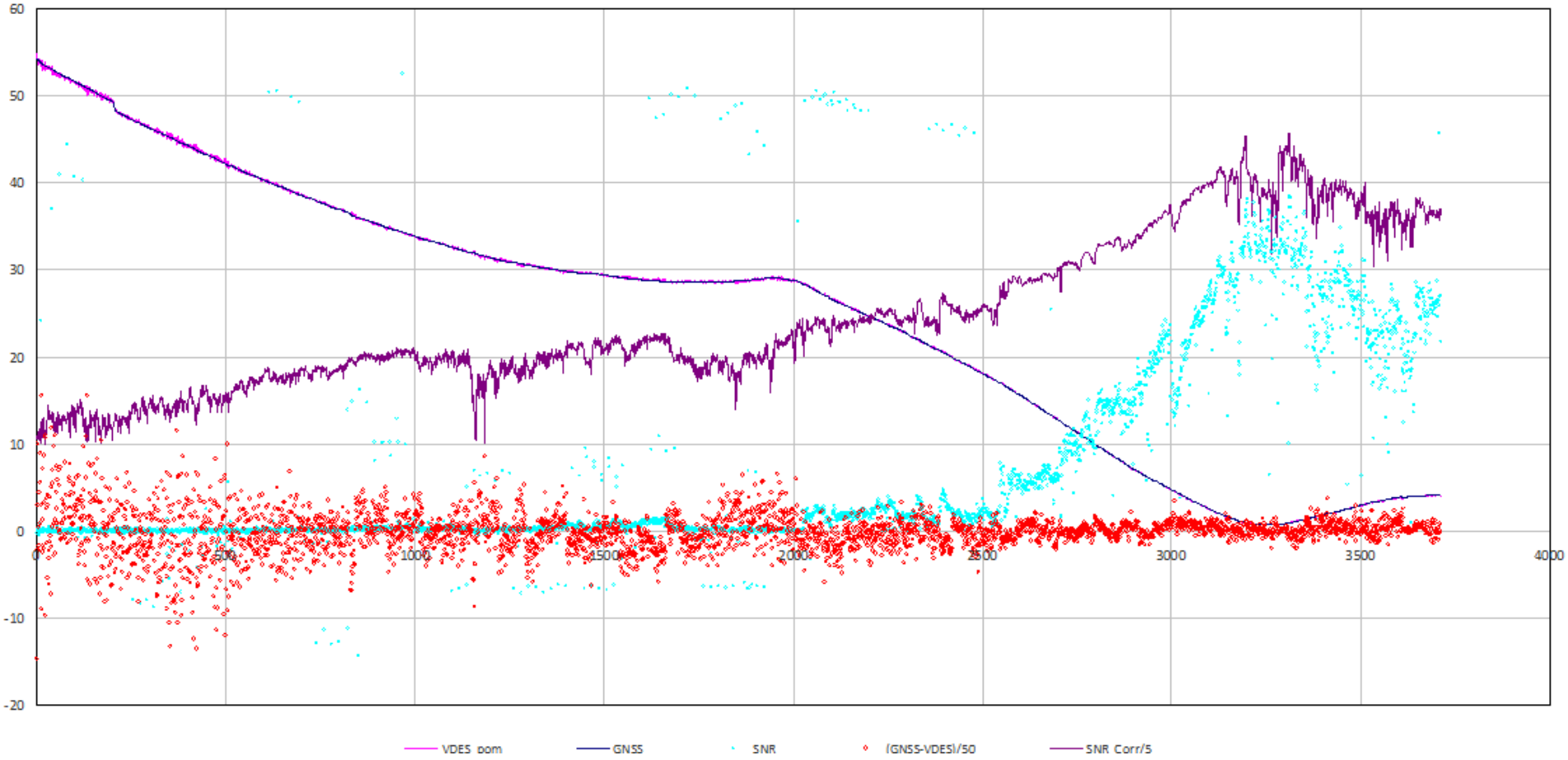

Figure 7: Measurement errors due to distance and signal SNR

The figure 8 below shows the results of distance measurements in R-Mode for VDES signals when the moving average corrections from 9 previous measurements are taken into account (the distance measurement and measurement error are marked in green):

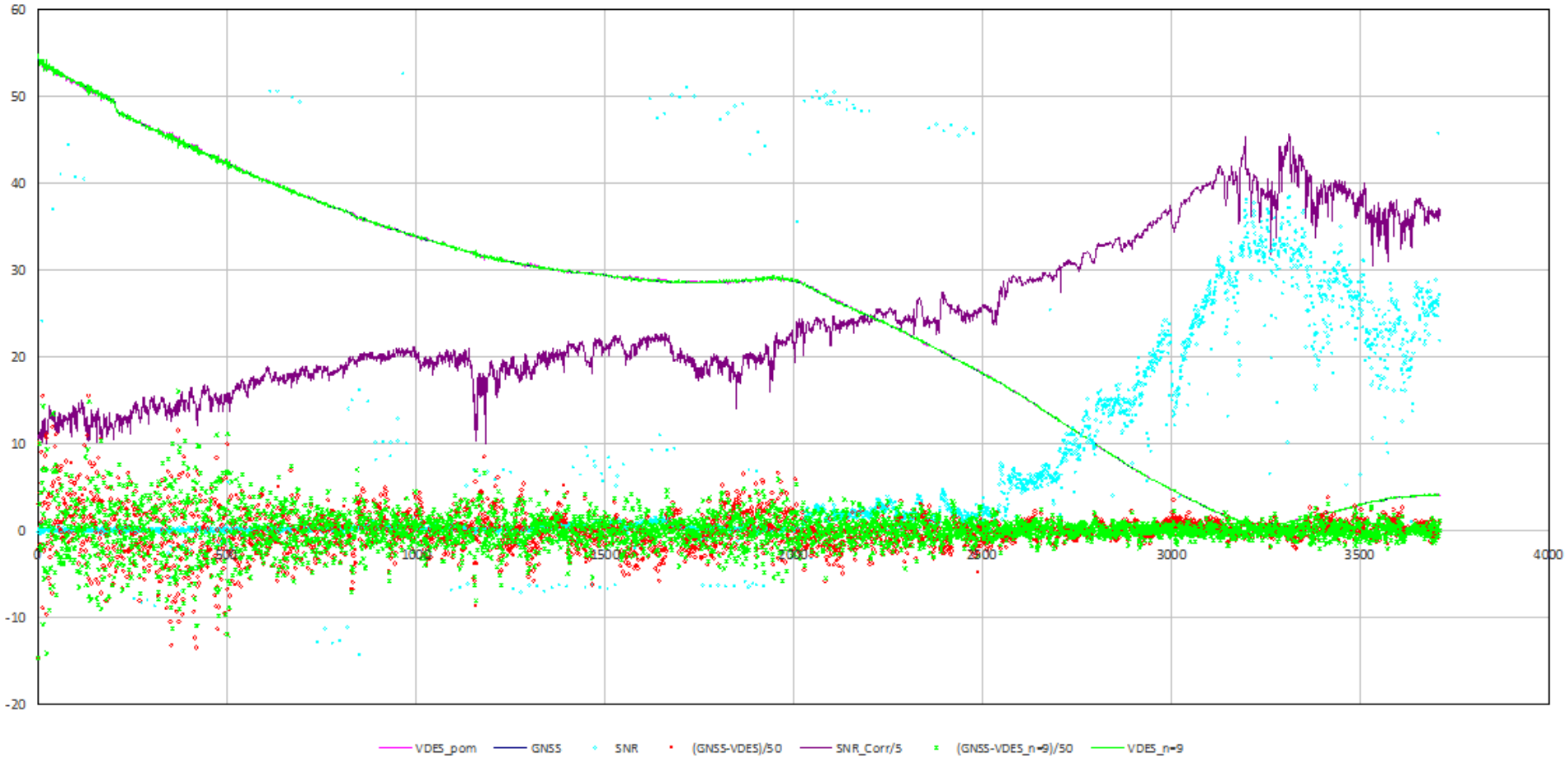

Figure 8: Results of distance measurements in R-Mode for VDES signals when the moving average corrections from 9 previous measurements are taken into account

Distances from the AIS transmitting station in the specified sub-ranges (table 3):

Table 3: Distances from the AIS transmitting station in the specified sub-ranges

Sub-ranges	Item No .:	Distance to the transmitting station [km]:	Item No .:	Distance to the transmitting station [km]:
analysis	2	54,105175	3712	-4,071342
1	2	54,105175	513	41,92534
2	514	41,89953	864	35,796988
3	865	35,779251	1178	31,617713
4	1179	31,61033	2009	28,709286
5	2010	28,704774	2544	17,081451
6	2545	17,052687	3010	4,528072
7	3011	4,528072	3369	-1,475202
8	3370	-1,489117	3712	-4,071342
9	2545	17,052687	3712	-4,071342

Table 4: The mean and standard deviation of the error of distance values depending on the analyzed sub-range

VDES	avg	standard deviation	avg	standard deviation	avg	standard deviation	avg	standard deviation	avg	standard deviation
	GNSS-VDES_n=0		GNSS-VDES_n=2		GNSS-VDES_n=3		GNSS-VDES_n=4		GNSS-VDES_n=9	
2:3712 (all)	-7,25659	113,871805	-0,094131	127,8119292	-0,084762	118,178445	-0,08607	115,9422019	-0,077848	108,740855
2:513	-7,227331	225,599996	-0,492605	270,4211818	-0,430462	245,580982	-0,36284	243,4624436	-0,7690264	224,6185778
514:864	-24,53078	117,340466	0,6292687	143,4590047	0,8787987	133,353858	0,824971	128,8982155	1,93407838	119,4886505
865:1178	8,8245751	98,2611631	-0,658617	103,3303616	-0,554509	99,522475	-0,37978	93,88977376	0,48584539	92,86635453
1179:2009	-10,55996	104,931399	0,1698685	99,84050295	0,0202273	95,4359503	-0,06691	93,21665897	-0,4542111	88,88575539
2010:2544	-30,79454	70,2411622	-0,487565	73,28238365	-0,446678	70,6743354	-0,40106	66,73818531	-0,4041854	67,40442003
2545:3010	-1,607477	39,0335274	0,4333102	30,66180906	0,4858743	30,6376183	0,512254	31,23424924	0,64983817	33,58741125
3011:3369	7,3763951	34,3024072	-0,644808	33,78295841	-0,698573	32,0441598	-0,76199	31,74234162	-0,8563135	30,46294547
3370:3712	17,381751	40,5924199	0,1110102	45,40326814	0,0525822	43,2535168	0,003121	41,98984044	-0,3740195	40,02864097
2545:3712	6,7302928	38,8867442	0,0072886	36,4562218	-0,005423	35,1786434	-0,02891	34,8541107	-0,1137677	34,7012058

Table 5: The mean and standard deviation of the error of SNR values depending on the analyzed sub-range

VDES	avg	standard deviation	avg	standard deviation	avg	standard deviation	avg	standard deviation
	GNSS-VDES_n=0		GNSS-VDES_n=9		SNR_VDES [dB]		SNR_Corr [dB]	
2:3712 (all)	-7,2565896	113,87181	-0,077848	108,74086	7,402839324	11,627447	122,417081	43,09622
2:513	-7,2273309	225,6	-0,7690264	224,61858	0,333799408	4,27668	67,8685104	7,0851324
514:864	-24,530785	117,34047	1,93407838	119,48865	0,579425999	5,7499803	89,7316299	5,0612991
865:1178	8,82457508	98,261163	0,48584539	92,866355	0,789638888	3,5763423	97,5407182	7,4892486
1179:2009	-10,559955	104,9314	-0,4542111	88,885755	1,158317704	6,3876902	99,8931	7,8988409
2010:2544	-30,794544	70,241162	-0,4041854	67,40442	4,119379696	9,9771696	122,348647	5,0904756
2545:3010	-1,6074772	39,033527	0,64983817	33,587411	11,25777166	5,5440474	158,031558	13,294377
3011:3369	7,37639507	34,302407	-0,8563135	30,462945	28,1607514	6,3059035	199,929953	11,413974
3370:3712	17,3817508	40,59242	-0,3740195	40,028641	8,162328163	4,8317619	185,225283	9,1141854
2545:3712	6,7302928	38,886744	-0,1137677	34,701206	20,27677753	9,3592707	178,895403	21,364483

Comparison of distance measurement results in R-Mode for AIS and VDES signals.

In the table 6 below, in the comparable ranges of distances from the transmitting station (the minus sign at the given distance, e.g. -4.066, means that the measuring point was to the west of the transmitting station), the calculated mean values and standard deviations were collected: distance measurement errors, SNR value of the used signal and SNR of the autocorrelation signal.

Table 6: Comparison of distance measurement results in R-Mode for AIS and VDES signals

Distance to the transmitting station [km]:	Sub-ranges	(GNSS-(AIS+pop_n=0)) [m]		(GNSS-(AIS+pop_n=2)) [m]		SNR of the AIS signal [dB]		SNR_Corr [dB]	
	analysis	avg	standard deviation	avg	standard deviation	avg	standard deviation	avg	standard deviation
-4,066 - 72,481	0:1059 (all)	267,197	1397,592	1,133565566	1158,922607	10,50062684	10,469830	37,5314753	7,111364419
-4,066 - 16,033	170:456	-15,744	100,2063	-0,70292683	50,83409629	19,7951476	7,0247047	43,8411547	3,449863294
16,121 - 36,423	457:649	-247,14	649,4163	-2,39896632	614,2783608	4,597879508	2,1676312	37,3882269	1,793278421
36,433 - 48,627	650:923	408,038	1579,127	0,737255474	1050,065614	1,346600906	0,7897415	31,9146854	2,284400955
Distance to the transmitting station [km]:	Sub-ranges	(GNSS-(VDES+pop_n=0)) [m]		(GNSS-(VDES+pop_n=9)) [m]		SNR of the VDES signal [dB]		SNR_Corr [dB]	
	analysis	avg	standard deviation	avg	standard deviation	avg	standard deviation	avg	standard deviation
-4,071 – 54,105	2:3712 (all)	-7,25659	113,8718	-0,077848	108,7409	7,40283932	11,62745	122,41708	43,09622
-4,071 – 17,052	2545:3712	6,730293	38,88674	-0,113768	34,70121	20,2767775	9,359271	178,8954	21,36448
17,081 – 35,779	865:2544	-13,38065	94,89414	-0,262579	83,41752	2,03236712	7,50128	106,60445	12,89116
35,796 – 54,105	2:864	-14,265	189,2823	0,3303824	188,9659	0,43370084	4,927614	76,760695	12,47531

The table 6 shows that the average value of SNR of approx. 20 dB for AIS and VDES signals, regardless of large differences in the value of SNR_Corr, results in the smallest error in the distance measurement, the standard deviation is, respectively, approx. 50.8 m for AIS and approx. 34.7 m for VDES (after applying the corrections).

For the average value of SNR below 5 dB, the errors in the distance measurement result in much larger errors expressed in the standard deviation; the errors in the case of using AIS signals are about 7 times greater than in the case of using VDES signals.

The influence of the SNR_Corr index seems to be less significant on the error of distance measurement.

R-Mode distance measurement analysis for VDES signals - campaign III

The figure 9 below shows the results of distance measurements in R-Mode for VDES signals without taking into account possible corrections, distance measurement (“VDES_pom”) - purple, GNSS reference measurement - dark blue, measurement error in relation to the GNSS signal (“B_odl_pom”) - orange, SNR value of the VDES signal (“SNR_VDES”) - yellow, SNR value of the correlation signal (“SNR_Corr”) - brown and sub-range indicators - green.

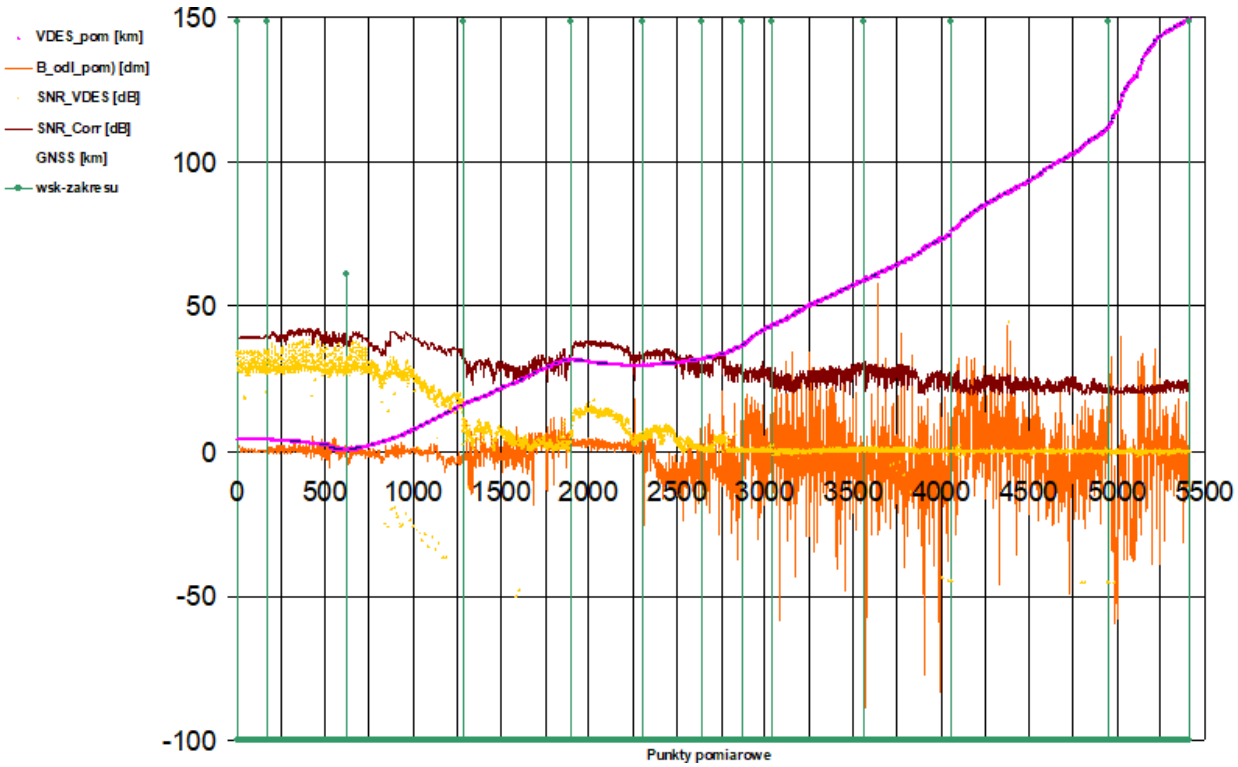

Figure 9: Measurements in the 3rd campaign as a function of measurement points

The figure 10 below shows the results of the distance measurements in the R-Mode for VDES signals without taking into account the possible corrections and shows the errors of distance measurement according to the moving average of 2 (blue) and 9 (black) previous measurements ("B_odl_pom") against the measurement error in relation to the signal GNSS without correction ("B_odl_am") (orange). Additionally, it shows the VDES distance measurement ("VDES_pom") (purple), GNSS reference measurement (dark blue), VDES signal SNR value ("SNR_VDES") (yellow), the SNR value of the correlation signal ("SNR_Corr ") (brown) and sub-range indicators - green.

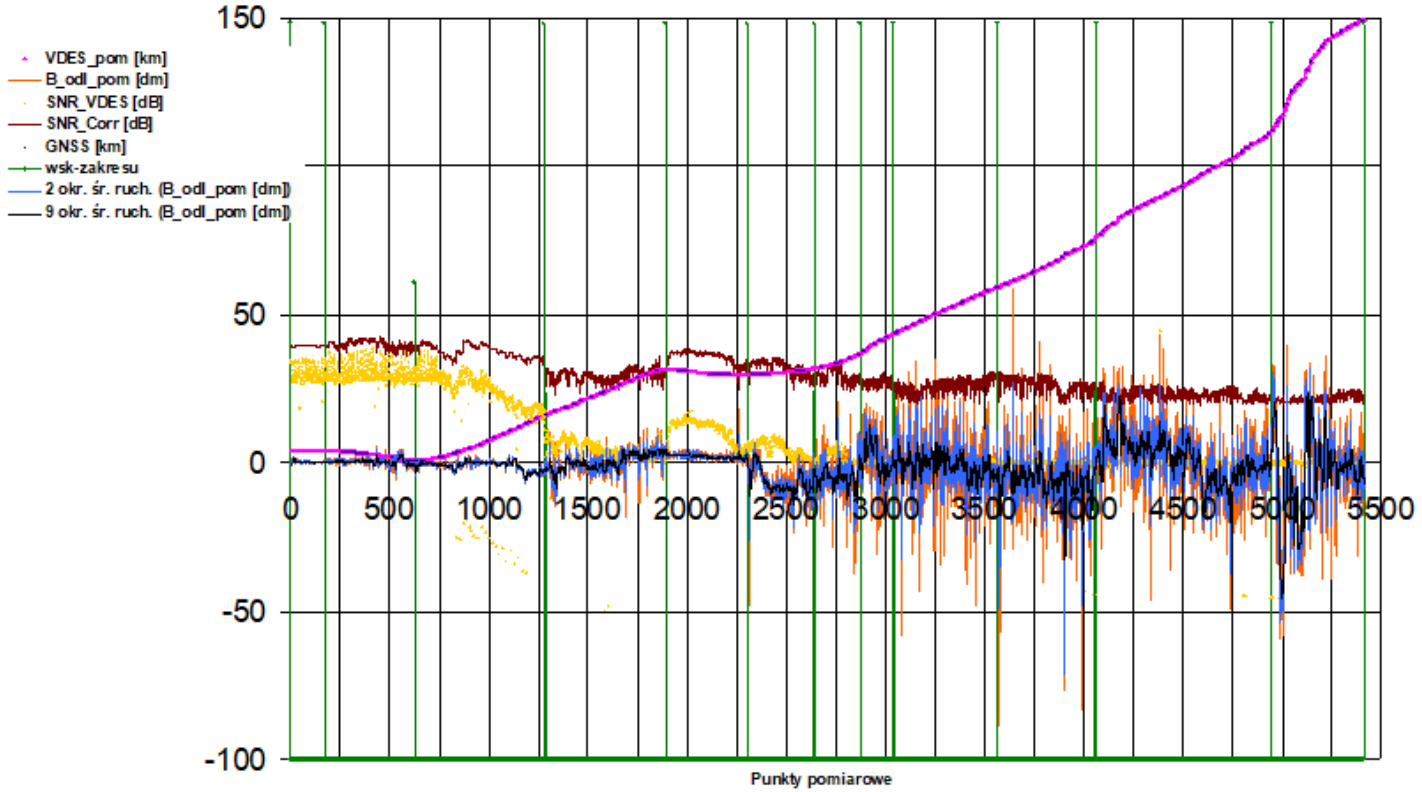

Figure 10: Measurements in the 3rd campaign as a function of measurement points

Division of the distance from the VDES broadcasting station into sub-ranges:

Due to large dispersions of the measurement parameters, such as: the value of the SNR_VDES coefficient, the size of measurement errors ("B_odl_pom") and the SNR_Corr coefficient, the entire measurment range is divided into sub-ranges. It enables the estimation of the mean value and standard deviation of the above parameters in particular sub-ranges.

Table 7 below breaks down the distance from the transmitting station into sub-ranges. The table 7 shows: sub-range numbers, position numbers in each sub-range and the distances' limits ("edges") in each sub-range in relation to the VDES signal transmitting station (the minus sign at the distance means that the measuring point is on the opposite side than the one with the plus sign):

Table 7: Division of the distance from the VDES broadcasting station into sub-ranges:

Sub-ranges:	Sub-range item numbers range:	Range and distance to the transmitting station in the sub-range [km]:
all	2 – 5417	(-4,067155) – 149,627112
1	2 – 169	(-4,067155) – (-4,066757)
2	170 – 1283	(-4,066427) – 16,183794
3	1284 – 1895	16,207486 – 31,857812
4	1896 – 2305	31,860096 – 29,828475
5	2306 – 2642	29,828939 – 32,041053
6	2643 – 2874	32,05065 – 36,912765
7	2875 – 3042	36,931596 – 43,601700
8	3043 – 3564	43,625508 – 59,237789
9	3565 – 4061	59,264493 – 76,438249
10	4062 – 4951	76,466765 – 112,256441
11	4952 – 5417	112,285921 – 149,627112

The table 8 below presents the calculated parameters of the distance measurement in particular sub-ranges.

Average values and standard deviations measured in Campaign III were calculated, as well as the parameters of the distance measurement and the VDES signal:

• Distance measurement error without correction (error in relation to the measurement using the GNSS signal) - the mean value and standard deviation are given,

• The error of the distance measurement with correction calculated using the "moving average" method with a period of 2 - the mean value and standard deviation are given,

• The error of the distance measurement with correction calculated using the "moving average" method with a period of 9 - the mean value and standard deviation are given,

• SNR value of received VDES signal - mean value and standard deviation are given

• Value of the SNR of the correlation signal - the mean value and standard deviation are given.

Table 8: Calculated parameters of distance measurement in individual ranges

Sub-ranges:	Sub-range item numbers range:	Range and distance to the transmitting station in the sub-range [km]:	Measurement error without correction; average [m]	Measurement error without correction; std dev. [m]	Measurement error 2-degree correction; average [m]	Measurement error 2-degree correction; std dev. [m]	Measurement error 9-degree correction; average [m]	Measurement error 9-degree correction; std dev. [m]	VDES signal SNR value average [dB]	VDES signal SNR value std. [dB]	Correlation signal SNR value mean [dB] y	Correlations signal SNR value std. [dB]
all	2 – 5417	(-4,067155) – 149,627112	-14,2678	93,76433	-14,2767	78,47518	-14,2253	61,32939	8,013756	11,91711	29,83525	6,435226
1	2 – 169	(-4,067155) – (-4,066757)	3,077912	4,735414	2,995101	4,518174	2,954309	3,743723	29,71513	3,277924	39,39171	0,192356
2	170 – 1283	(-4,066427) – 16,183794	-3,70375	16,09981	-3,67985	15,1721	-3,58342	13,66282	26,20587	9,250651	38,43174	2,285096
3	1284 – 1895	16,207486 – 31,857812	3,035999	38,06733	2,870430	32,19458	2,490747	25,17139	4,164515	4,070699	29,48266	2,042068
4	1896 – 2305	31,860096 – 29,828475	21,99459	13,0742	22,19381	9,7507	22,42908	6,025979	11,05310	3,730258	35,79585	1,940845
5	2306 – 2642	29,828939 – 32,041053	-64,7775	55,58351	-64,5601	45,52755	-64,3032	36,75252	4,685897	2,592835	32,21531	2,311041
6	2643 – 2874	32,05065 – 36,912765	-56,866	73,8123	-57,2169	54,39097	-57,229	30,05482	1,782477	1,681152	29,49032	2,403146
7	2875 – 3042	36,931596 – 43,601700	15,12052	91,84234	15,18082	69,26365	14,20047	48,31635	0,401427	0,305065	26,72711	1,522855
8	3043 – 3564	43,625508 – 59,237789	-9,23837	108,6168	-9,41762	77,47461	-9,01385	34,51662	0,310392	0,410517	26,01969	2,331249
9	3565 – 4061	59,264493 – 76,438249	-64,8249	129,1936	-64,6043	96,8369	-64,7369	52,75301	0,160653	2,971188	26,22819	2,540714
10	4062 – 4951	76,466765 – 112,256441	8,699403	106,7747	8,592832	85,634	8,512334	63,69102	-0,08800	3,378974	23,04351	1,678697
11	4952 – 5417	112,285921 – 149,627112	-48,8432	170,14	-48,7667	156,0258	-48,077	135,2955	-0,18692	2,97285	21,7218	1,155579

Comparison of distance measurement indicators and the parameters of the VDES signal in measurement campaigns II and III.

The table 9 below compares the distance measurement with the use of VDES signals in the 3rd and 2nd measurement campaigns. The criterion was the error of the distance measurement in similar distance ranges from the transmitting station (rows highlighted in blue were omitted) without applying corrections (e.g. the moving average method), and for these ranges the value of the SNR of the VDES signal was given. It can be noticed that the error of measuring the distance in Campaign III is about two times smaller than in Campaign II (the lines marked in blue, due to incomparable distances from the transmitting station of VDES signals, are not included in the comparison).

This result was obtained through:

• Changing the transmission conditions of the VDES signal and by

• Changing the method of determining the correlation of the received VDES signal.

Table 9: Comparison of distance measurement indicators and the parameters of the VDES signal in measurement campaigns II and III

Distance to the transmitting station [km]	Sub-scope - VDES III analyzes: sub-scope and item number		(GNSS-VDES III) pop_n=0 [m]		SNR of the VDES III signal [dB]		SNR_Corr III [dB]	
			avg	std dev	avg	std dev	avg	std dev
-4,067– 149,627	(całość)	2:5417	-14,2678	93,76433	8,013756	11,91711	29,83525	6,435226
-4,066 – 16,183	2	170:1283	-3,70375	16,09981	26,20587	9,250651	38,43174	2,285096
16,206– 36,912	3, 4, 5, 6	1284:2874	-15,1773	57,48269	5,7027886	4,746819	31,68951	3,394997
36,931– 59,237	7, 8	2875:3564	-3,30751	105,2374	0,3325572	0,389254	26,19194	2,182654
59,264– 76,438	9	3565:4061	-64,8249	129,1936	0,160653	2,971188	26,22819	2,540714
76,466– 149,627	10, 11	4062:5417	-11,0756	134,7643	-0,121999	3,244378	22,58929	1,643611
Distance to the transmitting station [km]	Sub-scope - VDES II analyzes: sub-scope and item number		(GNSS-VDES II) pop_n=0 [m]		SNR of the VDES II signal [dB]		SNR_Corr II [dB]	
			avg	std dev	avg	std dev	avg	std dev
-4,071 – 54,105	(całość)	2:3712	-7,25659	113,8718	7,40283932	11,62745	122,41708	43,09622
-4,071 – 17,052	6, 7, 8	2545:3712	6,730293	38,88674	20,2767775	9,359271	178,8954	21,36448
17,081 – 35,779	3, 4, 5	865:2544	-13,38065	94,89414	2,03236712	7,50128	106,60445	12,89116
35,796 – 54,105	1, 2	2:864	-14,2650	189,2823	0,43370084	4,927614	76,760695	12,47531

The figure 11 below shows selected measurement data in the 2nd and 3rd measurement campaigns and the boundaries of the division into sub-ranges of all measurement points. The measurement data includes: the value of the SNR of the VDES signal (“SNR_VDES”) in II (dark blue) and III (yellow) campaign, errors in measuring the distance (“B_odl_pom”) in II (blue) and III (orange) campaign, and sub-range indicators (range indication) in the II (light blue) and III (green) campaigns.

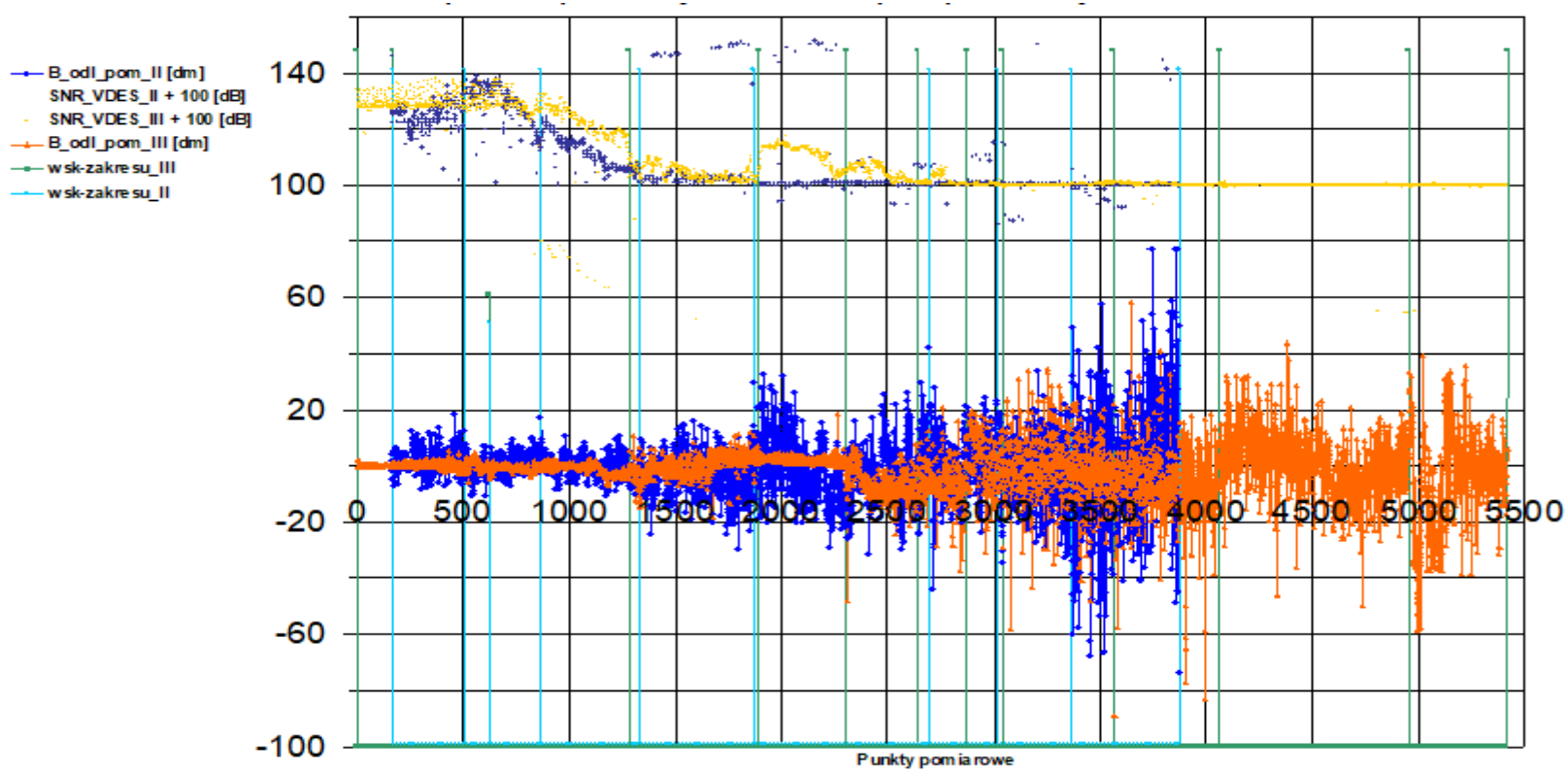

Figure 11: Measurement data (distance measurement error and SNR_VDES value) and range limits as a function of measurement points in the 2nd and 3rd measurement campaigns

The figure 12 below shows the error of distance measurement (“B_odl_pom”) as a function of the SNR of the VDES signal (SNR_VDES) obtained in the measurement campaigns II and III (see figures 9, 10 and 11 for campaign III - orange, and figure 11 for campaign II - blue).

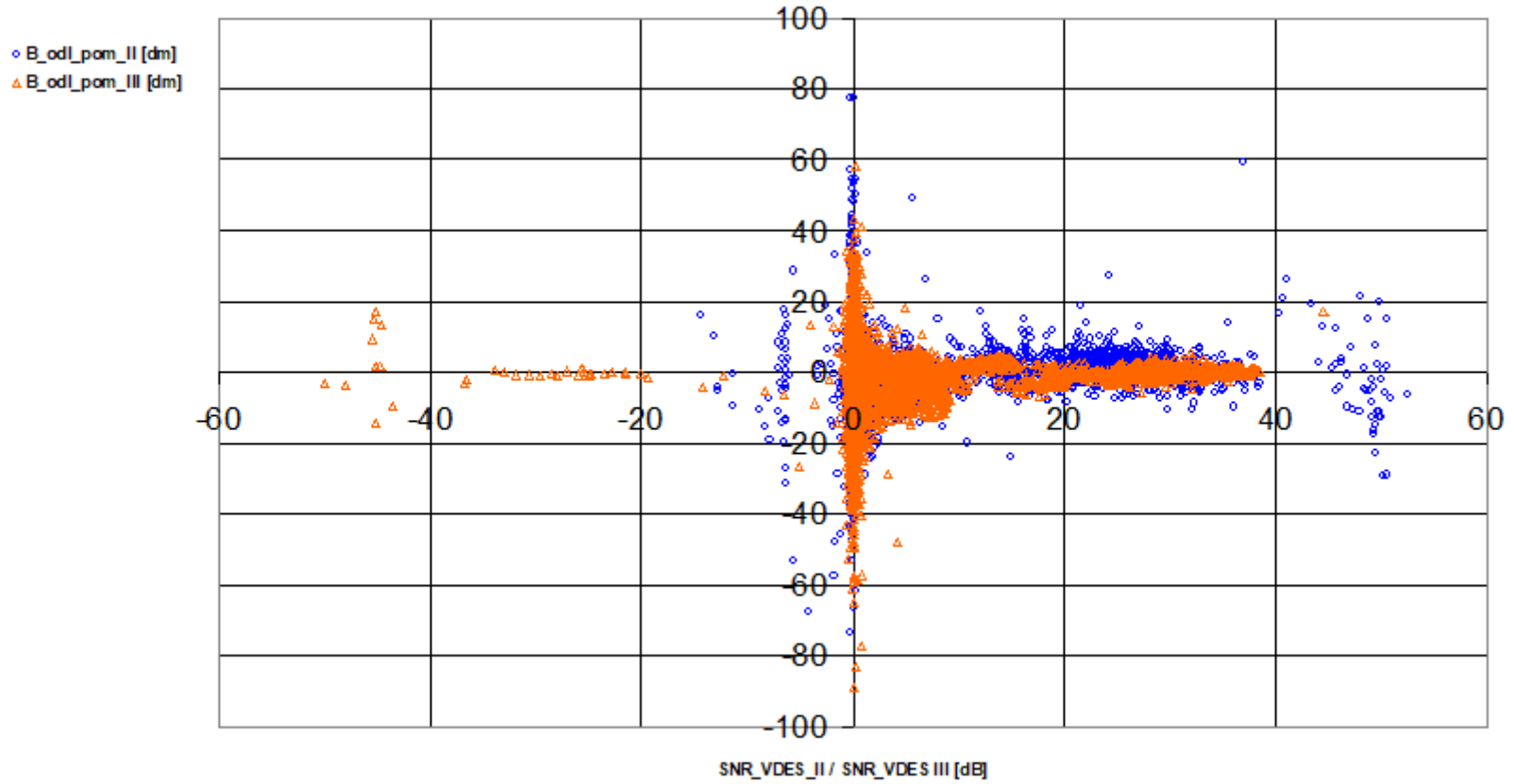

Figure 12: Distance measurement error in the SNR_VDES function

The figure 13 below shows the dependence of the distance measurement error (“B_odl_pom”: standard deviation value) on the SNR of the received VDES signal (“SNR_VDES”, average value) and the trend of these dependencies estimated in sub-ranges (by analyzing the distance from the transmitting station, see Table 7, 8 and 9 - rows marked in green and figures 9, 10 and 11 for campaign III and figure 11 for campaign II)

designated for measurement campaigns II and III. Comparing these dependencies, it can be seen that in the measurement campaign III in the entire range of the SNR change of the VDES signal, the value of the error in the distance measurement was educed two times (standard deviation).

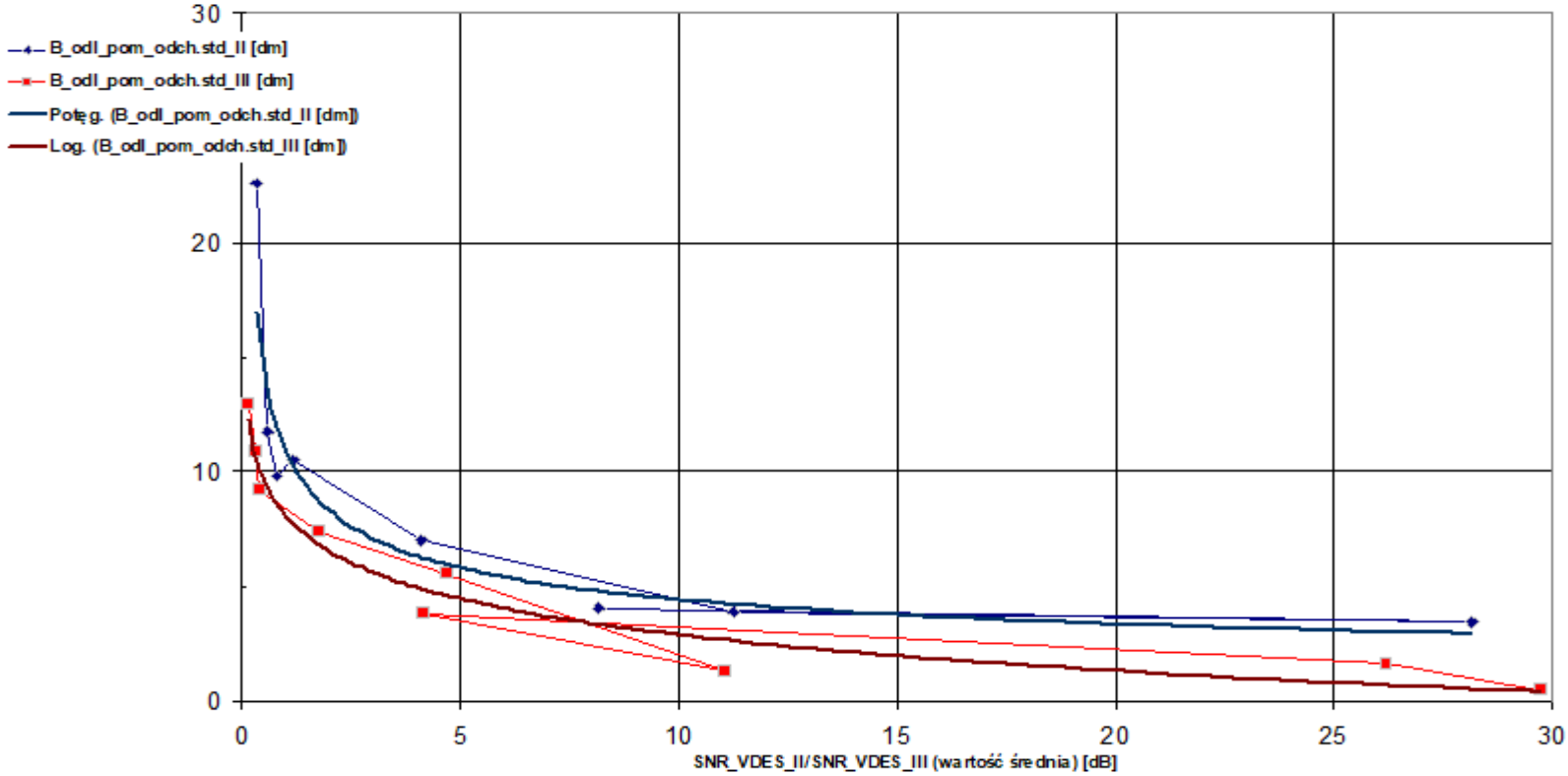

Figure 13: Distance measurement error (standard deviation) in the SNR_VDES function (average value)

The figure 14 shows the error of distance measurement (absolute value) as a function of the SNR of the VDES signal obtained at each measurement point and the superimposed curve of the standard deviation of the distance measurement as a function of the mean value of the SNR of the VDES signal obtained in the estimation of these values in the measurement sub-ranges, as well as the trend of this relationship, respectively for measurements in campaigns II and III.

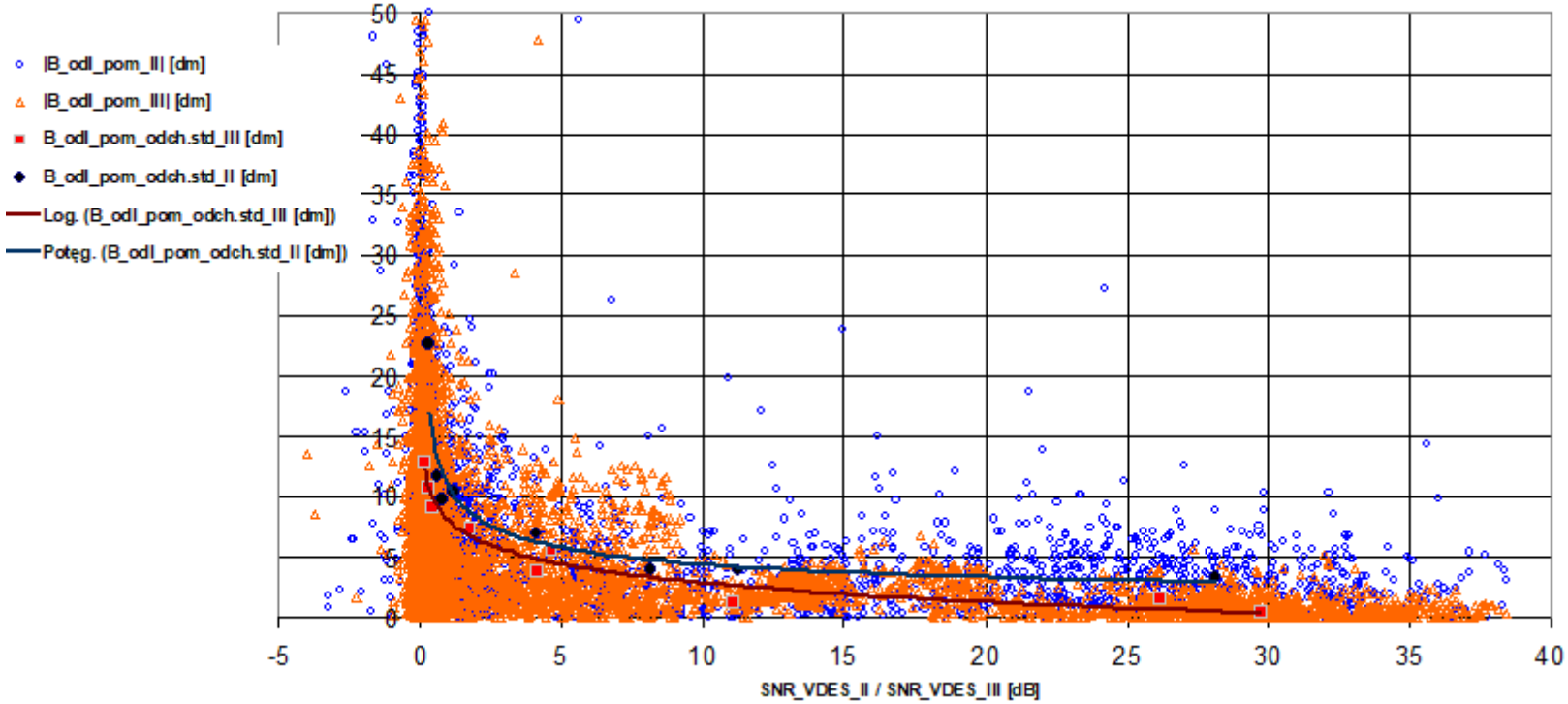

Figure 14: Distance measurement error (absolute point value and standard deviation value) in the function SNR_VDES (point value and average value)